NBS MONOGRAPH 67

Methods for the Dynamic Calibration Of Pressure Transducers

U.S. DEPARTMENT OF COMMERCE
NATIONAL BUREAU OF STANDARDS

THE NATIONAL BUREAU OF STANDARDS

Functions and Activities

The functions of the National Bureau of Standards are set forth in the Act of Congress, March 3, 1901, as amended by Congress in Public Law 619, 1950. These include the development and maintenance of the national standards of measurement and the provision of means and methods for making measurements consistent with these standards; the determination of physical constants and properties of materials; the development of methods and instruments for testing materials, devices, and structures; advisory services to government agencies on scientific and technical problems; invention and development of devices to serve special needs of the Government; and the development of standard practices, codes, and specifications. The work includes basic and applied research, development, engineering, instrumentation, testing, evaluation, calibration services, and various consultation and information services. Research projects are also performed for other government agencies when the work relates to and supplements the basic program of the Bureau or when the Bureau's unique competence is required. The scope of activities is suggested by the listing of divisions and sections on the inside of the back cover.

Publications

The results of the Bureau's research are published either in the Bureau's own series of publications or in the journals of professional and scientific societies. The Bureau itself publishes three periodicals available from the Government Printing Office: The Journal of Research, published in four separate sections, presents complete scientific and technical papers; the Technical News Bulletin presents summary and preliminary reports on work in progress; and CRPL Ionospheric Predictions provides data for determining the best frequencies to use for radio communications throughout the world. There are also five series of nonperiodical publications: Monographs, Applied Mathematics Series, Handbooks, Miscellaneous Publications, and Technical Notes.

A complete listing of the Bureau's publications can be found in National Bureau of Standards Circular 460, Publications of the National Bureau of Standards, 1901 to June 1947 ($1.25), and the Supplement to National Bureau of Standards Circular 460, July 1947 to June 1957 ($1.50), and Miscellaneous Publication 240, July 1957 to June 1960 (includes Titles of Papers Published in Outside Journals 1950 to 1959) ($2.25); available from the Superintendent of Documents, Government Printing Office, Washington D.C. 20402

UNITED STATES DEPARTMENT OF COMMERCE • Luther H. Hodges, *Secretary*

NATIONAL BUREAU OF STANDARDS • A. V. Astin, *Director*

Methods for the Dynamic Calibration of Pressure Transducers

J. L. Schweppe, L. C. Eichberger, D. F. Muster,
E. L. Michaels, and G. F. Paskusz

Prepared by Dresser Electronics, Southwestern
Industrial Electronics Division, under contract
with the National Bureau of Standards.

National Bureau of Standards Monograph 67

Issued December 12, 1963

For sale by the Superintendent of Documents, U.S. Government Printing Office
Washington, D.C., 20402 - Price 60 cents

Library of Congress Catalog Card Number: 63–60069

Contents

Foreword

Accurate dynamic measurements of pressure are a necessity in the design and development of modern rocket engines. Thus, with the growth of missile and space vehicle programs, such measurements have become increasingly important. To insure their accuracy, precise calibration methods must be employed. As pressure changes in rocket engines may exceed 200 psi at frequencies above 10kc/s. the measurement and calibration requirements of the dynamic pressure transducer are extremely rigorous.

This publication is designed to assist the practicing engineer who is faced with the problem of making dynamic measurements of such rapidly changing pressures. It provides a single reference source in which he may find, for a particular pressure transducer, the appropriate mathematical model, the mathematical and instrumental methods of analysis, the methods of calibration, and the specific methods for evaluation of test data from each method of calibration.

A. V. Astin, *Director.*

Preface

This Monograph is published as part of a continuing program on telemetering transducers which has been conducted in the Mechanical Instruments Section of the National Bureau of Standards under the sponsorship of the Bureau of Naval Weapons; Aeronautical Systems Division, U.S. Air Force; White Sands Missile Range, U.S. Army; and the National Aeronautics and Space Administration. Publication of the Monograph was conceived while Edward C. Lloyd was Chief of the Section, and under his direction Dr. Frederick F. Liu of Dresser Dynamics prepared a report entitled "The Dynamic Calibration of Transducers." Dr. Liu's report, which was completed in 1959, is a major source of the material included in this Monograph.

The final manuscript was prepared by Dresser Electronics, Southwestern Industrial Electronics Division, Houston, Texas under contract with the National Bureau of Standards. The text was written by Drs. J. L. Schweppe, L. C. Eichberger, D. F. Muster, E. L. Michaels, and G. F. Paskusz of the University of Houston. Dr. Knut Seeber and the late Dr. H. E. Hollman of Dresser Electronics, SIE Division made major contributions. Raymond O. Smith, Paul S. Lederer, and Dr. Hansjorg Oser of the National Bureau of Standards and Dr. Henry L. Mason, formerly of the National Bureau of Standards and now of the Veterans Administration, assisted materially with critical review, comments, and suggestions.

In order to calibrate and use dynamic pressure transducers, the practicing engineer needs to be familiar with (1) the characteristic differential equations and their solutions, (2) the methods of analyzing pairs of input and output functions to determine the transfer function and the frequency response curve, (3) the methods of generating precise input functions, and (4) the specific methods for using precise experimental measurements to determine the dynamic characteristics of a particular pressure transducer. The first two of these topics are covered in chapters 1 through 4, and the last two are covered in chapters 5 through 7.

Chapters 1 through 4 include an introduction to pressure transducer calibration, the characteristic differential equation, analytical methods of analysis for both linear and nonlinear transducers, and approximate methods of analysis for both linear and nonlinear transducers. Chapters 5 through 7 cover the description of many types of input function generators, the theory of calibration with each generator, the design of the calibration system, and the specific methods for evaluating the calibration data. Chapter 8 is devoted to a discussion of the applications and limitations of the electronic compensator, a device designed to compute the input function directly from the transducer output.

Arnold Wexler, *Chief*,
Mechanical Instruments Section.

List of Symbols

Symbol	Concept
a	arbitrary constant
	speed of sound
a_n	Fourier coefficient of cos $n\omega t$
A	arbitrary constant
	area, cross-sectional
	function
	maximum amplitude of $\frac{\sin x}{x}$
A_{ni}	coefficients
b	arbitrary constant
b_n	Fourier coefficient of sin $n\omega t$
B	arbitrary constant
	function
c	arbitrary constant
	damping constant
c_n	Fourier coefficient, eq (1.10)
C	arbitrary constant
	function
d	diameter
D	arbitrary constant
	function
e	base of Napierian or natural logarithm (e=2.718 . . .)
	function
	voltage or electromotive force
exp	e^a=exp a
E	error
	nonlinear differential equation
	function
E_n	function
f	frequency
	input function
F	amplitude of the input spectrum
	force
	Fourier transform of f
	Laplace transform of f
	maximum value of f
$\mathfrak{F}$	Fourier transform operator
$\mathfrak{F}^{-1}$	inverse Fourier transform operator
g	modified input function
G	Fourier transform of g
	function
h	function
H	amplitude of the transfer function (describing function)
	function
$\angle H$	phase angle of the describing function
	function
Im	imaginary part of a complex number
J	function
j	square root of minus one
k	amplitude factor
	scale factor
	spring constant
K	numerator of partial fraction
	arbitrary constant
K_m	bulk modulus
l	length
L	dimension of length
	inductance
	function

Symbol	Concept
$\mathcal{L}$	Laplace transform operator
$\mathcal{L}^{-1}$	inverse Laplace transform operator
m	mass
M	arbitrary constant
	Mach number
	function
n	nth quantity or number in general
N	dimensionless number
	modulus of inverse equivalent transfer function
	function
p	pressure
	velocity
p_i	generalized coordinate
P	pressure
	function
$P(q_k,\dot{q}_k)$	point located at coordinates $(q_k,\dot{q}_k)$
q	transducer output
q_i	generalized coordinate
Q	maximum value of q
r	root of auxiliary equation
R	function
	gas constant
	electrical resistance
Re	real part of a complex number
Rp	ramp function
s	complex variable $\sigma+j\omega$
S	excitation parameter
	function
	phase space
t	time
T	dimension of time
	operator
	period
	temperature
	total transmitted light
	triangular pulse function
u	velocity
u_1	gas velocity into which the shock moves
u_2	gas velocity out of which the shock moves
U	shock velocity
	unit step function
	unit pulse function
v	velocity component along x-axis ($\dot{x}$)
V	function
	volume
V_1	maximum value of x
x	coordinate along x-axis
	function
	instantaneous displacement
$\tilde{x}$	approximate solution or value
X	amplitude of the response spectrum
	function
	Fourier transform of x
	maximum displacement
	response function
	Re ($X(s)$), eq (3.73)
y	coordinate along y-axis
	function
Y	$Im(X(s))$, eq (3.74)

Symbol	Concept
z	arbitrary variable
	coordinate along z-axis
	response function
Z	arbitrary constant
$\tilde{z}$	approximate solution or value
α	angle
	attenuation constant
	output phase angle
$\alpha\tau$	logarithmic decrement
β	angle
	phase angle of the transfer function
	nonlinearity coefficient
	attenuation constant
γ	ratio of specific heats
Γ	function
δ	logarithmic decrement
	function
Δ	finite difference
ϵ	arbitrary constant
	phase angle
ζ	damping ratio
θ	angle
λ	wavelength
μ	absolute viscosity
ξ	phase angle
ρ	function
	mass density
	radius
ρ_0	maximum value of ρ
σ	angle
	real part of $s=\sigma+j\omega$
τ	normalized time ($=\omega t$)
	time constant
τ_i	time increment used in trapezoidal method (fig. 3.4c)
φ	input phase angle
	force ($c/\lvert\dot{x}\rvert$)
ϕ	function
ω	angular velocity (circular frequency)
ω_n	undamped natural frequency

Superscript	Concept
(n)	nth derivative of a quantity (the nth derivative of X is denoted $X^{(n)}$)
+ (plus)	limit of the function when the independent variable approaches the point to be evaluated from the right ($f(t)$ approaches the limit $f(0^+)$ as t approaches zero from the right)
—(bar)	mean value (written over, not after, the principal symbol to which it applies)
· (dot)	derivative with respect to time (number of dots over primary symbol indicates number of times derivative is taken)
*	approximation

Subscript	Concept
av	average
c	critical
	upper limit
d	damped
eff	effective
i	ith quantity or number in general
k	kth quantity or number in general
m	maximum
n	fundamental
	nth quantity or number in general
o	output
p	pulse
R	rectangular
Rp	ramp
s	steady-state or particular solution
S	step
t	transient or complementary solution
	transition point
T	triangular
0	(zero): initial condition
	peak value

NOTES: 1. This list of symbols is based on American Standards Letter Symbols for Rocket Propulsion, ASA Y10.14–1959. Some symbols have been added from other sources.

2. Vectors are indicated by an arrow over the principal symbol. The amplitude of a vector is represented by the principal symbol without the arrow.

3. In general functions of time are indicated by lower case letters, functions of frequency by capitals. The same letter is used so, when a given function such as $f(t)$ is transformed to the frequency domain it becomes $F(\omega)$.

1. INTRODUCTION

L. C. Eichberger [1] and J. L. Schweppe [2]

1. General

1.1. Statement of Objectives

The purpose of this publication is to provide assistance to the practicing engineer who is faced with the problem of making dynamic measurements of rapidly changing pressures. This chapter and the chapters which follow cover the mathematical models for transducers, the methods of analyzing pairs of input and output functions to determine the transfer function and the frequency response curve, the methods of generating precise input functions, and the specific methods for using precise experimental measurements to determine the dynamic characteristics of a pressure transducer.

The specific objectives of Chaper 1 are to introduce (1) the types and characteristics of pressure transducers, and (2) the concepts of calibration and analysis.

1.2. Background

The missile and space vehicle programs have brought about a need for precise measurements of rapidly changing pressures. Along with this need for high precision and response, there is an associated need for improved calibration techniques. As a result, both experimental and analytical methods have evolved rapidly.

For some time the frequency-response concept has been established in the electronic and servo fields. It is therefore a natural development for this concept to be applied to pressure transducers, which are components in electronic systems. This development has been accelerated by the increasing application of transform methods such as Fourier and Laplace. The frequency-response concept and the use of mathematical methods are introduced in this chapter.

2. Pressure Transducers

A pressure transducer is an electromechanical device through which an input pressure signal is converted to an output electrical signal. In most pressure transducers the pressure force causes the displacement of a spring. This displacement produces a change in some electrical property which in turn is measured by an appropriate electrical system. The electrical property of the transducer is most commonly the resistance of a potentiometer, the resistance of a bonded or unbonded strain gage, the capacitance between two plates, the inductance of a coil, or the piezoelectric property of a crystal. Depending on the physical combination of parts, any one of these gages may either approach a simple oscillator having one natural frequency, or it may have a combination of frequencies. And it may have a linear or nonlinear response to the input signal. Some good general references on pressure transducers are Hernandez [1] [3], Borden and Mayo-Wells [2], Lion [3], and Roberts [4].

2.1. Types of Pressure Transducers

The potentiometric transducer utilizes a potentiometer circuit in which the slider location is determined by the magnitude of the pressure force, figure 1.1. A multiplying linkage is used between the slider and the force-summing member to minimize the required movement of the latter part. The many moving parts make friction, vibration, and inertia substantial problems; and, although these transducers are carefully designed to reduce the effects of friction and vibration, they do not respond well to high rates of pressure change. However, because a high-output a-c or d-c signal may be obtained without use of an amplifier, the potentiometric transducer is widely used for measuring static and low-rate-of-change pressures.

The strain gage transducer system measures the pressure through its effect on a bonded or unbonded strained element in the transducer. In the example shown in figure 1.2, the strain gages are bonded to a cylindrical strain tube which is compressed when pressure is applied. A flush catenary diaphragm separates the transducer components from the pressure region and transmits the pressure to the strain tube. Two strain gages are bonded, one longitudinally and one circumferentially, to the outside of the tube to form the two active arms of a Wheatstone bridge. Two inactive precision resistors and a precision potentiometer are added externally to complete the bridge. The unbonded strain gage transducer utilizes the gage directly as the strained element. That is, no element comparable to the strain tube of figure 1.2 is used. For further details see Hernandez [1].

[1] Assistant Professor of Mechanical Engineering, The University of Houston; Technical Staff, Houston Engineering Research Corporation.
[2] Professor of Mechanical Engineering, The University of Houston; President, Houston Engineering Research Corporation.
[3] Figures in brackets indicate the literature references on page 9.

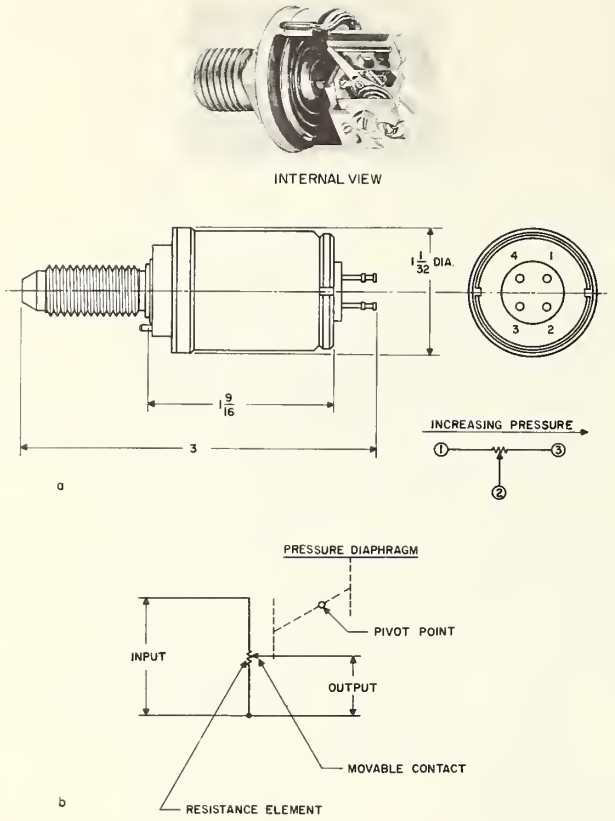

FIGURE 1.1. *Potentiometric pressure transducer.*

(a) Photograph and typical dimensions
(Reproduced by courtesy of Fairchild Controls Corporation)
(b) Schematic diagram

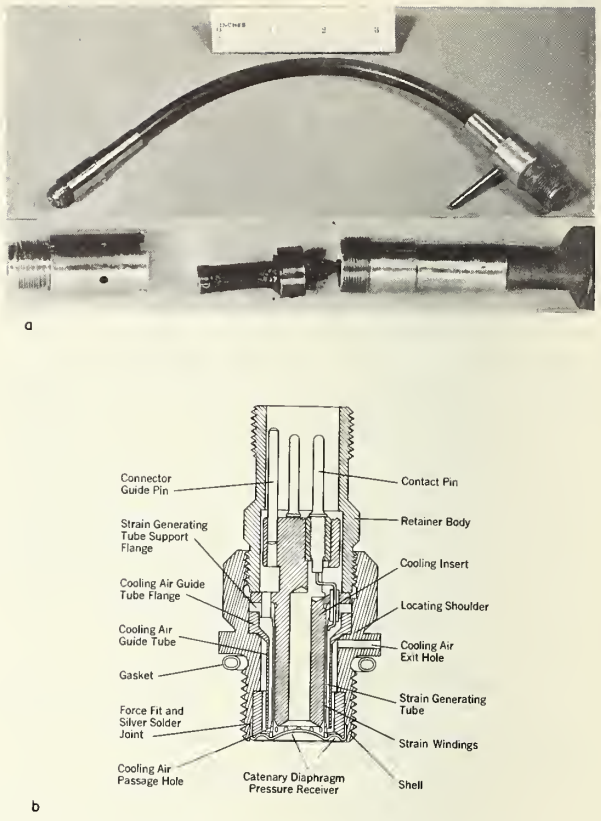

FIGURE 1.2. *Bonded strain gage pressure transducer.*

(Reproduced by courtesy of Norwood Controls Unit of Detroit Controls Corporation)
(a) Photograph with enlarged view of disassembled pickup
(b) Cross section of catenary diaphragm pressure transducer

Figure 1.3 shows one example of the unbonded strain gage transducer. Bonded and unbonded gages are available from a number of manufacturers and both may be used to measure either static or dynamic pressures.

Still another strain gage system measures pressure through its effect on the resistivity of a semiconductor crystal. In this system the crystal functions both as the strained element and the measuring element. The crystal is mounted between a fixed plane and a diaphragm which separates the components from the pressure region. The piezoresistive transducer has a gage factor of the order of magnitude of 150 compared to 2 to 4 for a conventional strain gage [5].

The capacitive transducer system measures the pressure through its effect on the electrical capacitance of a movable-plate condenser. In one system the movable-plate condenser is a part of a very-high-frequency circuit. As the capacitance changes, so does the impedance. Since for a fixed position of the movable plate the impedance is constant, the capacitive transducer system can be used for either static or dynamic pressure measurements. It is important to note that the coaxial cable which connects the transducer with the external circuit is a part of the circuit whose impedance change is an analog of pressure. Therefore electrical characteristics of the coaxial cable are critical. A photograph, a dimensional drawing, and a cross-sectional view of a typical capacitive transducer are shown in figure 1.4.

The inductive transducer measures the pressure by its effect on the inductance of a coil or on the inductance ratio of a pair of coils. In a typical instrument the pressure force moves a diaphragm and thereby changes the magnetic coupling between the coils, figure 1.5. The inductive transducer has the advantages that it can be used for static or dynamic measurements and that it has a high output and high signal-to-noise ratio. But it is influenced by stray magnetic fields and it has a low useful frequency range in the order of 500 c/s.

The piezoelectric transducer system measures the pressure through its effect on a piezoelectric material. When the crystal is distorted by the pressure force, an electric charge is generated. The amount of this charge, which is a function of the pressure force, is measured with an electrometer. Since the electric charge leaks off, the piezoelectric transducer is inherently a transient device and cannot be used for static measurements. A photograph and a cross-sectional view are shown in figure 1.6.

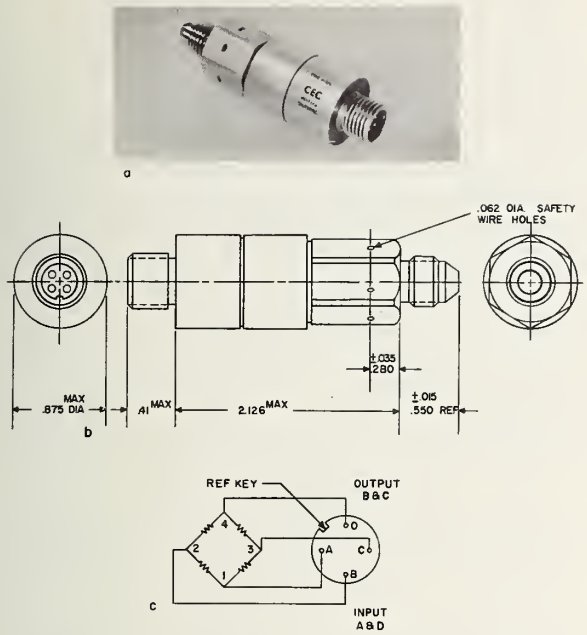

FIGURE 1.3. *Unbonded strain gage pressure transducer.*

(Reproduced by courtesy of Transducer Division, Consolidated Electrodynamics.)

(a) Photograph
(b) Typical dimensions
(c) Wiring diagram

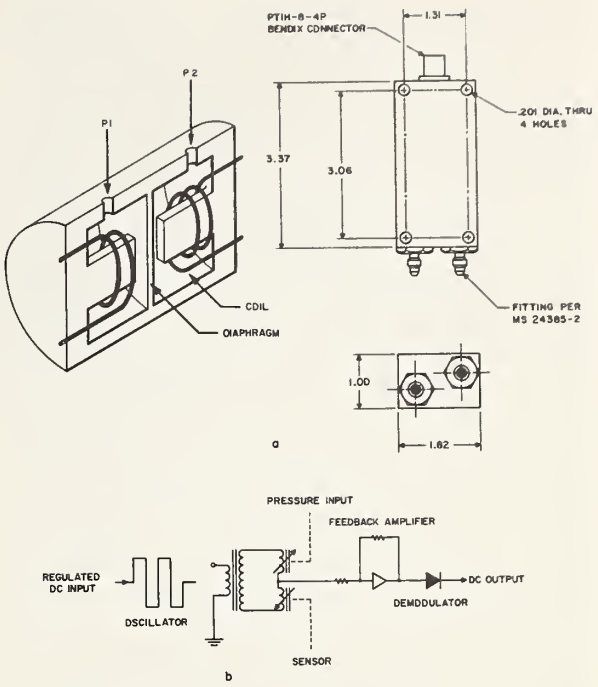

FIGURE 1.5. *Inductive pressure transducer.*

(Reproduced by courtesy of Astromics Division of Mitchell Camera Corporation.)

(a) Internal view and typical dimensions
(b) Circuit diagram

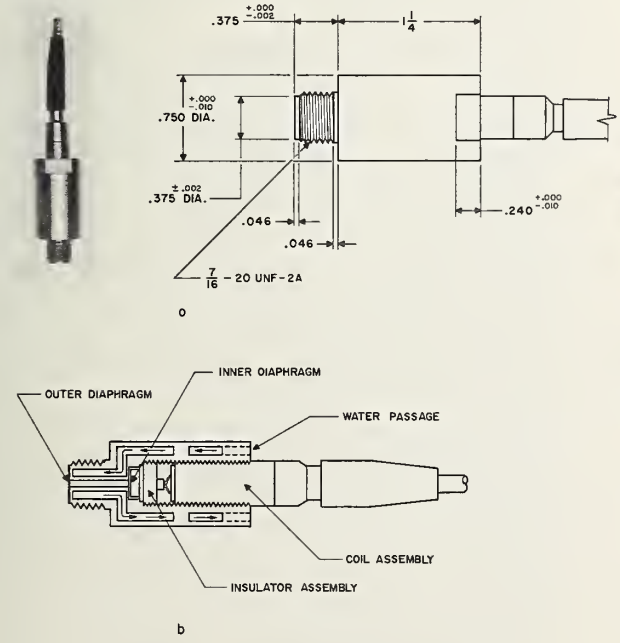

FIGURE 1.4. *Typical capacitive transducer.*

(a) Photograph and typical dimensions
(Reproduced by courtesy of Photocon Research Products.)
(b) Cross-sectional view

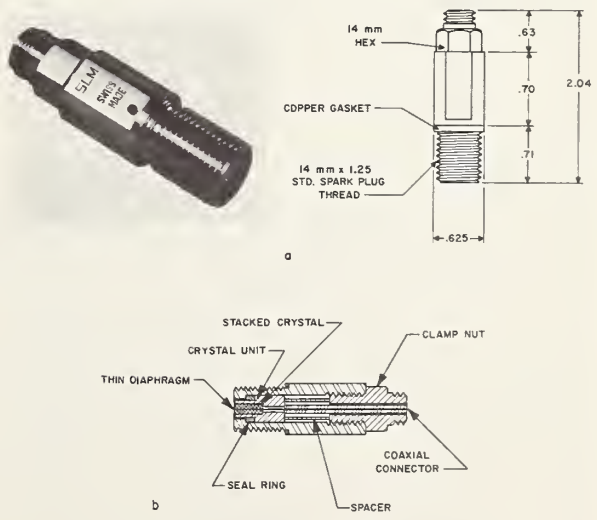

FIGURE 1.6. *Piezoelectric pressure transducer.*

(a) Photograph and typical dimensions
(Reproduced by courtesy of Kistler Instruments Corporation.)
(b) Cross section

2.2. Physical Characteristics of Transducers

The above descriptions of several types of transducers show the similarities and the differences in physical characteristics. First, each transducer must have certain major parts. These include an active or sensing element, a body to hold the active element in place in the wall of the pressure region, a diaphragm or other device to separate the components from the pressure region and to transmit the pressure force to the sensing element, and an electrical means of removing the output signal from the transducer. The signal output may be through a simple transmission line or a rather complicated electronic device such as a carrier bridge.

A simple or "ideal" transducer would have a linear response to the input pressure signal, and it would have a single degree of freedom. That is, the oscillatory movement would be limited to a direction parallel to the line of action of the applied force. Also, the "ideal" transducer would deflect little when the input pressure is applied, but would generate a substantial output signal.

A real transducer may have a response which approaches the ideal linear response to the input signal, but it will have more than one mode of oscillation. The number of additional modes and their importance depend on the particular transducer. In the analysis which follows, it will be assumed that the pressure input is applied directly to the diaphragm. That is, cavity effects will not be included. Also, it will be assumed that the body of the transducer is rigid—or that it has a natural frequency so far above the operating frequency that it need not be considered.

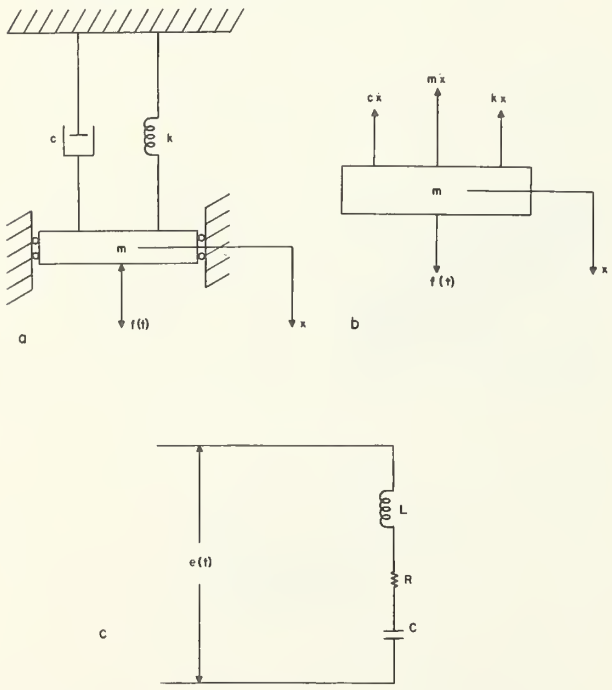

FIGURE 1.7. *Single-degree-of-freedom vibrating system.*

(a) Mechanical model
(b) Free-body diagram
(c) Electrical force-voltage analog

For each transducer, then, two parts are considered in the synthesis of the mechanical model. They are the sensing element and the diaphragm and, in many cases, the electrical equipment required to complete the energy transformation to the voltage or current analog. Each of these parts will have one or more modes of oscillation, with associated spring constants and damping factors. Mechanical models for several typical transducers are synthesized in the next section. It should be noted that such mechanical models do not always completely describe the transducer, but that often one or more additional electrical modes of oscillation need to be indicated. The mathematical treatment need not distinguish between mechanical and electrical resonances.

2.3. Mechanical Models

A mechanical model idealizes a vibrating system. The model consists of at least one inertial mass, a spring, a viscous resistance, and an external driving or exciting force. For the ideal transducer the spring force and the viscous resistance are linear, i.e., the spring force is directly proportional to the change in length and the viscous resistance is directly proportional to the velocity. Nonlinearity results if the spring force or the viscous resistance, or both, are nonlinear. The arrangement and number of components establish the number of degrees of freedom for the model, i.e., the minimum number of coordinates necessary to specify the configuration of the vibrating system at any time [6, 7].

A single-degree-of-freedom vibrating system can be idealized by the mechanical model shown in figure 1.7a. The characteristics of the capacitive and piezoelectric transducers are approximated by this model. For these transducers the response, or output, is normally dependent upon one of two masses: the mass of the sensing element, or the mass of the diaphragm. In the capacitive transducer the moving mass in the sensing element (air) is negligible compared to the mass of the diaphragm (active, or movable plate of the capacitor). In the piezoelectric transducer the mass of the diaphragm normally is negligible compared to the mass of the sensing element.

A two-degree-of-freedom vibrating system can be idealized by the mechanical model shown in figure 1.8a. Lederer and Smith of the National Bureau of Standards have shown that this model is a fair approximation for the strain gage transducer shown in figure 1.2. They considered the mass of the diaphragm to be negligible and the mass of the strain-generating tube to respond in two modes, a longitudinal mode and a radial mode.

In general, the synthesis of a mechanical model must be preceded by a detailed study of the arrangement, size, and orientation of the physical components of a transducer. The validity of the

synthesis is verified by comparing the response of the model to that of the transducer for a given input, or external driving function.

2.4. Characteristic Differential Equations

Once the mechanical model has been established, the characteristic differential equation which describes the motion of the system is obtained by application of d'Alembert's principle. For the single-degree-of-freedom vibrating system, figure 1.7b, summing the forces gives

$$m\ddot{x}+c\dot{x}+kx=f(t). \tag{1.1}$$

The damping constant, c, is the number of units of resistive force per unit velocity of motion; the spring constant, k, is the number of units of force required to stretch the spring a unit length; and $f(t)$ is the external driving force, a function of time.

Application of d'Alembert's principle to the two-degree-of-freedom vibrating system, figure 1.8b, yields

$$\begin{aligned} &m_1\ddot{x}_1+c_1\dot{x}_1+k_1x_1-c_2(\dot{x}_2-\dot{x}_1)-k_2(x_2-x_1)=0 \\ &m_2\ddot{x}_2+c_2(\dot{x}_2-\dot{x}_1)+k_2(x_2-x_1)=f(t). \end{aligned} \tag{1.2}$$

The number subscripts distinguish between like elements.

In general the number of such characteristic second-order differential equations of motion will agree with the number of degrees of freedom of the vibrating system.

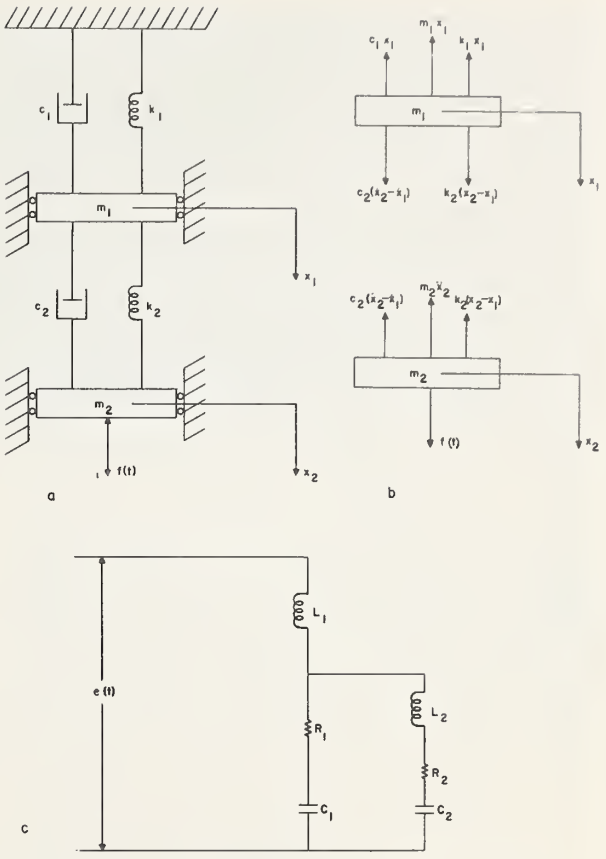

FIGURE 1.8. *Two-degree-of-freedom vibrating system.*

(a) Mechanical model
(b) Free-body diagram
(c) Electrical force-voltage analog

3. Transducer Calibration and Analysis

Calibration is the establishment of a known relation or transfer function between the input or driving function and the output or response function. This transfer function exists only if the transducer is describable by a linear differential equation. For a simple static calibration the transfer function is the ratio of output to input. For a dynamic calibration the transfer function is normally a complex function of frequency in which are included certain time constants. This function may be found in one of two ways: (1) If the transducer system can be described by a characteristic differential equation, the transfer function may be obtained by analytical solution of the equation. With this solution the response for a given input, or the input which will produce a given response, can be computed. Or (2) if the characteristic differential equation is not known, the transfer function can be obtained from knowledge of a pair of associated input and output functions. From this transfer function, frequency-response curves can be computed, and these curves can be used to determine the response for a given input, or the input which will produce a given response.

In the following, the reader is introduced to the analytical solution of the characteristic differential equations, experimental calibration methods, and the relationship of calibration to analysis.

3.1. Methods of Analysis

Methods used for solving differential equations of the motion of a vibrating system are dependent on the type of these differential equations. We shall deal here exclusively with homogeneous and nonhomogeneous linear, second-order, differential equations with constant coefficients.

Several methods are available to find solutions of these equations. The oldest method, which we shall refer to as the classical method, consists in finding one particular solution of the nonhomogeneous equation and adding to it the general solution of the homogeneous equation. The former solution is also called the steady-state solution, whereas the latter is the transient solution, which is found, for example, by substituting $\exp(rt)$ into the homogeneous equation. Calling the solutions of the resulting equation r_1 and r_2, we obtain the general solution of the homogeneous equation as

$c_1 \exp(r_1 t) + c_2 \exp(r_2 t)$, with arbitrary constants c_1 and c_2. They are determined from the initial conditions.

The operational methods are Laplace and Fourier transformations, which are dealt with in section 4 of this chapter. Both transient and steady-state solutions are obtainable by either of these methods.

Other methods of analysis make use of digital or analog computers. On the digital computer the solution is determined on a discrete set of values of time. Because of the cost of programming high-speed electronic computers, these machines are economical only if many differential equations of the same type have to be solved, or if high accuracy is desired which is not obtainable otherwise. However, since automatic programming is now available for almost any computer, programming costs have been reduced considerably.

The analog computer simulates the original differential equation, the dependent variable usually being a voltage which is made to satisfy the given differential equation and the initial conditions. It is an extremely versatile device which can also be made to simulate many types of mathematical nonlinearities or graphic relationships not expressible in analytic form, or even to permit the inclusion of actual transducer components in the simulated system. The output of the analog computer may be a continuous curve, e.g., an inked trace or a display on a cathode ray tube, or it may be digital through the use of analog-to-digital converters. Because the parameters and variables of a problem are uniquely evidenced by knob settings or dial readings during the solution, the rapid scanning of parameter influence is possible. This puts the analog computer clearly ahead of any other method if some quantitative results with moderate accuracy are desired.

Purely mathematical methods for other types of differential equations exist, but their discussion is outside the scope of this treatise.

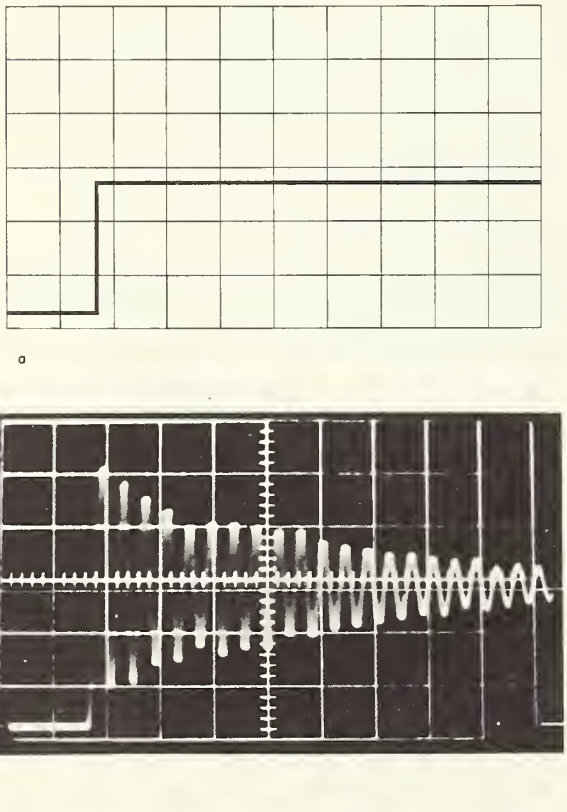

FIGURE 1.9. *Associated input and output functions from shock tube calibration of a pressure transducer.*

(a) Input function (b) Output function

3.2. Experimental Calibration Methods

In general, the imposed input for dynamic calibration may be either a nonperiodic or a periodic function. In either case the dynamic properties may be expressed as a plot of the instrument's response to the input. The nonperiodic function may be an impact of short duration which is quickly released, or it may be a step function which changes the pressure level from one specific value to another in a very short time. The dropping ball is an example of the impact-type, nonperiodic function generator. Step-function generators include quick-opening devices, explosive devices, and shock tubes. Figure 1.9 shows the response of a typical gage to a pressure step generated in a shock tube in the laboratory at the National Bureau of Standards.

The ideal periodic-function generator produces pure sine waves of controlled frequency and amplitude, and the frequency response curves are determined directly as they are for electronic circuits. Satisfactory sinusoidal calibration os microphones, a form of pressure transducer, if carried out in air over a wide frequency range but at very low amplitudes. Since accurately known sinusoidal input functions in the form of pressure cannot be generated in a gas at appreciable amplitudes [8, 9], other waveforms describable as the sum of a number of sinusoids are used when tests must be conducted at pressures up to 200 psia and at frequencies up to 30 kc/s. Periodic waveforms used for transducer calibration include repetitive impulses, square waves, sawtooth waves, and the like. Periodic-function generators include acoustical shock generators, rotating valves, sirens, piston-in-cylinder devices, and electrical and mechanical oscillators. Figure 1.10 shows the response of a typical pressure transducer to a sine wave generated by a hydraulic oscillator [10].

3.3. Relationship of Calibration to Analysis

Even though it may be possible to describe the characteristics of a real transducer by a simple mechanical model and the associated differential equation, the spring constants and damping coefficients still must be determined experimentally.

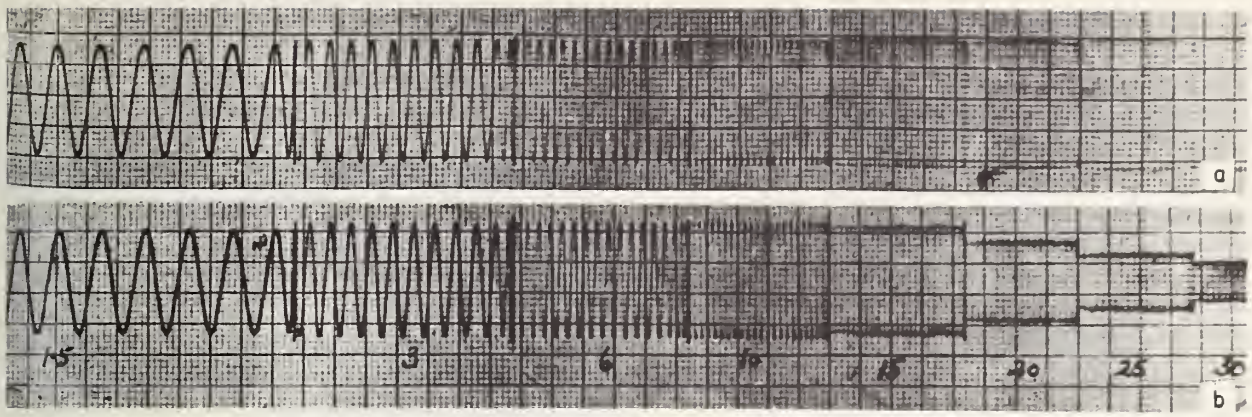

FIGURE 1.10. *Associated input and output functions from calibration of a pressure transducer with a hydraulic oscillator.*

(Reproduced from [10] with permission from J. Sci. Instr., published by The Institutes of Physics and The Physical Society.)
(a) Input function (b) Response function

And, when it is impossible or impractical to describe the characteristics of the transducer analytically, the transfer function must be obtained from a knowledge of a pair of associated input and output functions which must be imposed and measured experimentally.

These experimental input and output functions are recorded as a function of time, or are expressed in the time domain. In order to obtain the transfer function, which is expressed in the frequency domain, the input and output functions must be transformed into the frequency domain. Therefore, the method chosen for analyzing the experimental input and output functions must include this transformation. Fourier and Laplace analysis fulfill this requirement and, at the same time, are more efficient than methods which operate in the time domain. Accordingly, Fourier and Laplace methods are used exclusively in this work.

4. Fourier Methods and Spectral Analysis

4.1. Fourier Series and Line Spectra

Any periodic function $f(z)$ with period 2π can be expanded into a Fourier series of the form

$$f(x)=\frac{a_0}{2}+\sum_{n=1}^{\infty}(a_n\cos nz+b_n\sin nz), \quad (1.3)$$

where the Fourier coefficients a_n and b_n are given by

$$a_n=\frac{1}{\pi}\int_{-\pi}^{\pi}f(z)\cos nz\,dz \quad (1.4)$$

$$b_n=\frac{1}{\pi}\int_{-\pi}^{\pi}f(z)\sin nz\,dz. \quad (1.5)$$

The validity of the Fourier series of $f(z)$, eq (1.3), as used in engineering applications, is covered by the Dirichlet conditions. Dirichlet proved that, if $f(z)$ is finite in a given interval and has a finite number of maxima and minima in one period, the Fourier series of $f(z)$ is convergent, and its sum is equal to $f(z)$, if $f(z)$ is continuous at the point z. If $f(z)$ is discontinuous at the point z, then the Fourier series will converge to the average value of $f(z)$ at this point. Immediately near and on both sides of the discontinuity, the Fourier series overshoots the function $f(z)$. The amount of the overshoot is about 9 percent of the jump, so the Fourier series approximation is not very satisfactory for points very near to the discontinuity [11].

In most engineering applications, a function of time is given, and eqs (1.3), (1.4), and (1.5) must be modified. If T is the period in time of the given function $f(t)$, then $z=(2\pi/T)\,t=\omega t$, since z is the argument of the sine and cosine function and must be an angle. The circular frequency, ω, will always have the value of $2\pi/T$. Therefore

$$f(t)=\frac{a_0}{2}+\sum_{n=1}^{\infty}(a_n\cos n\omega t+b_n\sin n\omega t), \quad (1.6)$$

where, for $n=(0, 1, 2, \ldots)$

$$a_n=\frac{2}{T}\int_{-T/2}^{T/2}f(t)\cos n\omega t\,dt \quad (1.7)$$

$$b_n=\frac{2}{T}\int_{-T/2}^{T/2}f(t)\sin n\omega t\,dt. \quad (1.8)$$

Equation (1.6) can also be expressed in an alternate form:

$$f(t)=\frac{a_0}{2}+\sum_{n=1}^{\infty}c_n\cos(n\omega t-\varphi_n) \quad (1.9)$$

where

$$c_n=\sqrt{a_n^2+b_n^2} \quad (1.10)$$

and

$$\varphi=\tan^{-1}(b_n/a_n). \quad (1.11)$$

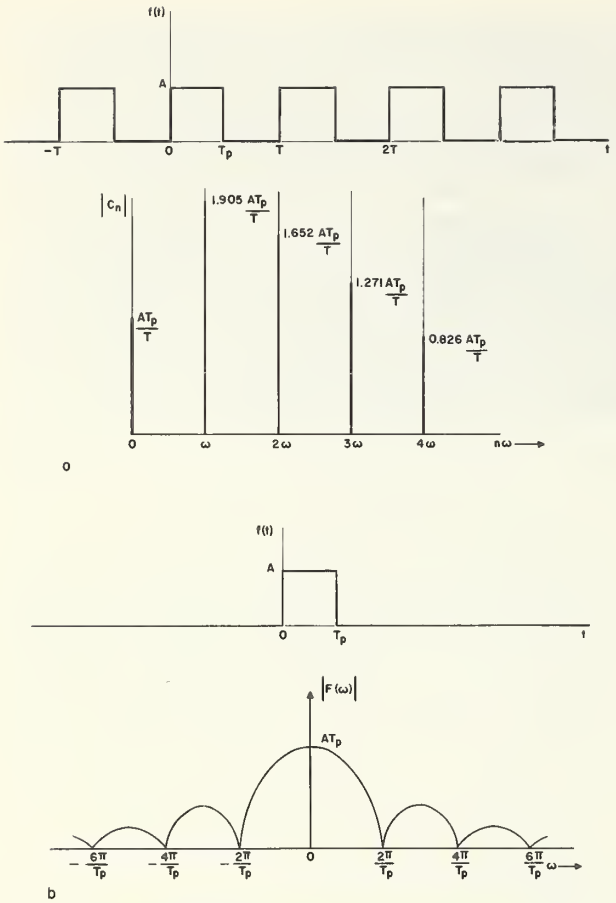

FIGURE 1.11. *Characteristic spectral plots.*

(a) Harmonic amplitude line spectrum
(b) Relative frequency distribution for a single rectangular pulse

Still another alternate form of the Fourier series is the complex exponential form which is used to introduce the Fourier integral and Fourier transform. This form is obtained by substituting the exponential equivalents of the sine and cosine terms into eq (1.3). Expanding, collecting like terms, and writing the results in a symmetrical form yields

$$f(t)=\sum_{n=-\infty}^{\infty} c_n e^{jn\omega t} \tag{1.12}$$

where

$$c_n=\frac{1}{T}\int_{-T/2}^{T/2} f(t)e^{-jn\omega t}dt. \tag{1.13}$$

Spectral analysis has evolved from Fourier analysis solutions [12]. A plot of c_n or φ_n from the Fourier series representation of $f(t)$, eq (1.9), as ordinate and $n\omega$ as abscissa, consists of discrete vertical lines and so is called a line spectrum. Specifically, the c_n and φ_n versus $n\omega$ plots are, respectively, the harmonic-amplitude spectrum and the phase-angle spectrum. In general, plots of this type are called by that quantity which is plotted against $n\omega$, and are a part of the family referred to as Fourier series spectra (see fig. 1.11a). For a more detailed discussion on Fourier series see Pipes [13].

4.2. Fourier Transform and Continuous Spectrum

The Fourier series is adequate to accomplish the expansion of any periodic function satisfying the Dirichlet conditions [11]. However, in many problems encountered, the given function of time is aperiodic and such a function cannot be handled directly by the Fourier series. However, in the limit, as the fundamental period T becomes infinite, the series passes into an integral form [14]. The resulting integral is called the Fourier integral and is expressed as

$$f(t)=\int_{-\infty}^{\infty} e^{2\pi j\sigma t}d\sigma \int_{-\infty}^{\infty} f(t)e^{-2\pi j\sigma t}dt \tag{1.14}$$

where σ is a real variable. This representation of $f(t)$ is valid, provided that in every finite interval $f(t)$ satisfies the Dirichlet conditions and the integral $\int_{-\infty}^{\infty}|f(t)|dt$ exists.

Equation (1.14) may be written in a slightly different form by the introduction of $\omega=2\pi\sigma$ as a new variable. With this,

$$f(t)=\frac{1}{2\pi}\int_{-\infty}^{\infty} e^{j\omega t}d\omega \int_{-\infty}^{\infty} f(t)e^{-j\omega t}dt. \tag{1.15}$$

Then, eq (1.15) becomes

$$f(t)=\frac{1}{2\pi}\int_{-\infty}^{\infty} F(\omega)e^{j\omega t}d\omega \tag{1.16}$$

where

$$F(\omega)=\int_{-\infty}^{\infty} f(t)e^{-j\omega t}dt. \tag{1.17}$$

Equations (1.16) and (1.17) constitute what is known as a Fourier transform pair; $F(\omega)$ is called the Fourier transform of $f(t)$ and, conversely, $f(t)$ is called the inverse Fourier transform of $F(\omega)$:

$$F(\omega)=\mathfrak{F}[f(t)] \tag{1.18}$$

$$f(t)=\mathfrak{F}^{-1}[F(\omega)] \tag{1.19}$$

The Fourier transformation of eq (1.18) transforms a function of t (in the time domain) into a function of ω (in the frequency domain). The inverse Fourier transformation of eq (1.19) transforms a function of ω (in the frequency domain) into a function of t (in the time domain).

4.3. Laplace Transform and Continuous Spectrum

If a function is identically zero before some time, say $t=0$, then it may be represented by the Fourier transform pair, eqs (1.16) and (1.17), if the lower limit of $F(\omega)$ is changed from $-\infty$ to 0 [16].

$$f(t)=\frac{1}{2\pi}\int_{-\infty}^{\infty}F(\omega)e^{j\omega t}d\omega \qquad (1.16)$$

$$F(\omega)=\int_{0}^{\infty}f(t)e^{-j\omega t}dt. \qquad (1.20)$$

Equations (1.16) and (1.20) are known as the unilateral Fourier transform.

In contrast to the line spectra concept from the Fourier series analysis of periodic functions, Fourier integral analysis of aperiodic functions yields a continuous amplitude spectrum. This transform, when applied to a single rectangular pulse, yields the spectrum of figure 1.11b.

Equations (1.16) and (1.20) are meaningless if the integral $F(\omega)$ does not exist. A sufficient condition for the existence of $F(\omega)$ is that $f(t)$ be absolutely integrable, i.e., that $\int_0^\infty |f(t)|dt$ exists. There are cases where $f(t)$ is not absolutely integrable, but still represents a physically well-behaved stimulus. Examples are the step function and sin ωt. For this reason there is a need for an extended definition of the transforms which yields $F(\omega)$ whenever that integral exists, and also gives a meaningful answer for some other cases of physical interest.

If for t tending towards infinity, $f(t)$ remains finite or tends to infinity at a rate less rapid than e^{bt}, then $\int_0^\infty |f(t)e^{-\sigma t}|dt$ exists for all $\sigma>b$. Under these conditions the transforms (1.16) and (1.20) can be considered for the function $g(t)=f(t)e^{-\sigma t}$, where $g(t)$ is the modified function and $f(t)$ is the function of actual interest. Applying the unilateral Fourier transform

$$g(t)=f(t)e^{-\sigma t}=\frac{1}{2\pi}\int_{-\infty}^{\infty}G(\omega)e^{j\omega t}d\omega$$

$$g(t)e^{\sigma t}=f(t)=\frac{1}{2\pi}\int_{-\infty}^{\infty}G(\omega)e^{(\sigma+j\omega)t}d\omega$$

$$G(\omega)=\int_{-\infty}^{\infty}g(t)e^{-j\omega t}dt=\int_{0}^{\infty}f(t)e^{-(\sigma+j\omega)t}dt.$$

In these equations let $s=\sigma+j\omega$ and $ds=j\,d\omega$. Since s is a function of ω, $G(\omega)$ can be replaced by $F(s)$.

$$f(t)=\frac{1}{2\pi j}\int_{\sigma-j\infty}^{\sigma+j\infty}F(s)e^{st}ds \qquad (1.21)$$

$$F(s)=\int_{0}^{\infty}f(t)e^{-st}dt. \qquad (1.22)$$

Equations (1.21) and (1.22) are the Laplace transform pair. The function $F(s)$ is known as the Laplace transform of $f(t)$, and the integral for $f(t)$ is known as the complex inversion integral:

$$F(s)=\mathcal{L}[f(t)] \qquad (1.23)$$

$$f(t)=\mathcal{L}^{-1}[F(s)]. \qquad (1.24)$$

The Laplace transform, therefore, is a special case of the unilateral Fourier transform, expressed symbolically as

$$\mathcal{L}[f(t)]=\mathfrak{F}[f(t)e^{-\sigma t}].$$

That is, the Laplace transform is identical with the unilateral Fourier transform of the same function multiplied by a convergence factor. Applications of both of these transforms are discussed in chapters 2 and 3.

5. References

[1] J. S. Hernandez, Introduction to Transducers for Instrumentation, Stratham Instruments, Inc. (Los Angeles, Calif.).

[2] P. A. Borden and W. J. Mayo-Wells, Telemetering Systems, Reinhold Publ. Corp. (New York, 1959).

[3] K. S. Lion, Instrumentation in Scientific Research—Electrical Input Transducers, McGraw-Hill Book Co., Inc. (New York, N.Y., 1959).

[4] H. C. Roberts, Mechanical Measurements by Electrical Methods, Instruments Publ. Co., Inc. (Pittsburgh, Pa., 1951).

[5] G. Landwehr and K. F. Zobel, A new device for measuring quickly changing high pressure (in German), Z. Instrumentenk. **65,** No. 11, 220 (1957).

[6] N. O. Myklestad, Fundamentals of Vibration Analysis, McGraw-Hill Book Co., Inc. (New York, N.Y., 1956).

[7] D. K. Cheng, Analysis of Linear Systems, Addison-Wesley Publ. Co., Inc. (Reading, Mass., 1959).

[8] Ralph A. Bowersox, Calibration of high-frequency-response pressure transducers, ISA J. **5,** 98 (1958).

[9] C. R. Tallman, Transducer frequency response evaluation for rocket instability research, ARS J. **29,** 119–122 (1959).

[10] A. W. Melville, Hydraulic oscillator for the dynamic calibration of pressure recording systems, J. Sci. Instr. **36,** 422 (1959).

[11] T. von Karman and M. A. Biot, Mathematical Methods in Engineering, p. 335, McGraw-Hill Book Co., Inc. (New York, N.Y., 1940).

[12] E. Weber, Linear Transient Analysis, Vol. 1, John Wiley & Sons, Inc. (New York, 1954).

[13] L. A. Pipes, Applied Mathematics for Engineers and Physicists, McGraw-Hill Book Co., Inc. (New York, N.Y., 1958).

[14] C. R. Wylie, Jr., Advanced Engineering Mathematics, McGraw-Hill Book Co., Inc. (New York, N.Y., 1951).

[15] R. V. Churchill, Operational Mathematics, McGraw-Hill Book Co., Inc. (New York, N.Y., 1958).

[16] M. F. Gardner and J. L. Barnes, Transients in Linear Systems, John Wiley & Sons, Inc. (New York, N.Y., 1942).

2. Analytic Methods for Linear Transducers

L. C. Eichberger [1]

In this chapter the reader is introduced to the procedural steps of analytical analysis. These steps are applied to a linear transducer which, for simplicity, is assumed to be a single-degree-of-freedom system represented by the mechanical model shown in figure 1.7a. The characteristic differential equation of motion for this system is given by eq (1.1). Response functions for the system are obtained for a given input function by both the classical and the operational methods of analysis. The periodic (sine, square wave, and rectangular pulse) and aperiodic (rectangular pulse and step) functions are the input functions considered. These functions represent the idealized inputs used in experimental dynamic calibration, as discussed in the later chapters of this work.

1. Input, Output, and Transfer Function Relations

1.1. Direct Input-Output Relation in the Time Domain

It is assumed that the characteristic differential equation of motion for the transducer is known, and that the input function f (periodic or aperiodic) can be expressed analytically as a function of time, $f(t)$. Then the general solution, or response function, $x(t)$, of the differential equation of motion can be obtained through the application of the classical method of analysis. The response function consists of a complementary function or transient solution, and a particular integral or steady-state solution. This operation is illustrated systematically in figure 2.1 by the path ABC in the time domain. The differential equation in this operation acts as a transfer function.

In the actual calculation of a response function as indicated above, it will be found that the classical method of analysis is more adaptable to the periodic class of input functions than the aperiodic class. Most periodic functions encountered in transducer analysis will satisfy the Dirichlet conditions [1] [2] and, therefore, can be approximated by a Fourier series. Standard solutions are readily available for the sine and cosine terms contained in the series, and by the principle of superposition the particular integral is readily obtained.

Aperiodic functions are readily treated by the Laplace transformation. This method transforms a given function in the time domain to one in the domain of the complex variable $s=\sigma+j\omega$, where ω is a real frequency. When an aperiodic input function and the associated differential equation are known analytically, then the entire equation is transformed to the frequency domain as an algebraic equation. The Laplace transform of the solution is obtained from this equation and the inverse transform of this expression yields the required response function.

On the other hand, if the response function has been expressed analytically and the characteristic differential equation of motion is known, the input function can in theory be determined by substituting the response function into the differential equation. In fact, only the particular integral part of the response function need be used, since

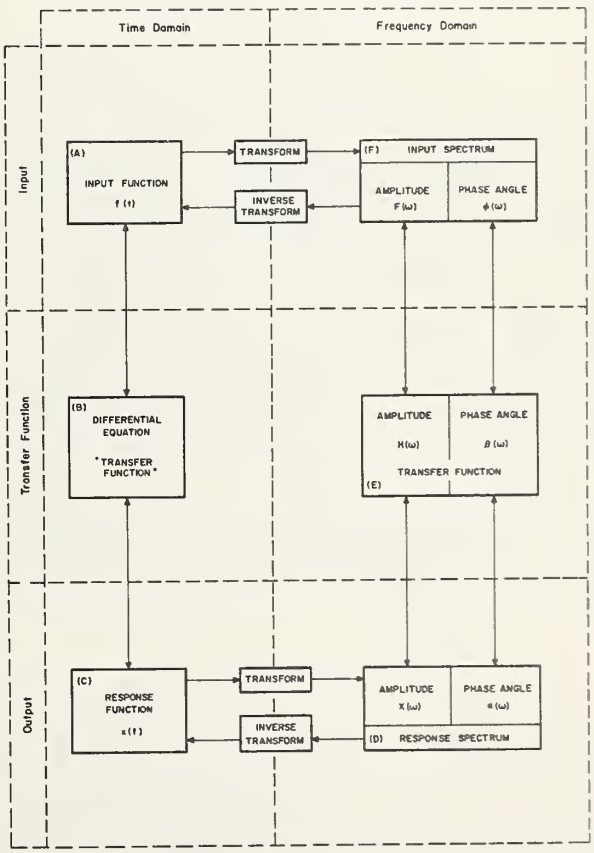

FIGURE 2.1. *Routes of analysis.*

[1] Assistant Professor of Mechanical Engineering, The University of Houston; Technical Staff, Houston Engineering Research Corporation.
[2] Figures in brackets indicate the literature references on p. 28.

the complementary function is the solution of the homogeneous part of the differential equation, i.e., when $f(t)$ is zero. This operation is illustrated in figure 2.1 by the path CBA.

1.2. Transformation From Time to Frequency Domain

With reference to figure 2.1, both the input function, $f(t)$, and the response function, $x(t)$, can be transformed from the time to frequency domain, respectively indicated by the paths from A to F and C to D. The transformed input function and response function are denoted as the input and response spectrum, respectively. Both spectra consist of two distinct parts, an amplitude and a phase angle. The input and response functions are related by a transfer function which also consists of an amplitude and a phase angle.

If the input function is periodic and satisfies the Dirichlet conditions, then it can be represented by a Fourier series. When the Fourier series is expressed in the form shown in eq (1.9), the amplitude $F(\omega)$ and the phase angle $\varphi(\omega)$ are given by the combined Fourier coefficient c_n and the phase angle φ_n, respectively.

The response of a linear system to a periodic input function is also periodic, and therefore can be represented by a Fourier series similar in form to that shown in eq (1.9), or

$$x(t)=X_0+\sum_{n=1}^{\infty} X_n \cos(n\omega t-\alpha_n).$$

The amplitude $X(\omega)$ of the response spectrum is given by X_n and its phase angle $\alpha(\omega)$ by α_n.

If the input function $f(t)$ is periodic or aperiodic and expressed analytically, then the input spectrum can be obtained directly from the Laplace transform providing that $f(t)=0$ for $t<0$ and the integral $\int_0^{\infty} |f(t)e^{-\sigma t}|dt$ exists. Since the Laplace transform of the input function is a complex number in the frequency domain, it provides both the amplitude and phase angle of the input spectrum. Likewise, the Laplace transform of the response function provides both the amplitude and the phase angle of the response spectrum.

It should be noted that the phase angles are an essential part of the frequency domain description for both periodic and aperiodic functions. In the time domain, any delay of an aperiodic function is described by the shift factor, e.g., $U(t-T_p)$, p. 22.

1.3. Transfer Function

The transfer function plays an important role in the analysis of a linear transducer. It allows the characteristics of the transducer to be described in the absence of the characteristic differential equation of motion. The transfer function is determined from the analytical expressions of the input and response spectrum. This requires that an accurate record of the response function for a known input function be made available, so that the response function can be expressed analytically by the methods given in chapter 3. Such a procedure for obtaining a response record for a known input function is included in the dynamic calibration of a transducer.

The transfer function is described by two separate characteristics, figure 2.1, which are defined as follows: the amplitude of the transfer function

$$H(\omega)=X(\omega)/F(\omega) \tag{2.1}$$

where $X(\omega)$ and $F(\omega)$ represent the amplitudes of the response and input spectra respectively, and the phase-angle of the transfer function

$$\beta(\omega)=\alpha(\omega)-\varphi(\omega), \tag{2.2}$$

where, respectively, $\alpha(\omega)$ and $\varphi(\omega)$ are the phase angles of the response and input spectra.

Among aperiodic functions, the pulse of infinitely short duration, but of unit area, has particular significance. The Laplace transform of the response to this input is the transfer function itself.

1.4. Input From Transfer Function and Response Record

If the transfer function for a transducer is known analytically, and a response record from the transducer for an unknown input is also known, then it is possible to determine an expression for the input function by operational methods. The stepwise procedure is described below:

(a) Express the response record as a function of time, $x(t)$.

(b) For a periodic function evaluate the amplitude and the phase-angle characteristics of the response spectrum by the Fourier series. For an aperiodic function, take the Laplace transform of the response function, which is the frequency response characteristic in amplitude and phase-angle. This is step C to D, figure 2.1.

(c) Evaluate the input spectrum by eqs (2.1) and (2.2). The amplitude and phase-angle transfer functions are known for the transducer, and the response spectrum was obtained in step (b). This step is represented by path DEF in figure 2.1.

(d) Finally, obtain the input function either by the Fourier series representation, i.e., by matching c_n and φ_n in eq (1.9), for periodic functions; or by the inverse Laplace transform for either periodic or aperiodic functions. This operation is illustrated in figure 2.1 by step F to A.

1.5. Phase-Plane Analysis

In the course of studying dynamical expressions which are invariant under canonical transformations, Poincaré [2, 3] used the concept of a phase space, a Cartesian space formed of coordinates q_i and p_i $(i=1, 2, \ldots n)$ in which the complete dynamical specification of a mechanical system is given by a point. Other investigators have

since used the phase plane (a two-dimensional phase space) to study the behavior of linear and nonlinear, damped and undamped dynamical systems. The most notable among the early papers on the graphical phase-plane method for the determination of transient response are, perhaps, those due to Lamoen [4, 5]. More recently the graphical phase-plane method was apparently rediscovered independently by Fuchs [6], Braun [7], and Rojansky [8]. Bishop [9] has published a comprehensive survey and Andronow and Chaikin [10], Minorsky [11], and Kryloff and Bogoliuboff [12] have included lengthy discussions of phase-plane techniques in their books on nonlinear mechanics.

In addition, Truxal [13] and Murphy [14] have shown the application of the phase-plane method to the analysis of servomechanisms, particularly those characterized by nonlinear behavior. Jacobsen and Ayre [15] use the method extensively in their recent book on vibrations. The current literature includes numerous applications to specific problems in the fields of dynamics, the design of the circuits in electronic instruments and servomechanisms, and transducer systems. These include contributions by Klotter [16, 17], Magnus [18], Gibson [19], Cosgriff [20], Bass [21], Ergin [22], Stout [23], Jacobsen [24], and Liu [25].

2. Periodic Input Functions

In this section, known periodic input functions are imposed on a hypothetical transducer for the purpose of illustrating the analytical methods of analysis presented in the previous section. The order of presentation is preserved and, for simplicity, a single-degree-of-freedom transducer is chosen for analysis. The mechanical model for this transducer is shown in figure 1.7a and its characteristic differential equation is given by eq (1.1). The inputs imposed on the transducer are the sine, square wave, and rectangular pulse functions. The analysis for the sine function is presented in detail, whereas only the results and pertinent details are given for the square wave and rectangular pulse function.

2.1. Sine Function

a. Direct Input-Output Relation in the Time Domain

The sine input function is shown in figure 2.2a,

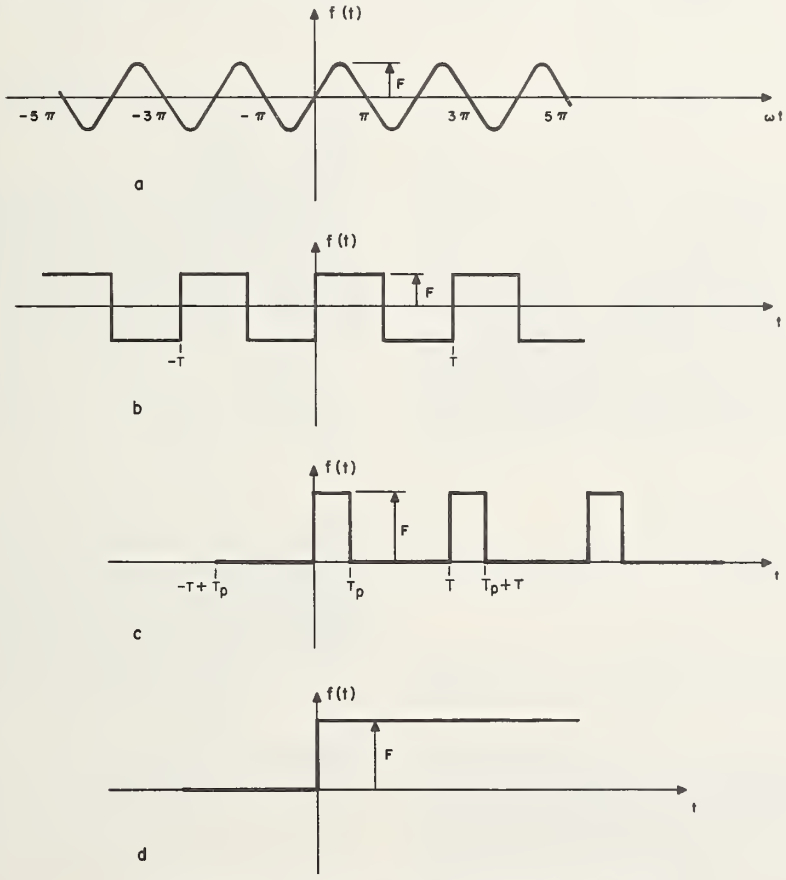

FIGURE 2.2. *Periodic and aperiodic input functions.*

(a) Sine function
(b) Square wave function
(c) Rectangular pulse train
(d) Step function

and is expressed by

$$f(t)=F \sin \omega t \tag{2.3}$$

where ω is the circular frequency in radians per unit time.

The characteristic differential equation of motion for a single-degree-of-freedom transducer, eq (1.1), becomes

$$m\ddot{x}+c\dot{x}+kx=F \sin \omega t. \tag{2.4}$$

The transient solution (complementary function) is obtained from the homogenous part of this equation, i.e.,

$$m\ddot{x}+c\dot{x}+kx=0. \tag{2.5}$$

The standard solution to a differential equation of this type is

$$x_t=C_1e^{r_1t}+C_2e^{r_2t} \tag{2.6}$$

where C_1 and C_2 are arbitrary constants and r_1 and r_2 are the two roots of the auxiliary equation

$$mr^2+cr+k=0. \tag{2.7}$$

Solution of eq (2.7) gives two roots

$$r_1=-c/2m+\sqrt{c^2/4m^2-k/m} \tag{2.8}$$

$$r_2=-c/2m-\sqrt{c^2/4m^2-k/m}. \tag{2.9}$$

Since m, c, and k are always positive, the type of root obtained is dependent upon the evaluation of the radical. If the radical in eqs (2.8) and (2.9) is positive, the motion given by eq (2.6) is of a gradually subsiding nature. If the radical is negative, the roots are complex numbers and the motion given by eq (2.6) is of a fluctuating nature. The limiting case is when the radical is equal to zero, for which $c^2=4km$. This value of c is called the critical damping c_c and is given by

$$c_c=2\sqrt{km}=2m\omega_n \tag{2.10}$$

where $\omega_n=\sqrt{k/m}$ is the natural circular frequency. The dimensionless ratio c/c_c is called the relative damping ratio ζ and is given by

$$\zeta=\frac{c}{c_c}=\frac{c}{2\sqrt{km}}=\frac{c}{2m\omega_n}. \tag{2.11}$$

When $\zeta>1$, the damping is called supercritical, and when $\zeta<1$, the damping is called subcritical. Since for practical transducers $\zeta<1$, it is more convenient to write eqs (2.8) and (2.9) in the form

$$r_1=-\zeta\omega_n+j\omega_n\sqrt{1-\zeta^2}$$

$$r_2=-\zeta\omega_n-j\omega_n\sqrt{1-\zeta^2}.$$

Then, eq (2.6) becomes for $\zeta<1$

$$x_t=e^{-\zeta\omega_nt}\left\{C_1e^{j\sqrt{1-\zeta^2}\omega_nt}+C_2e^{-j\sqrt{1-\zeta^2}\omega_nt}\right\}. \tag{2.12}$$

By introducing new arbitrary constants A and B, defined by

$$C_1=A/2+B/2j$$

$$C_2=A/2-B/2j,$$

and, using the exponential equivalents for the sine and cosine functions

$$\sin x=\frac{e^{jx}-e^{-jx}}{2j}$$

$$\cos x=\frac{e^{jx}+e^{-jx}}{2},$$

eq (2.12) becomes

$$x_t=e^{-\zeta\omega_nt}\{A \cos\sqrt{1-\zeta^2}\omega_nt+B \sin\sqrt{1-\zeta^2}\omega_nt\}, \quad (\zeta<1)$$

which may be written more conveniently in the form

$$x_t=X_0e^{-\zeta\omega_nt} \cos\{\sqrt{1-\zeta^2}\omega_nt-\varphi_0\} \quad (\zeta<1). \tag{2.13}$$

The constants X_0 and φ_0 can be evaluated at the initial conditions.

The steady-state solution (particular integral) is obtained by using the complete differential eq (2.4). For input functions which can be expressed in terms of sine and cosine functions, the steady-state solution is taken to be of the form

$$x_s=C \sin \omega t+D \cos \omega t, \tag{2.14}$$

where C and D are arbitrary constants. Successive differentiation of eq (2.14) gives

$$\dot{x}_s=C\omega \cos \omega t-D\omega \sin \omega t \tag{2.15}$$

$$\ddot{x}_s=-C\omega^2 \sin \omega t-D\omega^2 \cos \omega t. \tag{2.16}$$

Substituting eqs (2.14), (2.15), and (2.16) into eq (2.4) and collecting like terms yields

$$(k-m\omega^2)C \sin \omega t+(k-m\omega^2)D \cos \omega t$$
$$-c\omega D \sin \omega t+c\omega C \cos \omega t=F \sin \omega t. \tag{2.17}$$

Equating coefficients of like terms in eq (2.17) gives

$$(k-m\omega^2)C-c\omega D=F \tag{2.18}$$

$$c\omega C+(k-m\omega^2)D=0. \tag{2.19}$$

Solving eqs (2.18) and (2.19) simultaneously

yields

$$C=\frac{(k-m\omega^2)F}{(k-m\omega^2)^2+c^2\omega^2}$$

$$D=-\frac{c\omega F}{(k-m\omega^2)^2+c^2\omega^2},$$

and eq (2.14) becomes

$$x_s=\frac{F}{(k-m\omega^2)^2+c^2\omega^2}[(k-m\omega^2)\sin\omega t-c\omega\cos\omega t].$$

After normalizing the bracketed expression to give sin α and cos α, this may be written more conveniently in the form

$$x_s=X\cos(\omega t-\alpha) \tag{2.20}$$

where

$$X=\frac{F}{\sqrt{(k-m\omega^2)^2+c^2\omega^2}} \tag{2.21}$$

and

$$\alpha=\arctan\left(\frac{k-m\omega^2}{-c\omega}\right). \tag{2.22}$$

Therefore, the required response function (general solution) is given by

$$x=x_t+x_s$$

or

$$x=X_0e^{-\zeta\omega_n t}\cos(\sqrt{1-\zeta^2}\omega_n t-\varphi_0)+X\cos(\omega t-\alpha) \tag{2.23}$$

where X_0 and φ_0 are constants of integration which can be evaluated at the initial conditions; and X and α are given by eqs (2.21) and (2.22).

To obtain the input function when the characteristic differential equation of motion and the response function are known analytically, substitute the steady-state solution, eq (2.20), into the original differential equation of motion, eq (1.1), and solve for $f(t)$.

b. Transformation From Time to Frequency Domain

The transformation of the input and response functions from the time to the frequency domain requires that these functions be expressed as functions of time. Let us find the spectrum for the input function $F\sin\omega t$. Since this is a periodic function of time, it can be represented by a Fourier series of the form given in eq (1.9), i.e.

$$F\sin\omega t=c_1\cos(\omega t-\varphi_1). \tag{2.24}$$

Expanding the right hand side of eq (2.24) by the function for the sum of angles yields

$$F\sin\omega t=c_1\cos\omega t\cos\varphi_1+c_1\sin\omega t\sin\varphi_1,$$

and the equation is satisfied if $c_1=F$ and $\varphi_1=\pi/2$. Therefore, the input spectrum for $F\sin\omega t$ is

$$F(\omega)=c_n=F \tag{2.25}$$

and

$$\varphi(\omega)=\varphi_n=\pi/2 \tag{2.26}$$

where $F(\omega)$ and $\varphi(\omega)$ are the amplitude and phase angle of the input spectrum, respectively, and we see that both are constant for any value of ω.

The spectrum for the response function given by eq (2.23) is evaluated by the same procedure used for the input spectrum. However, to evaluate the response spectrum, only the steady-state solution of the response function need be considered. The steady-state solution of eq (2.23) is a periodic function of time and has a Fourier series representation of the form given in eq (1.9). Therefore,

$$X\cos(\omega t-\alpha)=c_1\cos(\omega t-\varphi_1).$$

By inspection $X=c_1$ and $\alpha=\varphi_1$. Then, the response spectrum is

$$X(\omega)=c_n=X,$$

and

$$\alpha(\omega)=\varphi_n=\alpha$$

where X and α are given by eqs (2.21) and (2.22) respectively. Therefore the amplitude of the response function becomes

$$X(\omega)=\frac{F}{\sqrt{(k-m\omega^2)^2+c^2\omega^2}} \tag{2.27}$$

and the phase angle

$$\alpha(\omega)=\arctan\left(\frac{k-m\omega^2}{-c\omega}\right). \tag{2.28}$$

c. Transfer Function

The transfer function defined by eqs (2.1) and (2.2) is obtained from the input and response spectra. Making use of the input spectra of eqs (2.25) and (2.26), and the response spectra of eqs (2.27) and (2.28), eqs (2.1) and (2.2) become

$$H(\omega)=\frac{1}{\sqrt{(k-m\omega^2)^2+c^2\omega^2}} \tag{2.29}$$

and

$$\beta(\omega)=\arctan\left(\frac{k-m\omega^2}{-c\omega}\right)-\pi/2 \tag{2.30}$$

where $H(\omega)$ and $\beta(\omega)$, respectively, are the amplitude and phase-angle of the transfer function.

d. Input From Transfer Function and Response Record

Determining an expression for the input function when the transfer function and the response record are known requires that the response record be expressible as a function of time. From the previous results the spectrum for the response function, eq (2.23), is given by eqs (2.27) and (2.28).

The transfer function is given by eqs (2.29) and (2.30). Equations (2.1) and (2.2) yield

$$F(\omega)=X(\omega)/H(\omega)=F=c_1$$

and

$$\varphi(\omega)=\alpha(\omega)-\beta(\omega)=\pi/2=\varphi_1.$$

Since a periodic response must be the result of a periodic input, the input function can be represented by a Fourier series of the form of eq (1.9),

$$f(t)=c_1 \cos(\omega t-\varphi_1)$$

where

$$\cos(\omega t-\varphi_1)=\cos(\omega t-\pi/2)=\sin \omega t.$$

Therefore

$$f(t)=F \sin \omega t.$$

This agrees with eq (2.3).

2.2. Square Wave Function

The square wave function, shown in figure 2.2b, is represented in the time domain for one complete period by

$$f(t)=-F \text{ for } -T/2<t<0 \qquad (2.31)$$

$$f(t)=F \text{ for } 0<t<T/2. \qquad (2.32)$$

The given square wave, being periodic and piecewise continuous, can be approximated by a Fourier series. Since the waveform is an odd function of t, no cosine terms can be present in the series, i.e., a_n in eq (1.6) must be zero. Therefore, it is only necessary to evaluate b_n, the Fourier coefficient of $\sin n\omega t$. By eq (1.8)

$$b_n=2/T\int_{-T/2}^{0}(-F)\sin n\omega t\,dt$$

$$+2/T\int_{0}^{T/2}F\sin n\omega t\,dt=\frac{4F}{n\omega T}\{1-\cos n\omega T/2\}.$$

Hence, the Fourier series representation for the square wave function described by eqs (2.31) and (2.32) is

$$f(t)=\frac{4F}{\omega T}\sum_{n=1}^{\infty}\frac{1}{n}\left(1-\cos\frac{n\omega T}{2}\right)\sin n\omega t. \qquad (2.33)$$

The circular frequency ω is equal to $2\pi/T$ and $\cos n\pi=1$ for n even; therefore eq (2.33) becomes

$$f(t)=\frac{4F}{\pi}\sum\frac{1}{n}\sin n\omega t, \text{ for } n \text{ odd}. \qquad (2.34)$$

a. Direct Input-Output Relation in the Time Domain

Substituting the Fourier series representation for the square wave driving function, eq (2.34), the differential equation of motion, eq (1.1), becomes

$$m\ddot{x}+c\dot{x}+kx=\frac{4F}{\pi}\sum\frac{1}{n}\sin n\omega t, \text{ for } n \text{ odd}. \qquad (2.35)$$

The transient solution of eq (2.35) is identical to the solution of eq (2.5), and is given by eq (2.13). The steady-state solution is obtained by assuming the solution to take the form of

$$x_s=\sum(C_n \sin n\omega t+D_n \cos n\omega t). \qquad (2.36)$$

The procedure for evaluating the constants C_n and D_n is the same as that presented in section 2.1 for the sine function. This procedure yields

$$C_n=\frac{4F(k-n^2m\omega^2)}{n\pi[(k-n^2m\omega^2)^2+n^2c^2\omega^2]}, \text{ for } n \text{ odd};$$

$$D_n=-\frac{4Fnc\omega}{n\pi[(k-n^2m\omega^2)^2+n^2c^2\omega^2]}, \text{ for } n \text{ odd}.$$

Therefore, eq (2.36) becomes

$$x_s=\frac{4F}{\pi}\sum\frac{1}{n[(k-n^2m\omega^2)^2+n^2c^2\omega^2]}[(k-n^2m\omega^2)\sin n\omega t$$

$$-nc\omega\cos n\omega t], \text{ for } n \text{ odd},$$

which may be written more conveniently in the form

$$x_s=\sum X_n \cos(r\omega t-\alpha_n), \text{ for } n \text{ odd} \qquad (2.37)$$

where

$$X_n=\frac{4F}{n\pi\sqrt{(k-n^2m\omega^2)^2+n^2c^2\omega^2}} \qquad (2.38)$$

and

$$\alpha_n=\arctan\left(\frac{k-n^2m\omega^2}{-nc\omega}\right). \qquad (2.39)$$

Therefore, the response function of eq (2.35) is

$$x=X_0e^{-\zeta\omega_n t}\cos(\sqrt{1-\zeta^2}\,\omega_n t-\varphi_0)$$

$$+\sum X_n \cos(n\omega t-\alpha_n), \text{ for } n \text{ odd}. \qquad (2.40)$$

The constants X_0 and φ_0 are evaluated from a set of initial conditions, and X_n and α_n are given by eqs (2.38) and (2.39) respectively.

To obtain the input function when the characteristic differential equation of motion and the response function are known analytically, substitute the steady-state solution of eq (2.40) into the original differential equation of motion, eq (1.1), and solve for $f(t)$.

b. Transformation From Time to Frequency Domain

As shown for the sine function, section 2.1, the input spectrum of a periodic function is obtained directly when c_n and φ_n of eq (1.9) are known for the input function. Therefore, rewriting eq (2.34)

with $\omega=2\pi/T$ and $\sin n\omega t=\cos(n\omega t-\pi/2)$ yields

$$f(t)=\sum \frac{8F}{n\omega T}\cos\left(n\omega t-\frac{\pi}{2}\right), \text{ for } n \text{ odd.} \quad (2.41)$$

Comparing eq (2.41) to eq (1.9), shows that

$$\frac{8F}{n\omega T}=c_n, \text{ for } n \text{ odd}$$

and

$$\frac{\pi}{2}=\varphi_n.$$

Therefore, the amplitude of the input spectrum is

$$F(\omega)=c_n=\frac{8F}{n\omega T}, \text{ for } n \text{ odd} \quad (2.42)$$

and the phase angle is

$$\varphi(\omega)=\varphi_n=\frac{\pi}{2}. \quad (2.43)$$

Similarly, the response spectrum can be evaluated when c_n and φ_n of eq (1.9) are known for the response function. These quantities are readily obtained by equating eq (2.37) to eq (1.9), where by inspection

$$X_n=c_n$$

and

$$\alpha_n=\varphi_n.$$

Therefore, the amplitude of the response spectrum is given by eq (2.38) with $\omega=2\pi/T$, or

$$X(\omega)=c_n=\frac{8F}{n\omega T\sqrt{(k-n^2m\omega^2)^2+n^2c^2\omega^2}}, \text{ for } n \text{ odd} \quad (2.44)$$

and the phase angle of the response spectrum is given by eq (2.39), or

$$\alpha(\omega)=\varphi_n=\arctan\left(\frac{k-n^2m\omega^2}{-nc\omega}\right), \text{ for } n \text{ odd.} \quad (2.45)$$

c. Transfer Function

The amplitude of the transfer function $H(\omega)$ is obtained by substituting the amplitude of the input spectrum $F(\omega)$ and the response spectrum $X(\omega)$ into eq (2.1). These quantities are given, respectively, by eqs (2.42) and (2.44). Therefore, the amplitude transfer function, eq (2.1), becomes

$$H(\omega)=1/\sqrt{(k-n^2m\omega^2)^2+n^2c^2\omega^2}, \text{ for } n \text{ odd.} \quad (2.46)$$

The phase angle of the transfer function $\beta(\omega)$ is defined by eq (2.2), where φ_n and α_n are given by eqs (2.43) and (2.45), respectively. Therefore, eq (2.2) becomes

$$\beta(\omega)=\arctan\left(\frac{k-n^2m\omega^2}{-n\omega c}\right)-\frac{\pi}{2}, \text{ with } n \text{ odd.} \quad (2.47)$$

d. Input From Transfer Function and Response Record

The input function can be described by a thorough knowledge of the input spectrum. The input spectrum is obtainable from eqs (2.1) and (2.2). Using the response spectrum described by eqs (2.44) and (2.45), and the transfer function given by eqs (2.46) and (2.47), the amplitude of the input spectrum is

$$F(\omega)=\frac{8F}{n\omega T}, \text{ for } n \text{ odd}$$

and the phase angle of the input spectrum is

$$\varphi(\omega)=\pi/2.$$

Therefore, since a periodic response is the result of a periodic input, the input function can be represented by a Fourier series of the form similar to that of eq (1.9), where

$$c_n=F(\omega)$$

and

$$\varphi_n=\varphi(\omega).$$

The input function then becomes

$$f(t)=\sum \frac{8F}{n\omega T}\cos(n\omega t-\pi/2), \text{ for } n \text{ odd}$$

or

$$f(t)=\frac{4F}{\pi}\sum \frac{1}{n}\sin n\omega t, \text{ for } n \text{ odd}$$

which agrees with eq (2.34).

2.3. Rectangular Pulse Train

The train of rectangular pulses to be analyzed is shown in figure 2.2c, with period T taken to lie between $-T/2$ and $T/2$. Therefore, one complete period can be represented in the time domain by

$$f(t)=0 \text{ for } -T/2<t<0 \quad (2.48)$$
$$f(t)=F \text{ for } 0<t<T_p \quad (2.49)$$
$$f(t)=0 \text{ for } T_p<t<T/2. \quad (2.50)$$

The Fourier series representation for this pulse train is obtainable by the evaluation of a_n and b_n given by eqs (1.7) and (1.8), respectively. These equations yield

$$a_n=\frac{2F}{n\omega T}\sin n\omega T_p \quad (2.51)$$

and

$$b_n=\frac{2F}{n\omega T}(\cos n\omega T_p-1). \quad (2.52)$$

For $n=0$, eq (2.51) becomes indeterminate. However, application of l'Hospital's rule yields

$$a_0=\frac{2FT_p}{T}. \quad (2.53)$$

Therefore, the Fourier series, eq (1.6), for the period rectangular pulse train described by eqs (2.48), (2.49), and (2.50) yields

$$f(t)=\frac{FT_p}{T}+\frac{2F}{\omega T}\sum_{n=1}^{\infty}\left[\frac{1}{n}\sin n\omega T_p\cos n\omega t - \frac{1}{n}(\cos n\omega T_p-1)\sin n\omega t\right]$$

which may be written more conveniently in the form

$$f(t)=\frac{FT_p}{T}+\sum_{n=1}^{\infty}c_n\cos(n\omega t-\varphi_n) \tag{2.54}$$

where

$$c_n=\frac{2\sqrt{2}F}{n\omega T}\sqrt{1-\cos n\omega T_p} \tag{2.55}$$

and

$$\varphi_n=\arctan\left(\frac{1-\cos n\omega T_p}{\sin n\omega T_p}\right). \tag{2.56}$$

Note that the average value FT_p/T is really part of the spectrum, and may be viewed as an "amplitude" at zero frequency.

a. Direct Input-Output Relation in the Time Domain

The differential equation of motion, eq (1.1), for the given rectangular pulse train input is

$$m\ddot{x}+c\dot{x}+kx=FT_p/T+\sum_{n=1}^{\infty}c_n\cos(n\omega t-\varphi_n) \tag{2.57}$$

where c_n and φ_n are given by eqs (2.55) and (2.56), respectively.

The transient solution of eq (2.57) is given by eq (2.13). The steady-state solution consists of two distinct parts: (a) a constant term corresponding to zero frequency, and (b) an oscillatory term with $n\omega>0$. For convenience, the solution is broken down into two problems, each considered to be independent of the other. The first problem is the solution of

$$m\ddot{x}+c\dot{x}+kx=FT_p/T, \tag{2.58}$$

for which the solution is a constant, and by inspection is

$$x_s]_{\omega=0}=\frac{FT_p}{kT}. \tag{2.59}$$

The second problem is the solution of

$$m\ddot{x}+c\dot{x}+kx=\sum_{n=1}^{\infty}c_n\cos(n\omega t-\varphi_n), \tag{2.60}$$

where c_n and φ_n are given by eqs (2.55) and (2.56), respectively. Rewriting eq (2.60) more conveniently

$$m\ddot{x}+c\dot{x}+kx=\frac{2F}{\omega T}\sum_{n=1}^{\infty}\left[\frac{1}{n}\sin n\omega T_p\cos n\omega t - \frac{1}{n}(\cos n\omega T_p-1)\sin n\omega t\right]. \tag{2.61}$$

Here again assume the solution of eq (2.61) to take the form of eq (2.36). Applying the same procedure as presented in section 2.1 for the sine wave to evaluate C_n and D_n yields

$$C_n=\frac{2F[nc\omega\sin n\omega T_p-(k-n^2m\omega^2)(\cos n\omega T_p-1)]}{n\omega T[(k-n^2m\omega^2)^2+n^2c^2\omega^2]} \tag{2.62}$$

and

$$D_n=\frac{2F[(k-n^2m\omega^2)\sin n\omega T_p+nc\omega(\cos n\omega T_p-1)]}{n\omega T[(k-n^2m\omega^2)^2+n^2c^2\omega^2]}. \tag{2.63}$$

Therefore, eq (2.36) becomes

$$x_s]_{n\omega>0}=\frac{2F}{\omega T}\sum_{n=1}^{\infty}\frac{1}{n[(k-n^2m\omega^2)^2+n^2c^2\omega^2]}\{[nc\omega\sin n\omega T - (k-n^2m\omega^2)(\cos n\omega T_p-1)]\sin n\omega t + [(k-n^2m\omega^2)\sin n\omega T_p + nc\omega(\cos n\omega T_p-1)]\cos n\omega t\}.$$

This expression may be written more conveniently in the form

$$x_s]_{n\omega>0}=\sum_{n=1}^{\infty}X_n\cos(n\omega t-\alpha_n), \tag{2.64}$$

where

$$X_n=\frac{2\sqrt{2F}}{n\omega T}\sqrt{\frac{1-\cos n\omega T_p}{(k-n^2m\omega^2)^2+n^2c^2\omega^2}} \tag{2.65}$$

and

$$\alpha_n=\arctan\left(\frac{nc\omega\sin n\omega T_p-(k-n^2m\omega^2)(\cos n\omega T_p-1)}{(k-n^2m\omega^2)\sin n\omega T_p+nc\omega(\cos n\omega T_p-1)}\right). \tag{2.66}$$

By the principle of superposition, the steady solution for eq (2.61) is

$$x_s=x_s]_{\omega=0}+x_s]_{n\omega>0}$$

or

$$x_s=\frac{FT_p}{kT}+\sum_{n=1}^{\infty}X_n\cos(n\omega t-\alpha_n) \tag{2.67}$$

where X_n and α_n are given, respectively, by eqs (2.65) and (2.66). Therefore, the response function of eq (2.61) is

$$x=X_0e^{-\zeta\omega_n t}\cos(\sqrt{1-\zeta^2}\omega_n t-\varphi_0)+\frac{FT_p}{kT}+\sum_{n=1}^{\infty}X_n\cos(n\omega t-\alpha_n) \tag{2.68}$$

where X_0 and φ_0 are evaluated from the knowledge of initial conditions; and, X_n and α_n are given by eqs (2.65) and (2.66), respectively.

To obtain the input function when the characteristic differential equation of motion and response

function are known analytically, substitute the steady-state response given by eq (2.67) into the original differential equation of motion, eq (1.1), and solve for $f(t)$.

b. Transformation From Time to Frequency Domain

The input spectrum is completely described by eq (2.54). The amplitude of the input spectrum $F(\omega)$ is obtained by adding the constant amplitude FT_p/T to the oscillatory amplitude c_n as given by eq (2.55). The phase angle is equal to φ_n and is given by eq (2.56).

Similarly, the response spectrum is determined by eq (2.67). The amplitude of the response spectrum $X(\omega)$ is equal to FT_p/kT plus X_n, where X_n is given by eq (2.65); and the phase angle $\alpha(\omega)$ is equal to α_n and is given by eq (2.66).

c. Transfer Function

The transfer function for the system is given by eqs (2.1) and (2.2). Since the amplitudes of the input and response spectra both consist of a constant and oscillatory part, then the amplitude of the transfer function will also contain these same characteristics. The amplitude $H(\omega)$ of the transfer function is obtained by dividing the constant amplitude FT_p/kT and the oscillatory amplitude X_n of the response spectrum, eq (2.67), respectively, by FT_p/T and c_n of the input spectrum, eq (2.54). This may be stated in equation form as

$$H(\omega)=H(\omega)]_{\omega=0}+H(\omega)]_{n\omega>0}$$

or

$$H(\omega)=\frac{1}{k}+\frac{1}{\sqrt{(k-n^2m\omega^2)^2+n^2c^2\omega^2}}. \qquad (2.69)$$

The phase angle $\beta(\omega)$ of the transfer function is obtained by subtracting $\varphi(\omega)$, eq (2.56), from $\alpha(\omega)$, eq (2.66), as indicated by eq (2.2).

$$\beta(\omega)=\text{arc tan}\left(\frac{nc\omega \sin n\omega T_p-(k-n^2m\omega^2)(\cos n\omega T_p-1)}{(k-n^2m\omega^2)\sin n\omega T_p+nc\omega(\cos n\omega T_p-1)}\right)$$

$$-\text{arc tan}\left(\frac{1-\cos n\omega T_p}{\sin n\omega T_p}\right) \qquad (2.70)$$

d. Input From Transfer Function and Response Record

The input spectrum can be found from $F(\omega)=X(\omega)/H(\omega)$ and $\varphi(\omega)=\alpha(\omega)-\beta(\omega)$, eqs (2.1) and (2.2) respectively. Using a transfer function expressed by eqs (2.69) and (2.70), and a steady-state response characteristic expressed by eqs (2.67) and (2.66), these relations become, respectively,

$$F(\omega)=\frac{FT_p}{T}+\frac{2\sqrt{2F}}{n\omega T}\sqrt{1-\cos n\omega T_p} \qquad (2.71)$$

and

$$\varphi(\omega)=\text{arc tan}\left(\frac{1-\cos n\omega T_p}{\sin n\omega T_p}\right). \qquad (2.72)$$

Equations (2.71) and (2.72) are, respectively, the amplitude and phase angle of the input spectrum. Therefore, the input function can be represented by a Fourier series of the form of eq (1.9), since the response function is periodic. Hence

$$f(t)=\frac{FT_p}{T}+\sum_{n=1}^{\infty} c_n \cos(n\omega t-\varphi_n) \qquad (2.73)$$

where c_n and φ_n are given by eqs (2.71) and (2.72), respectively.

Equation (2.73) agrees with the original Fourier series representation of the periodic rectangular pulse train, eq (2.54). The constant term FT_p/T is readily obtained from a static calibration of the system.

3. Aperiodic Input Functions

In this section aperiodic input functions are treated in a manner similar to that given the periodic functions in the previous section. A single degree-of-freedom transducer which can be represented by the mechanical model shown in figure 1.7a and eq (1.1) is chosen for analysis. The inputs imposed on the transducer are the rectangular pulse and step functions. The analysis illustrates the analytical methods presented in section 1 of this chapter. For the rectangular pulse function the analysis is presented in detail. For the step function only the results and pertinent details are given.

3.1. Rectangular Pulse Function

a. Direct Input-Output Relation in the Time Domain

The aperiodic rectangular pulse function consists of a single phase such as the first pulse shown in figure 2.2c and is expressed as a function of time by

$$f(t)=0 \text{ for } t<0 \qquad (2.74)$$

$$f(t)=F \text{ for } 0<t<T_p \qquad (2.75)$$

$$f(t)=0 \text{ for } t>T_p. \qquad (2.76)$$

Aperiodic functions are not representable by a Fourier series and, therefore, are best treated by the Laplace transformation, eq (1.22), which represents time functions in terms of the complex variable $s=\sigma+j\omega$. Both the aperiodic input function and the characteristic differential equation of motion are transformed to the frequency domain.

The Laplace transform for the rectangular pulse function described by eqs (2.74), (2.75), and (2.76) is obtained by eq (1.22).

$$F(s)=\int_0^\infty f(t)e^{-st}dt$$

$$F(s)=-\frac{1}{s}\int_0^{T_p} Fe^{-st}dt=-\frac{F}{s}\,(e^{-sT_p}-1). \quad (2.77)$$

Equation (2.77) represents the Laplace transform of the rectangular pulse function which is often written in the form

$$\mathcal{L}[f(t)]=\frac{F}{s}\,(1-e^{-sT_p}). \quad (2.78)$$

The characteristic differential equation of motion for the sytem under analysis is given by eq (1.1), and is

$$m\ddot{x}+c\dot{x}+kx=f(t)$$

where m, c, and k are constants. Applying the Laplace transformation to both sides of this equation yields

$$\mathcal{L}[m\ddot{x}+c\dot{x}+kx]=\mathcal{L}[f(t)]. \quad (2.79)$$

Equation (2.79) can be rewritten if we recognize that the Laplace transform of the sum of two functions is equal to the sum of the transforms of the individual functions, and that the Laplace transform of a constant times a function is the constant times the transform of the function [26, p. 161].

$$m\mathcal{L}[\ddot{x}]+c\mathcal{L}[\dot{x}]+k\mathcal{L}[x]=\mathcal{L}[f(t)].$$

Applying the differentiation theorem [27, p. 175] and substituting eq (2.78) into the equation yields

$$m\{s^2\mathcal{L}[x]-sx(0^+)-\dot{x}(0^+)\}+c\{s\mathcal{L}[x]-x(0^+)\}$$
$$+k\mathcal{L}[x]=\frac{F}{s}\,(1-e^{-sT_p}). \quad (2.80)$$

The initial displacement of the sensing element of the transducer is usually zero. However, if not zero, it will have a constant displacement which can be eliminated for the purpose of analysis by a shift in the coordinate system. The initial velocity of the sensing element is likewise usually zero. In this case, $x(0^+)=\dot{x}(0^+)=0$, and eq (2.80) becomes

$$ms^2\mathcal{L}[x]+cs\mathcal{L}[x]+k\mathcal{L}[x]=\frac{F}{s}\,(1-e^{-sT_p}). \quad (2.81)$$

Solving eq (2.81) for $\mathcal{L}[x]$,

$$\mathcal{L}[x]=\frac{F(1-e^{-sT_p})}{s(ms^2+cs+k)}. \quad (2.82)$$

The desired solution to the characteristic differential equation of motion is obtained by taking the inverse transform of eq (2.82), i.e.,

$$x=\mathcal{L}^{-1}\mathcal{L}[x]=\mathcal{L}^{-1}\left[\frac{F(1-e^{-sT_p})}{s(ms^2+cs+k)}\right]. \quad (2.83)$$

The inverse transform of most linear systems is determined by expanding into partial fractions the function upon which $\mathcal{L}^{-1}$ operates. The method of partial fractions enables us to utilize tables of Laplace transform pairs already evaluated for our convenience. Therefore, for the purpose of applying the method of partial fractions, eq (2.83) may be written more conveniently in the form

$$x=\frac{F}{m}\,\mathcal{L}^{-1}\left[\frac{1}{s\left(s^2+\frac{c}{m}s+\frac{k}{m}\right)}-\frac{e^{-sT_p}}{s\left(s^2+\frac{c}{m}s+\frac{k}{m}\right)}\right]. \quad (2.84)$$

The form of the partial fraction best suited to handle the two functions enclosed by the brackets in eq (2.84) is given by

$$\frac{A(s)}{B(s)}=\frac{1}{b}\left[\frac{K_1}{s-s_1}+\frac{K_2}{s-s_2}+\ldots+\frac{K_k}{s-s_k}+\ldots+\frac{K_n}{s-s_n}\right], \quad (2.85)$$

which is restricted to functions that are rational algebraic fractions with denominators of a higher degree than the numerators. In eq (2.85), b is a constant, and $s_1, s_2, \ldots, s_k, \ldots, s_n$ are the roots of $B(s)=0$. Equation (2.85) applies when the roots of $B(s)=0$ are all distinct, i.e., no two roots are equal. The numerators of the partial fractions, $K_1, K_2, \ldots, K_k, \ldots K_n$ are determined by

$$K_k=b\left\{(s-s_k)\frac{A(s)}{B(s)}\right\}_{s\to s_k}. \quad (2.86)$$

Therefore, the partial fraction for the first term enclosed by the brackets in eq (2.84) is obtained as follows by inspection:

$$A(s)=1$$

$$B(s)=s\left(s^2+\frac{c}{m}s+\frac{k}{m}\right).$$

The roots of $B(s)=0$ are

$$s_1=0 \quad (2.87)$$

$$s_2=-\frac{c}{2m}+\sqrt{\frac{c^2}{4m^2}-\frac{k}{m}} \quad (2.88)$$

$$s_3=-\frac{c}{2m}-\sqrt{\frac{c^2}{4m^2}-\frac{k}{m}}. \quad (2.89)$$

The roots defined by eqs (2.88) and (2.89) are identical to the roots r_1 and r_2 defined by eqs (2.8) and (2.9), respectively. Therefore, eqs (2.88)

and (2.89) may be written in the same form as r_1 and r_2:

$$s_2=-\zeta\omega_n+j\omega_n\sqrt{1-\zeta^2} \qquad (2.90)$$

$$s_3=-\zeta\omega_n-j\omega_n\sqrt{1-\zeta^2}. \qquad (2.91)$$

Once the roots of $B(s)=0$ are established, the numerator of the partial fractions can be evaluated by eq (2.86). Therefore, for $k=1$ eq (2.86) becomes:

$$K_1=b\left[\frac{s}{s\left(s^2+\frac{c}{m}s+\frac{k}{m}\right)}\right]_{s\to 0} =b\left[\frac{1}{\left(s^2+\frac{c}{m}s+\frac{k}{m}\right)}\right]_{s\to 0} =\frac{bm}{k}$$

However, $k/m=\omega_n^2$; therefore $K_1=b/\omega_n^2$. For $k=2$, eq (2.86) becomes

$$K_2=b\left[\frac{s-(-\zeta\omega_n+j\omega_n\sqrt{1-\zeta^2})}{s[s-(-\zeta\omega_n+j\omega_n\sqrt{1-\zeta^2})][s-(-\zeta\omega_n-j\omega_n\sqrt{1-\zeta^2})]}\right]_{s\to-\zeta\omega_n+j\omega_n\sqrt{1-\zeta^2}}$$

$$=b\left[\frac{1}{s[s+(\zeta\omega_n+j\omega_n\sqrt{1-\zeta^2})]}\right]_{s\to-\zeta\omega_n+j\omega_n\sqrt{1-\zeta^2}}=\frac{b}{2j\omega_n\sqrt{1-\zeta^2}(-\zeta\omega_n+j\omega_n\sqrt{1-\zeta^2})}$$

$$K_2=-\frac{b}{2\omega_n^2[(1-\zeta^2)+j\zeta\sqrt{1-\zeta^2}]}.$$

And, similarly, for $k=3$, eq (2.86) yields

$$K_3=-\frac{b}{2\omega_n^2[(1-\zeta^2)-j\zeta\sqrt{1-\zeta^2}]}.$$

Hence, the partial fraction expansion of eq (2.87) becomes

$$\frac{1}{s\left(s^2+\frac{c}{m}s+\frac{k}{m}\right)}=\frac{1}{\omega_n^2}\left(\frac{1}{s}\right)-\frac{1}{2\omega_n^2[(1-\zeta^2)+j\zeta\sqrt{1-\zeta^2}][s-(-\zeta\omega_n+j\omega_n\sqrt{1-\zeta^2})]}$$

$$-\frac{1}{2\omega_n^2[(1-\zeta^2)-j\zeta\sqrt{1-\zeta^2}][s-(-\zeta\omega_n-j\omega_n\sqrt{1-\zeta^2})]}. \qquad (2.92)$$

Taking the inverse transform of both sides yields

$$\mathcal{L}^{-1}\left[\frac{1}{s\left(s^2+\frac{c}{m}s+\frac{k}{m}\right)}\right]=\mathcal{L}^{-1}\left[\frac{K_1}{b}\left(\frac{1}{s}\right)-\frac{K_2}{b}\left(\frac{1}{s-s_2}\right)-\frac{K_3}{b}\left(\frac{1}{s-s_3}\right)\right],$$

where the constants K_1, K_2, and K_3 and the roots s_2 and s_3 are reintroduced for simplicity. By utilizing the summation and multiplication theorems [27, p. 161] this equation may be written as

$$\mathcal{L}^{-1}\left[\frac{1}{s\left(s^2+\frac{c}{m}s+\frac{k}{m}\right)}\right]=\frac{K_1}{b}\mathcal{L}^{-1}\left[\frac{1}{s}\right]-\frac{K_2}{b}\mathcal{L}^{-1}\left[\frac{1}{s-s_2}\right]-\frac{K_3}{b}\mathcal{L}^{-1}\left[\frac{1}{s-s_3}\right]. \qquad (2.93)$$

Referring to a table of Laplace transform pairs, the inverse transforms for eq (2.93) can be shown

to be

$$\mathcal{L}^{-1}\left[\frac{1}{s}\right]=1$$

$$\mathcal{L}^{-1}\left[\frac{1}{s-s_2}\right]=e^{s_2 t}$$

$$\mathcal{L}^{-1}\left[\frac{1}{s-s_3}\right]=e^{s_3 t}.$$

Therefore, eq (2.93) becomes

$$\mathcal{L}^{-1}\left[\frac{1}{s\left(s^2+\frac{c}{m}s+\frac{k}{m}\right)}\right]=\frac{K_1}{b}-\frac{K_2}{b}e^{s_2 t}-\frac{K_3}{b}e^{s_3 t}.$$

Introducing the expressions for K_1, K_2, K_3, s_2, and s_3, this equation becomes

$$\mathcal{L}^{-1}\left[\frac{1}{s\left(s^2+\frac{c}{m}s+\frac{k}{m}\right)}\right]$$
$$=\left\{\frac{1}{{\omega_n}^2}-\frac{\exp\left[(-\zeta\omega_n+j\omega_n\sqrt{1-\zeta^2})t\right]}{2{\omega_n}^2[(1-\zeta^2)+j\zeta\sqrt{1-\zeta^2}]}\right.$$
$$\left.-\frac{\exp\left[(-\zeta\omega_n-j\omega_n\sqrt{1-\zeta^2})t\right]}{2{\omega_n}^2[(1-\zeta^2)-j\zeta\sqrt{1-\zeta^2}]}\right\}$$

which reduces to

$$\mathcal{L}^{-1}\left[\frac{1}{s\left(s^2+\frac{c}{m}s+\frac{k}{m}\right)}\right]$$
$$=\frac{1}{{\omega_n}^2}\left\{1-e^{-\zeta\omega_n t}\left(\cos\sqrt{1-\zeta^2}\omega_n t\right.\right.$$
$$\left.\left.+\frac{\zeta}{\sqrt{1-\zeta^2}}\sin\sqrt{1-\zeta^2}\omega_n t\right)\right\}. \quad (2.94)$$

The second term enclosed by the brackets in eq (2.84) is identical to the first term multiplied by e^{-sT_p}. For such a case the shifting theorem [27, p. 166] applies and

$$f(t-T_p)U(t-T_p)=\mathcal{L}^{-1}[e^{-sT_p}F(s)].$$

This expression, where $U(t-T_p)$ is defined as a unit step occurring at T_p, shows that multiplication by a factor e^{-sT_p} simply amounts to a shift in the independent variable from t to $t-T_p$.

The procedure used in evaluating the inverse transform of the second term within the brackets of eq (2.84)

$$\frac{e^{-sT_p}}{s\left(s^2+\frac{c}{m}s+\frac{k}{m}\right)}$$

is as follows: first perform

$$\mathcal{L}^{-1}\left[\frac{1}{s\left(s^2+\frac{c}{m}s+\frac{k}{m}\right)}\right] \quad (2.95)$$

and then apply the shift in t, noting that $f(t-T_p)$ will be zero for $0<t<T_p$. The inverse transform of eq (2.95) is given by eq (2.94); therefore, applying the shift in t yields

$$\mathcal{L}^{-1}\left[\frac{1}{s\left(s^2+\frac{c}{m}s+\frac{k}{m}\right)}\right]$$
$$=\frac{1}{{\omega_n}^2}\left\{1-\exp\left(\left[-\zeta\omega_n(t-T_p)\right]\right.\right.$$
$$\left[\cos\sqrt{1-\zeta^2}\omega_n(t-T_p)+\frac{\zeta}{\sqrt{1-\zeta^2}}\right.$$
$$\left.\left.\left.\sin\sqrt{1-\zeta^2}\omega_n(t-T_p)\right]\right)\right\}U(t-T_p) \quad (2.96)$$

where

$$U(t-T_p)=0 \text{ for } t<T_p$$

and

$$U(t-T_p)=0 \text{ for } \geq T_p.$$

Substituting eqs (2.94) and (2.96) into eq (2.84), the complete solution to the characteristic differential equation of motion, or response function, is

$$x=\frac{F}{m{\omega_n}^2}\left\{1-\exp\left(-\zeta\omega_n t\right)\left[\cos\sqrt{1-\zeta^2}\omega_n t\right.\right.$$
$$\left.+\frac{\zeta}{\sqrt{1-\zeta^2}}\sin\sqrt{1-\zeta^2}\omega_n t\right]-\left(1-\exp\left[-\zeta\omega_n(t-T_p)\right]\right.$$
$$\left[\cos\sqrt{1-\zeta^2}\omega_n(t-T_p)+\frac{\zeta}{\sqrt{1-\zeta^2}}\right.$$
$$\left.\left.\left.\sin\sqrt{1-\zeta^2}\omega_n(t-T_p)\right]\right)U(t-T_p)\right\}. \quad (2.97)$$

To obtain the input function when the characteristic differential equation of motion and the response function are known analytically, substitute the response function, eq (2.97), into the original differential equation of motion, eq (1.1), and solve for $f(t)$. In this analysis keep in mind the properties of $U(t-T_p)$.

b. Transformation From Time to Frequency Domain

The transformation of an aperiodic function from the time to the frequency domain is accomplished by use of the Laplace transform, with $s=j\omega$. For the input function described by eqs (2.74), (2.75), and (2.76) the transformation has already been performed and is given by eq (2.77). For $s=j\omega$, eq (2.77) becomes

$$F(j\omega)=\frac{F}{j\omega}(1-e^{-j\omega T_p}) \quad (2.98)$$

where $F(j\omega)$ is denoted as the complex input

spectrum for real frequencies ω and can be simplified as follows:

$$F(j\omega)=\frac{2F}{\omega}\left[\frac{\exp\,(j\omega T_p/2)-\exp\,(-j\omega T_p/2)}{2j}\right]$$

$$[\exp\,(-j\omega T_p/2)]$$

$$=\left(\frac{2F}{\omega}\sin\frac{\omega T_p}{2}\right)\exp\,(-j\omega T_p/2). \qquad (2.99)$$

This complex number, eq (2.99), consists of two parts: (a) an absolute value or modulus, which is the amplitude of the input spectrum; and (b) an argument (the coefficient of j in the exponent), which is the phase angle. These are given, respectively, by

$$F(\omega)=\text{mod}\ F(j\omega)=\left|\frac{2F}{\omega}\sin\frac{\omega T_p}{2}\right| \qquad (2.100)$$

and

$$\varphi(\omega)=\arg F(j\omega)=-\frac{\omega T_p}{2}. \qquad (2.101)$$

Note that here $\omega T_p \neq 2\pi$ because T_p is not the period of a periodic function; therefore, ω is not fixed.

Taking the Laplace transform of the response function, eq (2.97), results in eq (2.82). For $s=j\omega$, eq (2.82) becomes

$$X(j\omega)=\mathcal{L}[x]=\frac{F(1-e^{-j\omega T_p})}{j\omega[(k-m\omega^2)+jc\omega]} \qquad (2.102)$$

where $X(j\omega)$ is denoted as the complex response spectrum. Equation (2.102) may be written in a more convenient form by noting that

$$\frac{F}{j\omega}[1-\exp\,(-j\omega T_p)]$$

$$=F(j\omega)=\left(\frac{2F}{\omega}\sin\frac{\omega T_p}{2}\right)[\exp\,(-j\omega T_p/2)]$$

and

$$(k-m\omega^2)+jc\omega$$

$$=\sqrt{(k-m\omega^2)^2+c^2\omega^2}\exp\left\{j\left[\arctan\left(\frac{c\omega}{k-m\omega^2}\right)\right]\right\}.$$

Therefore, eq (2.102) becomes

$$X(j\omega)=\frac{\frac{2F}{\omega}\sin\frac{\omega T_p}{2}}{\sqrt{(k-m\omega^2)^2+c^2\omega^2}}\,\frac{\exp\left(\frac{-j\omega T_p}{2}\right)}{\exp\left[j\arctan\left(\frac{c\omega}{k-m\omega^2}\right)\right]}$$

or

$$X(j\omega)=\frac{\frac{2F}{\omega}\sin\frac{\omega T_p}{2}}{\sqrt{(k-m\omega^2)^2+c^2\omega^2}}\exp\left\{-j\left[\frac{\omega T_p}{2}+\arctan\left(\frac{c\omega}{k-m\omega^2}\right)\right]\right\}. \qquad (2.103)$$

The amplitude of the response spectrum is given by

$$X(\omega)=\text{mod}\ X(j\omega)=\left|\frac{\frac{2F}{\omega}\sin\frac{\omega T_p}{2}}{\sqrt{(k-m\omega^2)^2+c^2\omega^2}}\right| \qquad (2.104)$$

and the phase angle by

$$\alpha(\omega)=\arg X(j\omega)=-\frac{\omega T_p}{2}-\arctan\left(\frac{c\omega}{k-m\omega^2}\right). \qquad (2.105)$$

c. Transfer Function

The transfer function for the system is defined by the relationships expressed by eqs (2.1) and (2.2), i.e., division of the moduli and subtraction of the arguments. The transfer function may also be expressed in complex number form as follows:

$$H(j\omega)=\frac{X(j\omega)}{F(j\omega)} \qquad (2.106)$$

where by eqs (2.99) and (2.103) the complex transfer function becomes

$$H(j\omega)=\frac{1}{\sqrt{(k-m\omega^2)^2+c^2\omega^2}}\times\left\{\exp\left[-j\arctan\left(\frac{c\omega}{k-m\omega^2}\right)\right]\right\} \qquad (2.107)$$

with

$$H(\omega)=\text{mod}\ H(j\omega)=\frac{1}{\sqrt{(k-m\omega^2)^2+c^2\omega^2}} \qquad (2.108)$$

and

$$\beta(\omega)=\arg H(j\omega)=-\arctan\left(\frac{c\omega}{k-m\omega^2}\right). \qquad (2.109)$$

d. Input From Transfer Function and Response Record

The input function is obtained through the knowledge of the response record and the transfer function for the system. A response record such as eq (2.97) has been shown to be Laplace transformable and can be expressed in the frequency domain by the substitution of $s=j\omega$ into the transform. This substitution results in the complex response spectrum $X(j\omega)$ given by eq (2.103). The complex transfer function $H(j\omega)$ has been derived in the previous section and is given by eq (2.107). Therefore, by eq (2.106) the complex input spectrum $F(j\omega)$ becomes

$$F(j\omega)=\frac{X(j\omega)}{H(j\omega)}$$

or

$$F(j\omega)=\left(\frac{2F}{\omega}\sin\frac{\omega T_p}{2}\right)\exp\left(\frac{-j\omega T_p}{2}\right). \qquad (2.110)$$

Equation (2.110) is identical to eq (2.99) which was shown to be derivable from eq (2.98) in

section c, or

$$F(j\omega)=\frac{F}{j\omega}(1-e^{-j\omega T_p}).$$

Taking the inverse Laplace transform of this expression, which is readily obtainable from a table of Laplace transform pairs and the shifting theorem, the input function is

$$f(t)=F[1-U(t-T_p)] \qquad (2.111)$$

where $U(t-T_p)$ has the properties previously defined. Equation (2.111) is in full agreement with the input described by eqs (2.74), (2.75), and (2.76).

3.2. Step Function

a. Direct Input-Output Relation in the Time Domain

The step function to be analyzed is shown in figure 2.2d and is expressed as a function of time by

$$f(t)=0 \text{ for } t<0 \qquad (2.112)$$

$$f(t)=F \text{ for } 0<t\leq\infty. \qquad (2.113)$$

The Laplace transformation for the step function described above is obtained through eq (1.22). Therefore,

$$F(s)=\int_0^\infty f(t)e^{-st}dt$$

or

$$\mathcal{L}[f(t)]=F(s)=\int_0^\infty Fe^{-st}\,dt=\frac{F}{s} \qquad (2.114)$$

where s is a complex number equal to $\sigma+j\omega$.

The characteristic differential equation of motion for the system analyzed is given by eq (1.1). Applying the Laplace transform operator to this equation, the form subsequently arrived at is equivalent to eq (2.81) except for the right hand side of eq (2.81):

$$ms^2\mathcal{L}[x]+cs\mathcal{L}[x]+k\mathcal{L}[x]=\frac{F}{s}$$

where

$$\mathcal{L}[x]=\frac{F}{s(ms^2+cs+k)}. \qquad (2.115)$$

Rewriting eq (2.115) in a more convenient form, and taking the inverse Laplace transform, yields the response function

$$x=\mathcal{L}^{-1}\mathcal{L}[x]=\frac{F}{m}\mathcal{L}^{-1}\left[\frac{1}{s\left(s^2+\frac{c}{m}s+\frac{k}{m}\right)}\right]. \qquad (2.116)$$

The inverse Laplace transform in eq (2.116) is identical to that given in eq (2.94). Therefore, the response function, eq (2.116) becomes

$$x=\frac{F}{m\omega_n^2}\left\{1-e^{-\zeta\omega_n t}\left(\cos\sqrt{1-\zeta^2}\omega_n t+\frac{\zeta}{\sqrt{1-\zeta^2}}\sin\sqrt{1-\zeta^2}\,\omega_n t\right)\right\}. \qquad (2.117)$$

When the characteristic differential equation of motion and the response function are expressed analytically, the input function is readily obtained either directly by substituting the response function eq (2.117) into eq (1.1), or by the Laplace transforms of these expressions.

b. Transformation From Time to Frequency Domain

The Laplace transform of the input function is given by eq (2.114). For $s=j\omega$, eq (2.114) becomes

$$F(j\omega)=\frac{F}{j\omega} \qquad (2.118)$$

where $F(j\omega)$ is the complex input spectrum. Equation (2.118) may be written in a more convenient form as

$$F(j\omega)=\frac{F}{\omega}e^{-j\frac{\pi}{2}} \qquad (2.119)$$

with the amplitude of the input spectrum given by

$$F(\omega)=\text{mod } F(j\omega)=\frac{F}{\omega} \qquad (2.120)$$

and the phase angle given by

$$\varphi(\omega)=\arg F(j\omega)=-\frac{\pi}{2}. \qquad (2.121)$$

The Laplace transform of the response function, eq (2.117), results in the complex response spectrum, eq (2.115). For $s=j\omega$, eq (2.115), becomes

$$X(j\omega)=\frac{F}{j\omega[(k-m\omega^2)+jc\omega]}. \qquad (2.122)$$

Equation (2.122) can be written in a more convenient form by recognizing that

$$\frac{F}{j\omega}=F(j\omega)=\frac{F}{\omega}e^{-j\frac{\pi}{2}}$$

and

$$(k-m\omega^2)+jc\omega$$

$$=\sqrt{(k-m\omega^2)^2+c^2\omega^2}\left\{\exp\left[j\arctan\left(\frac{c\omega}{k-m\omega^2}\right)\right].\right\}$$

Therefore, eq (2.122) can be written as

$$X(j\omega)=\frac{\frac{F}{\omega}}{\sqrt{(k-m\omega^2)^2+c^2\omega^2}} \times\left(\exp\left\{-j\left[\frac{\pi}{2}+\arctan\left(\frac{c\omega}{k-m\omega^2}\right)\right]\right\}\right) \quad (2.123)$$

with

$$X(\omega)=\text{mod } X(j\omega)=\frac{\frac{F}{\omega}}{\sqrt{(k-m\omega^2)^2+c^2\omega^2}} \quad (2.124)$$

and

$$\alpha(\omega)=\arg X(j\omega)=-\frac{\pi}{2}-\arctan\left(\frac{c\omega}{k-m\omega^2}\right). \quad (2.125)$$

c. Transfer Function

The complex transfer function $H(j\omega)$ is given by the division of $F(j\omega)$ into $X(j\omega)$, where these quantities are given by eqs (2.119) and (2.123), respectively. This division yields

$$H(j\omega)=\frac{1}{\sqrt{(k-m\omega^2)^2+c^2\omega^2}} \times\left\{\exp\left[-j\arctan\left(\frac{c\omega}{k-m\omega^2}\right)\right]\right\} \quad (2.126)$$

with

$$H(\omega)=\text{mod } H(j\omega)=\frac{1}{\sqrt{(k-m\omega^2)^2+c^2\omega^2}} \quad (2.127)$$

and

$$\beta(\omega)=\arg H(j\omega)=-\arctan\left(\frac{c\omega}{k-m\omega^2}\right). \quad (2.128)$$

Note that the transfer function is a characteristic of the linear transducer system and is not dependent upon the type of excitation or input to the system. This in part is substantiated by the fact that eq (2.126) is identical to eq (2.107), where the transfer function relations were derived for two different inputs.

d. Input From Transfer Function and Response Record

The input function is directly determined from the complex input spectrum $F(j\omega)$, which can be obtained from eq (2.106). This requires that the complex response function $X(j\omega)$ and transfer function $H(j\omega)$ be known analytically. For $X(j\omega)$ and $H(j\omega)$ given by eqs (2.122) and (2.126), respectively, the complex input spectrum is

$$F(j\omega)=\frac{F}{j\omega}.$$

By a table of Laplace transform pairs, the inverse transform of $F(j\omega)=F(s)$ is

$$f(t)=F.$$

The interpretation of this result is

$$f(t)=0 \text{ for } t<0$$

$$f(t)=F \text{ for } t>0,$$

which is based on the property of a function which is Laplace transformable. These results agree with the input function described by eqs (2.112) and (2.113).

4. Phase-Plane Method

4.1. Introduction

We introduce the concept of the phase-plane method here, in a section concerned with linear transducers, only to relate it to the more common methods by which the behavior of linear dynamical systems is characterized. In chapter 4, the application of the phase-plane method in characterizing the behavior of nonlinear transducers is discussed in detail. For linear systems (where the principle of superposition is valid), the classical, direct methods of analysis are more commonly used and the existence of a meaningful transfer function precludes the necessity for using the phase-plane method. For nonlinear systems the same transfer function does not exist; however, the time response of certain nonlinear systems can be determined by phase-plane techniques. Other methods for approximating the response of nonlinear transducer systems are described in chapter 4. Here we confine ourselves to an introductory exposition of the phase-plane method as it applies to linear systems.

4.2. The Phase Plane (Phase Space)

The phase plane is a two-dimensional phase space, the coordinates of which are related in that the one is the time derivative of the other. In the analysis of transducer systems, the appropriate phase-plane coordinates are the transducer output and its first time derivative, say, q and $\dot{q}$, respectively.

The general concept of a phase space is well known in physics and perhaps best known for its application to kinetic theory of gases. In such an application of the general concept, the disturbed response of a dynamical system with n degrees of freedom is characterized for time t by the set of $2n$ coordinates comprising the positional coordinates $q_i(i=1, 2, \ldots n)$ and their velocities

$\dot{q}_i (i=1, 2, \ldots n)$. The q_i, $\dot{q}_i$ may be considered as the coordinates of a space S of $2n$ dimensions called a *phase space*. At time t, for each state of the system there exists a point P with coordinates $(q_k, \dot{q}_k)$. As t is permitted to vary, the point P describes a curve called a *path* or *trajectory*, which characterizes a history of the system. An infinite number of such paths exists, each determined uniquely by specification of a single point of the path. For a given system the totality of such paths in the $(q_i, \dot{q}_i)$ space is the *phase portrait* of the system. Since each of the paths is determined uniquely by specifying a single point, it can be inferred that there is one and only one path through each point of the phase space.

4.3. The Phase-Plane Method Applied to Linear Systems

Let us consider the viscously damped, single-degree-of-freedom system described by the linear, second-order equation of motion

$$\ddot{q}+2\zeta\omega_n\dot{q}+\omega_n^2 q=0, \qquad (2.129)$$

where ω_n is the undamped natural frequency $(=\sqrt{k/m})$. The state of the system at any time is fixed by the values of q and $\dot{q}$; for example, if $q(0)$ and $\dot{q}(0)$ are known, the solution for all time $t>0$ is determined. This dependence of future states of the system on the initial conditions can be shown graphically in the phase plane, the $(q, \dot{q})$ plane. The phase portrait for the linear system of eq (2.129) with relative damping ratio $\zeta=0.5$ is shown in figure 2.3. Let us say that P_0 at q_0, $\dot{q}_0$ describes the initial state of the system. Then P_1, P_2 . . . describe successive states as t progresses. Note that time appears in the phase portrait only implicitly as a parameter changing value along any path.

Clearly, there is only one path through each point in the phase plane, since the solution of eq (2.129) is determined uniquely by specifying both q and $\dot{q}$ at a given instant of time. Thus, the phase portrait for the linear system is a family of noncrossing paths describing the system behavior after all possible initial conditions.

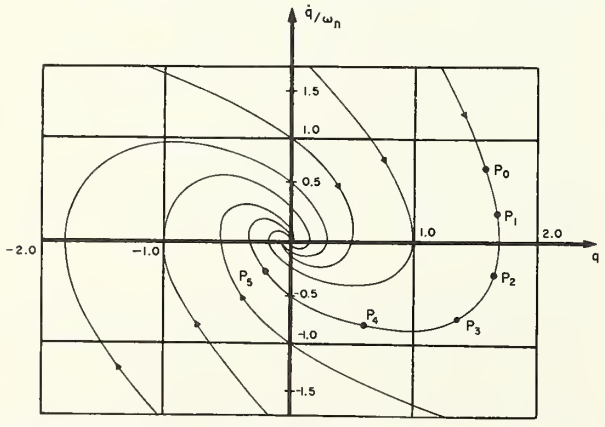

FIGURE 2.3. *Phase portrait of linear viscously damped system* $(\zeta=0.5)$.

(Reproduced from [35] with permission from Clarendon Press)

There are three methods for constructing the phase portrait: by direct solution of the differential equation, by reducing the order of the original differential equation and solving for $\dot{q}$ as a function of q, and by plotting the isoclines corresponding to various slopes of the phase paths. The three methods are described below in terms of eq (2.129) with $\zeta=0$, the equation of an undamped system,

$$\ddot{q}+\omega_n^2 q=0. \qquad (2.130)$$

a. Direct Solution

The solution of eq (2.130) is given by

$$q(t)=Q\sin(\omega_n t+\varphi) \qquad (2.131)$$

and the velocity by

$$\dot{q}(t)=Q\omega_n\cos(\omega_n t+\varphi). \qquad (2.132)$$

By squaring and adding eqs (2.131) and (2.132), time is eliminated as an explicit factor and we obtain

$$q^2+\frac{\dot{q}^2}{\omega_n^2}=Q^2, \qquad (2.133)$$

which describes the phase portrait of the system. The paths are ellipses with axes of magnitude Q and $Q\omega_n$, or, normalizing the velocity, the phase-plane coordinates are q, $\dot{q}/\omega_n$, and the corresponding phase paths are circles of radius Q. In either case, the initial conditions specify a particular ellipse (or circle) which characterizes the dynamic behavior of the system.

The same procedure, that is, direct solution of the differential equation, can be used infrequently in the analysis of nonlinear systems. However, this is discussed in chapter 4 where the phase-plane method is used to describe the behavior of nonlinear transducers.

b. Solution of the Equation for $\dot{q}$ as a Function of q

In certain systems, it is simpler to pass directly, without integration, from differential eq (2.130) to representation on the phase plane. The procedure by which this can be accomplished is, first, to replace the initial second-order equation by two equivalent, first-order equations.

$$\frac{dq}{dt}=p$$

$$\frac{dp}{dt}=\omega_n^2 q. \qquad (2.134)$$

But eq (2.134) can be written as the following first-order equation:

$$\frac{dp}{dq}=-\omega_n^2\frac{q}{p}. \qquad (2.135)$$

It can be seen that integration of eq (2.135) will yield

$$q^2+\frac{p^2}{\omega_n{}^2}=Q^2, \tag{2.136}$$

a solution (phase portrait) identical to that given by eq (2.133).

c. Method of Isoclines

An approximation of the phase portrait can be constructed by studying the slopes of the phase paths. This approximate method is, perhaps, most useful in the analysis of nonlinear systems or of linear systems where integration of the differential equation is difficult. The method of isoclines offers little advantage whenever, as in our illustrative case, separation of variables permits easy integration of the equation.

For the undamped linear system it is clear that the slopes of the totality of paths on the phase plane are given by eq (2.135). A locus of constant slope values is termed an *isocline*. The isocline corresponding to $dp/dq=\alpha$ can be found from the equation

$$\alpha=-\omega_n{}^2\frac{q}{p}. \tag{2.137}$$

The family of isoclines determined by eq (2.137) are straight lines passing through the origin of the phase plane with slope $-\omega_n/\alpha$ or, if the velocity p is normalized, with slope $-1/\alpha$.

The path from any given point (initial state) in the phase plane can be constructed in the following manner. Point P_0 in figure 2.4 lies on the isocline corresponding to $\alpha=1.00$. The motion of the path away from P_0 is clockwise with reference to the origin. The isocline adjacent to that through P_0 in a clockwise direction is that for $\alpha=-1.50$. From P_0 a directed line segment of slope -1.25 (the average of -1.00 and -1.50) is drawn to intersect the $\alpha=-1.50$ isocline at point P_1. From P_1 the process is repeated; a new line segment of slope -1.75 is drawn to intersect the $\alpha=-2.00$ isocline at point P_3. As the process is repeated an approximation of the phase path can be sketched by joining successive line segments.

The exactness of the approximation to the phase path is dependent upon the number of isoclines used in its construction: the greater the number, the more exact the approximation. Inherent in this lack of exactness lies the greatest disadvantage of the method. An important aspect of the phase portrait for nonlinear systems is the existence of closed paths. In some cases, with even a relatively dense array of isoclines upon which to base the construction, it is difficult to sketch accurately the phase path in the region of the origin. Is the path closed or is it, in fact, approaching the origin slowly with each circuit around the origin? As a practical consideration this deficiency is usually more disturbing than serious.

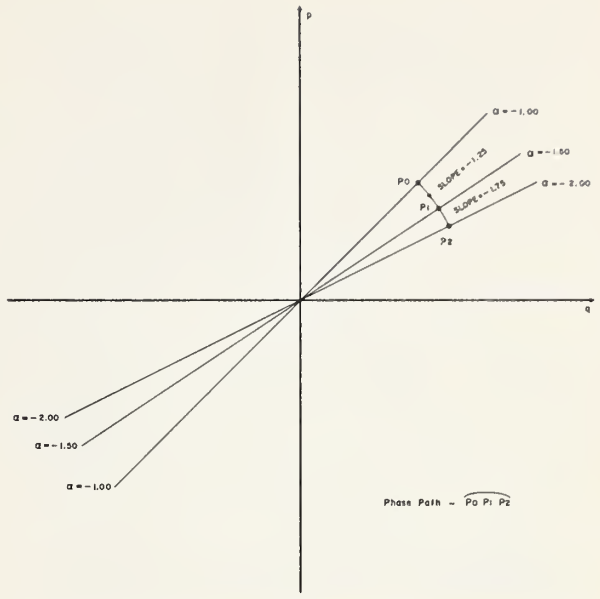

FIGURE 2.4. *Construction of phase path from isoclines.*

d. Application of the Phase-Plane Method to a Linear, Viscously Damped System by Means of Oblique Coordinates

If it is assumed that the initial conditions for the motion described by eq (2.129) are $q(0)=q_0$ and $\dot{q}(0)=p_0$, then the solution of (2.129) for $\zeta<1$ is

$$q=e^{-\zeta\omega_n t}\left(q_0\cos\omega_n\sqrt{1-\zeta^2}t+\frac{p_0+\zeta\omega_n q_0}{\omega_n\sqrt{1-\zeta^2}}\sin\omega_n\sqrt{1-\zeta^2}t\right), \tag{2.138}$$

which may be rewritten as

$$q=e^{-\zeta\omega_n t}S\cos(\omega_n\sqrt{1-\zeta^2}t-\varphi), \tag{2.139}$$

where

$$S^2=q_0{}^2+\left(\frac{p_0+\zeta\omega_n q_0}{\omega_n\sqrt{1-\zeta^2}}\right)^2 \tag{2.140}$$

and

$$\tan\varphi=\frac{p_0+\zeta\omega_n q_0}{q_0\omega_n\sqrt{1-\zeta^2}}.$$

By eq (2.140), the normalized velocity then becomes

$$\frac{\dot{q}}{\omega_n}=-e^{-\zeta\omega_n t}S\sin(\omega_n\sqrt{1-\zeta^2}t-\phi+\xi), \tag{2.141}$$

where the new phase angle ξ is defined by

$$\tan\xi=\frac{\zeta}{\sqrt{1-\zeta^2}}. \tag{2.142}$$

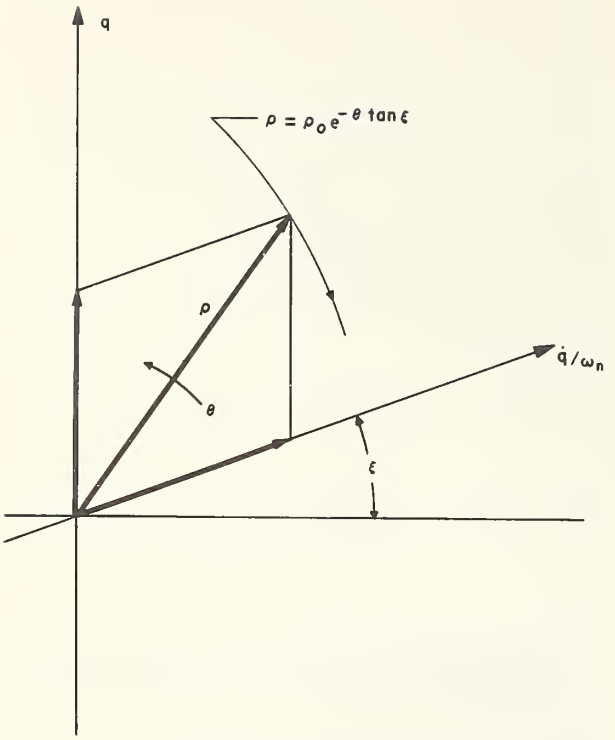

FIGURE 2.5. *Oblique-coordinate phase plane used for analysis of viscously damped systems.*

Earlier, in the undamped case, time was eliminated as an explicit parameter by squaring and adding the expressions for q and $\dot{q}/\omega_n$. Here, if the phase coordinates as given by eqs (2.139) and (2.141) are squared and added, the presence of the new phase angle ξ unduly complicates the resultant expression. However, the phase paths can be simplified if we use an oblique phase-plane coordinate system [15, 34].

Let q and $\dot{q}/\omega_n$ (the transducer output signal and its first normalized time derivative) be plotted on the oblique coordinates of figure 2.5. The magnitude of the radius vector ρ is

$$\rho^2 = \left(\frac{\dot{q}}{\omega_n}\cos\zeta\right)^2 + \left(q + \frac{\dot{q}}{\omega_n}\sin\xi\right)^2$$

$$= q^2 + (\dot{q}/\omega_n)^2 + 2q(\dot{q}/\omega_n)\sin\xi. \qquad (2.143)$$

By using eqs (2.139) and (2.141) in (2.143) we obtain

$$\rho = e^{-\zeta\omega_n t} S\cos\xi$$

$$= \rho_0 e^{-\zeta\omega_n t}, \qquad (2.144)$$

the equation of a logarithmic spiral in polar coordinates, which must be projected onto the oblique axes of figure 2.5 to give q and $\dot{q}/\omega_n$.

It was stated earlier that the time does not appear explicitly in the phase-plane representation of the motion of a system; however, time is given implicitly by the angular location of the phase points representing successive states of the system. In eq (2.139) the angle in the trigonometric argument is expressed in terms of the angular velocity $\omega_n\sqrt{1-\zeta^2}$. From this it can be concluded that the angular velocity of the phase point on the path will have this value. Consequently, the implied time for an angular movement of θ radians in the phase plane will be $\dfrac{\theta}{\omega_n\sqrt{1-\zeta^2}}$ and, upon substituting this in (2.144), the explicit equation of the spiral phase path in the oblique coordinate plane becomes

$$\rho = \rho_0 e^{-\theta\tan\xi}. \qquad (2.145)$$

Clearly, for each value of ζ, there exists a particular spiral.

While the construction of exponential spirals can be tedious, it presents no other problem. For values of $\zeta < 0.5$, Jacobsen [15, p. 204] suggests several approximate methods of construction.

5. References

[1] T. von Karman and M. A. Biot, Mathematical Methods in Engineering, p. 335, McGraw-Hill Book Co., Inc. (New York, N.Y., 1940).

[2] H. Poincaré, On the contours determined from a differential equation (in French), vol. I, Oeuvres de Henri Poincaré, Gauthier-Villars (Paris, 1928).

[3] H. Poincaré, New methods of Celestial Mechanics (in French), vol. I, Gauthier-Villars (Paris, 1892).

[4] J. Lamoen, On the dynamic entreaty of wind on tall structures (in French), Mem. Acad. Roy. Belgique, Classe Sci. **12,** 1437 (1932).

[5] J. Lamoen, Graphical study of the vibrations of single-degree-of-freedom systems (in French), Rev. Universelle Mines [8] **11,** No. F, 213 (May 1935).

[6] H. O. Fuchs, Spiral diagrams to solve vibration damping problems, Prod. Eng., 294–296 (Aug. 1936).

[7] E. Braun, On the graphical solution of the differential equation for forced vibration, considering an arbitrary law for damping, restoring force and driving force (in German), Ing. Archiv **8,** No. 3, 198–202 (1937).

[8] V. Rojansky, Gyrograms for simple harmonic systems subjected to external forces, J. Appl. Phys. **19,** No. 3, 297–301 (Mar. 1948).

[9] R. E. D. Bishop, On the graphical solution of transient vibration problems, Proc. IME (London) **168,** No. 10, 299–322 (1954).

[10] A. A. Andronov and C. E. Chaikin, Theory of Oscillations, Princeton Univ. Press (Princeton, N.J., 1949).

[11] N. Minorsky, Introduction to Non-Linear Mechanics, Edwards Brothers (Ann Arbor, Mich., 1947); also Non-Linear Oscillations, D. Van Nostrand Co., Inc. (Princeton, N. J., 1962).

[12] N. Kryloff and N. Bogoliuboff, Introduction to Non-Linear Mechanics (Kiev, USSR, 1937); trans. S. Lefschetz, Princeton Univ. Press (Princeton, N.J., 1943, 1947).

[13] J. G. Truxal, Automatic Feedback Control System Synthesis, McGraw-Hill Book Co., Inc. (New York, N.Y., 1955).

[14] G. J. Murphy, Control Engineering, D. Van Nostrand Co., Inc. (Princeton, N.J., 1959).

[15] L. S. Jacobsen and R. S. Ayre, Engineering Vibrations, p. 203, McGraw-Hill Book Co., Inc. (New York, N.Y., 1958).
[16] K. Klotter, How to obtain describing functions for non-linear feedback systems, Trans. ASME **79,** 509–512 (1957).
[17] K. Klotter, Steady-state oscillation in non-linear multiloop circuits, Trans. IRE, 13–18 (1954).
[18] K. Magnus, On a method for the analysis of non-linear vibration and control systems (in German), VDI Forschungsheft [13] **21,** 1–32 (1955).
[19] J. E. Gibson, Non-linear system design, Control Eng., 69–75 (Oct. 1951).
[20] R. L. Cosgriff, Non-Linear Control Systems, McGraw-Hill Book Co., Inc. (New York, N.Y., 1958).
[21] R. W. Bass, Proc. Symp. Non-Linear Circuit Analysis, Polytechnic Inst. Brooklyn, vol. 6, 1956.
[22] E. I. Ergin, Transient response of a non-linear spring-mass system, J. Appl. Mech. **23,** 635–641 (1956).
[23] T. M. Stout, Basic methods for non-linear control system analysis, Trans. ASME **79,** 497–508 (1957).
[24] L. S. Jacobsen, On the general method of solving second-order, ordinary differential equations by phase-plane displacements, J. Appl. Mech. **19,** 543 (1952).
[25] F. F. Liu, Recent advances in dynamic pressure measurement techniques, J. ARS **28,** 83–85, 128–132 (1958).
[26] D. K. Cheng, Analysis of Linear Systems, Addison-Wesley Pub. Co., Inc. (Reading, Mass. 1959).
[27] R. V. Churchill, Operational Mathematics, McGraw-Hill Book Co., Inc. (New York, N.Y., 1958).
[28] J. N. MacDuff and J. R. Curreri, Vibration Control, McGraw-Hill Book Co., Inc. (New York, N.Y., 1958).
[29] A. Bronwell, Advanced Mathematics in Physics and Engineering, McGraw-Hill Book Co., Inc. (New York, N.Y., 1953).
[30] W. R. LePage, Complex Variables and the Laplace Transform for Engineers, McGraw-Hill Book Co., Inc. (New York, N.Y., 1961).
[31] C. R. Wylie, Jr., Advanced Engineering Mathematics, McGraw-Hill Book Co., Inc. (New York, N.Y., 1951).
[32] L. A. Pipes, Applied Mathematics for Engineers and Physicists, McGraw-Hill Book Co., Inc. (New York, N.Y., 1958).
[33] N. O. Myklestad, Fundamentals of Vibration Analysis, McGraw-Hill Book Co., Inc. (New York, N.Y., 1956).
[34] Flügge-hotz, Irmgard, Discontinuous Automatic Control, p. 24, Princeton Univ. Press (Princeton, N.J., 1953).
[35] N. W. McLachlan, Ordinary Non-Linear Differential Equations in Engineering and Physical Sciences, Clarendon Press (Oxford, England, 1956).

3. Approximate Methods of Linear Transducer Analysis

L. C. Eichberger [1]

1. General

In chapter 2 it was assumed that the characteristic differential equation of motion of the transducer system is known. Corresponding response functions were then obtained analytically from the differential equation for a number of given input functions by classical or operational mathematics. This procedure of analysis is the exception rather than the rule. In general, the characteristic differential equation of motion is not known. What is known is the response of the transducer system to (1) a known input function and (2) the response of the same transducer system to an unknown input function. The response function will usually be in the form of a record—either a strip-chart record from an oscillograph or a photographic record from an oscilloscope. The response function will be referred to the time domain since its graphical representation is a function of time. The graphical form of the response function brings about a need for a method or methods by which the response function can either be expressed analytically as a function of time or transformed directly to the frequency domain. This chapter will be devoted to the various methods available for fulfilling this need. Once the response function has been expressed as a function of either time or frequency, the transfer function and the input function can be obtained by following the routes of analysis shown in figure 2.1 and illustrated in detail in chapter 2.

The major part of the analysis in this chapter is based on the evaluation of the Fourier integral eq (1.17). The integral, as it stands, is cumbersome to compute, and the solution to some very elementary situations often turns out to be a tedious and time-consuming task. To relieve this tedium, different approximations and/or computing aids are introduced to simplify the evaluation. Some of the approximations considered are harmonic analysis, staircase function, straight-line segment, trapezoidal, sin x/x, number series transformation, and the pseudo-rectangular pulse. The computing aids considered are Henderson's analyzer, Montgomery's optical Fourier analyzer, photoelectric Fourier transformer, and an electronic analyzer with magnetic transient storage used by Lederer and Smith.

Before discussing the approximations in detail let us examine the Fourier integrals, eqs (1.16) and (1.17), more closely. For convenience, let us rewrite eqs (1.16) and (1.17) as

$$x(t)=\frac{1}{2\pi}\int_{-\infty}^{\infty} X(j\omega)e^{j\omega t}d\omega \tag{3.1}$$

$$X(j\omega)=\int_{-\infty}^{\infty} x(t)e^{-j\omega t}dt, \tag{3.2}$$

where $x(t)$ is the response function and $X(j\omega)$ is its direct Fourier transform, the complex frequency response of the system.

Let us assume that the response function $x(t)$ is identically zero for $t<0$. This assumption for all practical purposes is true since it implies that the input function to the system is also identically zero for $t<0$. The acceptance of this assumption allows us to use either the real or imaginary part of $X(j\omega)$ and thus eliminates the exponential form of the transform [1].[2] This can be easily shown [2] by rewriting eq (3.2) with $X(j\omega)=X_1(\omega)+jX_2(\omega)$ and $e^{-j\omega t}=\cos\ \omega t-j\ \sin\ \omega t$. Therefore, eq (3.2) becomes

$$X_1(\omega)+jX_2(\omega)=\int_{-\infty}^{\infty} x(t)\ \cos\ \omega t\ dt \\ -j\int_{-\infty}^{\infty} x(t)\ \sin\ \omega t\ dt$$

from which

$$X_1(\omega)=\int_{-\infty}^{\infty} x(t)\ \cos\ \omega t\ dt$$

$$X_2(\omega)=\int_{-\infty}^{\infty} x(t)\ \sin\ \omega t\ dt.$$

Assuming that $x(t)$ is an even function, then $X_1(\omega)$ is even and determines the even part of $x(t)$ in eq (3.1), while $X_2(\omega)$ is odd and vanishes. Or assume $x(t)$ to have even and odd parts, then, since $x(t)$ is zero for $t<0$, the even and odd parts must cancel. It follows that they are identical for $t>0$. Therefore, one-half of either part or one-fourth of the total can be used to compute $x(t)$ for positive t. On the basis of this argument,

[1] Assistant Professor of Mechanical Engineering, The University of Houston; Technical Staff, Houston Engineering Research Corporation.

[2] Figures in brackets indicate the literature references on p. 51.

eqs (3.1) and (3.2) may be rewritten as

$$x(t)=\frac{2}{\pi}\int_0^\infty X_1(\omega)\cos\omega t\,d\omega \qquad (3.3)$$

$$X_1(\omega)=\int_0^\infty x(t)\cos\omega t\,dt, \qquad (3.4)$$

where $X_1(\omega)$ is a real function of a real variable.

2. Approximation of Periodic Functions

2.1. Harmonic Analysis

Harmonic analysis enables us to represent any known periodic phenomenon by an empirical function. The periodic phenomenon, the response function, can always be approximated by the Fourier series of the form

$$f(t)=a_0+a_1\cos\omega t+a_2\cos 2\omega t+\ldots+a_n\cos n\omega t$$
$$+b_1\sin\omega t+b_2\sin 2\omega t+\ldots+b_n\sin n\omega t. \qquad (3.5)$$

This function is periodic and has a period of 2π. If values of the dependent variable $f(t)$ are known for certain equidistant values of the independent variable ωt, then the unknown coefficients $a_0, a_1, a_2, \ldots, a_n, b_1, b_2 \ldots, b_n$ can be easily found. Values of $f(t)$ are readily obtainable from the record of the response function. This record may be in the form of numerical data, a graph, or a photograph. Once these values have been obtained the analysis for evaluating the coefficients is as follows: for illustrative purposes, let us assume that the function is periodic with period 2π as shown in figure 3.1, and that $f(t)$ is known for six equidistant values of ωt (or $k=3$ in fig. 3.1), i.e.,

ωt	0	60	120	180	240	300
$f(t)$	f_0	f_1	f_2	f_3	f_4	f_5

Equation (3.5), for the 6-ordinate system, becomes

$$f(t)=a_0+a_1\cos\omega t+a_2\cos 2\omega t+a_3\cos 3\omega t$$
$$+b_1\sin\omega t+b_2\sin 2\omega t. \qquad (3.6)$$

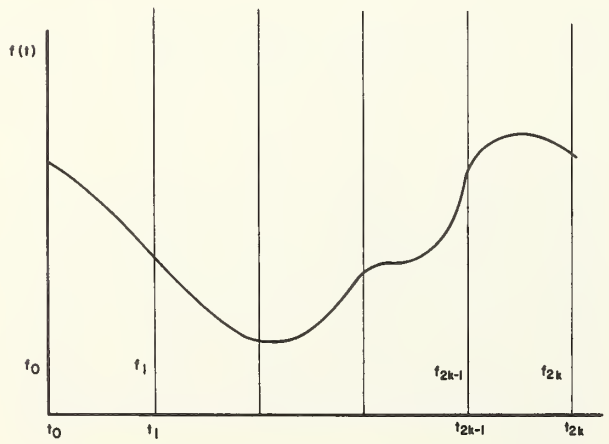

FIGURE 3.1. *Periodic response function.*

Substituting the corresponding set of values for $f(t)$ and ωt into eq (3.6), gives

$$\left.\begin{aligned}
f_0&=a_0+a_1+a_2+a_3\\
f_1&=a_0+\tfrac{1}{2}a_1-\tfrac{1}{2}a_2-a_3+\frac{\sqrt{3}}{2}b_1+\frac{\sqrt{3}}{2}b_2\\
f_2&=a_0-\tfrac{1}{2}a_1-\tfrac{1}{2}a_2+a_3+\frac{\sqrt{3}}{2}b_1-\frac{\sqrt{3}}{2}b_2\\
f_3&=a_0-a_1+a_2-a_3\\
f_4&=a_0-\tfrac{1}{2}a_1-\tfrac{1}{2}a_2+a_3-\frac{\sqrt{3}}{2}b_1+\frac{\sqrt{3}}{2}b_2\\
f_5&=a_0+\tfrac{1}{2}a_1-\tfrac{1}{2}a_2-a_3-\frac{\sqrt{3}}{2}b_1-\frac{\sqrt{3}}{2}b_2
\end{aligned}\right\}. \qquad (3.7)$$

To solve these equations for the a's and b's apply the following rule: To find a_n (or b_n), multiply each equation by the coefficient of a_n (or b_n) of that equation and add the results [3]. Applying this rule to eqs (3.7), yields

$$\left.\begin{aligned}
6a_0&=f_0+f_1+f_2+f_3+f_4+f_5\\
3a_1&=f_0+\tfrac{1}{2}f_1-\tfrac{1}{2}f_2-f_3-\tfrac{1}{2}f_4+\tfrac{1}{2}f_5\\
3a_2&=f_0-\tfrac{1}{2}f_1-\tfrac{1}{2}f_2+f_3-\tfrac{1}{2}f_4-\tfrac{1}{2}f_5\\
6a_3&=f_0-f_1+f_2-f_3+f_4-f_5\\
3b_1&=\frac{\sqrt{3}}{2}f_1+\frac{\sqrt{3}}{2}f_2-\frac{\sqrt{3}}{2}f_4-\frac{\sqrt{3}}{2}f_5\\
3b_2&=\frac{\sqrt{3}}{2}f_1-\frac{\sqrt{3}}{2}f_2+\frac{\sqrt{3}}{2}f_4-\frac{\sqrt{3}}{2}f_5
\end{aligned}\right\}. \qquad (3.8)$$

The values of the a's and b's could be obtained directly from these equations without too much difficulty. However, if the present intervals were halved, this would constitute a 12-ordinate system which would yield 12 equations similar to those shown above with some containing at least 12 terms. For such a system the evaluation of the a's and b's would be a tedious process. Therefore, let us show for the six-ordinate system how an addition and subtraction scheme can be developed to aid in the evaluation of the a's and b's.

Suppose the terms in eq (3.8) are regrouped as follows:

$$6a_0=(f_0+f_3)+(f_1+f_4)+(f_2+f_5)$$

$$3a_1=(f_0-f_3)+\tfrac{1}{2}(f_1-f_4)-\tfrac{1}{2}(f_2-f_5)$$

$$3a_2=(f_0+f_3)-\tfrac{1}{2}(f_1+f_4)-\tfrac{1}{2}(f_2+f_5)$$

$$6a_3=(f_0-f_3)-(f_1-f_4)-(f_2-f_5)$$

$$3b_1=\frac{\sqrt{3}}{2}(f_1-f_4)+\frac{\sqrt{3}}{2}(f_2-f_5)$$

$$3b_2=\frac{\sqrt{3}}{2}(f_1+f_4)-\frac{\sqrt{3}}{2}(f_2+f_5).$$

Let us now put

$$f_0+f_3=S_0 \qquad f_0-f_3=D_0$$

$$f_1+f_4=S_1 \qquad f_1-f_4=D_1$$

$$f_2+f_5=S_2 \qquad f_2-f_5=D_2.$$

Then these equations become

$$6a_0=S_0+S_1+S_2$$

$$3a_1=D_0+\tfrac{1}{2}D_1-\tfrac{1}{2}D_2$$

$$3a_2=S_0-\tfrac{1}{2}S_1-\tfrac{1}{2}S_2$$

$$6a_3=D_0-D_1-D_2$$

$$3b_1=\frac{\sqrt{3}}{2}D_1+\frac{\sqrt{3}}{2}D_2$$

$$3b_2=\frac{\sqrt{3}}{2}S_1-\frac{\sqrt{3}}{2}S_2.$$

Finally, substitute

$$S_0=U_0$$

$$S_1+S_2=U_1 \qquad S_1-S_2=V_1$$

$$D_0=R_0 \qquad D_1-D_2=P_1.$$

$$D_1+D_2=R_1$$

Then the equations for finding the coefficients in the Fourier series are

$$\left.\begin{aligned} a_0&=\tfrac{1}{6}(U_0+U_1)\\ a_1&=\tfrac{1}{3}(R_0+\tfrac{1}{2}P_1)\\ a_2&=\tfrac{1}{3}(U_0-\tfrac{1}{2}U_1)\\ a_3&=\tfrac{1}{6}(R_0-R_1)\\ b_1&=\frac{\sqrt{3}}{6}R_1\\ b_2&=\frac{\sqrt{3}}{6}V_1 \end{aligned}\right\}. \qquad (3.9)$$

The results of the addition and subtraction scheme could be tabulated as follows:

	f_0	f_1	f_2	S_0	S_1	D_0	D_1
	f_3	f_4	f_5		S_2		D_2
Sum	S_0	S_1	S_2	U_0	U_1	R_0	R_1
Diff.	D_0	D_1	D_2		V_1		P_1.

A reliable check on the computed a's and b's is obtained by a study of eqs (3.7) which yields

$$f_0=a_0+a_1+a_2+a_3$$

to be used as a check on the a's, and

$$f_1-f_5=\sqrt{3}(b_1+b_2)$$

for a check on the b's.

It should be noted that, since the terms of the Fourier series are additive, it is necessary that the coefficients all be computed to the same number of decimal places.

A system for any number of Fourier coefficients can be developed in the same manner. To expedite this procedure, it can be shown [4] that eqs (3.8) can be written directly from the following (with reference to fig. 3.1):

$$a_0=\frac{1}{2k}\sum_{i=0}^{2k-1} f_i$$

$$\left.\begin{aligned} a_j&=\frac{1}{k}\sum_{i=0}^{2k-1} f_i\cos\frac{ij\pi}{k}\\ b_j&=\frac{1}{k}\sum_{i=0}^{2k-1} f_i\sin\frac{ij\pi}{k} \end{aligned}\right\} j=1, 2, \ldots, k-1.$$

$$a_k=\frac{1}{2k}\sum_{i=0}^{2k-1} f_i\cos i\pi$$

Tables 3.1 and 3.2 give systems for determining 12 and 24 Fourier coefficients, respectively. For other systems the reader is referred to MacDuff and Curreri [4], 48-ordinate system; Running [5], 6-, 8-, 10-, 16-, 20-, etc., ordinate systems; and Pollak [6], 3- through 40-ordinate systems, inclusive.

Since periodic functions having a period different than 2π can be reduced to the form of eq (3.5) by a linear substitution of the independent variable [7], the procedures outlined in this section are also valid for functions having periods other than 2π.

TABLE 3.1. *12-ordinate system (12 Fourier coefficients)*

	f_0	f_1	f_2	f_3	f_4	f_5
	f_6	f_{11}	f_{10}	f_9	f_8	f_7
Sum	S_0	S_1	S_2	S_3	S_4	S_5
Diff.	D_0	D_1	D_2	D_3	D_4	D_5

	S_0	S_1	S_2	D_1	D_2
	S_3	S_5	S_4	D_5	D_4
Sum	U_0	U_1	U_2	R_1	R_2
Diff.	V_0	V_1	V_2	P_1	P_2

	U_1	P_1
	U_2	P_2
Sum	L	H
Diff.	M	G

$$a_0=\tfrac{1}{12}(U_0+L)$$

$$a_1=\tfrac{1}{6}\left(D_0+\frac{\sqrt{3}}{2}V_1+\tfrac{1}{2}V_2\right)$$

$$a_2=\tfrac{1}{6}(V_0+\tfrac{1}{2}M)$$

$$a_3=\tfrac{1}{6}(D_0-V_2)$$

$$a_4=\tfrac{1}{6}(U_0-\tfrac{1}{2}L)$$

$$a_5=\tfrac{1}{6}\left(D_0-\frac{\sqrt{3}}{2}V_1+\tfrac{1}{2}V_2\right)$$

$$a_6=\tfrac{1}{12}(V_0-M)$$

$$b_1=\tfrac{1}{6}\left(D_3+\tfrac{1}{2}R_1+\frac{\sqrt{3}}{2}R_2\right)$$

$$b_2=\frac{\sqrt{3}G}{12}$$

$$b_3=\tfrac{1}{6}(R_1-D_3)$$

$$b_4=\frac{\sqrt{3}H}{12}$$

$$b_5=\tfrac{1}{6}\left(D_3+\tfrac{1}{2}R_1-\frac{\sqrt{3}}{2}R_2\right)$$

Check formulas (check results for a's and b's):

$$\Sigma a=f_0$$

$$(b_1+b_5)\ +2b_3+\sqrt{3}(b_2+b_4)=D_1.$$

TABLE 3.2. *24-ordinate system (24 Fourier coefficients)*

	f_0	f_1	f_2	f_3	f_4	f_5	f_6	f_7	f_8	f_9	f_{10}	f_{11}
	f_{12}	f_{23}	f_{22}	f_{21}	f_{20}	f_{19}	f_{18}	f_{17}	f_{16}	f_{15}	f_{14}	f_{13}
Sum	S_0	S_1	S_2	S_3	S_4	S_5	S_6	S_7	S_8	S_9	S_{10}	S_{11}
Diff.	D_0	D_1	D_2	D_3	D_4	D_5	D_6	D_7	D_8	D_9	D_{10}	D_{11}

	S_0	S_1	S_2	S_3	S_4	S_5
	S_6	S_{11}	S_{10}	S_9	S_8	S_7
Sum	U_0	U_1	U_2	U_3	U_4	U_5
Diff.	V_0	V_1	V_2	V_3	V_4	V_5

	D_1	D_2	D_3	D_4	D_5
	D_{11}	D_{10}	D_9	D_8	D_7
Sum	R_1	R_2	R_3	R_4	R_5
Diff.	P_1	P_2	P_3	P_4	P_5

	U_0	U_1	U_2	P_1	P_2	L_1	G_1
	U_3	U_5	U_4	P_4	P_5	L_2	G_2
Sum	L_0	L_1	L_2	H_1	H_2	C	J
Diff.	M_0	M_1	M_2	G_1	G_2	E	N

$A=\sin 15°=0.2588190$
$B=\cos 15°=0.9659258$

$$a_0=\tfrac{1}{24}(L_0+C)$$

$$a_1=\tfrac{1}{12}\left(D_0+BV_1+\frac{\sqrt{3}}{2}V_2+\frac{1}{\sqrt{2}}V_3+\tfrac{1}{2}V_4+AV_5\right)$$

$$a_2=\tfrac{1}{12}\left(V_0+\frac{\sqrt{3}}{2}M_1+\tfrac{1}{2}M_2\right)$$

$$a_3=\tfrac{1}{12}\left[D_0+\frac{1}{\sqrt{2}}(V_1-V_3-V_5)-V_4\right]$$

$$a_4=\tfrac{1}{12}(M_0+\tfrac{1}{2}E)$$

$$a_5=\tfrac{1}{12}\left(D_0+AV_1-\frac{\sqrt{3}}{2}V_2-\frac{1}{\sqrt{2}}V_3+\tfrac{1}{2}V_4+BV_5\right)$$

$$a_6=\tfrac{1}{12}(V_0-M_2)$$

$$a_7=\tfrac{1}{12}\left(D_0-AV_1-\frac{\sqrt{3}}{2}V_2+\frac{1}{\sqrt{2}}V_3+\tfrac{1}{2}V_4-BV_5\right)$$

$$a_8=\tfrac{1}{12}(L_0-\tfrac{1}{2}C)$$

$$a_9=\tfrac{1}{12}\left[D_0-\frac{1}{\sqrt{2}}(V_1-V_3-V_5)-V_4\right]$$

$$a_{10}=\tfrac{1}{12}\left(V_0-\frac{\sqrt{3}}{2}M_1+\tfrac{1}{2}M_2\right)$$

$$a_{11}=\tfrac{1}{12}\left(D_0-BV_1+\frac{\sqrt{3}}{2}V_2-\frac{1}{\sqrt{2}}V_3+\tfrac{1}{2}V_4-AV_5\right)$$

$$a_{12}=\tfrac{1}{24}(M_0-E)$$

TABLE 3.2. *24-ordinate system (24 Fourier coefficients)*—Continued

$$b_1=\tfrac{1}{12}\left(AR_1+\tfrac{1}{2}R_2+\frac{1}{\sqrt{2}}R_3+\frac{\sqrt{3}}{2}R_4+BR_5+D_6\right)$$

$$b_2=\tfrac{1}{12}\left(\tfrac{1}{2}H_1+\frac{\sqrt{3}}{2}H_2+P_3\right)$$

$$b_3=\tfrac{1}{12}\left[R_2-D_6+\frac{1}{\sqrt{2}}(R_1+R_3-R_5)\right]$$

$$b_4=\frac{\sqrt{3}}{24}J$$

$$b_5=\tfrac{1}{12}\left(BR_1+\tfrac{1}{2}R_2-\frac{1}{\sqrt{2}}R_3-\frac{\sqrt{3}}{2}R_4+AR_5+D_6\right)$$

$$b_6=\tfrac{1}{12}(H_1-P_3)$$

$$b_7=\tfrac{1}{12}\left(BR_1-\tfrac{1}{2}R_2-\frac{1}{\sqrt{2}}R_3+\frac{\sqrt{3}}{2}R_4+AR_5-D_6\right)$$

$$b_8=\frac{\sqrt{3}}{24}N$$

$$b_9=\tfrac{1}{12}\left[D_6-R_2+\frac{1}{\sqrt{2}}(R_1+R_3-R_5)\right]$$

$$b_{10}=\tfrac{1}{12}\left(\tfrac{1}{2}H_1-\frac{\sqrt{3}}{2}H_2+P_3\right)$$

$$b_{11}=\tfrac{1}{12}\left(AR_1-\tfrac{1}{2}R_2+\frac{1}{\sqrt{2}}R_3-\frac{\sqrt{3}}{2}R_4+BR_5-D_6\right)$$

Check formulas (check results for a's and b's):

$$\Sigma a=f_0$$

$$2A(b_1+b_{11})+(b_2+b_{10})+\sqrt{2}(b_3+b_9)+\sqrt{3}(b_4+b_8)+2B(b_5+b_7)+2b_6=D_1.$$

3. Approximation for Aperiodic Functions

3.1. Staircase Function

Let us assume a response function as shown in figure 3.2a. This graphical record may be either a strip-chart record or a photographic record. From this record it is required that the frequency characteristics of the system be determined. Since analytical evaluation of eq (3.4) generally proves rather difficult, it would help us little to find a mathematical expression for $x(t)$. Therefore, an approximate integration by graphical means seems appropriate. To begin with, let us differentiate eq (3.1) with respect to t and eq (3.2) with respect to $j\omega$.

$$\dot{x}(t)=\frac{1}{2\pi}\int_{-\infty}^{\infty}X(j\omega)e^{j\omega t}(j\omega)\,d\omega=(j\omega)x(t) \quad (3.10)$$

and

$$\dot{X}(j\omega)=\int_{-\infty}^{\infty}x(t)e^{-j\omega t}(-t)\,dt=-tX(j\omega). \quad (3.11)$$

Substituting the results of eq (3.10) and (3.11), respectively, into eqs (3.2) and (3.1) gives

$$(j\omega)X(j\omega)=\int_{-\infty}^{\infty}\dot{x}(t)e^{-j\omega t}\,dt \quad (3.12)$$

$$-tx(t)=\frac{1}{2\pi}\int_{-\infty}^{\infty}\dot{X}(j\omega)e^{j\omega t}\,d\omega. \quad (3.13)$$

Equations (3.12) and (3.13) show that differentiation in the time domain corresponds to multiplication by $j\omega$ in the frequency domain, while differentiation in the frequency domain corresponds to multiplication by $-t$ in the time domain.

In a manner analogous to the derivation of eqs (3.3) and (3.4), with an assumption of fictitious odd and even components in $x(t)$ for $t<0$, a similar

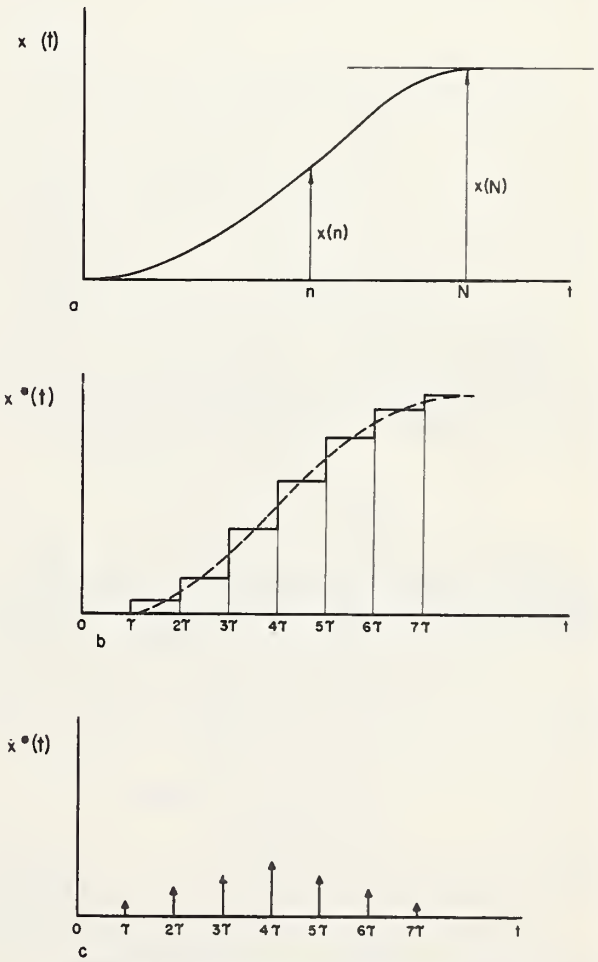

FIGURE 3.2. *Application of the staircase function approximation.*

(a) Response function
(b) Staircase function approximation of the response function
(c) First derivative of the staircase function approximation

set of equations can be derived for eqs (3.12) and (3.13); these are

$$x(t)=-\frac{2}{\pi t}\int_0^\infty \dot{X}_1(\omega)\sin\omega t\,d\omega \qquad (3.14)$$

$$X_1(\omega)=-\frac{1}{\omega}\int_0^\infty \dot{x}(t)\sin\omega t\,dt. \qquad (3.15)$$

Let us consider eq (3.15) and return to the original problem of evaluating the frequency characteristics from figure 3.2a. Eq (3.15) requires that the slope of the original function $x(t)$ be known. This is accomplished by approximating $x(t)$ by a staircase function as shown in figure 3.2b. The derivative of this function is the impulse distribution shown in figure 3.2c. Let the impulses (inclusive of their algebraic signs) be denoted by $a_1, a_2, \ldots, a_k$ and their time of occurrence by $t_1, t_2, \ldots, t_k$, then eq (3.15) yields

$$X_1(\omega)=-\frac{1}{\omega}(a_1\sin\omega t_1+a_2\sin\omega t_2+\ldots+a_k\sin\omega t_k) \qquad (3.16)$$

where k is the number of impulses.

The only error committed in the above analysis is that due to the staircase approximation of $x(t)$. The impulses shown in figure 3.2c are true impulses, so eq (3.16) is good for all values of the frequency ω. By making a less precise staircase approximation (which need not, incidentally, involve uniform increments) an expression for $x(t)$ can be obtained with fewer terms than before. However, this is done at the expense of accuracy. To obtain fewer terms in $x(t)$ without sacrificing accuracy it is necessary to take further advantage of the differentiation characteristics of eqs (3.1) and (3.2). This is discussed in more detail in the following section on straight-line segments.

3.2. Straight-Line Segments

Before introducing the straight-line segment approximation, let us examine more closely the successive differentiation of eqs (3.10) and (3.11) with respect to t and $j\omega$, respectively. Therefore

$$\ddot{x}(t)=(j\omega)\dot{x}(t)$$

and

$$\ddot{X}(j\omega)=-t\dot{X}(j\omega)$$

which by eqs (3.10) and (3.11) become

$$\ddot{x}(t)=(j\omega)^2x(t) \qquad (3.17)$$

and

$$\ddot{X}(j\omega)=(-t)^2X(j\omega). \qquad (3.18)$$

Substituting eqs (3.17) and (3.18) into eqs (3.2) and (3.1), respectively, yields

$$(j\omega)^2X(j\omega)=\int_{-\infty}^{\infty}\ddot{x}(t)e^{-j\omega t}dt \qquad (3.19)$$

and

$$(-t)^2x(t)=\frac{1}{2\pi}\int_{-\infty}^{\infty}\ddot{X}(j\omega)e^{j\omega t}d\omega. \qquad (3.20)$$

Comparing eq (3.20) with eqs (3.1) and (3.10) and eq (3.19) with eqs (3.2) and (3.11), the following general equations evolve:

$$(-t)^nx(t)=\frac{1}{2\pi}\int_{-\infty}^{\infty}X^{(n)}(j\omega)e^{j\omega t}d\omega \qquad (3.21)$$

and

$$(j\omega)^nX(j\omega)=\int_{-\infty}^{\infty}x^{(n)}(t)e^{-j\omega t}dt \qquad (3.22)$$

where the nth derivative of $X(j\omega)$ and $x(t)$ is denoted, respectively, by $X^{(n)}(j\omega)$ and $x^{(n)}(t)$.

The corresponding real part of the time function, eq (3.21) is

$$x(t)=\frac{2(-1)^{\frac{n}{2}}}{\pi t^n}\int_0^\infty X^{(n)}(j\omega)\cos\omega t\,d\omega, \qquad \text{for } n \text{ even} \qquad (3.23)$$

and

$$x(t)=\frac{2(-1)^{\frac{n+1}{2}}}{\pi t^n}\int_0^\infty X^{(n)}(j\omega)\sin\omega t\,dt, \qquad \text{for } n \text{ odd.} \qquad (3.24)$$

Similarly, the real part of the frequency function, eq (3.22), is

$$X_1(\omega)=\frac{(-1)^{\frac{n}{2}}}{\omega^n}\int_0^\infty x^{(n)}(t)\cos\omega t\,d\omega, \qquad \text{for } n \text{ even} \qquad (3.25)$$

and

$$X_1(\omega)=\frac{(-1)^{\frac{n+1}{2}}}{\omega^n}\int_0^\infty x^{(n)}(t)\sin\omega t\,dt, \qquad \text{for } n \text{ odd.} \qquad (3.26)$$

Let us now consider approximating $x(t)$ by straight-line segments as shown in figure 3.3a. Then its first derivative becomes a step approximation, figure 3.3b, and its second derivative a sum of impulses, figure 3.3c. The expression for $X_1(\omega)$ is given by eq (3.25) for $n=2$, therefore

$$X_1(\omega)=\frac{1}{\omega^2}(a_1\cos\omega t_1+a_2\cos\omega t_2+\ldots+a_k\cos\omega t_k) \qquad (3.27)$$

where $a_1, a_2, \ldots a_k$ and $t_1, t_2, \ldots, t_k$ are defined in the same manner as in eq (3.16), and k is now the number of impulses in the presentation of $\ddot{x}(t)$.

The basic difference between the staircase function approximation and the straight-line segment approximation can be readily seen by comparing figures 3.2c and 3.3c. Thus, the latter approximation results in fewer impulses, or an expression for $x(t)$ involving fewer terms. Therefore, for the same number of impulses as in the staircase function approximation, the straight-line segment approximation to $x(t)$ is better.

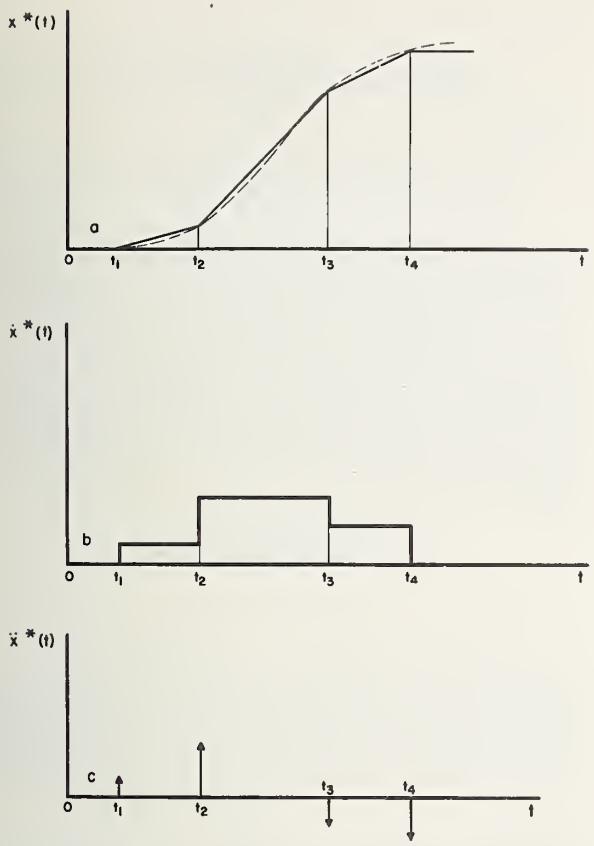

FIGURE 3.3. *Application of the straight line segment approximation.*

(a) Straight line segment approximation of the response function shown in fig. 3.2(a)
(b) First derivative of the straight line segment approximation
(c) Second derivative of the straight line segment approximation

The same line of reasoning can be extended to higher order approximation such as approximating the response function by a second-degree curve. The first derivative of such an approximation is a straight-line segment approximation, while its second derivative is a staircase function approximation. The third derivative is a sum of impulses. Thus, the expression for $x(t)$ is readily obtained by the appropriate form of eq (3.26). There is, however, a great deal of difficulty experienced in implementing this approximation and those of higher order. For this reason, higher order approximations will not be considered further. For a detailed discussion of higher order approximations the reader is directed to the work of Guillemin [1].

3.3. Trapezoidal Method

In section 1, the determination of the amplitude of the frequency characteristic for the stated problem is reduced to the approximate evaluation of eq (3.4), or

$$X_1(\omega)=\int_0^\infty x(t)\cos\omega t\,dt$$

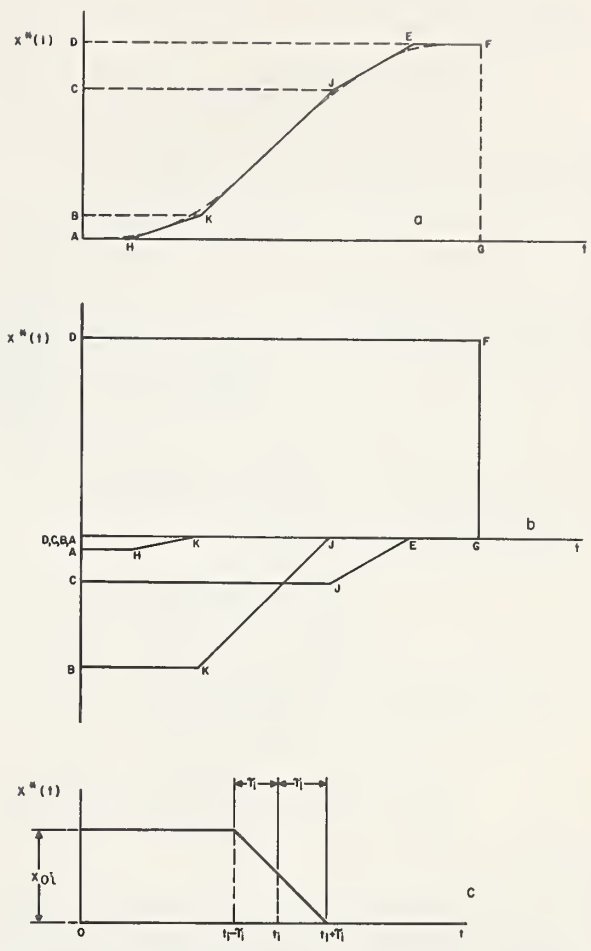

FIGURE 3.4. *Application of the trapezoidal method of approximation.*

(a) Trapezoidal approximation of the response function
(b) Approximating trapezoids
(c) Symhol description for trapezoid

where

$$X_1(\omega)=\mathrm{Re}\,[X(j\omega)].$$

Let us assume the response function to be that shown in figure 3.2a and let it be approximated by the straight-line segments shown in figure 3.3a. For convenience figure 3.3a is repeated as figure 3.4a. It can be seen that the curve $x(t)$ can be approximated piecewise by several trapezoidal boundaries as shown in figure 3.4a. Therefore

$$x(t)\approx\sum_{i=1}^{n}x^*_i(t) \qquad (3.28)$$

where the $x^*_i(t)$ denotes the ith trapezoidal boundary segment of n boundaries shown in figure 3.4b. Substituting eq (3.28) into eq (3.4) yields

$$X_1(\omega)=\sum_{i=1}^{n}\int_0^\infty x^*_i(t)\cos\omega t\,dt. \qquad (3.29)$$

Thus, the frequency response is the sum of inte-

grals of the form

$$X_1(\omega)_i=\int_0^{\infty} x^*_i(t)\cos\omega t\,dt \qquad (3.30)$$

where, with reference to figure 3.4c,

$$x^*_i(t)=\left\{\begin{array}{ll} x_{0i}=\text{const} & 0<t<(t_i-\tau_i) \\ x_{0i}\,\dfrac{t_i+\tau_i-t}{2\tau_i} & (t_i-\tau_i)<t<(t_i+\tau_i) \\ 0 & t>(t_i+\tau_i) \end{array}\right\}. \qquad (3.31)$$

Substituting eq (3.31) into eq (3.30) yields

$$X_1(\omega)=\int_0^{t_i-\tau_i} x_{0i}\cos\omega t\,dt + \int_{t_i-\tau_i}^{t_i+\tau_i} x_{0i}\left(\frac{t_i+\tau_i-t}{2\tau_i}\right)\cos\omega t\,dt$$

$$=x_{0i}\int_0^{t_i+\tau_i}\cos\omega t\,dt+\frac{x_{0i}(t_i+\tau_i)}{2\tau_i} \int_{t_i-\tau_i}^{t_i+t_i\tau_i}\cos\omega t\,dt-\frac{x_{0i}}{2\tau_i}\int_{t_i-\tau_i}^{t_i+\tau_i} t\cos\omega t\,dt.$$

Integrating gives

$$X_1(\omega)_i=\frac{x_{0i}}{\omega}\sin\omega t\Big|_0^{t_i-\tau_i}+\frac{x_{0i}(t_i+\tau_i)}{2\tau_i\omega}\sin\omega t\Big|_{t_i-\tau_i}^{t_i+\tau_i} -\frac{x_{0i}}{2\tau_i\omega}\,t\sin\omega t\Big|_{t_i-\tau_i}^{t_i+\tau_i}-\frac{x_{0i}}{2\tau_i\omega^2}\cos\omega t\Big|_{t_i-\tau}^{t_i+\tau^i}$$

$$=\frac{x_{0i}}{2\tau_i\omega}\Big\{2\tau_i\sin\omega(t_i-\tau_i)+(t_i+\tau_i) \times[\sin\omega(t_i+\tau_i)]-(t_i+\tau_i)\sin\omega(t_i-\tau_i) -(t_i+\tau_i)\sin\omega(t_i+\tau_i)+(t_i-\tau_i) \times[\sin\omega(t_i-\tau_i)]-\frac{1}{\omega}[\cos\omega(t_i+\tau_i) -\cos\omega(t_i-\tau_i)]\Big\}$$

or

$$X_1(\omega)_i=-\frac{x_{0i}}{2\tau_i\omega^2}[\cos\omega(t_i+\tau_i)-\cos\omega(t_i-\tau_i)] \qquad (3.32)$$

where

$$\cos\omega(t_i+\tau_i)-\cos\omega(t_i-\tau_i)=-2\sin\omega t_i\sin\omega\tau_i.$$

Therefore, eq (3.32) becomes

$$X_1(\omega)_i=\frac{x_{0i}}{\tau_i\omega^2}\sin\omega t_i\sin\omega\tau_i$$

or

$$X_1(\omega)_i=(x_{0i}t_i)\left(\frac{\sin\omega t_i}{\omega t_i}\right)\left(\frac{\sin\omega\tau_i}{\omega\tau_i}\right).$$

Therefore,

$$X_1(\omega)=\sum_{i=1}^{n}(x_{0i}t_i)\left(\frac{\sin\omega t_i}{\omega t_i}\right)\left(\frac{\sin\omega\tau_i}{\omega\tau_i}\right). \qquad (3.33)$$

The evaluation of eq (3.33) does not present any difficulties, especially if tables of the function $\frac{\sin x}{x}$ are available. For tables of $\frac{\sin x}{x}$ the reader is referred to the work by Solodovnikov [8], where five-place tables appear in Appendix 1 for arguments of ranging from 0 to 10 in increments of 0.01, from 10 to 20 in increments of 0.1, and from 20 to 100 in increments of 1.

3.4. $\frac{\text{Sin } x}{x}$ Approximation

In this section $\frac{\sin x}{x}$ will be used to approximate the response function $x(t)$. Shannon [9] noted that the spectrum for almost all response functions had an upper limit, say ω_c. Shannon also proved that a function of this type could be synthesized exactly by a sum of functions of the type $\frac{\sin x}{x}$. Synthesis of a response curve by $\frac{\sin x}{x}$ functions is shown in figure 3.5. For purposes of clarity only portions of the $\frac{\sin x}{x}$ curves are shown. The response function can be expressed as

$$x^*(t)=\sum_{n=0}^{\infty} A_n\frac{\sin\omega_c(t-n\tau)}{\omega_c(t-n\tau)}, \qquad (3.34)$$

where A_n, the amplitude of $\frac{\sin x}{x}$, is equal to the ordinate of the response function at $t=n\tau$, and τ is the time spacing, which must be smaller than or equal to π/ω_c.

Substituting eq (3.34) into eq (3.2) yields

$$X(j\omega)=\sum_{n=0}^{\infty}\int_{-\infty}^{\infty} A_n\frac{\sin\omega_c(t-n\tau)}{\omega_c(t-n\tau)}e^{-j\omega t}\,dt, \qquad (3.35)$$

where $X(j\omega)$ is the complex frequency characteristic of the system. To eliminate the exponential form of the transform, we evaluate the real part of eq (3.35). The Re $[X(j\omega)]$ is

$$X_1(\omega)=\sum_{n=0}^{\infty}\frac{A_n}{\omega_c}\int_{-\infty}^{\infty}\frac{\sin\omega_c(t-n\tau)}{(t-n\tau)}\cos\omega t\,dt. \qquad (3.36)$$

Hence, the frequency response is the sum of integrals of the form

$$X_1(\omega)_n=\frac{A_n}{\omega_c}\int_{-\infty}^{\infty}\frac{\sin\omega_c(t-n\tau)}{(t-n\tau)}\cos\omega t\,dt. \qquad (3.37)$$

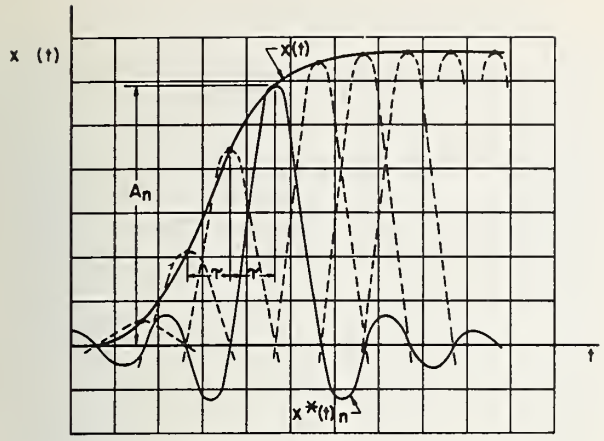

FIGURE 3.5. $\frac{\sin x}{x}$ *approximation of the response curve shown in figure 3.2.*

(Reproduced from [11] with permission from Proc. IRE)

Evaluation of eq (3.37) involves a number of trigonometric manipulations. The substitution of $\sin \omega_c t \cos n\omega_c\tau - \sin n\omega_c\tau \cos \omega_c t = \sin \omega_c(t-n\tau)$ into eq (3.37) gives

$$X_1(\omega)_n$$

$$= \frac{A_n}{\omega_c} \int_{-\infty}^{\infty} \left[\frac{(\sin \omega_c t \cos n\omega_c\tau - \sin n\omega_c\tau \cos \omega_c t)}{(t-n\tau)} \right] \times [\cos \omega t]\, dt$$

$$= \frac{A_n}{\omega_c} \left\{ \cos n\omega_c\tau \int_{-\infty}^{\infty} \frac{\sin \omega_c t \cos \omega t}{(t-n\tau)}\, dt - \sin n\omega_c\tau \int_{-\infty}^{\infty} \frac{\cos \omega_c t \cos \omega t\, dt}{(t-n\tau)} \right\}. \quad (3.38)$$

However, $\sin \omega_c t \cos \omega t = \frac{1}{2} \sin (\omega+\omega_c)t - \frac{1}{2} \sin [(\omega-\omega_c)]t$ and $\cos \omega_c t \cos \omega t = \frac{1}{2} \cos (\omega+\omega_c)t + \frac{1}{2} \cos [(\omega-\omega_c)]t$. Therefore, eq (3.38) becomes

$$X_1(\omega)_n = \frac{A_n}{2\omega_c} \left\{ \cos n\omega_c\tau \left[\int_{-\infty}^{\infty} \frac{\sin (\omega+\omega_c)t\, dt}{(t-n\tau)} - \int_{-\infty}^{\infty} \frac{\sin (\omega-\omega_c)t\, dt}{(t-n\tau)} \right] - \sin n\omega_c\tau \times \left[\int_{-\infty}^{\infty} \frac{\cos (\omega+\omega_c)t}{(t-n\tau)}\, dt + \int_{-\infty}^{\infty} \frac{\cos (\omega-\omega_c)t}{(t-n\tau)}\, dt \right] \right\}.$$

At this point let $t-n\tau=z$, thus $dt=dz$. The limits of $-\infty$ to ∞ remain unchanged for this substitution. Also let $\omega-\omega_c=\alpha$, and $\omega+\omega_c \| \beta$. Then

$$X_1(\omega)_n = \frac{A_n}{2\omega_c} \left\{ \cos n\omega_c\tau \left[\int_{-\infty}^{\infty} \frac{\sin \beta(z+n\tau)dz}{z} - \int_{-\infty}^{\infty} \frac{\sin \alpha(z+n\tau)dz}{z} \right] - \sin n\omega_c\tau \times \left[\int_{-\infty}^{\infty} \frac{\cos \beta(z+n\tau)dz}{z} + \int_{-\infty}^{\infty} \frac{\cos \alpha(z+n\tau)dz}{z} \right] \right\}.$$

Expanding the sine and cosine functions in the above equation for the sum and difference of two angles, and factoring out the non-integrable terms, $X_1(\omega)_n$ becomes

$$X_1(\omega)_n = \frac{A_n}{2\omega_c} \left\{ \cos n\omega_c\tau \left[\cos n\beta\tau \int_{-\infty}^{\infty} \frac{\sin \beta z\, dz}{z} + \sin n\beta\tau \int_{-\infty}^{\infty} \frac{\cos \beta z\, dz}{z} - \cos n\alpha\tau \int_{-\infty}^{\infty} \frac{\sin \alpha z\, dz}{z} - \sin n\alpha\tau \int_{-\infty}^{\infty} \frac{\cos \alpha z\, dz}{z} \right] - \sin n\omega_c\tau \times \left[\cos n\beta\tau \int_{-\infty}^{\infty} \frac{\cos \beta z\, dz}{z} - \sin n\beta\tau \int_{-\infty}^{\infty} \frac{\sin \beta z\, dz}{z} + \cos n\alpha\tau \int_{-\infty}^{\infty} \frac{\cos \alpha z\, dz}{z} - \sin n\alpha\tau \times \left(\int_{-\infty}^{\infty} \frac{\sin \alpha z\, dz}{z} \right) \right] \right\}. \quad (3.39)$$

The improper integrals in eq (3.39) are now in a form such that known properties of improper integrals may be introduced to aid in their evaluation. For example, integrands of the form $\frac{\cos cx}{x}$, where c is a constant, are odd functions which have a Cauchy Principal Value of

$$\int_{-\infty}^{\infty} \frac{\cos cx\, dx}{x} = 0. \quad (3.40)$$

Also, integrands of the form $\frac{\sin cx}{x}$ are even functions and

$$\int_{-\infty}^{\infty} \frac{\sin cx}{x} dx = 2 \int_{0}^{\infty} \frac{\sin cx}{x} dx. \quad (3.41)$$

The latter form of the improper integral is found in standard integral tables [10], which gives

$$\int_0^{\infty} \frac{\sin cx}{x} dx = \begin{cases} \frac{\pi}{2}, & c>0 \\ 0, & c=0 \\ -\frac{\pi}{2}, & c<0. \end{cases} \quad (3.42)$$

In eq (3.39) put $x=z$ and $c=\alpha=\omega-\omega_c$, where ω_c is the upper limit on the frequency. Therefore,

$\alpha<0$ and eq (3.41) yields

$$2\int_0^\infty \frac{\sin \alpha z}{z}\,dz \doteq -\pi. \tag{3.43}$$

Also, $c=\beta=\omega+\omega_c$; therefore $\beta>0$ and eq (3.41) gives

$$2\int_0^\infty \frac{\sin \beta z}{z}\,dz = \pi. \tag{3.44}$$

Substituting eqs (3.40), (3.43), and (3.44) into eq (3.39), eq (3.39) becomes

$$X_1(\omega)_n=\frac{\pi A_n}{2\omega_c}\{\cos n\omega_c\tau(\cos n\beta\tau+\cos n\alpha\tau) + \sin n\omega_c\tau(\sin n\beta\tau-\sin n\alpha\tau)\}. \tag{3.45}$$

Reintroducing $\alpha=\omega-\omega_c$ and $\beta=\omega+\omega_c$ into eq (3.45), expanding the sine and cosine for the sum and difference of two angles, multiplying and removing common factors, eq (3.45) finally becomes

$$X_1(\omega)_n=\frac{\pi A_n}{\omega_c}\cos n\omega\tau. \tag{3.46}$$

The frequency response for the system is

$$X_1(\omega)=\frac{\pi}{\omega_c}\sum_{n=0}^{\infty} A_n \cos n\omega\tau, \qquad \text{for } \tau\leq\frac{\pi}{\omega_c} \tag{3.47}$$

This equation relates the frequency response to the measured points A_0, A_1, A_2, . . . of the response curve.

In laying out the response function in equal intervals of τ at which the A's are to be measured, the first point ($n=0$) should not be more than one interval to the right of the first variation in the curve, figure 3.6. Also, the intervals should continue to the point where the curve ceases to vary.

In a problem similar to the above, Samulon [11] has developed an expression which considers measuring the first difference of the A's, A_n-A_{n-1} rather than A_n. He also developed a number of tables and nomographs to facilitate numerical evaluation. The original tables and nomographs are for 0.05 μ sec-intervals; however, these can be scaled to fit most problems.

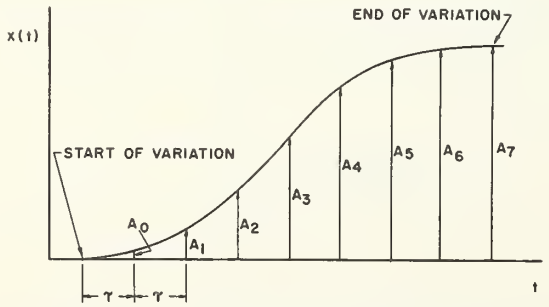

FIGURE 3.6. *Interval layout of response curve.*

3.5. Number Series Transformation

The number series transformation method was first introduced by Tustin [12] in 1947. Since that time Madwed [13] has been a principal contributor in this area. The fundamental idea behind the number series transformation method is the concept of representing or approximating a function $f(t)$ by a number series. For our purpose $f(t)$ will hereafter be denoted as the response function $x(t)$. Therefore, $x(t)$ is the dependent variable, displacement, and t is the independent variable, time. Since the independent variable is time, the number series is called a time series. To best present this method let us illustrate it in the form of an example. Again let us take the response function, shown in figure 3.2a, and approximate it in turn by a triangular, rectangular, step, and ramp time series transformation. The triangular time series transformation is presented in detail whereas only the results and pertinent details are given for the rectangular, step, and ramp time series transformation.

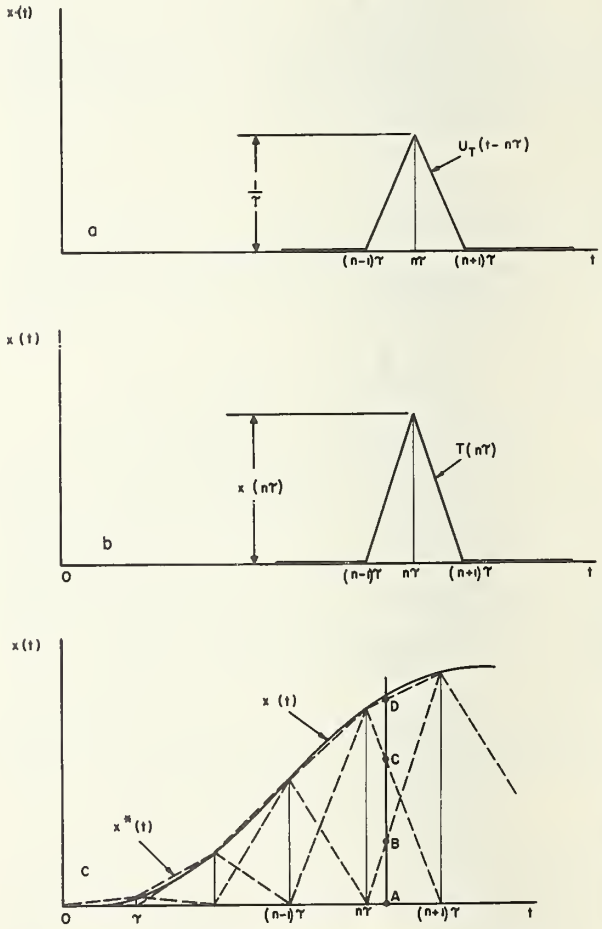

FIGURE 3.7. *Triangular time series transformation.*

(a) Unit triangular pulse function
(b) Triangular pulse function
(c) Triangular

a. Triangular Time Series Transformation

Any continuous arbitrary function $x(t)$ can be approximated by a set of triangular pulse functions, all of which have the same width, as shown in figure 3.7c. When $x(t)$ is approximated in this manner for analytical purposes, then by definition this approximation for $x(t)$ is called triangular time series transformation. For symbol simplicity all time series transformations or approximations of $x(t)$ will be denoted by $x^*(t)$. With reference to figure 3.7c, it is easily recognized that when a line is drawn parallel to the ordinate at point A on the abscissa, it cuts two adjacent pulses at B and C. The distance AD is laid off equal to the sum of AB and AC, and thus establishes a point on the approximate curve $x^*(t)$. It can be shown that repeating this process for an infinite number of points in a given time interval τ results in a chord approximation of $x(t)$ in that interval. Therefore, the sum of all the triangular pulse functions from $t=0$ to $t=\infty$ gives the chord approximation of $x(t)$ or $x^*(t)$.

Before developing an analytical expression for $x^*(t)$, let us first define two basic quantities used in the triangular time series transformation. The first quantity to be defined is the unit triangular pulse function rising at time $t=(n-1)\tau$, shown in figure 3.7a, and denoted by $U_T(t-n\tau)$. By definition the area enclosed between the unit triangular pulse function and the time axis is equal to unity. Therefore, with a base dimension of 2τ, the altitude of the unit triangular pulse function must be equal to $1/\tau$. The properties of the unit triangular pulse function then become

$$U_T(t-n\tau)=\begin{cases}0 & \text{for } t<(n-1)\tau\\ \dfrac{t-(n-1)\tau}{\tau^2} & \text{for } (n-1)\tau\leq t\leq n\tau\\ \dfrac{1}{\tau} & \text{for } t=n\tau\\ \dfrac{(n+1)\tau-t}{\tau^2} & \text{for } n\tau\leq t\leq(n+1)\tau\\ 0 & \text{for } t>(n+1)\tau.\end{cases} \tag{3.48}$$

The second quantity to be defined is the general triangular pulse function, shown in figure 3.7b, and denoted by T. By definition the triangular pulse function is equal to the area enclosed between the triangular pulse function and the time axis, multiplied by the unit triangular pulse function. Therefore, the nth triangular pulse function at $x(n\tau)$ is

$$T(n\tau)=\tau x(n\tau)U_T(t-n\tau). \tag{3.49}$$

It is now possible to write an analytical expression for the triangular time series transformation, since the response function can be approximated by summing the triangular pulse function, eq (3.49), from $n=0$ to $n=\infty$. Therefore

$$x^*(t)=\tau\sum_{n=0}^{\infty}x(n\tau)U_T(t-n\tau), \tag{3.50}$$

where $U_T(t-n\tau)$ is given by eq (3.48). Having once established the approximation to the response function $x^*(t)$, this approximation can then be substituted into the unilateral Fourier transform eq (1.20), thus achieving the desired transformation of the response function from the time to the frequency domain.

b. Rectangular Time Series Transformation

A unit rectangular pulse function, denoted by $U_R(t-n\tau)$, is shown in figure 3.8a. Since, by definition, the area enclosed by the unit rectangular pulse function and the time axis must be equal to unity, it can be seen that the height of the rectangle must be $1/\tau$. Therefore, the properties

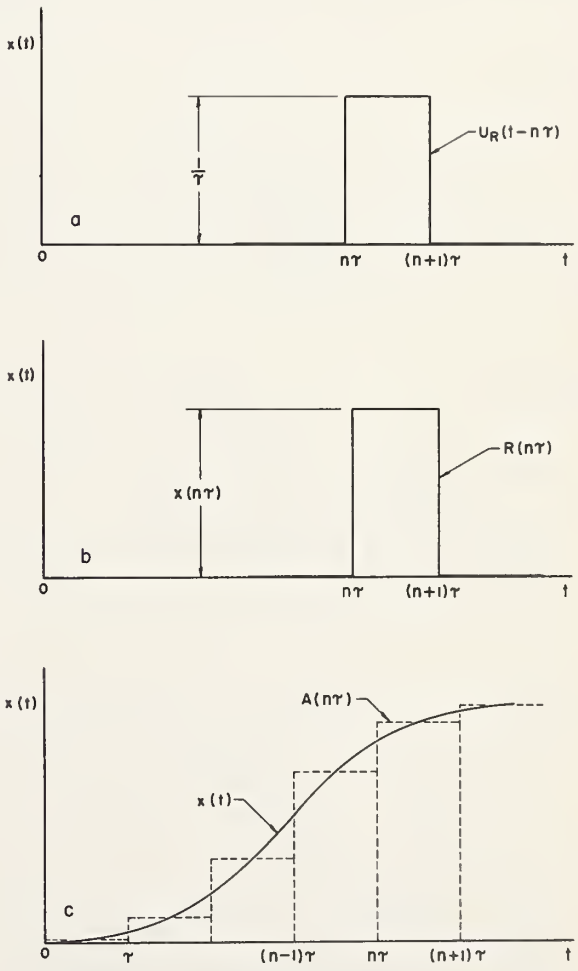

FIGURE 3.8. *Rectangular time series transformation.*

(a) Unit rectangular pulse function
(b) Rectangular pulse function
(c) Rectangular pulse function approximation of the response function

of the unit rectangular pulse function are

$$U_R(t-n\tau)=\begin{cases}0 & \text{for } t<n\tau\\ 1/\tau & \text{for } n\tau\le t\le(n+1)\tau\\ 0 & \text{for } t>(n+1)\tau.\end{cases} \quad (3.51)$$

The general rectangular pulse function, shown in figure 3.8b, is denoted by R and is defined as the area under the pulse function multiplied by the unit pulse function. That is,

$$R(n\tau)=\tau x(n\tau)U_R(t-n\tau). \quad (3.52)$$

Since the ordinate $x(n\tau)$ is not uniquely determined for the rectangular pulse function approximation, and since $\tau x(n\tau)$ is the area of the nth rectangular pulse, an approximation to the area under the curve $x(t)$ in the interval between $n\tau$ and $(n+1)\tau$ is

$$\tau x(n\tau)=A(n\tau)\approx\int_{n\tau}^{(n+1)\tau}x(t)dt, \quad (3.53)$$

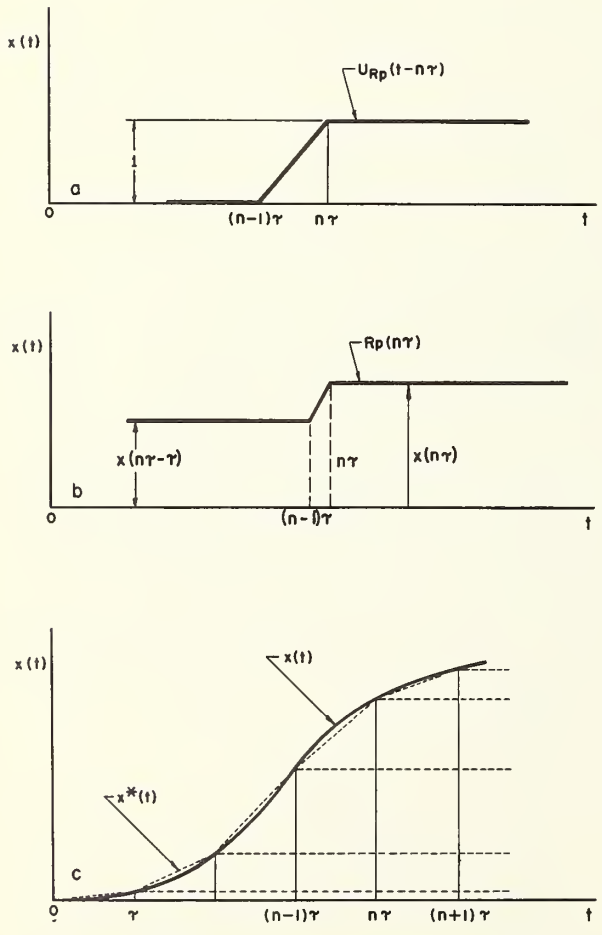

FIGURE 3.9. *Ramp time series transformation.*

(a) Unit ramp function
(b) Ramp function
(c) Ramp function approximation of the response function

where $A(n\tau)$ is the area under the nth rectangular pulse, then $x(n\tau)$ is defined to be

$$x(n\tau)=\frac{A(n\tau)}{\tau}\approx\frac{1}{\tau}\int_{n\tau}^{(n+1)\tau}x(t)dt. \quad (3.54)$$

Therefore, eq. (3.52) becomes

$$R(n\tau)=A(n\tau)U_R(t-n\tau) \quad (3.55)$$

and the rectangular time series transformation is given by

$$x^*(t)=\sum_{n=0}^{\infty}A(n\tau)U_R(t-n\tau), \quad (3.56)$$

where $U_R(t-n\tau)$ and $A(n\tau)$ are given, respectively, by eqs (3.51) and (3.53). The rectangular pulse function approximation is shown in figure 3.8c.

c. Ramp Time Series Transformation

Figure 3.9a shows a unit ramp function which is denoted by $U_{Rp}(t-n\tau)$. By definition the height of a unit ramp function is equal to unity. Therefore, the unit ramp function properties become

$$U_{Rp}(t-n\tau)=\begin{cases}0 & \text{for } t<(n-1)\tau\\ \dfrac{t-(n-1)\tau}{\tau} & \text{for } (n-1)\tau\le t\le n\tau\\ 1 & \text{for } t>n\tau.\end{cases} \quad (3.57)$$

The general ramp function, denoted by Rp and shown in figure 3.9b, can be defined as follows:

$$Rp(n\tau)=\{x(n\tau)-x(n\tau-\tau)\}U_{Rp}(t-n\tau). \quad (3.58)$$

Therefore, the ramp time series transformation is expressed as [3]

$$x^*(t)=\sum_{n=0}^{\infty}\{x(n\tau)-x(n\tau-\tau)\}U_{Rp}(t-n\tau) \quad (3.59)$$

where $U_{Rp}(t-n\tau)$ is defined by eq (3.57).

d. Step Time Series Transformation

The unit step function, shown in figure 3.10a, is denoted by $U_S(t-n\tau)$ and has the following properties

$$U_S(t-n\tau)=\begin{cases}0 & \text{for } t<n\tau\\ 1 & \text{for } t\ge n\tau.\end{cases} \quad (3.60)$$

The general step function is denoted by S and is shown in figure 3.10b. The expression for the nth step function is

$$S(n\tau)=[x(n\tau)-x(n\tau-\tau)]U_S(t-n\tau). \quad (3.61)$$

[3] From the definition of a unit triangular pulse function, it follows that a unit ramp function for $n=0$ can be expressed as a summation of the triangular pulse function, that is

$$U_{Rp}(t)=\tau\sum_{n=0}^{\infty}U_T(t-n\tau).$$

Also the triangular pulse and ramp function times series transformation results in a straight-line approximation of the original function.

Again the ordinates $x(n\tau)$ and $x(n\tau-\tau)$ are not uniquely determined for the step function approximation. However, let us define them, with reference to figure 3.10c, in a manner analogous to the evaluation of the ordinate $x(n\tau)$ for the rectangular pulse function approximation (i.e., $x(n\tau)$, defined by eq (3.54), repeated here for clarity):

$$x(n\tau)=\frac{A(n\tau)}{\tau}\approx\frac{1}{\tau}\int_{n\tau}^{(n+1)\tau}x(t)dt \qquad (3.54)$$

and

$$x(n\tau-\tau)=\frac{A(n\tau-\tau)}{\tau}\approx\frac{1}{\tau}\int_{(n-1)\tau}^{n\tau}x(t)dt. \qquad (3.62)$$

Therefore, eq (3.61) becomes

$$S(n\tau)=\frac{1}{\tau}\{A(n\tau)-A(n\tau-\tau)\}U_S(t-n\tau). \qquad (3.63)$$

Thus the step-time series transformation can be expressed as [4]

$$x^*(t)=\frac{1}{\tau}\sum_{n=0}^{\infty}\{A(n\tau)-A(n\tau-\tau)\}U_S(t-n\tau) \qquad (3.64)$$

where $A(n\tau)$ and $U_S(t-n\tau)$ are defined by eqs (3.53) and (3.60), respectively.

3.6. Pseudo-Rectangular Pulse Approximation

Let us consider the unilateral Fourier integral as given by eq (1.20) and rewritten in a notation that complies with the response, i.e.,

$$X(j\omega)=\int_0^{\infty}x(t)e^{-j\omega t}\,dt, \qquad (3.65)$$

where $X(j\omega)$ denotes the complex response spectrum of the response function $x(t)$.

Bowersox and Carlson [14] applied the fundamental theorem of calculus to eq (3.65) and obtained

$$X(j\omega)=\Delta t\sum_{n=1}^{\infty}x(n)e^{-jn\theta} \qquad (3.66)$$

where $\theta=\omega\Delta t$. Let us now consider a response function $x(t)$ which reaches a steady-state condition, such as the response shown in figure 3.2a. Then eq (3.66) becomes

$$X(j\omega)=\Delta t\left\{\sum_{n=1}^{N}x(n)e^{-jn\theta}+\Delta t x(N)\sum_{n=N+1}^{\infty}e^{-jn\theta}\right\} \qquad (3.67)$$

where $x(N)$ is the amplitude of the response function at time $t=N\Delta t$, the time for which the response function first reaches the steady-state condition. The summation part of the last term in eq (3.67) is recognized as the geometric series and can be written as

$$\sum_{n=N+1}^{\infty}e^{-jn\theta}=\frac{e^{-j(N+1)\theta}}{1-e^{-j\theta}}.$$

Therefore, eq (3.67) becomes

$$X(j\omega)=\Delta t\left\{\sum_{n=1}^{N}x(n)e^{-jn\theta}+\frac{x(N)e^{-j(N+1)\theta}}{1-e^{-j\theta}}\right\}. \qquad (3.68)$$

Schweppe [15] defined $X(j\omega)$ to be

$$X(j\omega)=(X+jY)e^{-\frac{j\theta}{2}\Delta t} \qquad (3.69)$$

for which the amplitude of the response spectrum

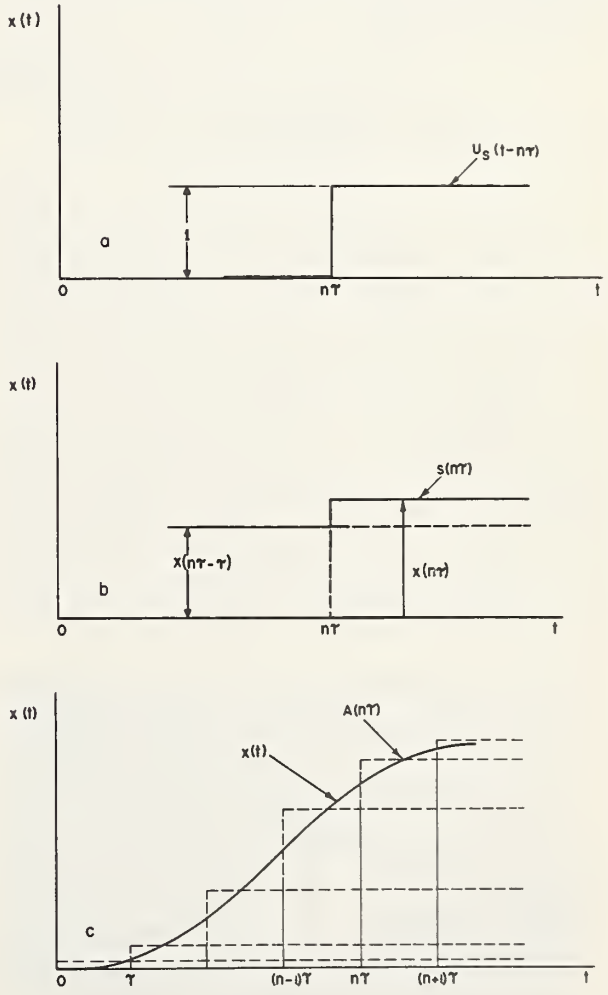

FIGURE 3.10. *Step time series transformation.*

(a) Unit step function
(b) Step function
(c) Step function approximation of the response function

[4] From the definition of a unit rectangular pulse function, it follows that a unit step function for $n=0$ can be expressed as a summation of the rectangular pulse function, that is

$$U_S(t)=\tau\sum_{n=0}^{\infty}U_R(t-n\tau).$$

Also, that the rectangular pulse and step function time series transformation results in a step curve approximation of the original function.

is given by

$$X(\omega)=\text{mod } X(j\omega)=\sqrt{X^2+Y^2} \qquad (3.70)$$

and its phase angle by

$$\alpha(\omega)=\arg X(j\omega)=\text{arc tan}\frac{Y}{X}-\frac{\theta}{2}. \qquad (3.71)$$

Rewriting eq (3.68) to include the definition of $X(j\omega)$, as given by eq (3.69), gives

$$(X+jY)e^{-\frac{j\theta}{2}}\Delta t=\Delta t\left\{\sum_{n=1}^{N}x(n)e^{-jn\theta}+\frac{x(N)e^{-j(N+1)\theta}}{1-e^{-j\theta}}\right\}. \qquad (3.72)$$

Equation (3.72) can be separated into real and imaginary parts [14]

$$X=\sum_{n=1}^{N}x(n)\cos n\theta-\frac{x(N)}{2}\left(\sin N\theta\cot\frac{\theta}{2}+\cos N\theta\right) \qquad (3.73)$$

$$Y=-\sum_{n=1}^{N}x(n)\sin n\theta-\frac{x(N)}{2}\left(\cos N\theta\cot\frac{\theta}{2}-\sin N\theta\right). \qquad (3.74)$$

Therefore, given a response function $x(t)$ which reaches a steady-state condition, the amplitude of the response spectrum is given by eq (3.70), and its phase by eq (3.71), where X and Y are given respectively by eqs (3.73) and (3.74), and $\theta=\omega\Delta t$.

The fundamental theorem of calculus is based on approximating the area under a curve by elemental rectangular areas. The error involved in such an approximation is directly related to the width of the elemental area, as, in this case, the time increment. A better approximation to the problem could be found in the adoption of the trapezoidal approximation or Simpson's rule [16].

4. Instrumental Aids

4.1. Henderson's Mechanical Harmonic Analyzer

The need to remove the tedium from numerical analysis is ever present. Henderson [17] developed the mechanical harmonic analyzer shown in figure 3.11 to fill this need. The analyzer is synthesized on the fact that any periodic function $f(t)$ can be represented by a Fourier series of the form given by eq (1.6), in which the coefficients are determined by the integral forms of eqs (1.7) and (1.8). Evaluation of these integrals for a given periodic function $f(t)$ is known as harmonic analysis, and is the sole job of the analyzer. The analyzer shown schematically in figure 3.12 essentially does just that. That is, on tracking a curve over one complete period, the displacement of the resolver plate gives a vector that represents the amplitude and phase of the derivative of a harmonic present in the curve. The fact that the instrument gives the derivative of the sinusoidal components, rather than the components themselves, is no disadvantage when analyzing periodic functions, as will be shown later.

With reference to figure 3.12, a brief description of the operation of the analyzer is as follows: the curve to be analyzed is placed on table a, which is moved from right to left either by a motor or by the handwheel labeled "traverse." As the table moves it drives a variable-speed gear, b,

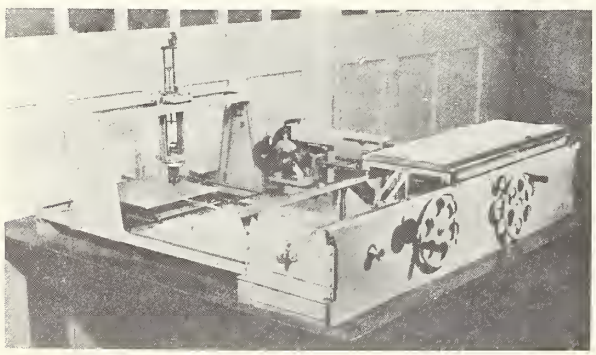

FIGURE 3.11. *Henderson's mechanical harmonic analyzer.*

(Reproduced from [17] with permission from Engineering)

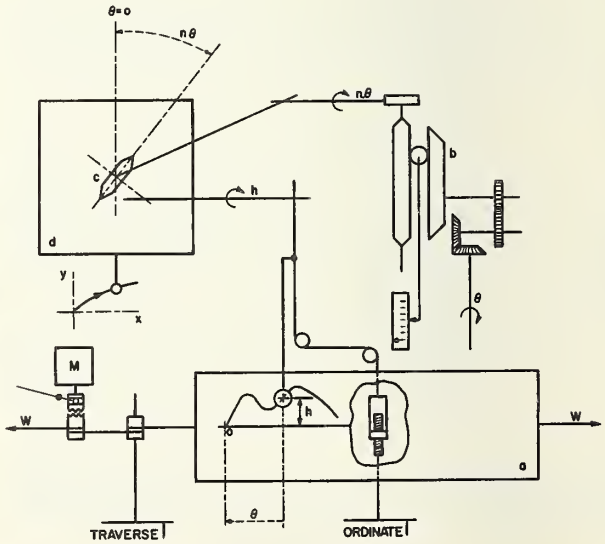

FIGURE 3.12. *Schematic of Henderson's mechanical harmonic analyzer.*

(Reproduced from [17] with permission from Engineering)

which causes the friction wheel, c, to rotate about its vertical axis, perpendicular to the resolver plate, d. The friction wheel makes contact with, and drives, the resolver plate, which is a flat plate free to move in the horizontal plane, but unable to rotate; its movement is recorded by a rigidly attached stylus. The friction wheel is driven about its horizontal axis by a flexible wire coupled to the cursor, which is operated manually by the handwheel labeled "ordinate." The rotary motion of the wheel is proportional to the change in the ordinate of the curve.

Before the start of analysis, the analyzer must first be initialized, that is, the friction wheel is alined with $\theta=0$, as indicated in figure 3.12, when the cursor is at the origin of the curve. Then the variable-speed gear is adjusted to give n (the harmonic of the curve to be determined) revolutions to the friction wheel as the cursor is moved through one period. The analyzer is now ready to determine the nth harmonic of the curve.

Let us consider the motion of the resolver plate when the curve has been moved an amount θ, and then incremented by $d\theta$. The corresponding change in the ordinate is dh, hence, the friction wheel, which is at an angle of $n\theta$ to its original direction, will drive the resolver plate $\alpha\, dh$ in the direction of $n\theta$. The constant α is denoted as the amplification factor. Then the displacements in the x and y directions become

$$dx=\alpha\frac{dh}{d\theta}\sin n\theta\, d\theta$$

and

$$dy=\alpha\frac{dh}{d\theta}\cos n\theta\, d\theta.$$

If the curve is tracked continuously throughout one period, the final coordinates of the locus traced by the resolver plate are given by

$$x=\alpha\int_0^{2\pi}\frac{dh}{d\theta}\sin n\theta\, d\theta \tag{3.75}$$

and

$$y=\alpha\int_0^{2\pi}\frac{dh}{d\theta}\cos n\theta\, d\theta \tag{3.76}$$

where $\frac{dh}{d\theta}=\frac{d}{d\theta}\,[f(\theta)]$. Substituting $\omega t=\theta$ into eq (1.6), $\frac{dh}{d\theta}$ becomes

$$\frac{dh}{d\theta}=-a_1\sin\theta-2a_2\sin 2\theta-\ldots-na_n\sin n\theta$$
$$+b_1\cos\theta+2b_2\cos 2\theta+\ldots+nb_n\cos n\theta. \tag{3.77}$$

Substituting eq (3.77) into eqs (3.75) and (3.76) gives

$$x=-n\alpha a_n\int_0^{2\pi}\sin^2 n\theta\, d\theta+n\alpha b_n\int_0^{2\pi}\sin n\theta\cos n\theta\, d\theta$$

$$y=-n\alpha a_n\int_0^{2\pi}\sin n\theta\cos n\theta\, d\theta+n\alpha b_n\int_0^{2\pi}\cos^2 n\theta\, d\theta$$

for which it can be readily shown that

$$\int_0^{2\pi}\sin^2 n\theta\, d\theta=\int_0^{2\pi}\cos^2 n\theta\, d\theta=\pi$$

$$\int_0^{2\pi}\sin n\theta\cos n\theta\, d\theta=0.$$

Therefore,

$$x=-\pi n\alpha a_n$$

$$y=\pi n\alpha b_n$$

or

$$a_n=-\frac{x}{\pi n\alpha} \tag{3.78}$$

$$b_n=\frac{y}{\pi n\alpha}. \tag{3.79}$$

Thus, the resultant vector of the locus traced by the resolver plate has rectangular components that are proportional to the Fourier coefficients a_n and b_n. Therefore, the resultant vector represents the amplitude and phase of the nth harmonic in the derivative of the tracked curve.

As mentioned earlier, the analyzer gives the derivatives of the sinusoidal components rather than the components themselves. Let us now look at this more closely. To aid us in this interpretation let us recognize that taking the derivative of a sinusoidal quantity results in another sinusoidal quantity n times larger and 90 degrees in advance of the first. That is $\frac{d}{d\theta}(\cos n\theta)$ $=-n\sin n\theta=n\cos\left(n\theta+\frac{\pi}{2}\right)$. Thus, by interchanging the designation of the reference axes and by dividing the projections of the resultant vector of the traced locus by the harmonic order, the true components present in the tracked curve are obtained. The equations for the coefficients a_n and b_n, eqs (3.78) and (3.79), respectively, must be rewritten to comply with this change as follows:

$$a_n=\frac{y}{\pi n^2\alpha} \tag{3.80}$$

and

$$b_n=-\frac{x}{\pi n^2\alpha}. \tag{3.81}$$

Let us further illustrate this point by an example. Figure 3.13a shows the waveform to be analyzed and figure 3.13b shows the results of the analysis for the first two harmonics. The projections of the resultant vector, shown as a dotted line extending from point O to A in figure 3.13b, on the x and y axes corresponding to the components present in the derivative curve. Thus, by eqs (3.78) and (3.79) the fundamental terms in the derivative of the waveform are $0.39\sin\theta$ and

0.714 cos θ. The analytical results for the fundamental terms of this same waveform are 0.7sinθ and 0.405 cos θ. Comparison of the fundamental terms shows that the coefficients should be interchanged for agreement. Therefore, eqs (3.80) and (3.81) will yield the correct results, since they were written purposely to incorporate this interchange.

The analyzer can also be used to obtain an approximate evaluation of Fourier integrals which have the form $\int_0^\infty x(t) \cos n\omega t \, dt$, where $x(t)$ is an aperiodic convergent function, since the displacement of the resolver plate represents the value of the integral, point by point, as the integration proceeds. It can also be shown, from the locus traced by the resolver plate after a sufficiently long period of integration, that the remaining portion of the integral is of negligible magnitude. Thus, the frequency response can be determined by analysis of the response function.

This analyzer can determine harmonics up to the 20th in curves of 27 in. period and 4 in. peak-to-peak amplitude. Analysis can be made on curves with smaller periods, however, at a proportional loss of harmonic range.

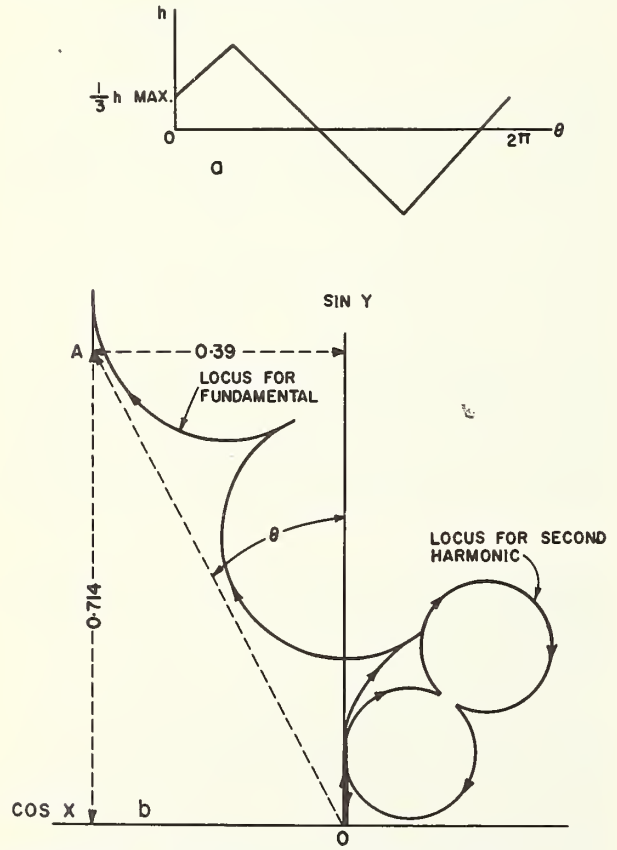

FIGURE 3.13. *Analysis of the 1st and 2d harmonic of a triangular wave by Henderson's mechanical harmonic analyzer.*

(a) Triangular wave
(b) Solution locus for triangular wave

(Reproduced from [17] with permission from Engineering)

4.2. Montgomery's Optical Harmonic Analyzer

Instead of evaluating the coefficients of the Fourier series for a periodic function by a mechanical method, Montgomery [18] utilizes the principles of optics to accomplish this feat. This method requires that the function to be analyzed be represented on a photographic film by one of two methods: (1) the variable area record, shown in figure 3.14a where the part between the curve and the t-axis is transparent, the remainder is opaque; and (2) the variable density record, shown in figure 3.14b. With either type of representation of a function $x(t)$, the amount of light transmitted through a narrow vertical strip of width dt is proportional to $x(t)dt$. If two or more such records are superimposed, the light transmitted through all of them will be proportional to the product of the recorded functions, provided that only one of the records is of the variable area type.

To determine the Fourier coefficients a_n and b_n, proceed as follows: consider the two records shown in figure 3.14, where $x(t)$ is a variable area record and cos$n\omega t$ is a variable density record. Here again the only requirement is that both should not be variable area records. Therefore, by superimposing one film on the other, the amount of light transmitted through both of them between the limits zero to 2π is $\int_0^{2\pi} x(t)\cos n\omega t dt$, and hence proportional to a_n. The coefficient b_n is obtained in the same manner, i.e., by replacing the cos $n\omega t$ film by a sin$n\omega t$ film. This can be accomplished very simply by moving the cos $n\omega t$

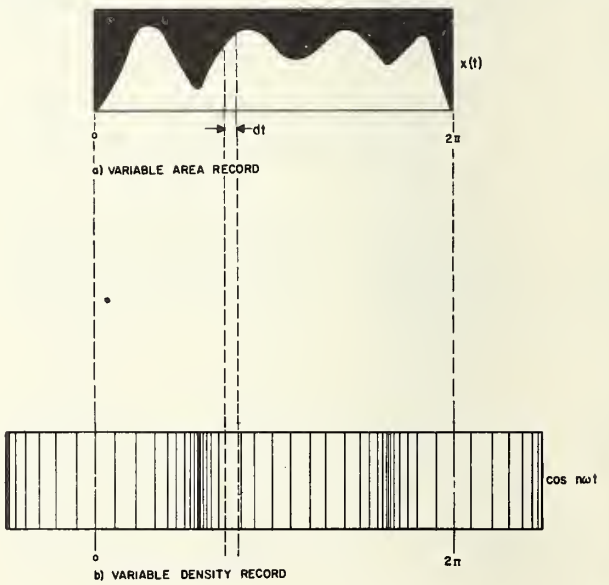

FIGURE 3.14. *Representation of* x(t) *and* cos nωt *on film.*

(Reproduced from [18] with permission from the Bell System Technical Journal.)

film one-quarter wavelength along the axis. Also, if the cosine film is moved a whole wavelength along the axis, the transmitted light will go through a maximum. This maximum value is proportional to c_n where $c_n=\sqrt{a_n^2+b_n^2}$, and the position of the cosine along the axis at which it occurs is the phase angle $\varphi_n=\text{arc tan}\,\frac{b_n}{a_n}$.

Since $x(t)$ and cos $n\omega t$, in general, will have both negative and positive values they cannot be directly represented by the transmission of light. Therefore, to eliminate this difficulty a constant is added to each function which results in a constant in the measured amplitude.

To illustrate this analytically, let us consider the optical transmission of the film on which $x(t)$ is recorded to be expressed as

$$A+x(t) \tag{3.82}$$

where A is a constant large enough to make the expression positive for all values of t. Similarly, the transmission of the cosine film is

$$B_n[1+M_n \cos\,(n\omega t-\theta)], \tag{3.83}$$

where θ denotes the position of the cosine film along the t-axis, M_n is a constant less than unity, known as the modulation of the record, and B_n is a constant which is the average optical transmission of the film.

Therefore, the total transmitted light when these two films are superimposed on each other is given by

$$\begin{aligned}T&=\int_0^{2\pi} B_n[A+x(t)][1+M_n \cos\,(n\omega t-\theta)]dt\\&=AB_n\int_0^{2\pi} dt+AB_nM_n\int_0^{2\pi} \cos\,(n\omega t-\theta)dt\\&\quad+B_n\int_0^{2\pi} x(t)dt+B_nM_n\int_0^{2\pi} x(t) \cos\,(n\omega t-\theta)dt.\end{aligned} \tag{3.84}$$

Integrating each term in eq (3.84) except the last integral yields

$$\begin{aligned}T&=2\pi AB_n+B_ng(t)\Big|_0^{2\pi}+B_nM_n\\&\quad\int_0^{2\pi} x(t) \cos\,(n\omega t-\theta)dt,\end{aligned} \tag{3.85}$$

where $g(t)=\int x(t)dt$. The last integral can be evaluated by a sequence of mathematical manipulations and previously derived expressions. Let us first rewrite the integral in the form

$$\int_0^{2\pi} x(t) \cos\,[(n\omega t-\varphi_n)-(\theta-\varphi_n)]dt.$$

Expanding the cosine function for the difference of two angles gives

$$\begin{aligned}&\cos\,(\theta-\varphi_n)\int_0^{2\pi} x(t) \cos\,(n\omega t-\varphi_n)dt+\sin\,(\theta-\varphi_n)\\&\times\left[\int_0^{2\pi} x(t) \sin\,(n\omega t-\varphi_n)dt\right].\end{aligned}$$

Again expanding the cosine term in the integrand yields

$$\begin{aligned}&\cos\,(\theta-\varphi_n)\left[\cos\varphi_n\int_0^{2\pi} x(t) \cos n\omega t\,dt+\sin\varphi_n\right.\\&\left.\times\left\{\int_0^{2\pi} x(t) \sin n\omega t\,dt\right\}\right]+\sin\,(\theta-\varphi_n)\left[\cos\varphi_n\right.\\&\left.\times\left\{\int_0^{2\pi} x(t) \sin n\omega t\,dt\right\}-\sin\varphi_n\int_0^{2\pi} x(t) \cos n\omega t\,dt\right].\end{aligned}$$

The integrals are now recognized as a_n and b_n, eqs (1.7) and (1.8) respectively, the coefficients of the Fourier series for a function $x(t)$ whose period is 2π. Therefore,

$$\begin{aligned}&\pi \cos\,(\theta-\varphi_n)[a_n \cos\varphi_n+b_n \sin\varphi_n]\\&\qquad+\pi \sin\,(\theta-\varphi_n)[b_n \cos\varphi_n-a_n \sin\varphi_n].\end{aligned}$$

From eq (1.11) it can be shown that cos $\varphi_n=a_n/c_n$ and sin $\varphi_n=b_n/c_n$; therefore

$$\int_0^{2\pi} x(t) \cos\,(n\omega t-\theta)dt=\pi c_n \cos\,(\theta-\varphi_n)$$

and eq (3.85) becomes

$$T=2\pi B_n(A+C)+\pi B_nM_nc_n \cos\,(\theta-\varphi_n) \tag{3.86}$$

where $C=\frac{g(t)}{2\pi}\Big|_0^{2\pi}$; c_n is the resultant of the Fourier series coefficient a_n and b_n, defined by eq (1.10); and φ_n is the phase angle defined by eq (1.11). To obtain a_n, take the difference in T for $\theta=0$ and π; therefore

$$a_n=\frac{T(0)-T(\pi)}{2\pi B_nM_n}. \tag{3.87}$$

Similarly, to obtain b_n, take the difference in T for $\theta=\pi/2$ and $3\pi/2$; thus

$$b_n=\frac{T\left(\frac{\pi}{2}\right)-T\left(\frac{3\pi}{2}\right)}{2\pi B_nM_n}.$$

As previously discussed, the maximum value of T occurs at $\theta=\varphi_n$ thus establishing φ_n. This can also be seen by referring to eq (3.86). The minimum T occurs at $\theta=\varphi_n+\pi$; thus the difference between maximum and minimum values of T gives

$$c_n=\frac{T_{\max}-T_{\min}}{2\pi B_nM_n}. \tag{3.88}$$

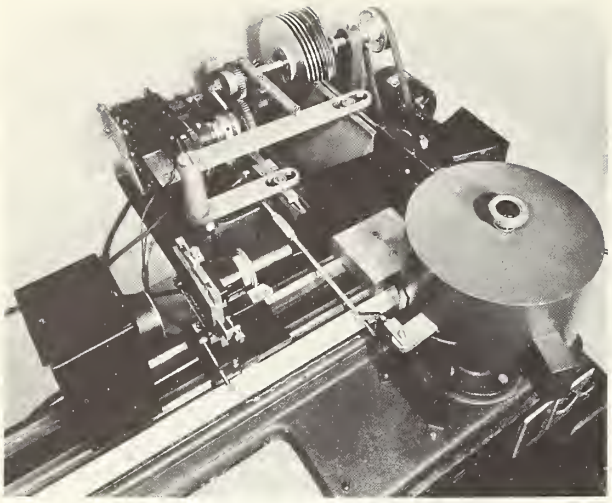

FIGURE 3.15. *Montgomery's optical harmonic analyzer.*

(Reproduced from [18] with permission from the Bell System Technical Journal)

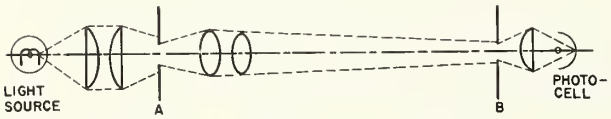

FIGURE 3.16. *Schematic of optical system in optical harmonic analyzer.*

(Reproduced from [18] with permission from the Bell System Technical Journal)

By making B_n and M_n approximately constant for all screens, the coefficients for either form of the Fourier series are directly proportional to the change in transmitted light for specified pairs of position of the cosine film.

The process which the analyzer is required to carry out consists of superimposing the function to be analyzed on a cosine film and measuring the variation in the transmitted light when the cosine film is moved along the t-axis. This is repeated with a different cosine film for each harmonic to be measured. Such an analyzer is shown in figure 3.15 and schematic of its optical system in figure 3.16. With reference to figure 3.16, the film containing $x(t)$ is placed in a holder at slot A and illuminated by passing light from an incandescent lamp through a condenser lens. An enlarged image of $x(t)$ is formed at B on a window bounded by two knife edges 0.750 in. apart. The portion of $x(t)$ to be analyzed must be adjusted so as to just fill the window. The cosine films slide in a track directly behind the window, and receive the image of $x(t)$. The transmitted light is collected by another lens and brought to a photocell. The photocell output is coupled directly to an oscillograph which records the variations in the form of a strip chart record. Each succeeding cosine film is brought into play and passed across the window at B automatically, by a series of cams and levers. The analysis is fully automatic except for adjustments at the beginning of each analysis.

The analyzer shown in figure 3.15 takes records of $x(t)$ between $\frac{1}{16}$ and $\frac{5}{16}$ in. in length and no higher than its length, and is capable of analyzing the first 30 harmonics.

4.3. Photoelectric Fourier Transformer

The photoelectric Fourier transformer is an optical analyzer which produces the Fourier transform of a given function automatically and instantaneously in the form of a graph on the screen of an oscilloscope. Furth and Pringle [19] based their analyzer on a principle similar to that used by Montgomery [18], but extended it for continuous Fourier analysis, i.e., Fourier integration. The analysis is based on the light transmitted through a closely spaced fringe pattern rotating in front of a narrow slit, beyond which is the mask with the pattern to be analyzed. The light reaching a photocell can be expressed by an equation similar to eq (3.84), or

$$T=AB_n\int_a^b dt+AB_nM_n\int_a^b \cos\,(n\omega t-\theta)\,dt$$

$$+B_n\int_a^b x(t)dt+B_nM_n\int_a^b x(t)\,\cos\,(n\omega t-\theta)dt, \quad (3.89)$$

where the only difference is in the range of integration. Let us consider only one standard fringe pattern, say cos ωt; therefore $n=1$ and integration of eq (3.89) gives

$$T=AB_1M_1g(\omega)+B_1M_1h(\omega)+C \quad (3.90)$$

$$g(\omega)=\frac{1}{\omega}\,[\sin\,(\omega b-\theta)-\sin\,(\omega a-\theta)] \quad (3.91)$$

$$h(\omega)=\int_a^b x(t)\,\cos\,(\omega t-\theta)dt \quad (3.92)$$

$$C=AB_1(b-a)+B_1\int^b x(t)dt. \quad (3.93)$$

If ω is now made to extend and shrink periodically in time between $\omega=0$ and an upper limit ω_c, the spacing of the standard fringe pattern along the t-axis (defined by $\lambda=2\pi/\omega$), will vary periodically in time between $\lambda_c=2\pi/\omega_c$ and infinity. Thus, the time dependence of the transmitted light will be represented by eq (3.90) with the limits of minus ω_c and plus ω_c. If $A=0$ (the given function is positive everywhere) or if $b=-a$ and $\theta=\pm\pi/2$, then eq (3.90) represents the Fourier transform of $x(t)$. The constant C in eq (3.90) is considered insignificant [19].

The transmitted light which is directly proportional to the Fourier transform of $x(t)$ is now concentrated on a photoelectric cell. The photoelectric cell produces a current proportional to the intensity of light received, and therefore pro-

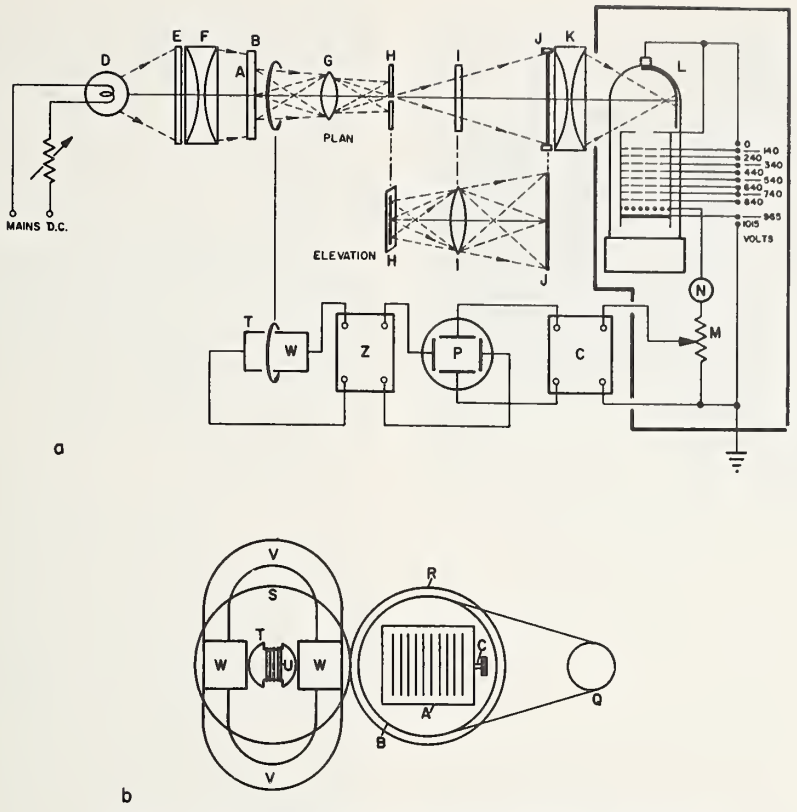

FIGURE 3.17. *Schematic of the photoelectric Fourier transformer.*

(Reproduced from [19] with permission from The Philosophical Magazine)
(a) Optical and recording system
(b) Plate drive and generator system

portional to the Fourier transform of $x(t)$. The current is then amplified and fed into an oscilloscope where it is made to deflect the beam in the vertical direction. At the same time a harmonic time base which is synchronized to the variation of ω is fed into the oscilloscope to drive the beam in the horizontal direction proportional to ω.

A schematic of the analyzer is shown in figure 3.17a. Light from an incandescent lamp D is passed through a diffuser E and a condenser lens F. The light is then passed through a small glass plate A, bearing a photographic pattern consisting of 20 fringes having a harmonic variation in optical transmission. The plate is mounted in a journal bearing B, so that it can be rotated with a constant angular velocity about the axis of the optical system. The light then passes through lens G which produces a reduced image on a fine adjustable vertical slit at H. The slit at H is arranged to make the axis of rotation pass exactly through the center of the slit. In this way a symmetrical distribution of light intensity is obtained along the slit as plate A is rotated. The width of the slit must be small compared to λ_c. The variation in the spacing of the light distribution, as plate A is rotated at constant angular velocity $\bar{\omega}$, is given by

$$\lambda = \frac{\lambda_c}{\sin \bar{\omega} t}. \qquad (3.94)$$

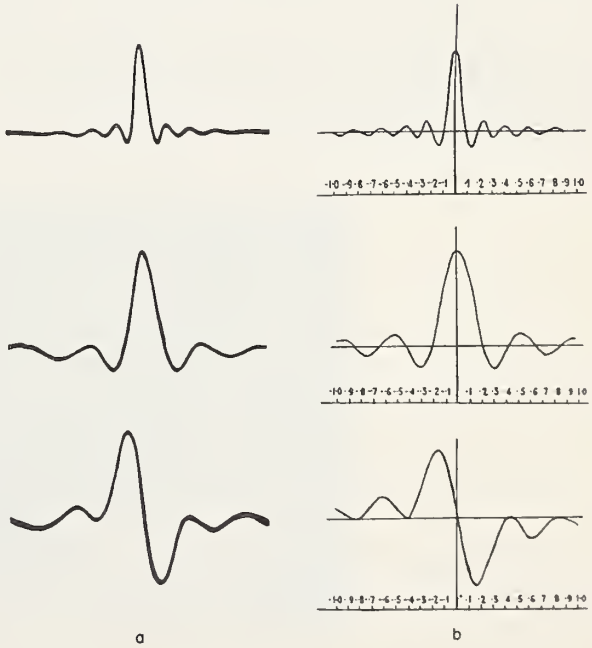

FIGURE 3.18. *Typical photoelectric Fourier transformer results with associated analytical solutions.*

(Reproduced from [19] with permission from The Philosophical Magazine.)
(a) Photoelectric Fourier transformer result
(b) Analytical solution

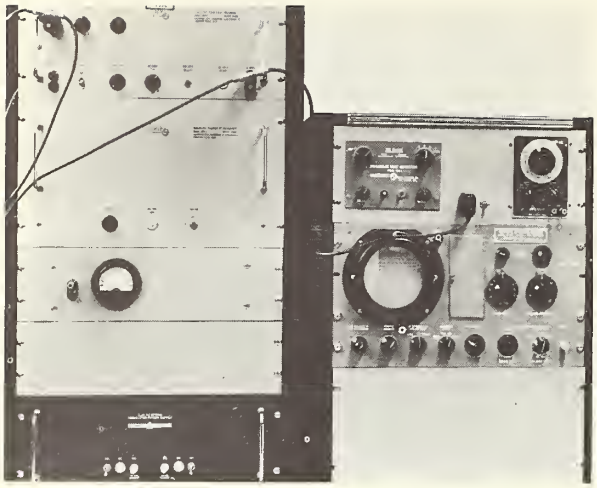

FIGURE 3.19. *Electronic and magnetic analyzer used by Lederer and Smith.*

Therefore, the angular frequency ω varies in time according to

$$\omega=\frac{2\pi}{\lambda}=\frac{2\pi}{\lambda_c}\sin\bar{\omega}t$$

or

$$\omega=\omega_c\sin\bar{\omega}t. \qquad (3.95)$$

From the slit at H, the light passes through a cylindrical lens I (with its longitudinal axis of symmetry perpendicular to the slit). The cylindrical lens rotates the vertical image at the slit H into an enlarged horizontal image at J. The image at J consists of a 3×3 in. fringe pattern which contracts and expands in time according to eqs (3.83) and (3.95). At J the record of the function to be analyzed is introduced, i.e., $x(t)$. The optical arrangement is completed by the condensing lens K and the photoelectric cell L.

The remaining pieces of equipment shown in figure 3.17a are the milliammeter N, the potentiometer M, amplifier O and Z, oscilloscope P, and a generator. The motor Q rotates plate A and indirectly rotates plate S of the generator. The generator consists of core T, magnets V, and iron pole pieces W. The purpose of the generator is to produce a voltage which is synchronized with the angular rotation of plate A to drive the beam of the oscilloscope in the horizontal direction.

Typical results from this analyzer are shown in figure 3.18a. In figure 3.18b are the analytical solutions worked out for the function analyzed. The analytical solutions are scaled to the identical scale used by the analyzer; therefore a direct comparison can be made.

4.4. Electronic Analyzer With Magnetic Transient Storage

Lederer and Smith of the National Bureau of Standards use a magnetic drum recorder to store the transient response of the pressure transducer and to repetitively play it back to a commercially available electronic analyzer, figure 3.19. The resonating frequencies may be viewed on the screen of the analyzer as shown in figure 3.20. The recorder has a variable recording time of 1 to 6 msec and a frequency range of 1 to 100 kc/s.

The analyzer will detect any resonance of amplitude not less than 1 percent of that of the calibrated resonance nearest in frequency through a frequency range of 1 to 100 kc/s, provided that the resonant frequencies are separated by at least 1 kc/s. In general, the greater the frequency separation, the lower the amplitude ratio at which resonances can be detected. At frequency separations of less than 1 kc/s resonance can be detected if the amplitude is high enough.

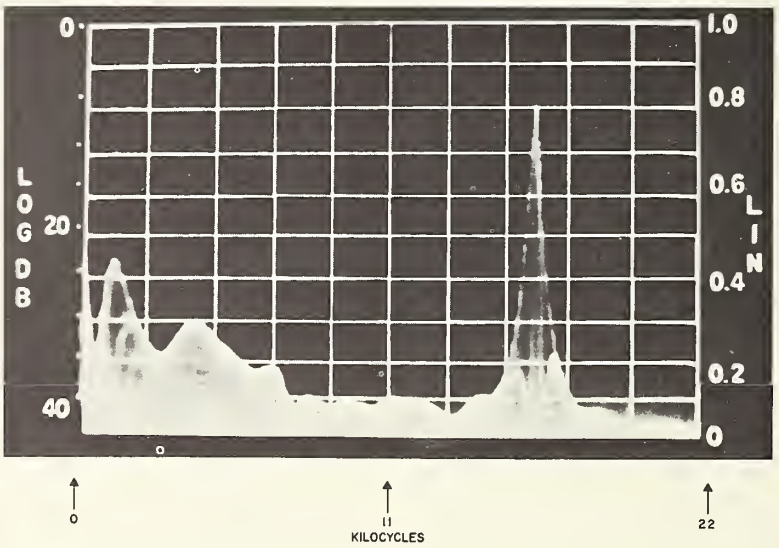

FIGURE 3.20. *Frequency analysis from analyzer used by Lederer and Smith.*

Information from this system is limited to the amplitude characteristic. No information regarding phase is obtained. Use of the information is based on the assumption that the transducer system has a sufficiently low damping constant to make possible construction of the frequency response curve. Thus it is possible to determine to what frequency the transducer can be used with acceptable fidelity.

5. References

[1] E. A. Guillemin, Computational techniques which simplify the correlation between steady-state and transient response of filters and other networks, Proc. Nat. Electron. Conf., 1953, **9,** 513–532 (1954).

[2] A. Sommerfeld, Partial Differential Equations of Physics (in German), W. Klemm (Wiesbaden, 1947).

[3] J. B. Scarborough, Numerical Mathematical Analysis, The Johns Hopkins Press (Baltimore, 1955).

[4] J. N. MacDuff and J. R. Curreri, Vibration Control, McGraw-Hill Book Co., Inc. (New York, N.Y., 1958).

[5] T. R. Running, Empirical Formulas, John Wiley & Sons, Inc. (New York, N.Y., 1917).

[6] L. W. Pollak, Multiplication Table for Harmonic Analysis (in German), J. A. Barth (Leipzig, 1926).

[7] L. A. Pipes, Applied Mathematics for Engineers and Physicists, McGraw-Hill Book Co., Inc. (New York, N.Y., 1958).

[8] V. V. Solodovnikov, Introduction to the Statistical Dynamics of Automatic Control Systems, Dover Publ., Inc. (New York, N.Y., 1960).

[9] C. Shannon, Communications in the presence of noise, Proc. IRE **37,** 10–21 (Jan. 1949).

[10] B. O. Peirce and R. M. Foster, A Short Table of Integrals, Ginn and Co. (Boston, Mass., 1956).

[11] H. A. Samulon, Spectrum analysis of transient response curves, Proc. IRE **39,** No. 2, 175–186 (Feb. 1951).

[12] A. Tustin, A method of analyzing the behavior of linear systems in terms of time series, J.I.E.E., Proc. Conv. Autom. Regulation and Servomechanisms, London, **94,** Part II–A, No. 1, p. 130 (May 1947).

[13] A. Madwed, Numerical analysis by the number series transformation method, Ch. 27, Instrument Engineering, Vol. II, by C. S. Draper, W. McKay, and S. Lees, McGraw-Hill Book Co., Inc. (New York, N.Y., 1953).

[14] R. B. Bowersox and J. Carlson, Digital-computer calculation of transducer frequency response from its response to a step function. Progress Report No. 20–331, Jet Propulsion Laboratory (July 26, 1957).

[15] J. L. Schweppe, Calibration of pressure transducers with aperiodic input-function generators, Paper 46.1.62 presented at the 17th Ann. ISA Instr.-Automation Conf. (Oct. 1962).

[16] R. W. Hamming, Numerical Methods for Scientists and Engineers, McGraw-Hill Book Co., Inc. (New York, N.Y., 1962).

[17] J. G. Henderson, Mechanical harmonic analyzer and some applications to servo systems, Eng. **173,** 52–53, 68–70 (Jan. 1952).

[18] H. C. Montgomery, An optical harmonic analyzer, Bell System Tech. J. **17,** 406–415 (July 1938); U.S. patent 2098326.

[19] R. Furth and R. W. Pringle, A photoelectric Fourier transformer, Phil. Mag. [7], **37,** No. 264, 1–13 (Jan. 1946).

[20] G. F. Floyd, Method of approximating the transient response from the frequency response, in Principles of Servo Mechanism by G. S. Brown and D. P. Campbell, Ch. 11, John Wiley & Sons, Inc. (New York, N.Y., 1948).

[21] L. C. Ludbrook, Step to frequency response transforms for linear servo systems, Electron. Eng. **27,** No. 311, 27–30 (Jan. 1954).

[22] F. H. Raven, Automatic Control Engineering, McGraw-Hill Book Co., Inc. (New York, N.Y., 1961).

[23] A. V. Bedford and G. L. Fredenall, Analysis, synthesis and evaluation of the transient response of television apparatus, Proc. IRE **30,** No. 10, 440–457 (Oct. 1942).

[24] R. Bowersox, Calibration of high frequency response pressure transducers, ISA J. **5,** No. 11, 98–103 (Nov. 1958).

4. Analysis of Nonlinear Transducers

D. Muster [1]

1. General

Physical nonlinear systems can be discussed only in terms of mathematical models that are characterized by differential equations amenable to some form of solution over restricted regions of the motion parameter(s), or for specific mathematical descriptions of the damping and/or restoring force terms. In addition, little can be done by analysis to predict a response function for systems which cannot be represented by one- or possibly two-degree-of-freedom models.

For damped linear systems, if $x_1(t)$ is a solution of $m\ddot{x}+c\dot{x}+kx=F_1(t)$, and $x_2(t)$ is a solution of $m\ddot{x}+c\dot{x}+kx=F_2(t)$, then $x=x_1+x_2$ is a solution of $m\ddot{x}+c\dot{x}+kx=F_1(t)+F_2(t)$. This fundamental fact, a direct consequence of the linearity of the differential equation, is called the *principle of superposition*. It is important to note explicitly that the principle does not hold for nonlinear differential equations. It follows as well that the concepts of free and forced oscillation, classical normal-mode analysis and resonance, all intimately related to the principle of superposition, have real meaning *only* for linear systems. As a consequence of these limiting conditions, any form of analysis conducted to evaluate specific characteristics of nonlinear systems is restricted stringently. The investigator is confronted immediately with the decision: which optimum mathematical model, among those amenable to useful solution, will provide an adequate characterization of the nonlinear system's behavior?

The decision on an optimum mathematical model raises several specific questions. Can the system be adequately described by a single-degree-of-freedom system? Is the nonlinearity of the damping (restoring) force sufficiently small that it can be represented adequately by viscous damping (a linear spring)? Is the region of interest sufficiently narrow that a linear approximation will be adequate? Can a solution be obtained by considering the system characteristics as being piece-wise linear (say, bilinear)? In summary, every attempt is made to represent the system by linear damping and restoring force characteristics or, if this is not possible, to minimize the magnitude and subsequent effect of the nonlinearity.

Fortunately, the response of most pressure transducers (as well as other electromechanical sensing devices) can be represented adequately by solutions of linear differential equations. Here we will discuss some of the methods of analysis for those transducer systems with sufficiently great nonlinear restoring force or damping characteristics, that linear analysis is not adequate, but not so great that solution is a practical impossibility. We will restrict the discussion to nonlinearities of the type and relative magnitude likely to be encountered in pressure transducer systems.

In this chapter, we discuss first the physical and analytical aspects of nonlinearity. In the main, this discussion will focus on the physical parameters of damping and stiffness and the manner of their representation in the analysis of transducer systems. The remainder of the text is concerned with analytical methods as they are applied to nonlinear systems. Particular attention is drawn to those methods and solutions of systems where the nonlinearity is confined to the restoring force term only and, later, to those where it is confined to the damping term only. Among the methods of analysis, the describing-function method, the bilinear approximation and the phase-plane method are discussed in some detail.

At the end of the chapter, there is a combined bibliography and reference list. The literature sources cited in the chapter text are listed first: uncited sources used for background information and general reference in preparing the chapter are listed last. Among the general references are several to which we draw the reader's special attention: the translations of the books by Andronov and Chaikin [1],[2] Minorsky [2], and Kryloff and Bogoliuboff [3], the vibrations text by Jacobsen and Ayre [4], that on nonlinear analysis by Cunningham [5], and those concerned with the design of control-systems by Truxal [6] and Murphy [7]. In addition, there is a review by Ku [8] of recent advances in analytical methods for studying nonlinear control problems. The extensive bibliography in the Ku paper is oriented primarily towards the theory of nonlinear control systems; however, many references to general analytical methods are included. Analysts interested in other nonlinear systems will find them useful.

Obviously, the adequacy of the results obtained with any method of analysis is intimately related to the values assigned to the damping and stiffness parameters in the governing differential equation. There are no standard accepted procedures for determining these values. Usually, the stiffness

[1] Professor of Mechanical Engineering, The University of Houston.

[2] Figures in brackets indicate the literature references on p. 66.

of a mechanical system is determined from a static test and the assumption is made that dynamic effects are either negligible or behave in accordance with a known relationship. The magnitude and form of the damping characteristic are usually assumed to be those associated with either viscous or coulomb damping. For a damped, one-degree-of-freedom system, the differential equation for free vibration can be integrated completely in only two cases; that is, when the damping force is proportional to the first power of the velocity, or is a constant value with a sign the same as that of the velocity—the coulomb friction type. In case the damping force is proportional to the square of the velocity, a first integral can be obtained and from this a relationship between two successive maximum displacements can be established [9]. The inverse problem, that of determining the damping parameter from a set of observed values, has been solved in general terms only for systems in which viscous or coulomb damping occur separately or jointly [10]. The case of combined viscous-coulomb damping has been studied by Den Hartog [11] and applied to the frequency response of vibration instruments [12].

For more general damping laws, when the damping force is proportional to either any power of the velocity or sums of such terms (or powers of the displacement or displacement amplitudes), neither the direct problem of finding an expression for the attenuation nor the inverse problem of determining the damping law from observed values has been solved in general terms. The reason for this has been mentioned earlier; the governing nonlinear differential equations are such that they do not admit of closed form solutions. However, if the damping forces are sufficiently weak, an approximate method due to Kryloff and Bogoliuboff [3] leads to a closed-form description of the attenuation of free damped vibrations for a variety of damping laws. Klotter [13] has shown that from the expressions for the attenuation it is possible to deduce, from a set of observed values, the damping law which governs the behavior of a system. In [13], damping laws are deduced for cases where the damping forces are proportional to a single power of the velocity, displacement or displacement amplitude, or to the sum of two such terms.

In summary, the relationships that govern the stiffness and damping parameters can be deduced from observations for a limited class of cases (usually, for one-degree-of-freedom systems characterized by relatively weak damping forces). For other cases, the assigned values are obtained through trial and error or through intuition.

2. Physical Aspects of Nonlinearity

One of the most desirable characteristics of a transducer is for it to respond in a linear manner over its useful dynamic range. In general, transducers are designed so as not to exhibit appreciable nonlinearity; for example, in the case of static calibration, there is no significant departure from linearity between input and output functions, or, under dynamic conditions, the transducer does not exhibit such phenomena as jumps and sub- or super-harmonic resonances. In the presence of significant nonlinearities in damping or stiffness, the principle of superposition does not hold, with the consequences enumerated earlier.

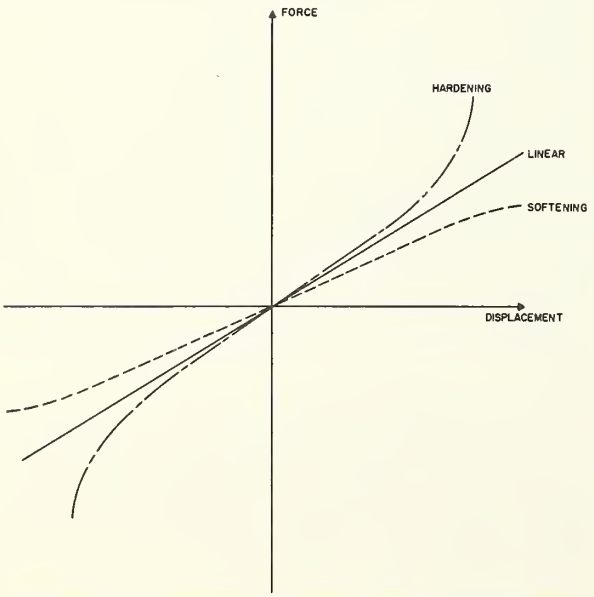

FIGURE 4.1. *Hardening, softening, and linear springs.*

In figure 4.1, softening (sub-linear) and hardening (supra-linear) stiffness curves are superposed on that for a linear spring. The nonlinear character of these curves can often be approximated by the addition of a cubic term, that is, the restoring force of a transducer may be given by

$$k(x \pm \beta^2 x^3), \tag{4.1}$$

where the relative magnitude of the nonlinearity is given by the coefficient β (with dimension L^{-1}) and the hardening or softening influence of the cubic term is indicated by the plus or minus sign, respectively. Consider the motion of an undamped transducer with sinusoidal forcing and a hardening stiffness characteristic given by eq (4.1). If the transducer system can be represented by a one-degree-of-freedom idealization, the equation characterizing its motion is

$$m\ddot{x} + k(x \pm \beta^2 x^3) = F \cos \omega t, \tag{4.2}$$

the well-known Duffing equation [4]. The steady-state response of a system governed by eq (4.2) is shown in figure 4.2 for a hardening stiffness characteristic and in figure 4.3 for a softening characteristic. After [4], the response is given in terms of the dimensionless excitation parameter

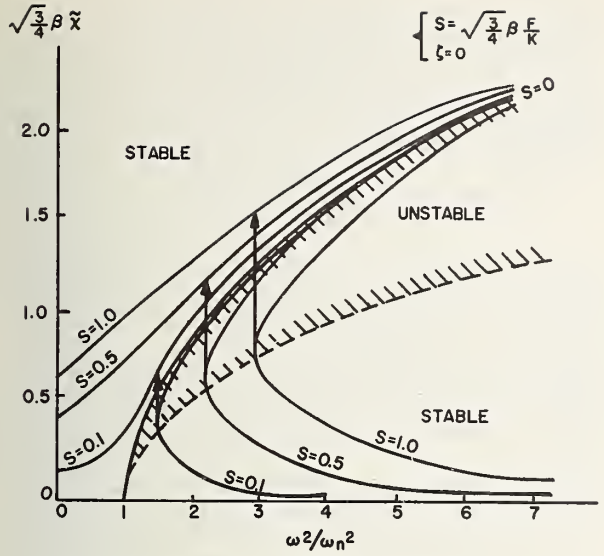

FIGURE 4.2. *Response curves for Duffing-equation model with hardening spring, no damping (jump phenomena).*

(Reproduced from [4] with permission from McGraw-Hill Book Co., Inc.)

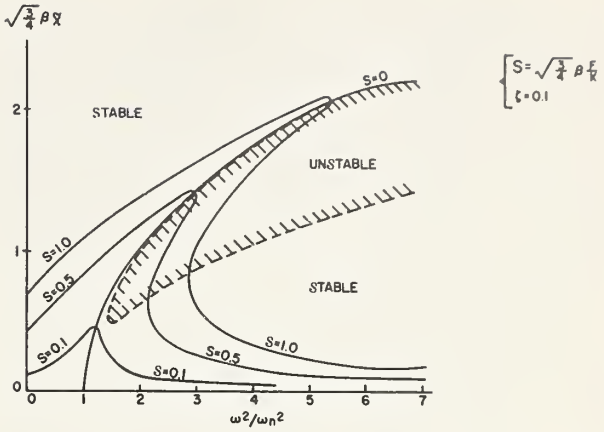

FIGURE 4.4. *Same as for figure 4.2, but with viscous damping ($\zeta=0.1$); no jump for $S=0.1$.*

(Reproduced from [4] with permission from McGraw-Hill Book Co., Inc.)

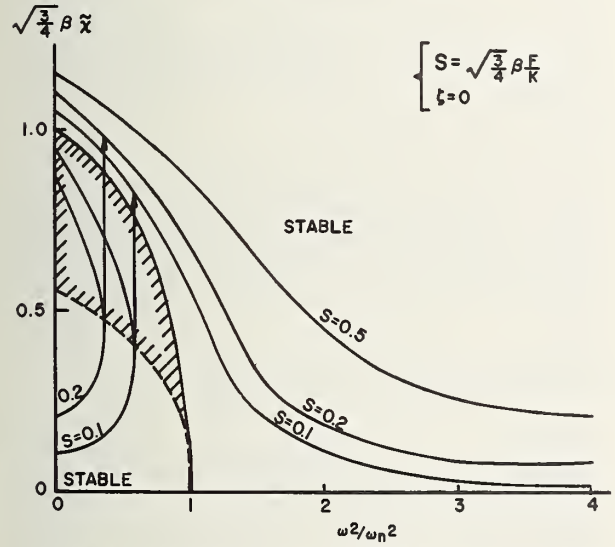

FIGURE 4.3. *Response curves for Duffing-equation model with softening spring, no damping (jump phenomena).*

(Reproduced from [4] with permission from McGraw-Hill Book Co., Inc.)

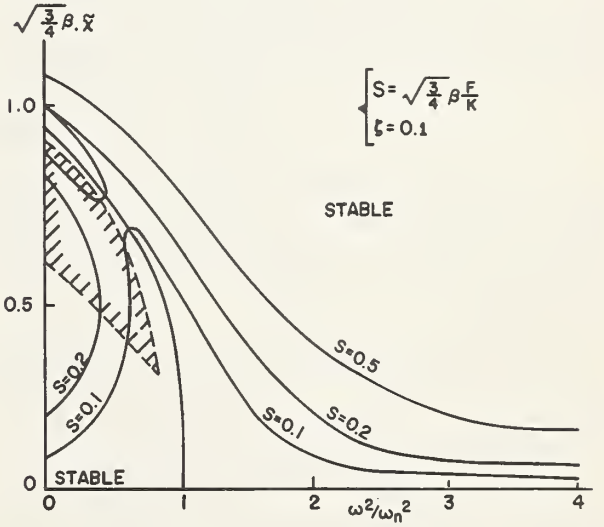

FIGURE 4.5. *Same as for figure 4.3, but with viscous damping ($\zeta=0.1$); jump phenomena exists for $S=0.1$.*

(Reproduced from [4] with permission from McGraw-Hill Book Co., Inc.)

S (where $S=(\sqrt{3/4}\beta F/k)$). The ordinate is the dimensionless parameter $\sqrt{3/4}\beta\tilde{x}$ where $\tilde{x}$ denotes an approximate solution of Duffing's equation obtained by, say, the Ritz averaging method [4]; the abscissa is $\omega^2/\omega_n{}^2$ (where $\omega_n{}^2=k/m$). The cross-hatched area in each figure indicates the areas of unstable motion and the vertical lines represent the jump phenomenon, in which the displacement changes suddenly from a lower to a higher value with no change in applied force.

The quantitative effect of hardening stiffness (that is, systems in which $\beta^2>0$) is to bend the $S=0$ curve of figure 4.2 toward larger values of ω/ω_n, while for softening-stiffness systems (fig. 4.3), for which $\beta^2<0$, the $S=0$ curve bends toward values of $\omega/\omega_n<1$. The greater the value of $|\beta^2|$, the more marked the bend in the response curves. The $S=0$ curves referred to above represent the free vibration case of the Duffing-equation model. It can be shown [4] that the natural frequency and

the displacement amplitude are related by

$$\omega_d=\omega_n\sqrt{1\pm\tfrac{3}{4}\beta^2\tilde{x}^2}. \tag{4.3}$$

The response functions of actual physical systems exhibiting hardening or softening stiffness characteristics will vary in detail from those of figure 4.2 and 4.3 but not in general appearance. The tendency for the response to lean towards larger values of ω/ω_n is associated with a hardening characteristic, the tendency to bend towards values of $\omega/\omega_n<1$ with a softening characteristic. The existence of regions of instability (jump phenomena) are characteristic of the presence of either hardening or softening.

The effect of nonlinear damping on the response of a mechanical system is more subtle. Whereas the stiffness characteristic determines the basic shape of the response function (that is, no bend for the linear case and bent response curves for the nonlinear cases), a nonlinear damping characteristic only modifies the shape and extent of the domains of instability (if they exist) and makes the resonance amplitudes finite. In systems with linear restoring force and with damping proportional to, say, the nth power of the velocity, it can be shown [14] that the steady-state response can be approximated closely by assuming that the actual damping term can be replaced by an equivalent viscous term. The criterion of equivalence is that of equal dissipative work per quarter cycle of the motion of the system.

As an example of the influence of damping upon response curves, let us consider a viscously damped Duffing-equation model. The governing differential equation of motion is

$$\ddot{x}+2\zeta\omega_n\dot{x}+\omega_n^2(x\pm\beta^2x^3)=\frac{F}{m}\cos\,\omega t, \tag{4.4}$$

where the damping ratio is $\zeta=c/c_c=c/2m\omega_n$ and c is the damping coefficient. Response curves analogous to those of figure 4.2 and 4.3 are shown in figures 4.4 and 4.5, respectively. It can be seen that the damping has made the resonance amplitudes finite and that the maximum amplitudes of the system are but very slightly larger than the response amplitudes. The two domains of stable motion in figures 4.2 and 4.3 are seen to merge in the damped response plot of figures 4.4 and 4.5, since the backbone of the plot (the $S=0$ curve) is no longer a boundary. As before, the unstable domain is bounded by the locus of the vertical tangents to the families of constant-excitation S curves.

In the case of damping proportional to the nth power of the velocity, the general configuration of the plots in figures 4.4 and 4.5 remains the same, but the crossings of the resonance-point loci with the $S=0$ curves change quantitatively.

3. Methods of Analysis (Nonlinear Systems)

By comparing the response curves of the nonlinear cases above with those for the linear cases discussed in chapter 2, it can be shown [4] that nonlinear behavior makes it difficult (if not practically impossible) to evaluate the dynamic characteristics of some transducers. For transducers with relatively weak nonlinearities, the response function can be approximated by that for a linear system with characteristics which are first-order approximations of those of the actual system. An alternate approach is to assume that the behavior of a system is linear in the neighborhood of an operating point or between two points on the curves describing the system parameters [15].

In the remainder of this chapter, the nonlinearities of stiffness and damping are assumed to be sufficiently great that it is necessary to recognize the system as being nonlinear. Within this framework, we will discuss the methods available for the analysis of such systems as they actually are. We will divide these methods into three major categories:

1. Perturbation, iteration, and variational methods.
2. Linearization methods (describing functions).
3. Phase-plane methods (including the method of isoclines and other graphical methods).

The mathematical methods of the first category are most useful in determining the approximate steady-state response of nonlinear systems and, in many cases, cannot be used to determine transient response. For the latter reason, and because of the sometimes formidable algebraic computation associated with their use, they enjoy, perhaps, the least popularity among analysts concerned with calibration problems. As computers and analog-to-digital conversion devices become more readily available, mathematical computation procedures will probably find wider acceptance.

The perturbation method was developed by Poincaré [16] and Lindstedt [17], primarily for application to astronomical problems. Somewhat later, Ritz [18] and then Galerkin [19] developed equivalent approximate methods for solving steady-state responses of linear as well as nonlinear problems. Duncan [20, 21] and others used the method to treat problems concerning the statics and dynamics of elastic bodies. Prior to the early 1950's, when Klotter called attention to the interdependence and equivalence of the two forms in which the method was known, it had been used only infrequently to solve dynamical problems (other than eigenvalue problems). Since that time (usually under the name of the Ritz averaging method), it has been used extensively [4, 22, 23, 24, 25]. In particular, the method can be applied to an oscillatory system described by differential equations of the type

$$E_n(\ddot{q}_n,\ \dot{q}_n,\ q_n,\ t)=0, \tag{4.5}$$

for example, eqs (4.2) and (4.4).

The exact solution would yield the coordinates $q_n(t)$ characterizing the response of the system at any time t. In the absence of a theory or method for obtaining the exact solution of eq (4.5) and hence of (4.2), (4.4), . . ., the Ritz averaging method will yield an approximate *steady-state* solution by the following procedure:

1. Each of the coordinates q_n is replaced by an assumed approximate solution of the form:

$$q_n(t)=\sum A_{ni}\varphi_i(t)$$

$$(n=1, 2, 3, \ldots), (i=1, 2, 3, \ldots) \quad (4.6)$$

where the A_{ni} are a set of unknown coefficients and the functions $\varphi_i(t)$ are assumed functions expected to yield the best average solution over a period.

2. Then the assumed solutions are introduced into eq (4.5) and integrations of the following type performed over the period indicated:

$$\int_0^{2\pi/\omega} E_n(\ddot{q}_n, \dot{q}_n, q_n, t)\varphi_i(t)dt=0$$

$$(n=1, 2, 3, \ldots), (i=1, 2, 3, \ldots). \quad (4.7)$$

A set of (mn) algebraic equations is obtained from which the coefficients A_{ni} can be determined.

Examples in which the method is applied appear in the literature and in later sections of this chapter.

As might be expected, the usefulness of perturbation, iterative, and variational procedures has been enhanced by the development of electronic computers and programing techniques. Bowersox and Carlson [26] and Hylkema and Bowersox [27] have investigated the digital-computer calculation of transducer frequency response from its response to a step function. The recent development of electronic devices which can convert the analog output of a transducer to a digital form acceptable to a computer suggests new possibilities for more effective use of mathematical computing procedures. At present, however, there is no simply applied, effective method of analysis available to all engineers, rather than only to specialists with access to extensive electronic computer facilities.

Among the linearization methods of the second category, we have selected the "describing-function" method [28] as, perhaps, the most practical method for application to determine the response of nonlinear transducers. The approximation involved in the method is similar to that used earlier by Kryloff and Bogoliuboff [3]. Independent development of essentially the same method as Kryloff-Bogoliuboff was made by Goldfarb [29], Tustin [30], and Oppelt [31].

A second method discussed later is that due to Ergin [32]. He has shown that for even substantial nonlinearities in restoring force, a bilinear approximation can be used with satisfactory results.

The third category covers phase-plane methods. For a general development of the method (including the method of isoclines) and for applications of it to linear systems, we refer the reader to section 4 of chapter 2. Here we will restrict the discussion to nonlinear systems. Transient disturbances as well as free vibrations of such systems can be treated by phase-plane methods, but the steady-state forced vibrations of any system are not readily dealt with by these methods unless the periodic excitation functions are of the square-wave type.

4. The Concept and Application of the Describing-Function Method [6, 28]

In linear systems the concept of frequency response, in the form of a (direct or inverse) transfer function, is used to describe the dynamic behavior of transducers. The concept of such a transfer function is not valid for transducer systems with substantial nonlinearity. Kochenburger [28] has proposed a nonlinear counterpart to the transfer function, a so-called "describing function" based on the frequency response. The method has been used extensively and extended in the recent past, primarily by Klotter [33, 34, 35], West [36], Grief [37], Johnson [38], Tou and Schultheiss [39], and Truxal [6].

The describing-function method of analysis is based on three assumptions [28]:

1. There is only one nonlinear element in the system.
2. The output of the nonlinear element depends only on the present value and past history of the input. No time-varying characteristics are included in the nonlinear element.
3. If the input of the nonlinear element is a sinusoidal function, only the fundamental component of the element output is considered.

The implications of these assumptions are discussed in more detail by Truxal [6].

In order to demonstrate the use of the method, let us consider a transducer system consisting of a mass m, a coulomb damper (that is, a dry friction device), and a diaphragm of negligible stiffness. The governing differential equation for the sinusoidally forced motion of the system is [5]

$$m\ddot{x}+\frac{\varphi\dot{x}}{|\dot{x}|}=F\cos\omega t \quad (4.8)$$

where φ is the magnitude of the force needed to overcome the static friction of the damper. The sign of this force is the same as the sign of the velocity.

The exact steady-state solution of eq (4.8) can be determined by a piecewise linear solution of two equations, with the applicable equation depending upon the sign of $\dot{x}$. The equations, with their regions of applicability, are

$$\dot{x} \geq 0: \beta \leq \omega t \leq \pi + \beta$$

$$\ddot{x} = \frac{F}{m}\left(\cos \omega t - \frac{\varphi}{F}\right)$$

$$\dot{x} = \frac{F}{m\omega}\left[\sin \omega t - \frac{\varphi}{F}\left(\omega t - \frac{\pi}{2} - \beta\right)\right] \quad (4.9a)$$

$$\dot{x} \leq 0: \pi + \beta \leq \omega t \leq 2\pi + \beta$$

$$\ddot{x} = \frac{F}{m}\left(\cos \omega t + \frac{\varphi}{F}\right)$$

$$\dot{x} = \frac{F}{m\omega}\left[\sin \omega t + \frac{\varphi}{F}\left(\omega t - \frac{3\pi}{2} - \beta\right)\right] \quad (4.9b)$$

where $\sin \beta = -\pi\varphi/2F$. A plot of the variation of force and velocity is shown in figure 4.6, where the arbitrary choice has been made, $\varphi/F = 1/\pi$, so that $\beta = -30°$. The velocity vanishes at values of ωt determined by the phase angle β. The latter is negative and tends to zero for values of φ, which are negligibly small with respect to F. The upper limit of real values for β is $\varphi/F = 2/\pi$. If $\varphi/F > 2/\pi$, the velocity does not vary smoothly through zero, but so-called dead bands exist in which there is no motion. In fact, by examining eq (4.9a), it can be seen that, if $\varphi/F > 1$, no steady-state motion is possible.

The fundamental component of the velocity expressed by eq (4.9a) can be found by Fourier analysis. The amplitudes of the sine and cosine terms of the fundamental will be found to be, respectively,

$$b_1 = \frac{1}{m\omega}\left(F + \frac{4\varphi}{\pi}\sin \beta\right)$$

$$a_1 = \frac{1}{m\omega}\left(\frac{4\varphi}{\pi}\cos \beta\right). \quad (4.10)$$

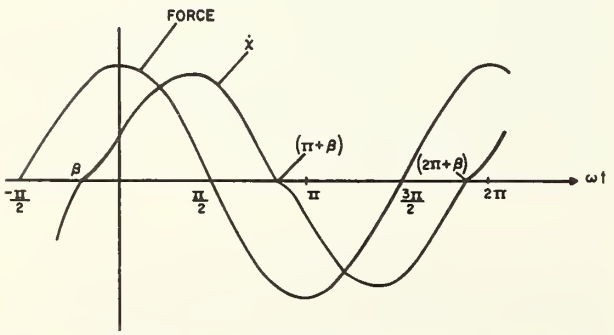

FIGURE 4.6. *Variations in force and velocity for system governed by* $m\ddot{x} + \varphi\dot{x}/|\dot{x}| = F \cos \omega t (\varphi/F = 1/\Pi, \beta = -30°)$.

(Reproduced from [5] with permission from McGraw-Hill Book Co., Inc.)

The describing function we seek is defined as the ratio

$$H = \frac{V}{F} \quad (4.11)$$

where

$$V = a_1 \cos \omega t + b_1 \sin \omega t.$$

Thus,

$$H = \frac{1}{m\omega}\left[\frac{4\varphi}{\pi F}\cos \beta \cos \omega t + \left(1 + \frac{4\varphi}{\pi F}\sin \beta\right)\sin \omega t\right] \quad (4.12)$$

where

$$\sin \beta = -\frac{\pi\varphi}{2F}.$$

The amplitude of the describing function is

$$|H| = \frac{1}{m\omega}\sqrt{1 - \left(\frac{\pi^2}{4} - 1\right)\left(\frac{4\varphi}{\pi F}\right)^2} \quad (4.13a)$$

with phase

$$\angle H = -\text{arc tan}\,\frac{b_1}{a_1}$$

$$= -\text{arc tan}\left[\left(\frac{\pi F}{4\varphi} + \sin \beta\right)\sec \beta\right] \quad (4.13b)$$

In theory, the relations given in eqs (4.13) are valid for $\varphi/F \leq 2/\pi$. In practice, a describing function is meaningful only so long as the variations are reasonably close approximations of simple harmonic functions. This requirement limits φ/F to small values. In table 4.1, there is a comparison between velocity values obtained by the exact analysis of eq (4.9a) and the describing function of eq (4.12). As in figure 4.6, the ratio of friction force to driving force is chosen to be $\varphi/F = 1/\pi$, from which it follows that $\beta = -30°$.

TABLE 4.1. *Comparison of exact solution to describing function*

ωt	$\dot{x}m\omega\pi/F$	$Hm\omega\pi$
0	1. 05	1. 09
$\pi/6$	2. 10	2. 21
$\pi/4$	2. 49	2. 54
$\pi/3$	2. 71	2. 71
$\pi/2$	2. 62	2. 51
$2\pi/3$	1. 66	1. 62
$3\pi/4$	0. 92	1. 00
$5\pi/6$	0	0

The values of $m\omega|H|$ and $\angle H$ from eqs (4.13) are plotted in figure 4.7. It can be shown that similar describing functions can be obtained by the Ritz averaging method [5] and also by assuming that the coulomb friction force can be replaced by an equivalent damping force [5].

In summary, the describing-function concept as developed by Kochenburger [28] embodies the idea that, in a nonlinear element, a steady-state sinusoidal input will produce a periodic but nonsinusoidal output. It is assumed that adequate

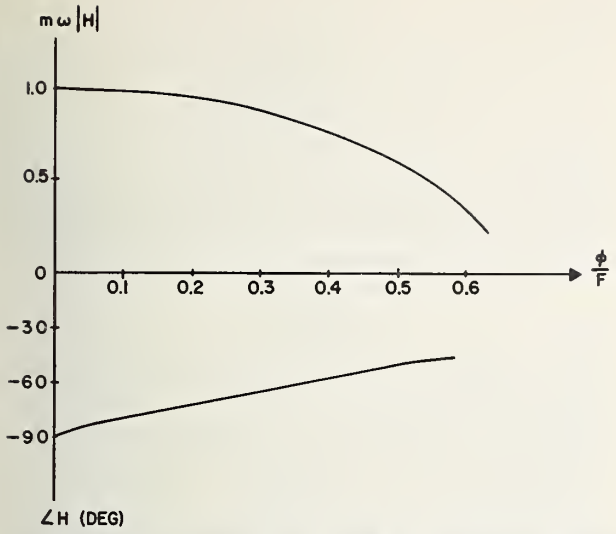

FIGURE 4.7. *Magnitude and phase of describing-function for system governed by eq (4.8).*

(Reproduced from [5] with permission from McGraw-Hill Book Co., Inc.)

results can be obtained by using only the fundamental component of this output.

Klotter [33] called attention to the fact that the cases which had been treated (until 1957) were those where the relationship between input and output can be given by a nonlinear expression of the variables themselves as contrasted to other cases in which the nonlinear element is characterized by differential relationships between the variables. In the literature, cases can be cited where the nonlinearity is caused by dead bands [40, 41], saturation [40], limiting [42], linkages [43], contactors [28], and coulomb friction [44]. (For the last situation see the illustrative problem discussed above, eq (4.8) et seq.) In [33] Klotter presents a method by which describing functions for nonlinear elements whose behavior is described by nonlinear differential equations can be obtained without solving the differential equations. The fundamentals of the method are explained in [22] and [24]; here we will focus our efforts on demonstrating its use. Let

$$E \equiv M(z) - k^2 y(t) = 0 \tag{4.14}$$

denote the nonlinear differential equation of the element under consideration with $y(t) = F \cos \omega t$ standing for the input and z for the unknown output. After [22], we will treat the second-order differential equation

$$E = \ddot{z} + 2\zeta\omega_n g(\dot{z}) + \omega_n^2 f(z) - \omega_n^2 F \cos \omega t = 0, \tag{4.15}$$

which contains two nonlinear terms $g(\dot{z})$ and $f(z)$. For simplicity of presentation, let us assume that $g(\dot{z})$ and $f(z)$ are odd functions of their respective arguments.[3] As an example, we will choose the parameters of eq (4.15) to be those of a Duffing-equation model with viscous damping (see eq (4.4) et seq.), that is,

$$g(\dot{z}) = \dot{z}$$

$$f(z) = z + \beta^2 z^3 \tag{4.16}$$

$$E \equiv \ddot{z} + 2\zeta\omega_n \dot{z} + \omega_n^2 (z + \beta^2 z^3) - \omega_n^2 F \cos \omega t = 0. \tag{4.17}$$

We seek an approximation $\tilde{z}$ to the output function $z(t)$ of the form (assumption 3)

$$\tilde{z} = Z \cos (\omega t - \epsilon), \tag{4.18}$$

with the parameters Z and ϵ chosen in such a way that they represent "best" values.

Because the function $\tilde{z}(t)$ of eq (4.18) cannot satisfy the differential equation of eq (4.17) at every instant, we will satisfy it in some weighted average. In [22] and [24], it is shown that appropriate weighting functions are cos ωt and sin ωt. By the Ritz averaging method then, the integrals

$$\left.\begin{aligned} \int_0^{2\pi} E[\tilde{z}(\sigma)] \cos \sigma \, d\sigma = 0 \\ \int_0^{2\pi} E[\tilde{z}(\sigma)] \sin \sigma \, d\sigma = 0 \end{aligned}\right\}. \tag{4.19}$$

From these two equations, we will determine the parameters Z and ϵ in the approximating function of eq (4.18). The steps for accomplishing this are:

Step 1. From the two functions $f(z)$ and $g(\dot{z})$, eq (4.16), we derive two new functions $\phi(Z)$ and $\Gamma(Z, \omega)$ by performing the following integrations:

$$\left.\begin{aligned} \phi(Z) = \frac{4}{\pi} \frac{1}{Z} \int_0^{\pi/2} f(Z \cos \sigma) \cos \sigma \, d\sigma \\ \text{or equivalently} \\ = \frac{4}{\pi} \frac{1}{Z} \int_0^{\pi/2} f(Z \sin \sigma) \sin \sigma \, d\sigma \end{aligned}\right\} \tag{4.20a}$$

and

$$\left.\begin{aligned} \Gamma(Z, \omega) = \frac{4}{\pi} \frac{1}{\omega_n} \frac{1}{Z} \int_0^{\pi/2} g(Z\omega \sin \sigma) \sin \sigma \, d\sigma \\ \text{or equivalently} \\ = \frac{4}{\pi} \frac{1}{\omega_n} \frac{1}{Z} \int_0^{\pi/2} g(Z\omega \cos \sigma) \cos \sigma \, d\sigma \end{aligned}\right\}. \tag{4.20b}$$

Equations (4.20) are equivalent to the following procedure: Introduce $Z \cos \omega t$ and $Z\omega \sin \omega t$ for z and $\dot{z}$, respectively; replace the functions f and g of these arguments by functions of multiple arguments ($2\omega t$ $3\omega t$, . . .) and retain the fundamental terms only.

Step 2. Using the functions ϕ and Γ of eqs (4.20), we obtain the amplitude Z and the phase ϵ from the two equations (which follow from eq

[3] In [22] the treatment is outlined also for the case of even functions.

(4.19))

$$\left[\phi-\left(\frac{\omega}{\omega_n}\right)^2\right]^2+4\zeta^2\Gamma^2=\left(\frac{F}{Z}\right)^2 \tag{4.21a}$$

and

$$\tan\epsilon=\frac{2\zeta\Gamma}{\phi-\left(\frac{\omega}{\omega_n}\right)^2}. \tag{4.21b}$$

In terms of the parameters of eq (4.17), the functions ϕ and Γ are

$$\left.\begin{aligned}\phi&=1+\tfrac{3}{4}\beta^2Z^2\\ \Gamma&=\frac{\omega}{\omega_n}\end{aligned}\right\} \tag{4.22}$$

by which eqs (4.21) become

$$\left[1+\tfrac{3}{4}\beta^2Z^2-\left(\frac{\omega}{\omega_n}\right)^2\right]+4\zeta^2\left(\frac{\omega}{\omega_n}\right)^2=\left(\frac{F}{Z}\right)^2 \tag{4.23a}$$

and

$$\tan\epsilon=\frac{2\zeta\left(\frac{\omega}{\omega_n}\right)}{1+\tfrac{3}{4}\beta^2Z^2-\left(\frac{\omega}{\omega_n}\right)^2}. \tag{4.23b}$$

Equations (4.23) give both the modulus $|N|=\frac{F}{Z}$ and the argument ϵ of the "inverse equivalent transfer function" [4]

$$N=\left(\frac{F}{Z}\right)e^{j\epsilon}. \tag{4.24}$$

This (complex) transfer function can be plotted as a family of curves, either with βZ, as a parameter of the family and ω/ω_n varying along the individual curves, or vice versa.

In summary, an equivalent transfer function (describing function) for the output of a viscously damped, Duffing-equation model has been derived. The expression for it is given by eq (4.24) and the modulus $|N|=\frac{F}{Z}$ and argument ϵ by eqs (4.23).

5. Bilinear Approximation Method for Determining the Transient Response of a Nonlinear System [32]

A line-segment approximation method by which the transient response of a nonlinear transducer can be determined has been developed by Ergin [32]. In particular, the method is applicable to systems with a nonlinear restoring force characteristic. Ergin shows that for many problems involving even large nonlinearities, two line segments are sufficient to yield an adequate approximate solution. At least for the examples chosen by Ergin, the bilinear approximation gives more accurate results than the classical perturbation methods of Poincaré [16], Linstedt [17], and Kryloff and Bogoliuboff [3], and it is faster than graphical and numerical methods. It may also be adapted to an iterative procedure, should it be desirable to improve the accuracy of the method.

There are other allied problems in which the effect of a nonlinear restoring-force function is represented by linear or piecewise linear functions of the displacement; for example, simple piecewise linear problems are considered by Hansen and Chenea [45], and others are discussed in some detail by Flugge-Lotz [46]. More recently, Mahalingham [47] developed a one-term approximate solution for the amplitudes of a single-degree-of-freedom system with nonlinear (nonsymmetrical) spring characteristics. The method of [47] is similar to that of Martienssen [48], but the construction uses a modified frequency function in place of the actual spring characteristic, the function being so chosen that it yields the correct frequency of free vibration. A system with a trilinear restoring-force function (that is, one which is piecewise linear by joining successively an initial linear section, a softening section, and a hardening section) has been studied by Dost and Atkinson [49] by means of an electronic differential analyzer. In addition, we include the following literature references to similar problems: Atkinson and Heflinger [50], Katz [51], Evaldson, Ayre and Jacobsen [52], Ludeke [53], Wylie [54], Jacobsen and Jespersen [55], Rauscher [56], and Burgess [57].

In most of the cases cited above, a solution is obtained for systems in which a nonlinear restoring-force function is piecewise linear, either bi- or trilinear. It is worth noting explicitly that Ergin [32] solved a somewhat different problem; namely, that of

(a) approximating the nonlinear restoring-force function of a system by a bilinear approximation and then

(b) finding a solution such that the mean-square error between the actual nonlinear restoring-force function and the assumed bilinear approximation is a minimum.

It is a well-known principle that any function can be approximated by a number of straight-line segments. Each line can be determined by its slope and a point through which it passes; this joint can be picked to be the transition point where two segments meet. The slopes and transition points can be determined so that the mean-square error between the function and the series of line segments is minimized within a range of variables. The application of this concept to the solution of nonlinear differential equations is a direct one. Any nonlinearity, which is a function

[4] In an attempt to emphasize the analogy to the corresponding linear concept, Klotter [33] chooses to replace the term "describing function" by "equivalent transfer function" with qualifying adjectives, such as inverse, direct, etc., as the case may be. For comparison, see eq (4.11).

of the independent variable only, can be described by a number of line segments chosen so as to approximate the nonlinear function as closely as possible. The nonlinear problem, then, reduces to the solution of the same number of linear equations as there are line segments, with the proper matching of displacement and velocity at the transition points. The determination of the optimum slopes and transition point locations for line segments requires the solution of $(2n-1)$ nonlinear simultaneous algebraic equations.

There are certain simplifications which make this method of linear approximations feasible. Most functions encountered in practice can be approximated satisfactorily by only two line segments. In addition, it is possible to choose the slope of the first line segment as the specified slope of the function at the origin without significant loss of accuracy. This simplifies the problem to the determination of the slope of the second line segment and the location of the transition point; the choice of both being such that the mean square error is minimized.

In [32] it is shown that, for any nonlinearity which can be expressed as a power of the independent variable, the second slope and the location of the transition point are simple functions of the maximum displacement amplitude. It is also shown that for small nonlinearities, the solution in many cases is insensitive to the precise choice of the maximum deflection used to calculate the parameters of the bilinear approximation.

In what follows we will state the basic relations upon which the method is based and apply it to the undamped Duffing-equation model of eq (4.2).

Consider the original nonlinear differential equation which governs the motion of a transducer system to be of the form [32]

$$\ddot{x}+k_1x+h(x)=f(t). \tag{4.25}$$

We assume that eq (4.25) can be approximated by the two linear equations:

$$\ddot{x}+g_1(x)=f(t) \text{ for } |x|<x_t \tag{4.26}$$

$$\ddot{x}+g_2(x)=f(t) \text{ for } |x|>x_t \tag{4.27}$$

where $g_1(x)$ and $g_2(x)$ are linear functions of x, and x_t is the "transition amplitude" where the linear restoring-force changes from $g_1(x)$ to $g_2(x)$.

As mentioned earlier, $g_1(x)$ is taken equal to k_1x, where k_1 is the slope of the nonlinear restoring-force function at the origin. Then,

$$\left.\begin{aligned} g_1(x)&=k_1x \\ g_2(x)&=k_2x+(k_1-k_2)x_t \end{aligned}\right\}, \tag{4.28}$$

where k_2 and x_t are as yet undetermined constants. The form of $g_1(x)$ and $g_2(x)$ require that the piecewise-linear approximation is continuous at $x=x_t$.

The parameters k_2 and x_t are to be determined such that the mean square error $(\bar{E})^2$ between the nonlinear restoring-force function and the bilinear approximation of it is minimized;

$$(\bar{E})^2=\frac{1}{x_m}\left\{\int_0^{x_t}[g_1(x)-g(x)]^2\,dx + \int_{x_t}^{x_m}[g_2(x)-g(x)]^2\,dx\right\} \tag{4.29}$$

where $g_1(x)$ and $g_2(x)$ are defined by eq (4.28); $g(x)=k_1(x)+h(x)$; and x_m is the maximum displacement amplitude of the motion.

The conditions that $(\bar{E})^2$ has an extremum are [58]

$$\frac{\partial(\bar{E})^2}{\partial x_t}=0 \tag{4.30}$$

and

$$\frac{\partial(\bar{E})^2}{\partial k_2}=0. \tag{4.31}$$

Since $g_1(x)$ and $g(x)$ are not functions of x_t, and $g_1(x_t)=g_2(x_t)$, then eq (4.30) reduces to

$$\int_{x_t}^{x_m}[g_2(x)-g(x)]dx=0. \tag{4.32}$$

Similarly, eq (4.31) reduces to

$$\int_{x_t}^{x_m}[g_2(x)-g(x)]\frac{\partial g_2(x)}{\partial k_2}\,dx=0 \tag{4.33}$$

but

$$\frac{\partial g_2(x)}{\partial k_2}=x-x_t,$$

which when used in eq (4.33) and recalling (4.32) yields

$$\int_{x_t}^{x_m}[g_2(x)-g(x)]x\,dx=0. \tag{4.34}$$

By appropriate substitution of $g_2(x)$ and $g(x)$, eqs (4.32) and (4.34) can be simplified to

$$k_2-k_1=\frac{2}{(x_m-x_t)^2}\int_{x_t}^{x_m}h(x)dx \tag{4.35}$$

and

$$k_2-k_1=\frac{6}{(x_m-x_t)^2(2x_m+x_1)}\int_{x_t}^{x_m}h(x)x\,dx, \tag{4.36}$$

from which the desired values of x_t and k_2 can be found.

For the case where $h(x)$ is of the form

$$h(x)=\epsilon x^n \qquad (n>1) \tag{4.37}$$

and

$$x_t=ax_m, \tag{4.38}$$

where a is a constant of proportionality, the simultaneous solution of eqs (4.35) and (4.36) is

relatively easy.[5] We see that they then become, respectively,

$$k_2-k_1=\frac{2\epsilon x_m^{n-1}(1-a^{n+1})}{(1-a)^2(n+1)} \tag{4.39}$$

and

$$k_2-k_1=\frac{6\epsilon x_m^{n-1}(1-a^{n+2})}{(1-a)^2(a+2)(n+2)}. \tag{4.40}$$

Solving for the constant a in the latter two equations, we obtain

$$a+2=\frac{3(n+1)(1-a^{n+2})}{(n+2)(1-a^{n+1})}. \tag{4.41}$$

Since $a<1$ and $n>1$ then $\frac{(1-a^{n+2})}{(1-a^{n+1})}\approx 1$ and eq (4.41) yields

$$a=\frac{n-1}{n+2}, \tag{4.42}$$

where n is the power of the nonlinear restoring-force term (4.37). In turn, with this value of a, the slope of the second line segment can be computed from eq (4.39) and x_t from eq (4.38).

Let us apply [32] the results of the analysis above to the transient response of an undamped Duffing-equation model to the half-sine pulse excitation of the form

$$\ddot{x}+\omega_n^2(x+\beta^2x^3)=\sin \omega t \text{ for } 0<t<\tau \tag{4.43}$$

$$=0 \text{ for } t>\tau \tag{4.44}$$

where τ, the pulse length, is π/ω. For $t=\pi/\omega$, the solutions of eqs (4.43) and (4.44) must be equal. Since an exact solution of homogeneous eq (4.44) exists [59], our main interest lies in finding an approximation to eq (4.43) such that the motion during the pulse can be obtained.

For convenience in computing the results, let us assume the initial conditions are at $t=0$:

$$x(0)=\dot{x}(0)=0$$

and

$$\omega_n^2=\beta^2=1, \qquad \omega=2$$

Then, eqs (4.43) and (4.44) become

$$\ddot{x}+x+x^3=\begin{cases}\sin 2t \text{ for } 0<t<\frac{\pi}{2}\\ 0 \text{ for } t>\frac{\pi}{2}.\end{cases} \tag{4.45}$$

For a cubic nonlinearity, the transition amplitude x_t is, from eqs (4.38) and (4.42)

$$x_t=0.4x_m \tag{4.46}$$

and the second slope k_2,

$$k_2=k_1+1.35x_m^2=1+1.35x_m^2. \tag{4.47}$$

The parameter x_m is computed as the maximum amplitude of the linear solution of eq (4.45)[6]; hence

$$\ddot{x}+x=\sin 2t,$$

the solution of which for the same initial conditions is

$$x=\tfrac{1}{3}(2\sin t-\sin 2t)$$

and, in the range $0<t<\pi/2$, $x_m=0.667$. Thus,

$$x_t=0.267 \text{ and } k_2=1.60. \tag{4.48}$$

The two bilinear equations to be solved are

$$\ddot{x}_1+x_1=\sin 2t;\ x_1(0)=\dot{x}_1(0)=0 \text{ for } |x|<x_t \tag{4.49}$$

$$\ddot{x}_2+1.6x_2-0.16=\sin 2t;\ x_2(t_t)=x_1(t_t);\ \dot{x}_2(t_t)=\dot{x}_1(t_t) \tag{4.50}$$

where t_t is the transition time, the time which it takes x_1 to reach x_t. The solution of eq (4.49) is

$$x_1=\tfrac{1}{3}(2\sin t-\sin 2t),$$

from which the transition parameters are

$$\left.\begin{aligned}&x_1(t_t)=x_t=0.267\\ &t_t=1.011 \text{ (radians)}\\ &\dot{x}(t_t)=0.646\end{aligned}\right\}. \tag{4.51}$$

The solution of eq (4.50) which satisfies the conditions $x_2(t_t)=0.267$ and $\dot{x}_2(t_t)=0.646$ is

$$x_2=0.1+0.582\sin\left(\sqrt{1.6}t-0.084\right)-\frac{1}{2.4}\sin 2t. \tag{4.52}$$

The displacement and velocity at the end of the pulse ($t=\pi/2$) are, respectively

$$x_2\left(\frac{\pi}{2}\right)=0.651 \text{ and } \dot{x}_2\left(\frac{\pi}{2}\right)=0.592.$$

Comparable values obtained by numerical iteration to four-place accuracy are

$$x\left(\frac{\pi}{2}\right)=0.6518 \text{ and } \dot{x}\left(\frac{\pi}{2}\right)=0.6001,$$

that is, the approximate results obtained by solving the two bilinear eqs (4.49) are within 0.5 percent in displacement and 1.5 percent in velocity of a numerical solution of eq (4.45) when the nonlinear force at the maximum deflection point is about 60 percent of that for the linear model.

In summary, a method is shown for approximating a nonlinear restoring-force function by a particular bilinear approximation for which the slope and location of the transition point have been selected so that the mean square error between the original function and the approximation is minimized.

[5] Note that the Duffing-equation type of restoring-force function, eq (4.1) is included.

[6] In [32] this is shown to be a reasonable assumption.

6. The Phase-Plane Method [4, 5]

A general exposition of the phase-plane method (including the method of isoclines) is given in section 4 of chapter 2. Here we will restrict the discussion to three central points:

(a) the method of isoclines applied to a nonlinear system,
(b) the phase-plane-delta method as applied to a nonlinear system, and
(c) the determination of displacement-time plots from phase portraits.

As mentioned earlier, a dynamical system with n degrees of freedom depends on n positional coordinates $\dot{q}_i$. The state of the system at any instant of time depends upon the values of q_i, and the velocities $\dot{q}_i$. Thus, a phase-space of $2n$ dimensions is associated with the behavior of the dynamical system. To each state of the system there corresponds the point Q with coordinates (q_i, q_i) in the phase space; as t varies, the point Q describes a curve called a path or trajectory, which describes the history of the system. The totality of all paths is called the phase portrait of the system. It represents all the possible histories of the system, any one of which is determined by specifying a single state Q_0. In a geometric sense, this means there is *one and only one* path through each point of the phase space.

6.1. Method of Isoclines [1]

It is upon this last concept that the method of isoclines is based. In chapter 2, the method is applied to linear systems. Here we will recall only the essentials of the method and apply it to a nonlinear system.

Only certain equations are amenable to solution by the isocline method, namely, those which can be reduced to a single first-order equation. An example is

$$\ddot{x}+f(\dot{x}, x)=0. \tag{4.53}$$

Equations (4.2), (4.4), (4.8), (4.43), and (4.45) in homogeneous form are all examples of eq (4.53), an autonomous equation.[7] It may be reduced to a first-order equation by introducing the new variable $v=\dot{x}$; then,

$$\ddot{x}=\dot{v}=\left(\frac{dv}{dx}\right)\left(\frac{dx}{dt}\right)=\frac{vdv}{dx},$$

and eq (4.53) becomes

$$\frac{dv}{dx}=-\frac{f(v, x)}{v}. \tag{4.54}$$

This is a first-order differential equation in the independent variable x and hence can be treated by the isocline method. It is convenient in some cases to normalize the velocity coordinate, that is, to specify the coordinates of the phase plane as (x, ν), where $\nu=\dot{x}/\omega_n$.

As an application of the isocline method to the solution of a nonlinear differential equation, let us consider [59] a system whose motion is governed by the van der Pol equation

$$\ddot{x}-\epsilon(1-x^2)\dot{x}+x=0, \tag{4.55}$$

the equation for an oscillatory system with variable damping. In our illustrative [8] problem, let $\epsilon=0.1$. In eq (4.55), let us introduce the variable $v=\dot{x}$, then

$$\frac{dv}{dx}=\epsilon\,\frac{(1-x^2)v-x}{v}.$$

The algebraic equation for an isocline curve is then

$$v=\frac{x}{\epsilon(1-x^2)-m},$$

where m is a specified value of dv/dx, the slope of a solution curve (phase path). Isoclines found from this relationship with indicated values of m are plotted in figure 4.8. Because the equation is nonlinear, the isoclines are curves and not straight lines as in figure 2.4 of chapter 2. An infinity of isoclines come together at the origin, which is a singularity.[9] For $\epsilon=0.1$, the isoclines have a rather simple geometrical shape, suggestive of figure 2.4. Line segments with appropriate slope are located along the isoclines of figure 4.8. For a precise construction of the phase trajectories, more isoclines and line segments are needed than are shown here.

A most interesting property of the solution for the van der Pol equation is that there is a particular closed solution curve that is ultimately achieved, regardless of the initial conditions. This closed curve represents a *steady-state periodic* oscillation, determined only by the properties of the equation itself, and independent of the way the oscillation is started. It is a phenomenon characteristic of oscillating systems with nonlinear damping and cannot occur in a linear system. A more intensive investigation of the phenomenon [10] shows that, if the initial point is inside this closed curve, the corresponding phase path (solution curve) spirals outward. If the initial point is outside the curve, the phase path spirals inward. In either case, ultimately the phase paths approach this closed curve, called a *limit cycle* by Poincaré [60]. An important property of this limit cycle for eq (4.55) is that the maximum magnitude of x is always close to two units, regardless of the value of ϵ.[11]

[7] An autonomous equation is one in which the independent variable (here time t) appears in the derivatives only.

[8] The relative magnitude of ϵ has significant effect upon the configuration of the phase paths which characterize the behavior of systems governed by eq (4.55). For a study of the effect of varying ϵ and the concept of limit cycles, see [9], p. 148 et seq., and [5], p. 35 et seq.

[9] For a system whose motion is characterized by an autonomous equation (such as equation (4.53)), the points at which both $\dot{x}$ and $\dot{v}$ vanish are called singular points. For a discussion of such points, see [1], p. 9.

[10] For example, see [59], p. 148 et seq.

[11] See [59], figures 58 and 59; see [5], figures 3.4 and 3.5.

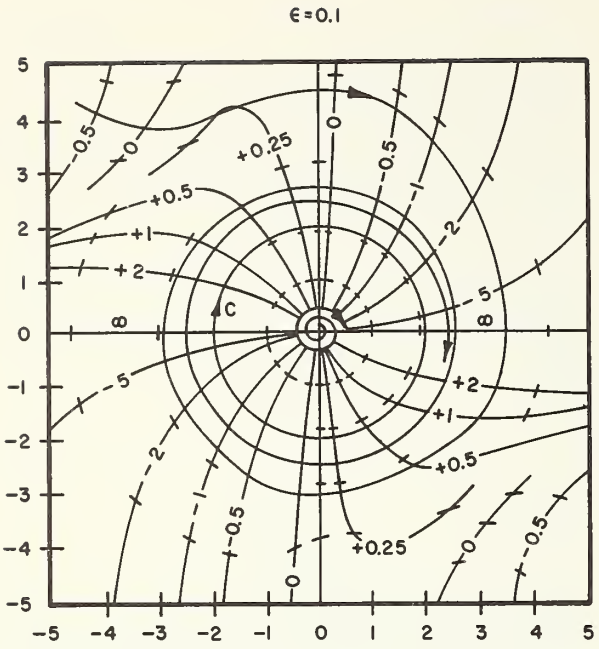

FIGURE 4.8. *Phase path for equation* $\ddot{x}-\epsilon(1-x^2)\,\dot{x}+x=0$ *for* $\epsilon=0.1$.

The closed curve C is the limit cycle. Isoclines are given for constant m

(Reproduced from [59] with permission from The Clarendon Press, Oxford)

6.2. Phase-Plane Delta Method [61]

In starting a solution by the isocline method, the entire plane must be filled with line segments which fix the slope of the phase paths. If only a single such trajectory is sought, only a few of these line segments are actually used. Considerable simplification would result if only information related directly to the desired solution curve were used. Jacobsen [61] has proposed just such a method. It is an extension and refinement of the earlier work by Lamoen [62] and Fuchs [63]. In [61], Jacobsen generalizes and consciously formulates the method as an efficient working tool.

Let us assume that either inherently or by a suitable division it is possible to reduce the equation governing the motion of a system to the form [12]

$$\ddot{x}+H(\dot{x}, x, t)=0 \tag{4.56}$$

without specifying any particular kind of function H. Then, after choosing an arbitrary constant k (of dimension T^{-1}), eq (4.56) may be written as

$$\ddot{x}+k^2h(\dot{x}, x, t)=0 \tag{4.56a}$$

with h of the same dimension as x. If we introduce the phase-plane coordinates x and $y=\dot{x}/k$, we may replace eq (4.56a) by

$$\begin{aligned}\dot{x}&=ky\\ \dot{y}&=-kh\end{aligned} \tag{4.57}$$

[12] Note the nonautonomous nature of eq (4.56) in contrast to eq (4.53) et seq.

from which we may obtain the differential equation of the trajectories in the phase plane.

$$\frac{dy}{dx}=-\frac{h}{y}. \tag{4.58}$$

In the phase-plane, the tangent of the path through P, figure 4.9, will be perpendicular to line QP. A graphical procedure, leading to an approximation of the trajectory by a sequence of arclike segments, can be based on this geometric relationship.

It is apparent that if k (as used here) is the same as the quantity ω_n (used in the chapter 2 discussion of the phase-plane), the coordinates y and v will coincide. The length h (fig. 4.9) may be divided into the two components x and δ, from which it follows that

$$\frac{dv}{dx}=-\frac{x+\delta}{v}, \tag{4.59}$$

where $v=\dot{x}/\omega_n$ and $\delta=\delta(v, x, t)=h(v, x, t)-x$. Equation (4.59) is similar to eq (4.54) used in the discussion of the isocline method. For δ constant, the variables of eq (4.59) are separable and can be integrated to yield

$$v^2+(x+\delta)^2=\text{constant}=\rho^2, \tag{4.60}$$

the equation of a circle of radius ρ with its center at $(x, v)=(-\delta, 0)$. Thus, for a suitably small increment, the trajectory is the arc of a circle having these properties. In reality δ is not a constant. This implies that the true centers of curvature of the path segments are located somewhere on the line PQ (fig. 4.9), but not necessarily at Q.

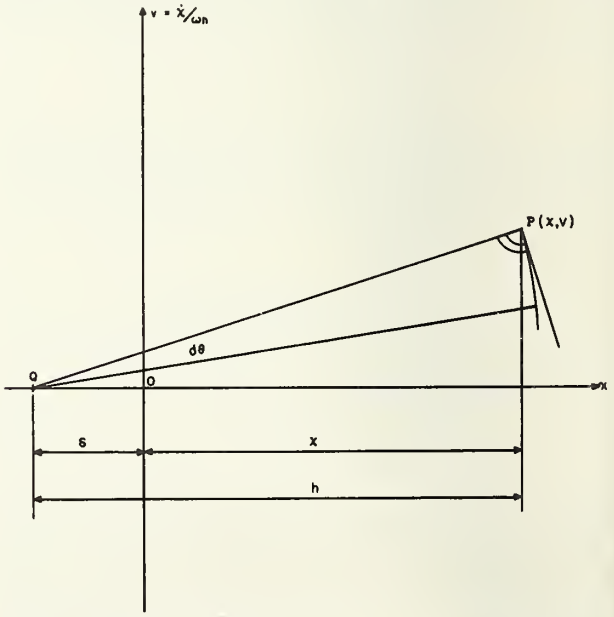

FIGURE 4.9. *Graphical representation of segment of phase path at* P(x, v).

Let us apply the delta method to a Duffing-equation model: let the motion of such a system be governed by [61]

$$\ddot{x}+25(1+0.1x^2)x=0 \qquad (4.61)$$

with initial conditions at $t=0$: $x=3$, $\dot{x}=0$. Then, putting the equation in the form of eq (4.56a),

$$\ddot{x}+\omega_n^2 h=0$$

where $\omega_n^2=25$, $h=x+\delta=x+0.1x^3$, and (in terms of the phase-plane coordinates)

$$\frac{dv}{dx}=-\frac{x+0.1x^3}{v}.$$

In figure 4.10, a plot of the solution curve for eq (4.61) is shown.

Construction of the approximation to the curve is shown on the figure. The initial point is $x(0)=3$, $v(0)=0$. As the first step, it is assumed that x decreases to the value 2.8, or $\Delta x^{(1)}=-0.2$, as shown. The average of x during this interval is $x_{av}^{(1)}=2.9$, for which the value of δ can be read directly as $\delta_{av}^{(1)}=2.4$, approximately. Thus, the center for the first circular arc is located at $x=-2.4$ and $v=0$. The radius is $(3+2.4)=5.4$, and with this radius an arc is drawn to the point where $x=2.8$, indicated in the figure by the small dot marked $x(0)+\Delta x^{(1)}$.

By continuing in this manner, the entire solution curve can be built up as a sequence of circular arcs. Dots along the curve of figure 4.10 indicate the junction points of successive arcs used in obtaining the phase path.

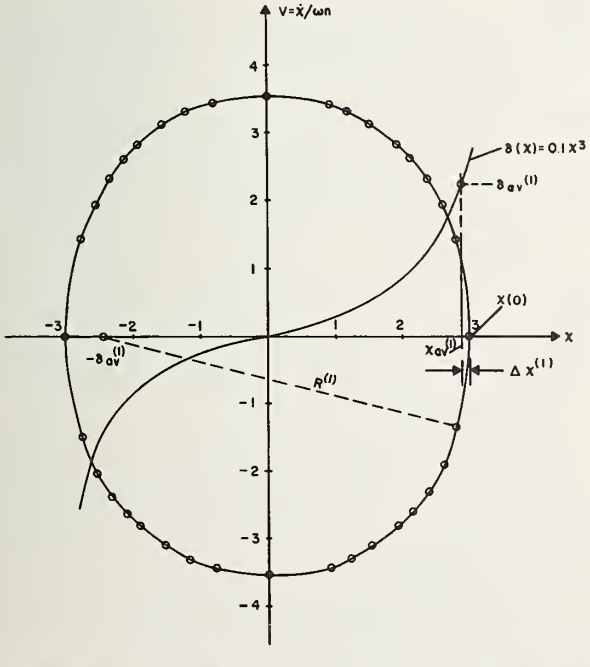

FIGURE 4.10. *Phase path for* $\ddot{x}+25(1+0.1x^2)x=0$ *constructed by delta method.*

Dots on phase path indicate junction point on arcs

(Reproduced from [5] with permission from McGraw-Hill Book Co., Inc.)

While the delta method is most immediately applicable to equations with oscillatory solutions (that is, closed-curve phase-paths), it can be applied to other types of equations as well. Chu and Abramson [71] have applied it to systems with several degrees of freedom.

In summary, the phase-plane-delta method relegates all the terms of an ordinary second-order differential equation into the type form

$$\ddot{x}+\omega_n^2(x+\delta)=0. \qquad (4.62)$$

Using the graphical procedure described above and the parameters of eq (4.62), an approximation to the sought-for solution curve is plotted in terms of the phase-plane coordinates (x, v). The accuracy of the graphical procedure depends upon judicious choice of the size of the x increments. Test cases in [61] involving elliptic integrals, Bessel and Neumann functions, show good accuracy for increments of practicable size. For reasons of accuracy, the method is not recommended for solutions involving long durations; for example, as in Mathieu-type equations.[13]

In the case of forced-motion systems, eq (4.56) may be written as

$$m\ddot{x}+H(\dot{x}, x, t)=f(t).$$

Rearrangement into the type-form (eq (4.62)) yields

$$\ddot{x}+\omega_n^2\left[x+\delta-\frac{1}{k}f(t)\right]=0,$$

from which

$$\delta_{eff}=\delta-\frac{1}{k}[f(t)].$$

If the external driving term $x^*(t)$ is a forced motion of the "ground" end of the spring element of a spring-mass system, then eq (4.56) may be written as

$$m\ddot{x}+k[x-x^*(t)+\delta]=0.$$

If the relative displacement of the mass is denoted by $y=x-x^*(t)$, then we have

$$\ddot{y}+\omega_n^2\left[y+\delta+\frac{1}{\omega_n^2}\ddot{x}^*(t)\right]=0$$

from which

$$\delta_{eff}=\delta+\frac{1}{\omega_n^2}\ddot{x}^*(t).$$

Solutions for systems of these types are treated in [61] for several step-function excitations.

6.3. Displacement-Time Plots From Phase Paths [14]

Phase-plane trajectories involve time implicitly but it can be determined explicitly and the dis-

[13] See [59], chapter 7.

[14] A graphical integration and also a geometrical method are given in [6, p. 623].

placement plotted as a function of time. One method requires step-by-step integration and can be performed as follows:

For small increments Δx and Δt, the average velocity is

$$v_{av}=\frac{1}{\omega_n}\frac{\Delta x}{\Delta t}.$$

A small increment Δx can be measured on the phase path and the corresponding v_{av} determined. The increment in time needed to traverse the increment Δx is then

$$\Delta\tau\equiv\omega_n\Delta t=\frac{\Delta x}{v_{av}}.$$

In figure 4.11a, a portion of the phase path of figure 4.10 is shown. We recall that the initial conditions for this case are, at $t=0$, $x=3$, $\dot{x}=v=0$. Increments (negative here) in x are assigned as $\Delta x^{(1)}$, $\Delta x^{(2)}$, $\Delta x^{(3)}$ . . ., and corresponding average velocity values are $v_{av}{}^{(1)}$, $v_{av}{}^{(2)}$, $v_{av}{}^{(3)}$ . . ., (also negative). The corresponding increments in $\tau(=\omega_n\Delta t)$ are then detremined from eq (4.63) and are positive. Individual points obtained in this way are plotted in figure 4.11b. As in any numerical integration procedure, the choice of the magnitude for Δx is a compromise. In general, Δx should be chosen sufficiently small so that the corresponding changes in x and v are also small.

6.4. Other Phase-Plane Methods

A review of six general types of recent analytic techniques and new transforms (particularly, as they apply to nonlinear control systems) appears in [8]. In addition, Liu [64] has developed an electronic system which plots directly on an oscilloscope tube-face the phase path for a specified motion of a system (say, the response of a pressure transducer to a pulse excitation). Timing marks for constant Δt are marked on the phase path by an internal circuit. The inherent advantages of such a direct display of test information are obvious. However, detailed information concerning the stiffness and damping relations which govern the motion must be obtained by additional tests.

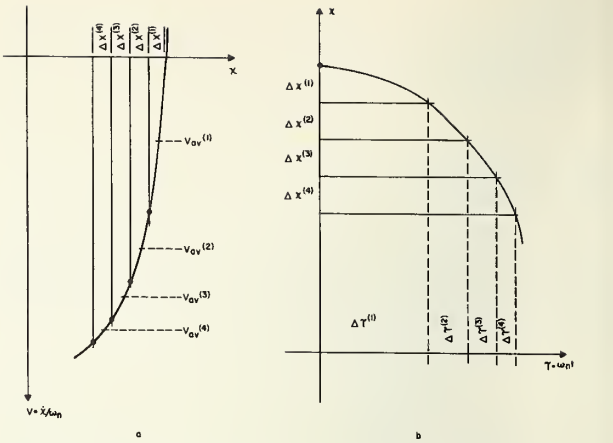

FIGURE 4.11. *Numerical integration method for obtaining displacement-time plot.*

7. References

[1] A. Andronov and C. E. Chaikin, Theory of Oscillations, Princeton Univ. Press (Princeton, N.J., 1949).

[2] N. Minorsky, Introduction to Non-Linear Mechanics, Edwards Brothers (Ann Arbor, Michigan, 1947); "Non-linear Oscillations", revised ed., D. Van Nostrand Co., Inc. (Princeton, N.J., 1962).

[3] N. Kryloff and N. Bogoliuboff, Introduction to nonlinear mechanics (trans. and ed. S. Lefschetz, "Ann. Math. Studies", No. 11), Princeton Univ. Press (Princeton, N.J., 1947).

[4] L. S. Jacobsen and R. S. Ayre, Engineering Vibrations, p. 286 et seq., McGraw-Hill Book Co., Inc. (New York, N.Y., 1958).

[5] W. J. Cunningham, Introduction to Non-linear Analysis, p. 208, McGraw-Hill Book Co., Inc. (New York, N.Y., 1958).

[6] J. G. Truxal, Automatic Feedback Control Synthesis, McGraw-Hill Book Co., Inc. (New York, N.Y., 1955).

[7] G. J. Murphy, Control Engineering, D. Van Nostrand Co., Inc. (Princeton, N.J., 1959).

[8] Y. H. Ku, Theory of non-linear control, J. Franklin Inst. **271,** 108–144 (1961).

[9] W. E. Milne, Damped vibrations, Univ. Oregon Publ. **2,** No. 2 (Aug. 1923).

[10] K. F. Rubbert, On vibrations with combined damping, Ing. Arch. **17,** No. 3, 165–166 (1949).

[11] J. P. Den Hartog, Forced vibrations with combined coulomb and viscous friction, Trans. ASME **53,** 107–115 (1931).

[12] T. A. Perls and E. S. Sherrard, Frequency response of second-order systems with combined coulomb and viscous damping, J. Research NBS **57,** No. 1 (July 1956) RP 2693.

[22] K. Klotter, Non-linear vibration problems treated by the averaging method of W. Ritz, pp. 125–131, Proc. 1st U.S. Natal Cong. Appl. Mech., ASME (1951).

[23] C. P. Atkinson and C. P. Bourne, The solution of Duffing's equation for a softening spring system using the Ritz-Galerkin method with a three-term

[13] K. Klotter, The attenuation of damped free vibrations and the derivation of the damping law from recorded data, p. 85, Proc. 2d U.S. Nat'l Cong. Appl. Mech., ASME (1954).

[14] L. S. Jacobsen, Steady forced vibrations as influenced by damping, Trans. ASME **52,** 169 (1930).

[15] J. E. Gibson, Non-linear system design, Control Eng., 69–75 (Oct. 1951).

[16] H. Poincaré, New Methods of Celestial Mechanics (in French), vols. I and II, Gauthier-Villars (Paris, 1892, 1893).

[17] A. Lindstedt, Differential equations of perturbation theory (in German), Mem. Acad. Imp. Sci. St. Petersburg **31,** No. 4 (1883).

[18] W. Ritz, On a new method of solution of certain variation problems of mathematical physics (in German), Crelles J. f.d. reine w. ang. Math. **135,** 1–61 (1909).

[19] B. G. Galerkin, Series solution of some problems of elastic equilibrium of rods and plates, Vestnik Inzhenerov Petrograd, No. 19, 897 (1915).

[20] W. J. Duncan, Galerkin's method in mechanics and differential equations, Aero. Research Com. (London), R&M No. 1798 (Aug. 1937).

[21] W. J. Duncan, The principles of the Galerkin method, Aero. Research Com. (London), R&M No. 1848 (Sept. 1938).

approximation, pp. 71–77, Proc. 3d U.S. Nat'l Cong. Appl. Mech. ASME (1958).
[24] K. Klotter, Steady-state vibrations in systems having arbitrary restoring and damping forces, pp. 234–258, Proc. Symp. Non-linear Circuit Analysis **2,** Brooklyn Poly. Inst. (1953).
[25] K. Klotter and P. R. Cobb, On the use of non-sinusoidal approximating functions for non-linear oscillation problems, J. Appl. Mech. [E] **27,** No. 3, 579–583 (1960).
[26] R. B. Bowersox and J. Carlson, Digital-computer calculation of transducer frequency response from its response to a step function, Progr. Rept. 20–331, Jet Propulsion Laboratory (July 1957).
[27] C. G. Hylkema and R. B. Bowersox, Experimental and mathematical techniques for determining the dynamic response of pressure gages, Memo No. 20–68, Jet Propulsion Laboratory (Oct. 1953).
[28] R. J. Kochenburger, A frequency response method for analyzing and synthesizing contactor servomechanisms, Trans. AIEE **69,** Pt. 1, 270 (1950).
[29] L. C. Goldfarb, On some non-linear phenomena in regulatory systems (in Russian), Avtomat. i Telemekh. **8,** No. 5, 349–383 (1947).
[30] A. Tustin, The effects of backlash and of speed-dependent friction on the stability of closed-cycle control systems, J. Inst. Elec. Engr. (London), Pt. **94,** II–A, 152–160 (1957).
[31] W. Oppelt, On the ortho-curve method as applied to an example with friction (in German), Z. Ver. deut. Ing. (Berlin) **90,** 179–183 (1948).
[32] E. I. Ergin, Transient response of a non-linear system, J. Appl. Mech., **23,** No. 4, 635–641 (1956).
[33] K. Klotter, How to obtain describing functions for non-linear feedback systems, Trans. ASME **79,** 509–512 (1957).
[34] K. Klotter, An extension of the conventional concept of the describing function, pp. 151–162, Proc. Symp. Non-linear Circuit Analysis **6,** Brooklyn Polytechnic Institute (1957).
[35] K. Klotter, On the Use of Replacing the Transient Response Function of the Solution of Non-linear Feedback Systems (in German), Fachtagung Regelungestechnik (Heidelberg, 1956).
[36] J. C. West, The Use of Frequency Response Analysis in Non-linear Control Systems, Fachtagung Regelungetechnik (Heidelberg, 1956).
[37] H. D. Grief, Describing function method of servomechanism analysis applied to most commonly encountered nonlinearities, Trans. AIEE **72,** Pt. II, 243–248 (1953).
[38] E. C. Johnson, Sinusoidal techniques applied to nonlinear feedback systems, pp. 258–273, Proc. Symp. Nonlinear Circuit Analysis, Vol. 2, Brooklyn Polytechnic Institute (1953).
[39] J. Tou and P. M. Schultheiss, Static and sliding friction in feedback systems, J. Appl. Phys. **24,** 1210–1217 (1953).
[40] H. Chestnut, Approximate frequency-response methods for representing saturation and dead band, Trans. ASME **76,** 1345–1364 (1954).
[41] C. H. Thomas, Stability characteristics of closed-loop systems with dead band, Trans. ASME **76,** 1365–1382 (1954).
[42] R. J. Kochenburger, Limiting in feedback control systems, Trans. AIEE **72,** Pt. 2, 180–194 (July 1953).
[43] E. C. Johnson, Sinusoidal analysis of feedback-control systems containing nonlinear elements, Trans. AIEE **71,** Pt. 2, 169 –181 (July 1952).
[44] V. B. Haas, Jr., Coulomb friction in feedback control systems, Trans. AIEE **72,** Pt. 2, 119–126 (1953).
[45] H. M. Hansen and P. F. Chenea, Mechanics of Vibration, John Wiley & Sons, Inc. (New York, N.Y., 1952).
[46] I. Flugge-Lotz, Discontinuous Automatic Control, Princeton Univ. Press (Princeton, N.J., 1953).
[47] S. Mahalingham, Forced vibrations of systems with nonlinear, nonsymmetrical characteristics, J. Appl. Mech. **24,** No. 3, 435–439 (1957).
[48] O. Martienssen, On a new response phenomena in alternating current circuits (in German), Phys. Z. **11,** 448 (1910).
[49] M. Dost and C. P. Atkinson, Electronic computer stimulation of a system with a trilinear restoring function, pp. 133–140, Proc. 3d U.S. Nat'l. Cong. Appl. Mech., ASME (1958).
[50] C. P. Atkinson and I. Heflinger, Subharmonic and superharmonic oscillations of a bilinear vibrating system, J. Franklin Inst. **262,** No. 3, 185–190 (Sept. 1956).
[51] A. M. Katz, Biharmonic vibrations of a dissipative nonlinear system activated or kept activated by a harmonic disturbing force, Appl. Math. and Mech. Inst. Mech. Acad. Sci., U.S.S.R., **18,** 425–444 (1954).
[52] R. L. Evaldson, R. S. Ayre, and L. S. Jacobsen, Response of an elastically nonlinear system to transient disturbances, J. Franklin Inst. **248,** 548–562 (1949).
[53] C. A. Ludeke, An experimental investigation of forced vibrations in mechanical systems having a nonlinear restoring force, J. Appl. Phys. **17,** 603–609 (1946).
[54] C. R. Wylie, On the forced vibration of non-linear springs, J. Franklin Inst. **236,** 273–284 (1943).
[55] L. S. Jacobsen and H. J. Jespersen, Steady forced vibration of a single mass system with a non-lincar restoring force, J. Franklin Inst. **220,** 467–496 (1935).
[56] M. Rauscher, Steady oscillations of systems with nonlinear and unsymmetrical elasticity, Trans. ASME **60,** A169–A177 (Dec. 1938).
[57] J. C. Burgess, Harmonic, superharmonic and subharmonic responses for single degree of freedom systems of the Duffing type, Tech. Rept. No. 27, Div. Eng. Mech., Stanford Univ. (Sept. 1954).
[58] R. Courant, Differential and Integral Calculus, vol. 1, p. 160 et seq, Interscience Publ., Inc. (New York, N.Y., 1937).
[59] N. W. McLachlan, Ordinary Non-linear Differential Equations in Engineering and Physical Sciences, p. 24 et seq, Oxford Univ. Press (London, 1950).
[60] J. H. Poincaré, On the curves defined by a differential equation (in French), J. Math. **8,** 251 (1882).
[61] L. S. Jacobsen, On a general method of solving second-order ordinary differential equations by phase-plane displacements, J. Appl. Mech. **19,** No. 4, 543–553 (1952).
[62] J. H. Lamoën, Graphic study of vibrations of systems with one degree of freedom (in French), Rev. Univ. Mines [8] **11,** No. 7, 213 (May 1935).
[63] H. O. Fuchs, Spiral diagrams to solve vibration problems, Prod. Eng. **271,** 108–144 (1961).
[64] F. F. Liu, Recent advances in dynamic pressure measurement techniques, J. ARS, Jet Propulsion **28,** 83–85, 128–132 (1958).
[65] R. E. D. Bishop, On the graphical solution of transient vibration problems, Proc. IME (London) **168,** No. 10, 299–322 (1954).
[66] F. J. Beutler and E. O. Gilbert, Applying phase-plane techniques to a non-linear system, ISA J. **8,** No. 7, 47–50 (1961).
[67] R. D. Mindlin, Dynamics of package cushioning, Bell System Tech. J. **24,** 353–461 (1945).
[68] J. J. Stoker, Non-linear Vibrations in Mechanical and Electrical Systems, Interscience Publ., Inc. (New York, N.Y., 1950).
[69] M. A. Sadowsky, Nonlinear strings, J. Franklin Inst. **240,** 469–476 (1945).
[70] N. Minorsky, Modern non-linear trends in engineering, Appl. Mech. Rev. **4,** No. 5, 266–267 (1951).
[71] H. N. Abramson and W. H. Chu, Application of the generalized phase-plane δ method to multi-degree-of-freedom vibrating systems, J. Appl. Mech. **29,** Series E, No. 3, 580–582 (1962).

5. Simple Aperiodic-Function Generators

J. L. Schweppe [1]

1. General

All methods of transducer calibration require that a known input be applied and that the output be measured precisely. In this and the following chapters, methods of producing the required input and methods of evaluating the measured response will be discussed. This chapter covers three types of simple aperiodic-function generators: the dropping ball, the quick-opening device, and the explosive device.

1.1. Types of Simple Aperiodic-Function Generators

Perhaps the most simple, though not the most satisfactory, aperiodic-function generator is the dropping ball. The transducer is set in motion by bouncing a ball bearing on the diaphragm, an action which approaches a true impulse.

Quick-opening devices include both quick-opening valve and burst-diaphragm devices. The pressure change produced approaches a step-function with the direction of the step either positive or negative.

Finally, a pressure step or pulse can be produced by an explosion. This is an adaptation of the closed bomb which has been used traditionally to determine thermodynamic properties and to determine the rate of reaction of fuels and oxidants.

1.2. Place in Pressure Transducer Calibration

The dropping ball was perhaps the first effective aperiodic generator which could be used for the determination of the natural frequency of transducers [1].[2] The method has a number of limitations which are discussed in section 2 of this chapter. Because of these limitations the dropping ball is not used extensively, although it can be used at higher frequencies than any of the other simple devices.

The quick-opening devices are used to provide precise pressure steps for amplitude calibration. In general, they are too slow for effective frequency calibration.

The explosive devices do not provide precise pressure steps. Therefore, calibration requires comparison with a gage which has been calibrated by some other method. For this reason explosive devices are not used extensively.

1.3. Range of Operation

The range of operation for each of the devices discussed in this chapter is given in table 5.1. The amplitude ranges are those reported by the laboratory or manufacturing concern where the device was built or used. The rise time of a pressure step of given amplitude (represented by the response of a "fast" transducer to the pressure step) is also that reported by the laboratory. The frequency ranges show the highest frequency mode of oscillation of the transducer which can be excited by a given aperiodic generator. These are approximations based on the assumption that the rise time for maximum swing of the transducer must not exceed one-fourth of the period of oscillation of the transducer.

TABLE 5.1. *Range of Simple Aperiodic-Function Generators*

Device	Amplitude range to	Time for pressure step		Frequency range to
		Rise	Rise time	
	psia	*psia*	*μsec*	*c/s*
Dropping ball	Not applicable			100, 000
Quick-opening				
JPL burst-diaphragm	200	200	250	1,000
Eisele's valve	3,000	1, 250	200×10^3	
NBS valve	50,000	23, 500	25	10, 000
Explosive				
JPL	700	700	300	8, 000
NOL	40,000	40, 000	400×10^3	

2. Dropping Ball

2.1. Description

The first simple aperiodic-function generator to be considered here is the dropping ball. This generator in its most simple form consists of a small ball which is dropped onto the sensing end of the transducer [1, 2, 3], figure 5.1. Ordinary ball bearings have good elastic properties and are customarily used. The ball is released by cutting off the current to an electromagnet which holds the ball directly above the transducer. The transducer system's response to the impact is displayed on an oscilloscope. The oscilloscope sweep may be triggered by the transient voltage generated across the electromagnet when the current is cut off, or by a microswitch or photocell actuated by the ball dropped on the transducer or by a second ball dropped at the same time, figure 5.1a.

2.2. Theory

The dropping ball transmits its kinetic energy to the transducer during the very short time the two masses are in contact. The ball then bounces away and the transducer is left to vibrate at its

[1] Professor of Mechanical Engineering, The University of Houston; President, Houston Engineering Research Corporation.

[2] Figures in brackets indicate the literature references on p. 75.

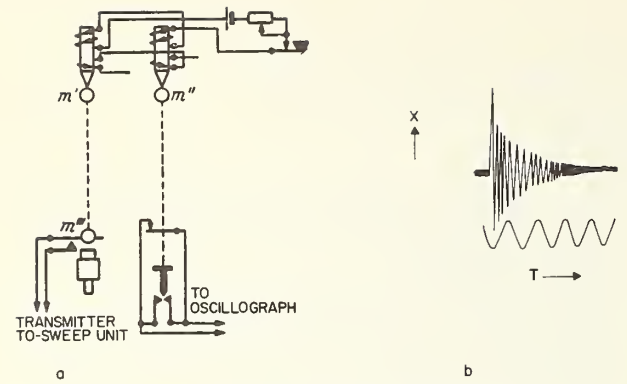

FIGURE 5.1. *Dropping ball calibrator.*

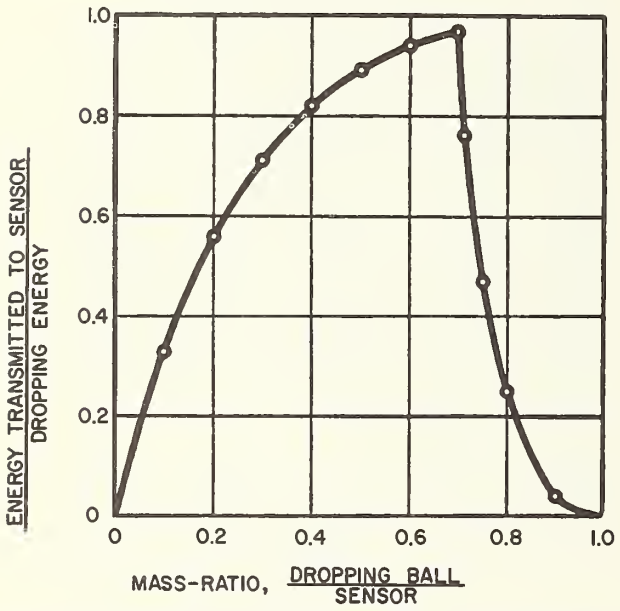

FIGURE 5.2. *Effect of mass-ratio on vibration energy of transducer.*

own natural frequency. If the ball and the sensor were perfectly elastic, and if the sensor deflection were zero, all of the kinetic energy of the dropping ball would be retained by the ball when it bounced away. This condition is approached as the mass of the dropping ball approaches zero. As the mass of the ball is increased from zero, the amount of energy transmitted to the sensor increases, reaches a maximum, and then decreases again [2], figure 5.2.

The fraction of the dropping energy transmitted to any given pressure transducer is affected by a number of factors. Some of these factors are the elasticities of the ball and the sensor, the relation between the force applied to the sensor and deflection of the sensor, and the relation between the rate of application of force and rate of deflection.

2.3. System Design

The design of a dropping-ball system for calibrating pressure transducers must take into account the factors which are discussed in section 2.2. Further consideration must be given to the selection of the dropping ball, the height of the drop, the oscilloscope sweep speed, and the triggering time. Since the proper choice of these design variables is generally different for each transducer to be tested, the testing system should allow for adjustments in these variables.

2.4. Evaluation of Test Data

The product of a dropping-ball calibration is an amplitude versus time plot of the transducer output. Four factors limit the value of this output function: (1) The forcing function cannot be determined precisely. (2) The response during the finite period when ball and transducer are in contact is a function of the joint mass. (3) Thin diaphragm transducers are sensitive to noise. And (4) the dropping ball exerts a point-concentrated force on the transducer and, depending on the configuration of the transducer, the response may not be the same as the response to a uniformly distributed pressure force. It is, however, usually possible to determine the frequency of the predominant mode and to treat the transducer as if this were the only mode of oscillation. The dropping-ball method is not recommended for amplitude response determinations. This method is useful for determining the transducer's predominant mode of oscillation in the range of 2 to 100 kc/s.

3. Quick-Opening Devices

In general, the quick-opening device utilizes two pressure chambers—a small gage chamber and a relatively large reservoir. Initially the two chambers are at different pressures and the pressure step is generated by opening quickly the passage between the two chambers. Since either chamber may be at the higher pressure initially, the pressure step may either rise or fall. Hylkema [4] states that, for the JPL (Jet Propulsion Laboratory) device, the pressure-fall (or negative-going step) arrangement develops a closer approach to the ideal step function. While this is generally true for quick-opening devices, it is important to recognize that all gages do not have the same character of response to negative- and positive-going steps. With the negative-going step the transducer oscillates about a median which is near the zero-pressure point. As a result it is possible for the diaphragm to lose contact with the force-summing component, in which case the recorded transducer response differs from that for oscillation about a median at a significant positive pressure point.

3.1. Description of Burst-Diaphragm Device

One of the simplest quick-opening devices for pressure gage calibration utilizes a thin plastic diaphragm as the separator between the two pressure chambers. Because of the bursting characteristics of the diaphragm, a pressure fall in the gage chamber produces a sharper pressure step than a pressure rise.

Hylkema and Bowersox [4] of the Jet Propulsion Laboratory have reported the construction details of one typical burst-diaphragm device, figure 5.3a. The JPL device has a 200-in.^{3} reservoir chamber and a very small gage chamber separated by a thin plastic diaphragm. Either chamber can be pressurized with an inert gas. The diaphragm is punctured by a 1/4-in. knife operated by a solenoid. A microswitch on the knife assembly triggers the sweep of the monitoring oscilloscope. In the JPL device, both chambers are lined with felt to eliminate pressure oscillations due to reflected pressure waves.

The JPL calibrator can operate at pressures up to 200 psi. The time to reach a steady pressure is about 250 μsec for a 200-psi change. This device can be used to shock a transducer into oscillation when the predominate resonance frequency is below about 1000 c/s. At higher resonance frequencies the device is limited to amplitude calibration.

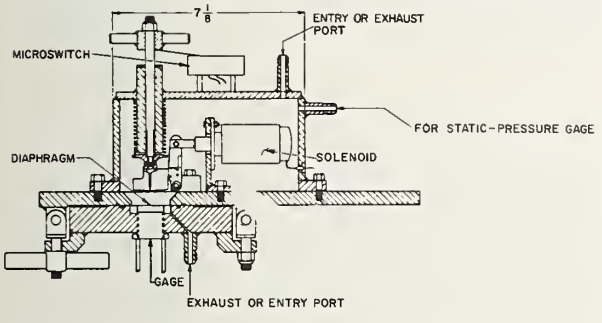

a

b

FIGURE 5.3. *Burst-diaphragm device.*

(a) Cross section of JPL device
(Reproduced from [4] with permission from Proc. ISA.)
(b) Wiancko device
(Reproduced by courtesy of WIANCO Engineering Co.)

Burst diaphragm devices (fig. 5.3b) are available commercially and custom models are being used in a number of laboratories. P. M. Aronson of the Naval Ordnance Laboratory, White Oak, Md., has built a device which operates at pressures up to 1000 psi.

3.2. Description of Eisele's Device

In some quick-opening devices a valve is used in place of a burst-diaphragm. The general principle of operation is the same. In Eisele's device [3] the reservoir is pressured with compressed air, the pressure is adjusted to the desired level with a needle-valve, and then a quick-opening hand valve is opened to admit the high-pressure air to the gage chamber, figure 5.4.

In principle Eisele's device can be operated at any pressure for which equipment can be designed and at which gas is available. The particular device described here can be operated at pressures up to 3000 psi. The pressure rise rate is much lower than for the burst diaphragm device, 6.2×10^3 versus 8×10^5 psi per second. Application is limited to amplitude calibration.

3.3. Description of NBS Device

D. P. Johnson of the National Bureau of Standards has developed a quick-loading, liquid-medium pressure calibrator which is now in service in the Mechanical Instruments Section of the Bureau (figs. 5.5, 5.6, and 5.7). In this device the two chambers are separated by a special quick-opening valve. The gage is mounted in the smaller chamber, and the pressure step is obtained by opening the valve between the two chambers. In Johnson's device the main reservoir is about 1000 times that of the gage chamber and its length is about 40 times as great.

The operating procedure is as follows: (1) Open the bleeder. (2) Open the poppet by opening and closing the quick-acting dump valve. (3) Fill the system by pumping. (4) Close the bleeder. (5) Close the poppet by increasing the differential pressure between the piston and the main reservoir several psi (pump-to-piston valve open and pump to main reservoir valve closed). (6) Open pump to main reservoir valve and pump to desired pressure behind piston and in main reservoir. (7) Open bleeder. If some main reservoir pressure is lost, repump. During pumping leave pump to main reservoir and pump to piston valves open. (8) Close pump to main reservoir and pump to piston valves. (9) Close bleeder. (10) Dump pressure behind piston by operation of quick opening valve.

Note that, as long as the poppet valve is closed, the reservoir pressure exerts a force which tends to hold the valve head in the closed position. As the actuating force is increased, the tension in the

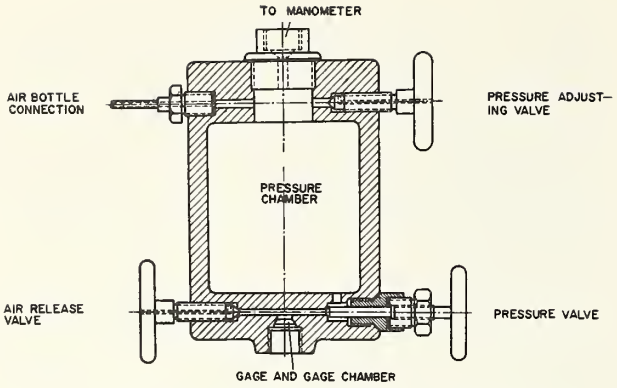

FIGURE 5.4. *Eisele's quick-opening device.*

(Reproduced from [3] with permission from Archiv fur Technisches Messen.)

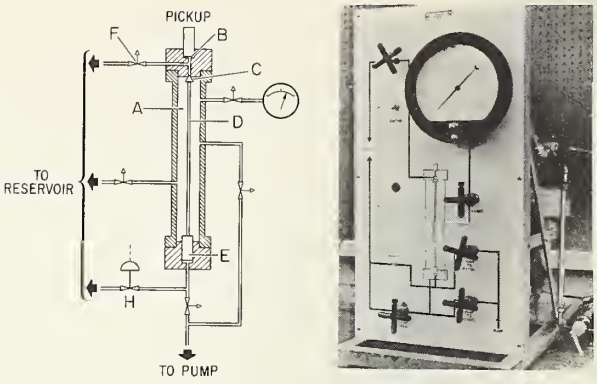

FIGURE 5.5. *NBS quick-loading calibrator.*

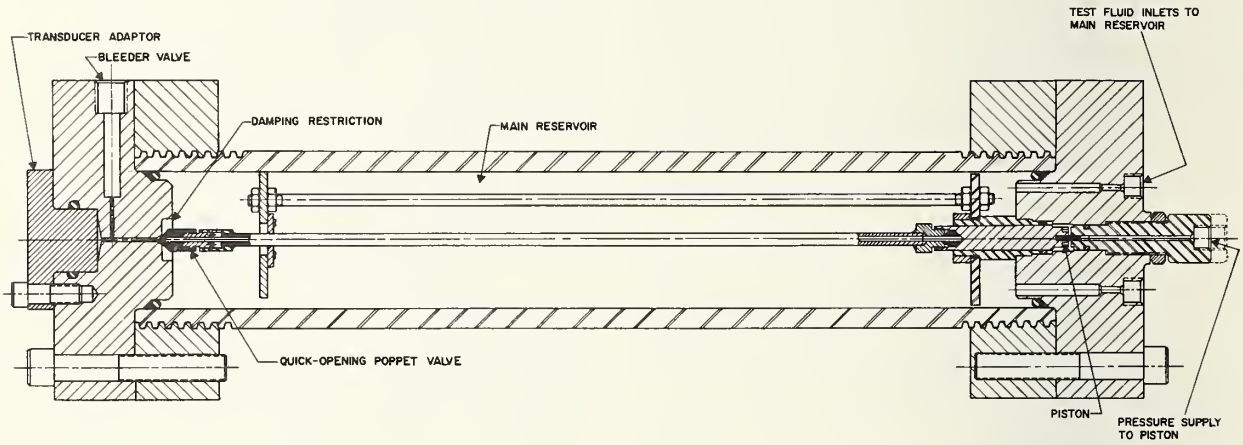

FIGURE 5.6. *Principal parts of NBS quick-loading calibrator.*

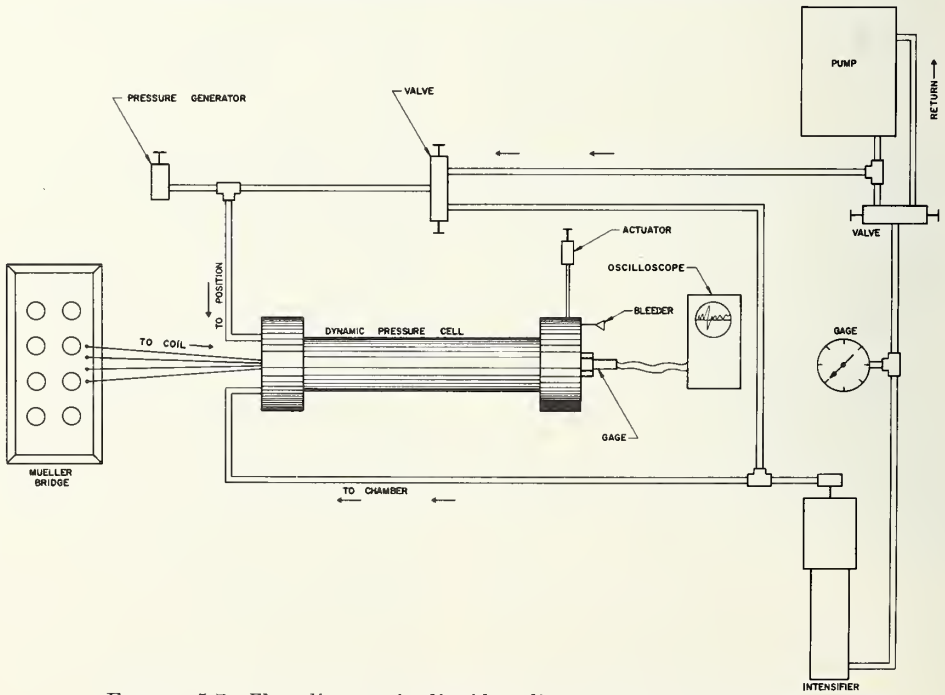

FIGURE 5.7. *Flow diagram for liquid-medium pressure-step generator.*

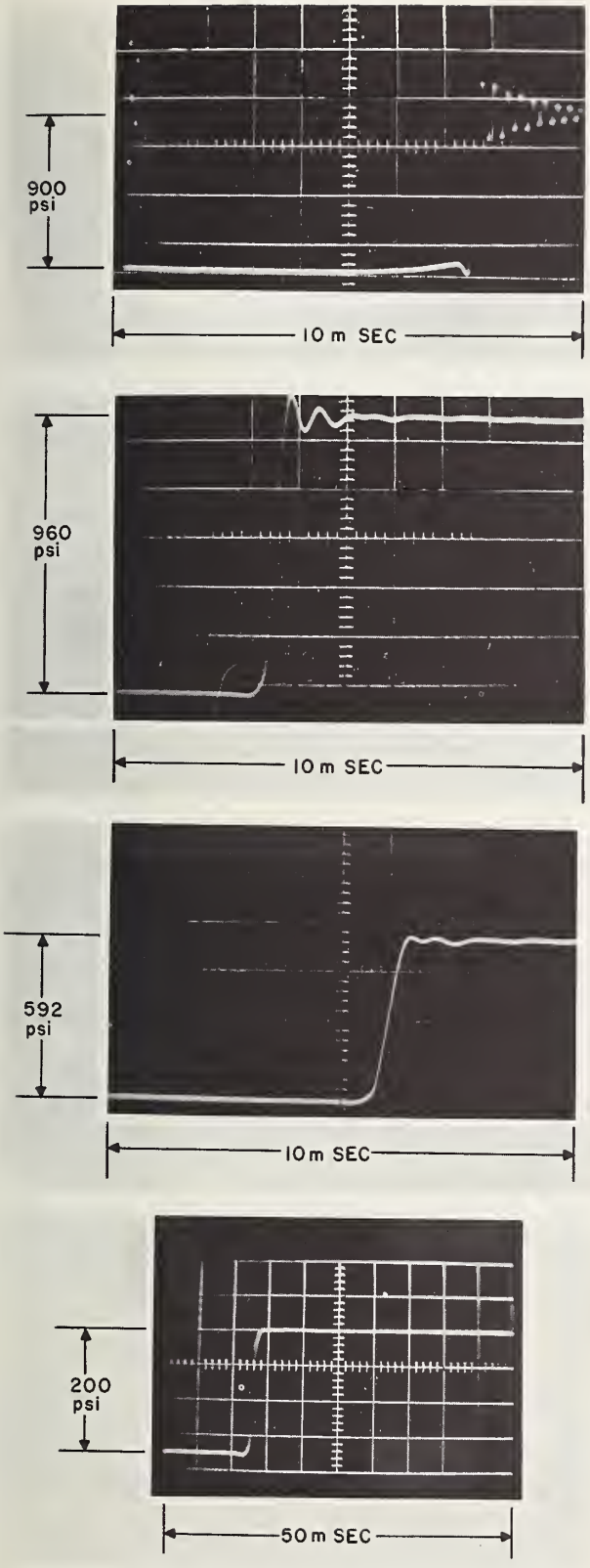

FIGURE 5.8. *Transducer response to NBS calibrator.*

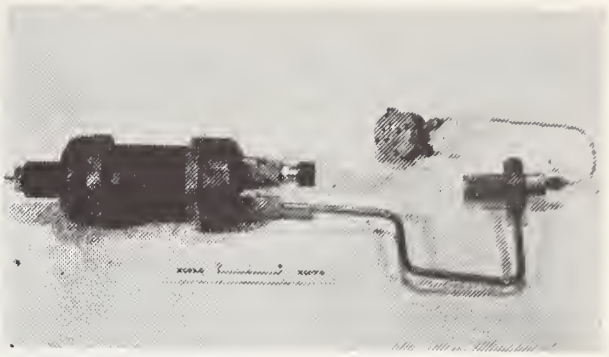

FIGURE 5.9. *JPL closed bomb.*

(Reproduced from JPL Memorandum No. 20–168 with permission from Jet Propulsion Laboratory)

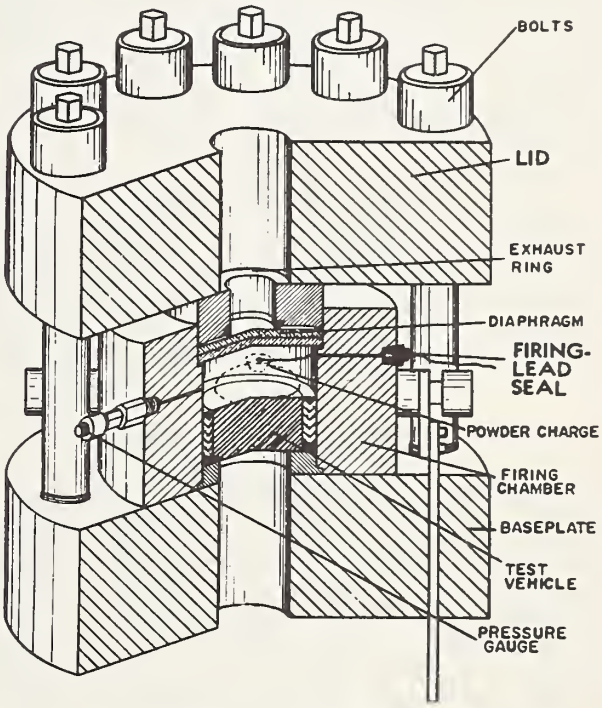

FIGURE 5.10. *NOL closed bomb.*

(Reproduced from 5 with permission from Trans. ASME.)

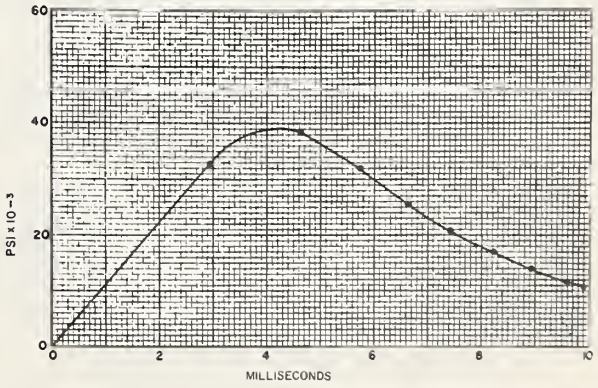

FIGURE 5.11. *Typical dynamic pressure pulse in NOL closcd bomb.*

(Reproduced from 5 with permission from Trans. ASME.)

valve stem increases almost to the breaking point. An expansion wave travels down the stem moving the poppet first in the direction of tighter closure, then in the opposite direction. The elastic force in the stem snaps the valve open at a rapid rate.

In Johnson's device the hydrostatic pressure in the reservoir is measured by its effect on the resistance of a manganin wire. The gage sensitivity is estimated to be 0.5 psi at 30,000 psi with a calibration repeatability of ± 0.1 percent. The calibration accuracy of the device is limited by two inherent errors. (1) Closure of the bleeder valve (step 8) reduces the volume of the gage cavity, thus raising the pressure to something above 0 psig. (2) It takes 5 to 10 msec for the piston to complete its travel. The volume of the main reservoir is increased by the travel of the piston so that the gage experiences a transient pressure somewhat higher than the steady final pressure. Both errors appear to be independent of pressure, so that for a given configuration of the device there is a pressure below which the error is not acceptable.

The time required for the pressure in the gage chamber to reach the main reservoir pressure depends on the gage cavity size, the gage cavity aperture diameter and length, the viscosity of the liquid, and the poppet valve stem stress. The damping restriction shown in figure 5.6 is designed to utilize the viscosity of the liquid to damp the oscillations of the poppet. With the most rapid pressure rise, the pressure step causes the gage cavity to ring at a frequency of about 10 kcs. This ringing frequency limits the use of the liquid-medium calibrator for testing the periodic response of a gage in a liquid. By increasing the time for the pressure rise to about 2 msec, a very nearly monotonic step can be produced for testing the nonperiodic transient errors. Typical response curves are shown in figure 5.8.

3.4. Evaluation of Test Data

All of the quick-opening devices provide a positive means for amplitude calibration within the ranges of pressure specified for each device. Evaluation of the amplitude data simply involves a determination of the output-input ratio as a function of the input magnitude.

None of these devices is particularly suited for the determination of frequency response. Since each is a step generator the rise time must be short in comparison with the period of the main resonant frequency of the transducer, if the transducer is to be shock excited. This requirement limits the usefulness of the quick-opening devices to a frequency range of about 0 to 10,000 c/s. The frequency response data which are valid can be evaluated by the methods described in chapters 2 and 3.

4. Explosive Devices

4.1. Description of JPL Bomb

Among the closed-bomb pressure generators which have been described in the literature is a simple calibration device developed at Jet Propulsion Laboratory [4]. This bomb was designed by L. R. Williamson and was described by C. G. Hylkema and R. D. Bowersox (fig. 5.9). The outer structure is a heavy-walled steel pipe nipple, about 6 in. long, fitted with screwed pipe caps. Aluminum liners are used to protect the outer case from exploded fragments and to vary the internal volume. The pressure is generated by exploding a dynamite cap within the bomb, and the peak pressure is adjusted by varying the internal volume. Since blasting caps are not perfectly uniform, successive shots may not produce the same pressure. This makes it necessary to use a calibrated comparison gage to determine the actual pressures attained.

Although bombs can be designed for very high pressures, the JPL bomb is limited to a maximum pressure of 700 psi. Rise time, using blasting caps, is about 300 μsec. The average rise rate of 2.3×10^6 psi per second is comparable to that of the quick-opening devices.

4.2. Description of NOL Bomb

Mickevicz [5] of the Naval Ordnance Laboratory has described a device which operates at much higher pressures (fig. 5.10). Mickevicz' dynamic pressure pulse generator is capable of generating reproducible pressure-time pulses in the order of 40,000 psi. The pressure is generated by igniting a propellent powder within the bomb, and the pulse is produced by releasing the pressure through a rupture disk when it reaches a predetermined value. The pressure transducer is mounted in the side of the firing chamber.

A typical dynamic pressure plot is shown in figure 5.11. The pulse rise rate is dependent on the powder grain size, and the decay rate is dependent on the escape aperture size. Rise rates of 14×10^6 psi per second have been attained, corresponding to 40,000 psi in 4,000 μsec. Dynamic calibration is accomplished by comparing the response of the unknown gage with that of a calibrated high-frequency response gage.

4.3. Evaluation of Test Data

The explosive devices produce somewhat more rapid pressure rise rates than the quick-opening devices. However, they are not adequate for determining frequency response above about 8,000 c/s.

Since precise pressure steps are not produced, amplitude calibration can be determined only by comparison with a gage which has been calibrated by some other method. Further, any determination of frequency response also involves the use

of a previously calibrated gage. Evaluation then requires a determination of the input function through use of the transfer function and the output of the calibrated gage, followed by evaluation of the transfer function for the gage being tested. The methods used are described in chapters 2 and 3. The explosive device provides only a secondary method for calibration.

5. References

[1] W. Gohlke, Quartz pressure measuring apparatus for high natural frequencies (in German), VDI-Forschungsheft **407** (1941).

[2] W. Gohlke, Introduction to Piezoelectric Measuring Techniques (in German), 2d ed., Academic Publ. Co. Geest & Partig K.–G. (Leipzig, 1959).

[3] E. Eisele, Calibration of indicators II. Dynamic calibration, Archiv. Tech. Messen J–137–7 (May 1951).

[4] C. G. Hylkema and R. D. Bowersox, Mathematical and experimental techniques for the determination of dynamic performance of pressure gages, Proc. ISA **8**, 115 (1953).

[5] E. J. Mickevicz, Techniques and equipment for generation of dynamic high pressures, Trans. ASME **75**, 325–327 (1953).

6. Shock Tube Methods

J. L. Schweppe [1]

1. General

1.1. The Shock Tube as a Step-Function Generator

In chapter 5 a number of simple aperiodic function generators are described and limitations in performance are pointed out. All of these simple generators produce pressure steps or pulses with relatively slow rates of pressure change or with uncertain magnitude or both. The rates of pressure change are such that dynamic calibration with these devices is limited to transducers with predominant modes of oscillation at frequencies below 10,000 c/s. Since calibration is required for transducers having predominant modes of oscillation in the range of 50,000 to 100,000 c/s or higher, the step-function generator must be capable of changing the pressure from one known level to another in a sufficiently short time to shock excite these high-frequency transducers.

The shock tube meets the requirement for a very short rise time between pressure levels—as short as 10^{-9} sec for a positive pressure step [1].[2] With proper design the pressure can be held steady for 4 or 5 μsec after the step change in a shock tube of moderate length. Step amplitudes are easily controlled from a few psi to about 600 psi in a shock tube of relatively simple construction.

1.2. Information Obtained From Shock Tube Calibration

The direct product of the shock tube calibration procedure is a time-base record of the response of the transducer to the step input. This record is obtained by photographing the trace made by the transducer output on an oscilloscope (figure 1.9).

Methods described in chapter 2, section 3.2 may be used to determine the frequency response from the transient response to a step-function input. Numerical methods also may be used effectively with the aid of a digital computer [2].

2. Description

2.1. Description of Components

The shock tube consists of two elongated chambers, usually of constant cross section, separated by a burst diaphragm. Initially the gas pressure in one chamber is higher than in the other. When the diaphragm ruptures the expansion of the high-pressure gas into the low-pressure chamber generates a shock wave which travels faster than the expanding gas. In addition to the compression and expansion chambers and the diaphragm-puncturing mechanism, the equipment includes a gas supply and regulating system, static pressure and temperature-measuring devices, a shock velocity-measuring system, and a transducer output recording system. See figure 6.1.

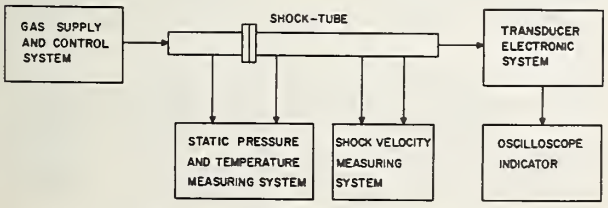

FIGURE 6.1. *Shock tube schematic.*

2.2. Qualitative Description of Shock Tube Phenomena [3]

Initially, the gas in the compression chamber is at a higher pressure than the gas in the expansion chamber, figure 6.2a. When the diaphragm bursts, the contact surface between the gas originally in the expansion chamber and that originally in the compression chamber moves into the expansion chamber. The pressure and the velocity of the medium on either side of the contact surface must be the same, but the temperature and density differ. A short time after the diaphragm bursts the idealized waves appear as shown in figure 6.2b.

The leading edge of the rarefaction wave moves into the compression chamber at the velocity of sound for the undisturbed medium while the trailing edge moves in the same direction at a lower velocity. The reduced velocity of the trailing edge results from the fact that it moves in a medium which is at a reduced temperature and it moves against the velocity of the stream. The rarefaction wave will, in time, reach the end of the compression chamber where it will be reflected as a rarefaction, figure 6.2c. After reflection the wave will move in the same direction as the shock

[1] Professor of Mechanical Engineering, The University of Houston; President, Houston Engineering Research Corporation.

[2] Figures in brackets indicate the literature references on p. 85.

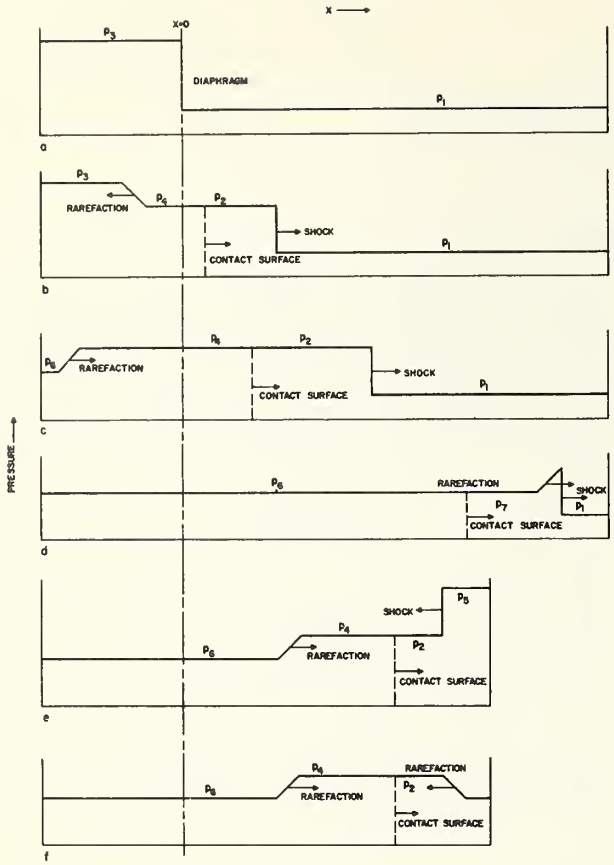

FIGURE 6.2. *Pressures and waves in shock tube.*

(a) Before diaphragm is burst
(b) After burst and before reflection of rarefaction
(c) After reflection of rarefaction
(d) Reflected rarefaction overtakes shock wave
(e) Shock wave reflected by closed end of tube
(f) Rarefaction wave reflected by open end of tube

wave at the velocity of sound in the medium plus the particle (contact surface) velocity. If the tube is long enough the rarefaction wave will overtake the shock wave, figure 6.2d. Under this circumstance the strength of the shock drops off.

For a shorter tube, the shock wave reaches the end and is reflected before the rarefaction wave overtakes it. If the end of the tube is open the reflection is a rarefaction and if the tube is closed the reflection is a shock wave of more than twice the magnitude of the incident pressure step, figures 6.2e and 6.2f.

3. Shock Tube Theory

3.1. General

The theory of shock waves is covered thoroughly in a number of references [3, 4, 5, 6, 7, 8, 9, and 10]. The general equations for shock and expansion waves may be used to analyze the flow conditions in a shock tube. In figure 6.3 the region of flow ahead of the shock in the expansion chamber is designated (1), the shock front is represented by a line of slope $1/U$, and the contact

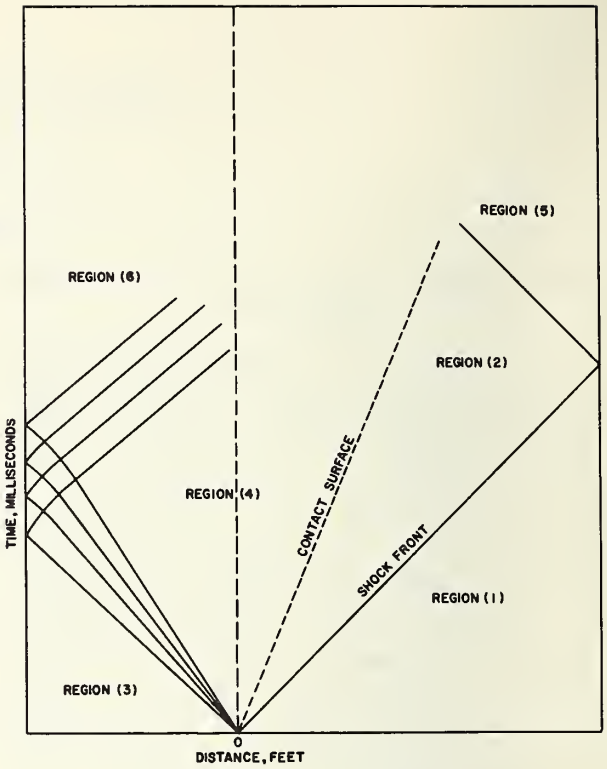

FIGURE 6.3. *Distance/time plot of events.*

surface by a line of slope $1/u$. The region between the shock front and the contact surface is designated (2), the region in front of the head of the rarefaction wave is designated (3), and the region between the contact surface and the tail of the rarefaction wave is designated (4).

Let us consider right-traveling shocks as in figure 6.3. The velocity of the shock relative to the gas into which it moves is $U-u_1$, and relative to the gas out of which it moves is $U-u_2$. The flow through a shock discontinuity may be treated as though the flow were steady at each instant of time and the relations for steady-flow normal shocks may be applied if the coordinate system moves with the shock [6, p. 995]. The following basic equations are taken from Shapiro [6], chapter 25, where detailed derivations are presented. The plus sign refers to a right-traveling and the minus sign to a left-traveling shock wave. (See List of Symbols.)

Translation particle velocity (Shapiro, eq 25.20, p. 1001):

$$\frac{u_2-u_1}{a_1}=\frac{\pm 2}{\gamma+1}\left[\frac{U-u_1}{a_1}-\frac{a_1}{U-u_1}\right]=\frac{\pm 2}{\gamma+1}\left[M_1-\frac{1}{M_1}\right]. \tag{6.1}$$

Shock wave pressure (Shapiro, eq 25.23, p. 1002):

$$\frac{P_2}{P_1}=1+\frac{2\gamma}{\gamma+1}\left[\left(\frac{U-u_1}{a_1}\right)^2-1\right]=1+\frac{2\gamma}{\gamma+1}\left(M_1^2-1\right). \tag{6.2}$$

Relation between particle velocity and velocity of sound (Shapiro, eq 24.20, p. 945):

$$\frac{a_2}{a_1}=1\pm\frac{\gamma-1}{2}\left(\frac{u_2-u_1}{a_1}\right). \tag{6.3}$$

Contact surface velocity (Shapiro, eq 25.32c, p. 1008):

$$\frac{u_2}{a_1}=\frac{\frac{P_2}{P_1}-1}{\gamma\left[1+\frac{\gamma+1}{2\gamma}\left(\frac{P_2}{P_1}-1\right)\right]^{1/2}}. \tag{6.4}$$

Relation between reflected and incident shock (Shapiro, eq 25.35, p. 1020):

$$\frac{P_5}{P_2}=\frac{\left(1+2\frac{\gamma-1}{\gamma+1}\right)\frac{P_2}{P_1}-\frac{\gamma-1}{\gamma+1}}{\frac{\gamma-1}{\gamma+1}\left(\frac{P_2}{P_1}\right)+1}. \tag{6.5}$$

Relation between incident and reflected pressure step (Shapiro, eq 25.36, p. 1021):

$$\frac{P_5-P_2}{P_2-P_1}=\frac{\frac{2\gamma}{k+1}}{\frac{P_1}{P_2}+\frac{\gamma-1}{\gamma+1}} \tag{6.6}$$

Relation between temperature and shock velocity (Shapiro, eq 25.5, p. 995):

$$\left(\frac{a_2}{a_1}\right)^2=\frac{T_2}{T_1}=\frac{\left(1+\frac{\gamma-1}{2}M_1^2\right)\left(\frac{2\gamma}{\gamma-1}M_1^2-1\right)}{\frac{(\gamma+1)^2}{2(\gamma-1)}M_1^2}. \tag{6.7}$$

3.2. Contact Surface Velocity

For a shock front which moves toward the right into a region at rest, $u_1=0$ and the positive sign is selected in eq (6.1). The resulting relation is not closely checked by experiment, but it is useful for planning experiments and for designing shock tubes.

$$\frac{u_2}{a_1}=\frac{2}{\gamma+1}\left[\frac{U_1}{a_1}-\frac{a_1}{U_1}\right]=\frac{2}{\gamma+1}\left[M_1-\frac{1}{M_1}\right]. \tag{6.8}$$

In eq (6.8), γ refers to the ratio of specific heats for the gas in region (1). For air, $\gamma=7/5$ and eq (6.8) becomes

$$\frac{u_2}{a_1}=\frac{5}{6}\left[\frac{U_1}{a_1}-\frac{a_1}{U_1}\right]=\frac{5}{6}\left[M_1-\frac{1}{M_1}\right]. \tag{6.9}$$

Since in a helium-to-air tube the shock front also moves into air in region (1), eq (6.9) applies.

3.3. Shock Wave Pressure

Equation (6.2) relates the shock velocity to the shock wave pressure. In the derivation of this equation it is assumed that the perfect gas laws apply, that the specific heats are constant, and that flow is adiabatic. For $u_1=0$

$$\frac{P_2}{P_1}=1+\frac{2\gamma}{\gamma+1}\left[\left(\frac{U_1}{a_1}\right)^2-1\right]=1+\frac{2\gamma}{\gamma+1}(M_1^2-1). \tag{6.10}$$

A second equation, which relates the compression-expansion pressure ratio to the shock-wave pressure, is developed as follows: Write eq (6.3) for a rarefaction wave moving left into region (3) at the velocity of the region (4) front. In this case γ is the ratio of specific heats (assumed constant) for the gas in the compression chamber and $u_3=0$. Also assume that the isentropic relation between a and p applies. That is,

$$\frac{P}{P_1}=\left(\frac{a}{a_1}\right)^{\frac{2\gamma}{\gamma-1}}.$$

Then

$$\frac{u_4}{a_3}=\frac{2}{\gamma_3-1}\left(1-\frac{a_4}{a_3}\right)=\frac{2}{\gamma_3-1}\left[1-\left(\frac{P_4}{P_3}\right)^{\frac{\gamma_3-1}{2\gamma_3}}\right]. \tag{6.11}$$

But $u_4=u_2$ and $P_4=P_2$. Therefore

$$\frac{u_2}{a_3}=\frac{2}{\gamma_3-1}\left[1-\left(\frac{P_2}{P_1}\right)^{\frac{\gamma_3-1}{2\gamma_3}}\left(\frac{P_1}{P_3}\right)^{\frac{\gamma_3-1}{2\gamma_3}}\right].$$

Now combine the above equation with eq (6.4) and solve for P_1/P_3. The result is

$$\frac{P_1}{P_3}=\frac{P_1}{P_2}\left\{1-\frac{a_1(\gamma_3-1)\left(\frac{P_2}{P_1}-1\right)}{2a_3\gamma_1\left[1+\frac{\gamma_1+1}{2\gamma_1}\left(\frac{P_2}{P_1}-1\right)\right]^{1/2}}\right\}^{\frac{2\gamma_3}{\gamma_3-1}} \tag{6.12}$$

If the same gas is present at the same temperature in both the compression and expansion chambers, $\gamma_3=\gamma_1$, $a_3=a_1$, and

$$\frac{P_1}{P_3}=\frac{P_1}{P_2}\left[1-\frac{\gamma-1}{2\gamma}\frac{\frac{P_2}{P_1}-1}{\left[1+\frac{\gamma+1}{2\gamma}\left(\frac{P_2}{P_1}-1\right)\right]^{1/2}}\right]^{\frac{2\gamma}{\gamma-1}} \tag{6.13}$$

For air in both chambers, eqs (6.10) and (6.13) reduce to

$$\left(\frac{P_2}{P_1}-1\right)=\frac{7}{6}(M_1^2-1) \tag{6.14}$$

$$\frac{P_3}{P_1}=\frac{\frac{P_2}{P_1}}{\left\{1-\left(\frac{P_2}{P_1}-1\right)\left[49+42\left(\frac{P_2}{P_1}-1\right)\right]^{-1/2}\right\}^7}. \tag{6.15}$$

For helium-to-air, eq (6.14) applies and eq (6.12) reduces to

$$\frac{P_3}{P_1}=\frac{\frac{P_2}{P_1}}{\left\{1-\frac{a_1}{a_3}\frac{5}{21}\left(\frac{P_2}{P_1}-1\right)\left[1+\frac{6}{7}\left(\frac{P_2}{P_1}-1\right)\right]^{-1/2}\right\}^5}. \tag{6.16}$$

If the temperatures in the two chambers are assumed to be the same, and the velocity of sound is computed assuming perfect gases

$$\frac{P_3}{P_1}=\frac{\frac{P_2}{P_1}}{\left\{1-\left(\frac{P_2}{P_1}-1\right)\left[150.4+128.7\left(\frac{P_2}{P_1}-1\right)\right]^{-1/2}\right\}^5}. \tag{6.17}$$

3.4. The Reflected Shock Wave

The pressure ratio for the reflected-to-incident shock wave is given by eq (6.6). In both air-to-air and helium-to-air tubes the equation is the same.

$$\frac{P_5-P_2}{P_2-P_1}=\frac{7P_2}{6P_1+P_2} \tag{6.18}$$

or

$$\frac{P_5-P_1}{P_2-P_1}=2\left[\frac{7P_1+4(P_2-P_1)}{7P_1+(P_2-P_1)}\right]. \tag{6.19}$$

Combining eq (6.19) with eq (6.14) yields a more convenient relation:

$$\frac{P_5-P_1}{P_1}=\frac{7}{3}(M_1^2-1)\left[\frac{2+4M_1^2}{5+M_1^2}\right]. \tag{6.20}$$

The relative Mach number of the reflected shock may be determined by writing eq (6.1) for the left-traveling reflected shock with $u_5=0$. Thus

$$-\frac{u_2}{a_2}=\frac{-2}{\gamma+1}\left(M_5-\frac{1}{M_5}\right). \tag{6.21}$$

Since this left-traveling shock moves into region (2), its absolute velocity to the left is reduced by the amount of the right-traveling particle velocity in region (2).

$$U_5=u_2-M_5a_2. \tag{6.22}$$

The velocity of sound in region (2) is given by eq (6.21), and the Mach number M_5 by eq (6.2) written for the shock between regions (5) and (2):

$$M_5^2=\left(\frac{P_5}{P_2}-1\right)\frac{\gamma+1}{2\gamma}+1. \tag{6.23}$$

Then

$$U_5=-u_2\frac{(\gamma+1)+(\gamma-1)\frac{P_5}{P_2}}{2\left(\frac{P_5}{P_2}-1\right)}. \tag{6.24}$$

The negative sign indicates that the reflected shock moves left.

3.5. The Rarefaction Wave

When the diaphragm bursts a rarefaction wave travels to the left into the expansion chamber, region (3), as shown on figure 6.3. The rarefaction wave tip travels at the speed of sound, a_3, in the negative direction until it is reflected by the closed end of the expansion chamber. It then travels in the positive direction; first at a changing rate through the expansion fan, then at a constant rate until it reaches a point where it overtakes the contact surface or meets the reflected shock, or both. The duration of the pressure step in the shock tube depends on the time required for the head of the rarefaction wave to meet the reflected shock. Wright [7] and others have described how to determine the position of the rarefaction wave tip as it moves through the expansion fan.

Passage through the expansion fan slows the rarefaction wave tip slightly, and hence shifts the region (4) distance-time curve to the left. If this shift is neglected and the constant velocity into region (4) is used to compute the position of the rarefaction tip, the result is an estimate of the duration of the pressure step which tends to be shorter than the actual step. Design based on the above assumption is therefore conservative. It is recommended that design be based on a negative rarefaction wave tip velocity of a_3 and a positive rarefaction wave tip velocity of

$$\frac{dx}{dt}=u_4+a_4. \tag{6.25}$$

3.6. Pressure Limitations

Consider eq (6.12), which relates the initial compression and expansion chamber pressures to the size of the pressure step. If P_1/P_3 approaches zero, P_1/P_2 becomes very small. But P_1 cannot be zero in a real shock tube. Therefore we can divide both sides of eq (6.12) by P_1 and rearrange.

$$\frac{P_2}{P_3}=\left[1-\frac{a_1(\gamma_3-1)\left(\frac{P_2}{P_1}-1\right)}{2a_3\gamma_1\left[1-\frac{\gamma_1+1}{2\gamma_1}\left(\frac{P_2}{P_1}-1\right)\right]^{1/2}}\right]^{\frac{2\gamma_3}{\gamma_3-1}} \tag{6.26}$$

Now P_3 may become very large, but since P_2 must always have a finite value, the ratio P_2/P_3 can approach zero as a limit. At this limit P_2 reaches a maximum value. Solving eq (6.26) at $P_2/P_3=0$,

$$\left(\frac{P_2}{P_1}-1\right)_{\max}=\left(\frac{a_3}{a_1}\right)^2\frac{\gamma_1(\gamma_1+1)}{(\gamma_3-1)^2}+\frac{a_3}{a_1}\frac{\gamma_1}{\gamma_3-1}\sqrt{\left(\frac{a_3}{a_1}\right)^2\left(\frac{\gamma_1+1}{\gamma_3-1}\right)^2+4}. \tag{6.27}$$

Inserting eq (6.27) into eq (6.10) and solving

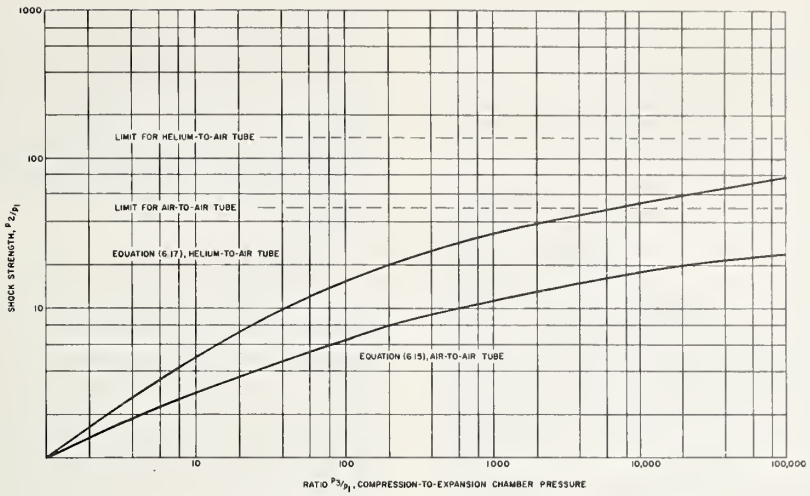

FIGURE 6.4. *Relation between compression chamber pressure and shock strength.*

for M_1,

$$(M_1)_{max}=\frac{1}{2}\frac{a_3}{a_1}\frac{\gamma_1+1}{\gamma_3-1}+\frac{1}{2}\sqrt{\left(\frac{a_3}{a_1}\right)^2\left(\frac{\gamma_1+1}{\gamma_3-1}\right)^2+4}. \quad (6.28)$$

For the air-to-air shock tube, eqs (6.27) and (6.28) reduce to

$$\left(\frac{P_2}{P_1}-1\right)_{max}=\frac{\gamma(\gamma+1)}{(\gamma-1)^2}+\frac{\gamma}{\gamma-1}\sqrt{\left(\frac{\gamma+1}{\gamma-1}\right)^2+4} \quad (6.29)$$

$$(M_1)_{max}=\frac{1}{2}\frac{\gamma+1}{\gamma-1}+\frac{1}{2}\sqrt{\left(\frac{\gamma+1}{\gamma-1}\right)^2+4}. \quad (6.30)$$

The maximum pressure ratio P_2/P_1 for an air-to-air shock tube is 44.1 and the maximum Mach number is 6.16.

Higher pressure ratios and Mach numbers may be obtained by using properly selected gases in the compression and expansion chambers. Higher ratios also may be obtained by increasing the energy ratio by heating the compression chamber or cooling the expansion chamber, or both. Figure 6.4 shows the solutions of eqs (6.15) and (6.17) for air-to-air and helium-to-air shock tubes with the same initial temperatures in the compression and expansion chambers.

Extremely high compression-to-expansion pressure ratios are required to approach the limiting maximum pressure step. For example, to reach a shock strength of $P_2/P_1=10$ a compression-to-expansion ratio of about 600 is required for an air-to-air tube. The same shock strength can be obtained in a helium-to-air tube with a compression-to-expansion ratio of 43. Table 6.1 below shows the effect of compression and expansion chamber pressure on shock amplitude for both air-to-air and helium-to-air tubes.

TABLE 6.1

Shock tube	P_3	P_1	P_2	P_2-P_1
Air-to-air	500	7.5	41.5	34
	500	15.0	66	51
	500	30.0	104	74
	1,000	15.0	83	68
Helium-to-air	500	15.0	132	117

3.7. Real Shock Tube Behavior

Experimental measurements indicate that values of shock strength computed from eq (6.12) are higher than those actually attained. The difference between the theoretical and experimental results can be explained by reviewing the assumptions made in the derivation of eq (6.12). The following assumptions were made: (1) the perfect gas laws apply; (2) flow is adiabatic; (3) the isentropic relation between a and p applies; (4) the specific heats are constant; (5) the diaphragm burst is instantaneous; and (6) viscous forces are negligible. The first three assumptions are somewhat more realistic than the last three. Glass and Patterson [9] have discussed the conditions under which variations of specific heat are of importance. We will concentrate here on a discussion of the influence of diaphragm burst and viscous forces.

The diaphragm is, of course, a necessary component of the shock tube system. It separates the high-pressure gas in the compression chamber from the relatively low-pressure gas in the expansion chamber. It is stretched nearly to the bursting point by the high pressure of the expansion chamber and is caused to burst by the action of a knife or punch. Two factors related to the diaphragm cause the real shock strength to be less than theoretical. First, energy is required to separate and fold back a metal diaphragm or to

accelerate the particles of a friable diaphragm to the flow velocity of the gas. And second, the diaphragm burst delays the formation of a one-dimensional shock wave. For each shock a certain distance must be traveled before the wave is fully developed.

In their paper on experimental aspects of shock wave attenuation, Glass and Martin [10] discuss both the growth and development of the shock wave and the effect of viscous forces. As the wave moves down the tube it tends to decelerate due to the growth of the boundary layer. At the same time the contact surface accelerates. Although real shock tube behavior is not ideal, in a well-designed tub the attenuation of the wave is small.

4. Design for Pressure-Gage Testing

4.1. General Requirements

Satisfactory pressure-gage calibration with a step-function generator requires generation of a step of reasonable duration and known amplitude over the necessary pressure range. To accomplish this with the shock tube, the compression and expansion chamber lengths must be properly proportioned, the tube must be designed for minimum wave distortion, minimum mechanical vibration, and minimum secondary shock or noise; and the shock velocity must be precisely measured.

4.2. Tube Dimensions

The expansion chamber must be at least long enough for a plane wave to develop. Although there is no theoretical relation for determination of this length, experience shows that a length of ten times the largest dimension of the cross section is sufficient [11]. The size of the cross section therefore affects the minimum length of the expansion chamber and hence the length of the tube.

The vertical or largest dimension of the cross section must be large enough for the test purpose. Wolfe [12] chose a 1⅜ in. square section for pressure gage testing because a very few pressure transducers have diameters greater than 1 in. If one-dimensional investigations are to be made (or if optical timing devices are to be used) the width or smallest dimension should be as small as possible, but large enough that the shock wave will deflect light rays for distinct schlieren pictures. Bitondo and Lobb [11] found that a 2-in. width is adequate for this purpose (they did not determine the minimum adequate width).

The compression chamber must be long enough to keep the rarefaction wave from overtaking the shock wave before it passes through the test section. The time required for this process, and hence the best compression chamber length, depends on the initial pressure ratio between the two chambers and the gases initially present in the chambers. For side gage location the maximum constant-pressure interval is achieved when the compression-expansion chamber length ratio is such that the reflected rarefaction reaches the gage port simultaneously with the reflected shock. For end gage location the maximum constant-pressure interval occurs when the compression-expansion chamber length ratio is such that the rarefaction tip, the contact surface, and the reflected shock reach the same point in the tube at the same instant [12].

Since most pressure transducers exhibit some response to mechanical vibration, it is desirable to reduce the mechanical vibration to a minimum. This can best be accomplished by making the tube massive and rigid. The tube at the NBS used for pressure gage testing weighs about 1500 lb, and has a minimum wall thickness of ¾-in.

For satisfactory performance a shock tube must be built within reasonable dimensional tolerances. It is generally agreed that the inside surface should be machined but that surface grinding is an unnecessary refinement. Bitondo and Lobb [11] point out that waviness in the longitudinal direction is especially to be avoided and they suggest a manufacturing tolerance of 0.035 in. in a 12-in. length. If the tube bends the shock wave will not remain perpendicular to the wall as it travels down the tube.

4.3. Burst-Diaphragm Selection

In section 3 of this chapter theoretical relations were developed based on the assumption that the diaphragm bursts instantaneously and completely. Real diaphragms are rated by the degree to which they satisfy this assumption.

Glass and Patterson [9] have reported that, for low-pressure operation, Red Zip cellophane has the best rupture properties and leaves the smallest obstruction. Glass and Patterson and others have also reported good results with cellulose acetate film and with Monsanto's Vuepak F. All of the plastic materials give best results when they are loaded near the bursting point before the rupturing mechanism is activated.

For high pressures, metal diaphragms must be used. Copper or aluminum sheets have been used successfully and particularly good results have been reported for hard or half-hard brass shim stock. Annealed shim stock gives poor results.

4.4. Gas Supply and Control System

The gas supply and control system indicated in figure 6.1 includes the source of gas or gases, the pressure-regulation system, the loading system, and the diaphragm-puncture system.

The gas source is usually purchased in cylinders for use in the laboratory, although a compressor may supply air for an air-to-air tube. In either

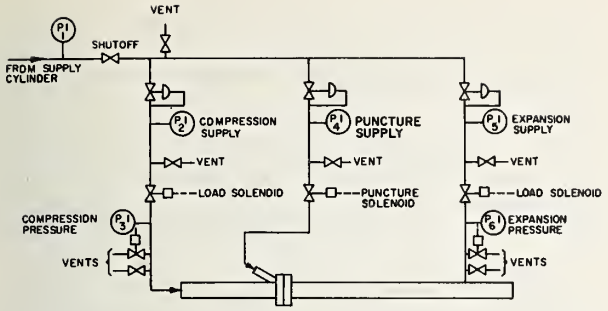

FIGURE 6.5. *Gas supply and control system.*

case the gas is stored in high-pressure cylinders prior to use in the tube, and in either case moisture free gas must be provided. On the way to the shock tube the gas passes through a regulator which is set at a pressure somewhat above the maximum desired in the shock tube chamber, figure 6.5. The puncture pressure is set some 250 psia above the desired compression chamber pressure. The load and vent switches are operated manually to adjust the pressures in the compression and expansion chambers. The compression chamber is loaded first to avoid distortion of the diaphragm. When the desired pressures have been attained and pressures and temperatures have been recorded, the tube is fired by actuating the puncture solenoid.

4.5. Shock-Velocity Measurement

Shock wave velocities are measured by determining the time required for the wave to traverse the measured distance between two points. Because of the high velocity of the wave, the instrument used to detect the passing of the wave must have a rapid response and the instrument used to measure the time interval must be capable of counting in very small increments. Methods of detecting the shock wave and determining the velocity are discussed by Cady and Bleakney in section C of Physical Measurements in Gas Dynamics and Combustion [13]. Cady describes ion-tracer techniques, use of luminous particles, electric discharge anemometry, and acoustic Mach meters, and Bleakney describes the light-screen techniques. The latter method is perhaps used most commonly to measure shock wave velocity. Pressure transducers are also used to detect the passage of the shock wave.

The light-screen technique is used in one of two types: schlieren or reflection. In the schlieren system for detecting the passage of the shock wave, the camera or viewing screen is replaced by a photocell. The reflection method uses the shock front as a reflecting surface to bend the light rays along a path through three staggered knife edges. The two light-screen methods are equally accurate, but the reflection method has the advantage of simplicity and cheapness.

The light-screen methods permit defection of the arrival of a shock wave within 1 μsec. In general, detection with a pressure transducer is somewhat less accurate.

4.6. Transducer Output Records

The calibration system must include equipment for recording the transducer output in some permanent form, either on photographic film or in punched or printed form, or both. The transducer system includes the electronic circuits which are directly associated with a given transducer. Examples are the piezoelectric transducer and electrometer, the capacitance-type transducer and oscillator-detector, and the strain gage transducer and Wheatstone bridge.

Additional electronic equipment must be included as a part of the calibration system. Triggering and time delay circuits must be provided to start the recording equipment a few microseconds before the shock wave reaches the transducer. And appropriate recording equipment must be available, figure 6.6.

The input to the trigger circuit may be the output from one of the detectors in the shock-velocity measuring system. This trigger-pulse is fed to an adjustable time-delay generator which puts out a pulse to the recording equipment a few microseconds before the shock wave hits the transducer which is being tested. The output from the transducer system also goes to the recording system.

The simplest recorder is an oscilloscope fitted with a camera. The scope is set to give a single sweep when triggered, and by holding the camera shutter open during the sweep, a photographic record can be obtained. This record can be superimposed on a voltage-calibrated grid if the grid is lighted during the time the photograph is being exposed. The photographic record can then be analyzed to determine the response spectrum of the transducer system.

The photographic output record can be converted to numerical data by manual graphical means, or it can be scanned by an electronic device which "reads" the curve at fixed time increments and records the numerical values in printed or punched-card form. The conversion of the transducer system output directly to a numerical output would be more satisfactory, but

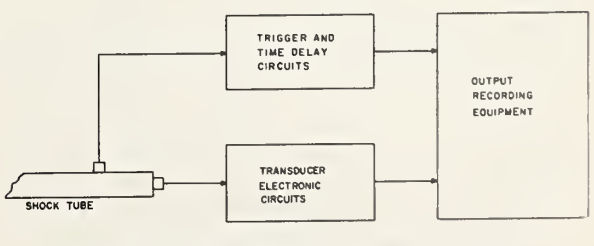

FIGURE 6.6. *Transducer output recording system.*

it is difficult to provide analog-to-digital equipment which can operate sufficiently fast.

A third means of recording the transducer system output was described in chapter 3, section 4. This is a magnetic drum recording which can be played over and over again into a frequency analyzer.

5. Evaluation of Test Data

The transducer system is evaluated on the basis of the recorded response to the step-function input. From this recorded response the amplitude characteristic of the response can be compared to the input step, the predominant frequency or frequencies and the logarithmic decrement or damping characteristic can be determined, and the amplitude and phase characteristics of the complex transfer function can be computed. The general background and the relation of calibration to analysis are covered in chapter 1, section 3, and the methods for determining the transfer function are presented in chapters 2 and 3. Here we concentrate on the application of methods described elsewhere.

5.1. Amplitude Characteristic of Response Function

Before shock tube tests are made the transducer system should be calibrated with a static calibration device if possible. For transducer systems which include piezoelectric transducers, for example, leakage prevents accurate calibration by strictly static means. In such cases, pseudo-static or short-time-period static calibration replaces static calibration. The result of either of the above calibrations is transducer system response in terms of an electrical output as a function of pressure input. A typical calibration curve is shown in figure 6.7.

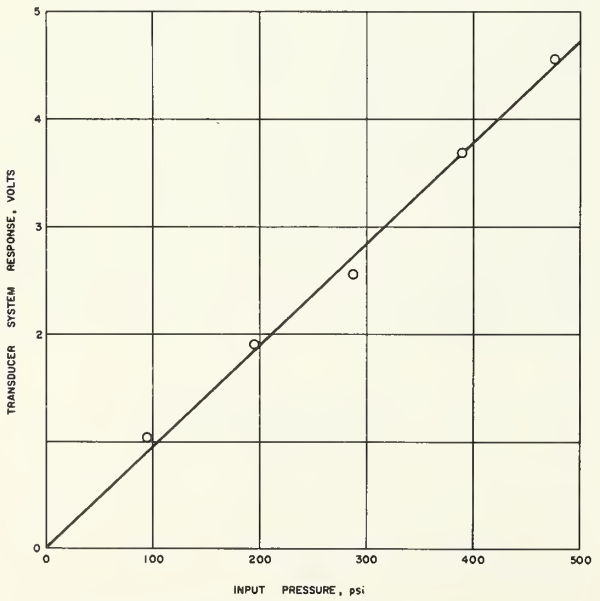

FIGURE 6.7. *Static calibration of transducer system.*

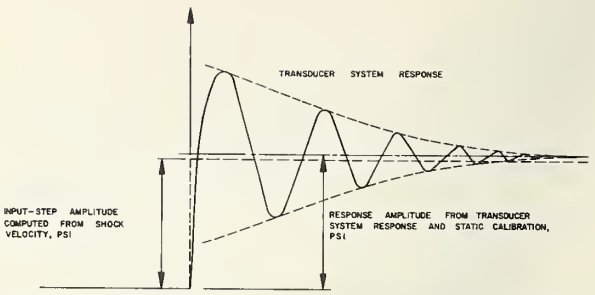

FIGURE 6.8. *Response of transducer system to step input.*

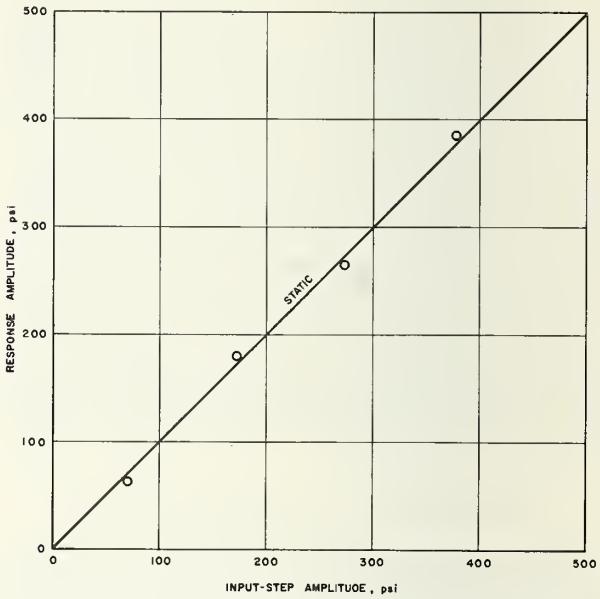

FIGURE 6.9. *Response amplitude versus input-step amplitude.*

Figure 6.8 shows an idealized response to a step-function input. For the air-to-air tube the step amplitude is computed from eq (6.14) for side mounted gages and from eq (6.20) for end-mounted gages. The step amplitude may also be evaluated from the transducer response—either by a graphical averaging process or by arithmetic average of numerical values taken at equal time increments. Since the transducer response is in electrical units, it must be converted to pressure for comparison with the input pressure step. This conversion is made with the aid of the static calibration. A typical plot of response amplitude versus input-step amplitude is given in figure 6.9.

5.2. Predominant Frequency or Frequencies

When the predominant frequency of oscillation of the transducer is far removed from other

oscillating frequencies and/or the magnitude of the predominant oscillations is much greater than that of the other modes of oscillation, the transducer response can be approximated by a single-degree-of-freedom model. In this case it is a simple matter to scale the transducer response record and count the number of oscillations in a given period of time. The computation of the damped frequency is then straightforward.

If more than one major frequency exists (that is, if the transducer has two or more degrees of freedom), determination of these frequencies is not so simple, and a more sophisticated method of analysis is required. One such method is discussed below in section 5.4; other methods are discussed in chapter 3.

5.3. Logarithmic Decrement or Damping Characteristic

In a typical transducer system, actual damping is only a small fraction of the critical damping. This is the case for the system illustrated in figure 6.8 and we assume that the systems we are concerned with here are all of this "underdamped" category. For underdamped, single-degree-of-freedom systems the logarithm of the ratio of the magnitudes of successive maximum (or minimum) displacements is constant. The following expression is known as the logarithmic decrement [14, p. 205]:

$$\delta=\ln\left(\frac{y_n}{y_{n+2}}\right). \tag{6.31}$$

The logarithmic decrement is related to the fraction of critical damping by the equation

$$\frac{c}{c_c}=\frac{\delta}{\sqrt{\delta^2+4\pi^2}}. \tag{6.32}$$

Knowledge of the damping ratio and the damped frequency can be used to compute the undamped natural frequency, ω_n.

$$\omega_n=\frac{\omega}{\sqrt{1-\left(\frac{c}{c_c}\right)^2}}. \tag{6.33}$$

Performance of the transducer system may then be predicted from standardized curves of magnification ratio and phase angle versus ω/ω_n, *for a single-degree-of-freedom system* [14, pp. 208–9]. For more complex systems, more sophisticated methods of analysis are required. One such method is discussed in the following section.

5.4. Determination of the Transducer System Transfer Function

Approximation of the response function may be carried out by any one of the methods described in chapter 3. As an example, use the method of section 3.6 based on closely spaced coordinates. It is necessary to express the step input-function in the complex plane in a form compatible with the approximation of the response function. For a step input, the Laplace transform may be shown [2] to be

$$F(s)=\int_0^\infty Fe^{-st}dt=-\frac{1}{2}\Delta tF\left(1+j\cot\frac{\theta}{2}\right). \tag{6.34}$$

Equation (6.34) represents a complex vector of amplitude $F(\omega)=F\Delta t/2\sin(\theta/2)$ and phase angle $\varphi(\omega)=(-90°-\theta/2)$.

The amplitude characteristic of the transfer function is given by eq (2.1). For a frequency $\omega=\theta/\Delta t$, the transfer function is

$$H(\omega)=\frac{X(\omega)}{F(\omega)}=\frac{\sqrt{X^2+Y^2}}{\frac{F\Delta t}{2\sin\left(\frac{\theta}{2}\right)}}=\frac{2}{F}\sin\frac{\theta}{2}\sqrt{X^2+Y^2}. \tag{6.35}$$

The phase characteristic $\beta(\omega)$ of the transfer function is given by eq (2.2).

$$\beta(\omega)=\alpha(\omega)-\varphi(\omega)=\tan^{-1}\left[\left(\frac{Y}{X}\right)+90°\right] \tag{6.36}$$

where

$$\alpha(\omega)=\tan^{-1}\left(\frac{Y}{X}-\frac{\theta}{2}\right).$$

We have shown here one method for determining the amplitude and phase characteristics of the complex transfer function for a transducer system. The response function was approximated by numerical methods and the transfer function might be computed with the aid of a digital computer. The methods of analysis are described more completely in chapter 2 and the methods of approximation are given in chapter 3.

6. References

[1] G. R. Cowan and D. F. Hornig, The experimental determination of the thickness of a shock front in a gas, J. Chem. Phys. **18,** 1008–1018 (Aug. 1950).

[2] R. B. Bowersox and J. Carlson, Digital-computer calculation of transducer frequency response from its response to a step function, Prog. Rept. No. 20–331, Jet Propulsion Laboratory (July 26, 1957).

[3] W. Bleakney, D. K. Weiner, and C. H. Fletcher, The shock tube as a facility for investigation in fluid dynamics, Rev. Sci. Instr. **20,** 807 (1949).

[4] R. Courant and K. O. Friedricks, Supersonic Flow and Shock Waves, Interscience Publ., Inc. (New York, N.Y., 1948).

[5] A. H. Shapiro, The Dynamics and Thermodynamics of Compressible Fluid Flow, vol. I, The Ronald Press Co. (New York, N.Y., 1953).

[6] A. H. Shapiro, The Dynamics and Thermodynamics of Compressible Fluid Flow, vol. II, The Ronald Press Co. (New York, N.Y., 1954).

[7] J. K. Wright, Shock Tubes, John Wiley & Sons, Inc. (New York, N.Y., 1961).

[8] L. D. Landau and E. M. Lifschitz, Fluid Mechanics (transl. from the Russian by J. B. Sykes and W. H. Reid), Addison-Wesley Publ. Co., Inc. (Reading, Mass., 1959).

[9] I. I. Glass and G. N. Patterson, A theoretical and experimental study of shock tube flow, J. Aeronautical Sci. **22,** 73–100 (Feb. 1955).

[10] I. I. Glass and W. A. Martin, Experimental and theoretical aspects of shock wave attenuation, J. Appl. Phys. **26,** 113–120 (1955).

[11] D. Bitondo and R. K. Lobb, The design and construction of a shock tube, Toronto University Institute of Aerophysics Rept. No. 3, pp. 48 (1950).

[12] A. E. Wolfe, Shock tube for gage performance studies, Rept. No. 20–87, Jet Propulsion Laboratory (May 1955).

[13] R. W. Ladenburg, B. Lewis, R. N. Pease, and H. S. Taylor, Physical Measurements in Gas Dynamics and Combustion, vol. IX, High Speed Aerodynamics and Jet Propulsion, Princeton Univ. Press (Princeton, N.J., 1954).

[14] C. R. Wylie, Jr., Advanced Engineering Mathematics, McGraw-Hill Book Co., Inc. (New York, N.Y., 1960).

7. Periodic-Function Generators

D. F. Muster [1]

1. General

1.1. Types of Periodic-Function Generators

In chapters 2 and 4, respectively, the response of linear and nonlinear pressure transducers to periodic input functions is discussed. It is demonstrated that (even in theory) there are inherent advantages to calibrating certain transducers with steady-state (repetitive or periodic) inputs rather than step inputs. The relative value of these advantages will be discussed with reference to each of the periodic-function generators mentioned below.

For convenience, let us restrict this initial discussion to linear transducers; the effect of nonlinearities (particularly, of stiffness) is discussed separately. As sensed and displayed by a linear transducer system, the shape, magnitude and time of occurrence of an arbitrary forcing function are modified. In effect, the transducer system filters the input and the displayed response is modified accordingly. If the forcing function is a sinusoid, the response of a linear transducer will also be a sinusoid; thus, the shape of the input and response are the same. However, the magnitude and phase of the response may be markedly different from that of the input. As was mentioned earlier, this fact places sinusoidal forcing functions in a unique position in the dynamic calibration of all categories of transducers. Further, it gives experimentalists a feel for the physical significance of Fourier analysis and the concept of frequency spectra. If any input can be represented as the sum of a number of sinusoids, then it follows that the output of a linear transducer can be represented by these same sinusoids modified only in amplitude and phase. Each is sensed and displayed by the transducer as if it were present alone (the principle of superposition). The response function is the sum of the output sinusoids.

It is shown in chapter 2 that from a knowledge of the steady-state characteristic of a system the response waveform for any specified input waveform can be computed. For example, if the specified input includes components at frequencies in a given range and it is known that the transducer system is linear in the same frequency range, then the following relationship will hold:

$$X(\omega)=kF(\omega)e^{-j\phi}, \qquad (7.1)$$

where $X(\omega)$ and $F(\omega)$ are the output and input spectra, respectively, k an amplitude factor, and φ the phase shift, all in the given frequency range.

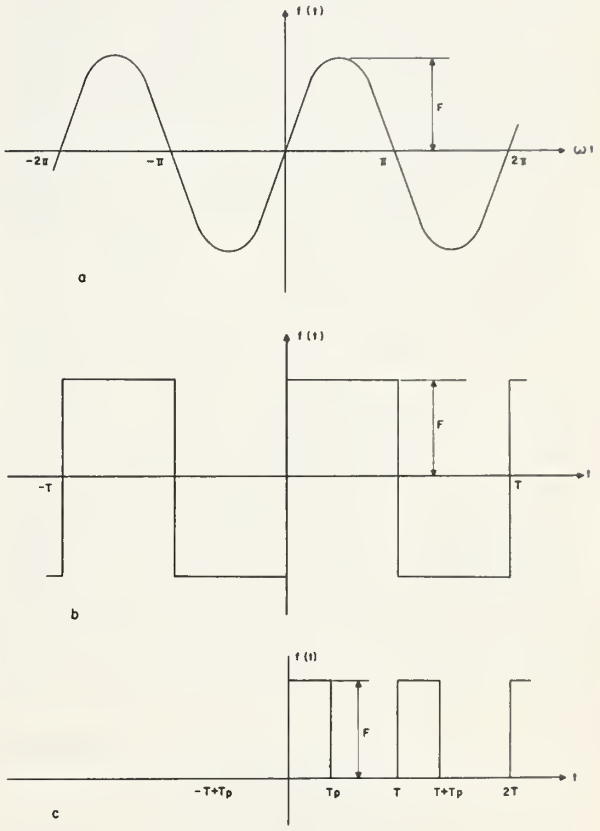

FIGURE 7.1. *Periodic input functions.*
(a) Sine function
(b) Square-wave functions
(c) Pulse function

The specific periodic functions of primary use in the dynamic calibration of pressure transducers are sinusoids, square-wave, and impulse functions (fig. 7.1). In consequence, in this chapter we will be concerned primarily with generators capable of producing pressure changes which approximate closely one of these wave forms. These include acoustical shock generators, rotating valve and piston-in-cylinder devices, sirens, and electrical, mechanical, and electro-mechanical exciters.

1.2. Place in Pressure Transducer Calibration

The descriptive phrase "frequency response" implies that the response under consideration (pressure, acceleration, velocity, etc.) is a function of frequency. Two examples are the measured

[1] Professor of Mechanical Engineering, The University of Houston.

output of an electronic amplifier in response to sinusoidal inputs of known frequency from an oscillator, and the oscillating electrical output of a microphone in response to known sinusoidal changes in pressure level. In the first case, it is relatively easy to generate sinusoidal signals up to frequencies in the megacycle per second range. In the second case, it is difficult to generate a relatively distortion-free sinusoidal sound field at high amplitudes and/or high frequencies. The latter is in conflict with the requirements for shock wave and rocket-engine research, where the ambient acoustic environment may be characterized by amplitudes of greater than one atmosphere ($\approx$ 188 db re 0.0002 microbar) and frequency components up to 30 kc/s. To date, sinusoidal pressure oscillations at these amplitudes and frequencies cannot be produced in a gaseous medium. At lower amplitudes and/or frequencies calibrating devices have been developed and are described in a later section.

The lack of an acoustic high-amplitude, high-frequency sinusoidal calibration device is not due to a lack of ingenuity on the part of experimentalists. It is due to certain fundamental physical limitations associated with the problem of attempting to force the motion of gases in a sinusoidal manner over a wide range of frequencies. If the amplitude is kept constant, as the forcing frequency is increased the wave form degenerates from a sinusoid to a saw tooth. This is due to thermodynamic causes, particularly to shock wave interaction. As a result, sinusoidal acoustic exciters in pressure transducer calibration are limited to pressure levels and frequencies considerably lower in scale than those associated with most rocket-engine research.

In some cases, input functions to a pressure transducer in the range of frequencies and/or amplitudes of interest can be more easily generated as a square wave or repetitive impulse. The superposition principle will still apply, if the transducer system is linear, and the frequency response for either input will be the same as for the sinusoid, although the method of interpreting the results is different.

There are two principal limitations on calibration with impulse generators. The impulse must be of short duration compared with duration of the finest detail of the output transient which is to be reproduced accurately; that is, the impulse spectrum must be flat over the entire frequency range of the device under test. In turn, this implies that, in order to achieve a significant response at some frequencies the impulse must be so great in amplitude that the transducer system under test is often forced out of its linear range at other frequencies.

The second disadvantage is that, when testing wide-band devices, low-frequency effects are difficult to observe. The one-test advantages of impulse methods are offset by the incapability of transducer systems to react in the same way to all frequencies and, as a consequence, low-frequency cutoff limits their effectiveness.

In summary, in the low- and medium-pressure range, the available methods of dynamic calibration include the use of repetitive acoustical-shock generators, sirens, rotating-valve and electromechanical exciters. Piezoelectric devices are useful in the higher frequency and pressure-level ranges; strictly mechanical devices are most useful in the lower frequency and, most often, the lower pressure-level ranges.

2. Acoustical-Shock Generator

2.1. Description

The acoustical-shock generator is well adapted to the dynamic calibration of microphones and other low-pressure transducers. It is characterized by the following features: low power requirement, suitability for automatic operation, and the high-energy, short-duration acoustic pulses it generates are accurately reproducible.

In principle, the operation of the device is similar to suddenly bursting an inflated paper bag. A piston in a cylinder is forced against a compression spring and held in this retracted position. The open end of the cylinder is covered by a paper strip. When the piston is released, the air ahead of it is compressed adiabatically until the paper strip breaks at a certain critical pressure. The piston is again retracted. A fresh strip of paper is drawn over the end of the cylinder and the process repeated. The device is motor-driven and the length of time between impulses is controlled through a gear train. In a typical generator, the pressure at bursting is about 50 psi, the time between pulses from 3 to 30 secs.

2.2. Theory

The shock wave associated with each burst is propagated in an essentially spherical manner. The value of the energy in the pressure wave can be computed by integrating the square of the pressure-level function from $t=0$ to $t\rightarrow\infty$. To the first order, the pressure wave may be assumed to have the shape of a saw-tooth, whose base represents the duration of the wave (say, 0.4 msec). At a radius of 1 m and for a pressure of 200 dynes/cm^2, the energy content of the shock wave is approximately 0.25 watt-sec and the power of the acoustic source is about 600 acoustic watts.

2.3. Evaluation of Test Data

Oscillograms of the pressure pulses from an acoustical-shock generator (as measured at a given radius and various angles with the generator at the origin) show that the shock wave propagates spherically. The main pulse is essentially triangular and a typical value of its duration is, say, 250 μsec. Whereas the amplitude of the main

pulse may be almost 100 db (re 0.0002 microbar), the amplitude of succeeding pulses is considerably less (down 20 db or more).

A typical frequency spectrum is essentially flat from about 1000 to 8000 c/s. This is roughly two octaves below and one octave above the center frequency of 4000 c/s, which corresponds to the duration of the main pulse. At higher frequencies, the diameter of the generator opening is not small compared to the acoustic wavelengths and the pressure waves associated with these frequencies are not propagated spherically. As a consequence, each frequency spectrum will display directional characteristics and the measured spectrum is no longer flat.

In addition to the gradual decrease in level associated with the radiation characteristics of the source, there are resonances and anti-resonances observed in the measured spectra. These are due to the presence of a short tube just in front of the generator cylinder and along an extension of its axis. At the moment of burst the cylinder plus tube acts as a quarter-wave resonator. At the end of the piston stroke, the tube alone acts in the same manner. In effect, this affects the frequency spectra by strengthening certain frequency components and weakening others, causing relative peaks and nulls in the measured pressure levels.

The reproducible quality of the pulses from an acoustical-shock generator have been well established. A generator was placed in an anechoic chamber and the relative maximum sound-pressure levels per octave were measured. The results of many tests were analyzed in this way and the per-octave sound pressure levels compared. The deviations are less than ± 0.5 db for all octaves from 100 to 6400 c/s; thus, the reproducible quality of the pulses produced by the generator was established. Above 6400 c/s, the deviation was as much as ± 3 db.

3. Rotating-Valve Generator

3.1. Description

It is often desirable in the calibration of pressure transducers that the forcing function be of the form of a series of repetitive, precisely controlled pressure pulses. A mechanical device which generates such a forcing function (but which is necessarily limited to low frequencies) is reported by Hermann and Stiefelmeyer [1] [2] (and attributed to Staiger and Mohilo). A schematic representation of the device is shown in figure 7.2a and of a similar device developed by Eisele [2] in figure 7.3a.

Pressure fluctuations of the kind in figure 7.2b [1] or 7.3b [2] are possible by suitably arranging the rotating valves and the sources of high-pressure gas. The levels of the pressure in either figure 7.2b or 7.3b can be preset precisely by means of pressure gages. By adjusting the speed of the driving motor, a series of valves are opened and closed sequentially at the desired repetition rates. The transducer is subjected to a sequence of predetermined pressure changes, the duration of which are determined by the speed of the rotation.

3.2. Evaluation of Test Data

At higher repetition rates, Eisele [2] has found that the pressure steps are distorted by resonance effects which can be attributed to the inertia of the gas column in the valve system (fig. 7.3b). As a consequence, the usefulness of the device as a calibrator is limited to frequencies below where these effects are observed.

Normally, the square pressure pulses generated by the rotating-valve device are not truly shock waves. Unlike the short-term, high-intensity pulses generated by the acoustical-shock generator, the pulses from the rotating-valve generator are of longer duration (say, about 100 msec as compared to 250 μsec) and lesser intensity (say, about

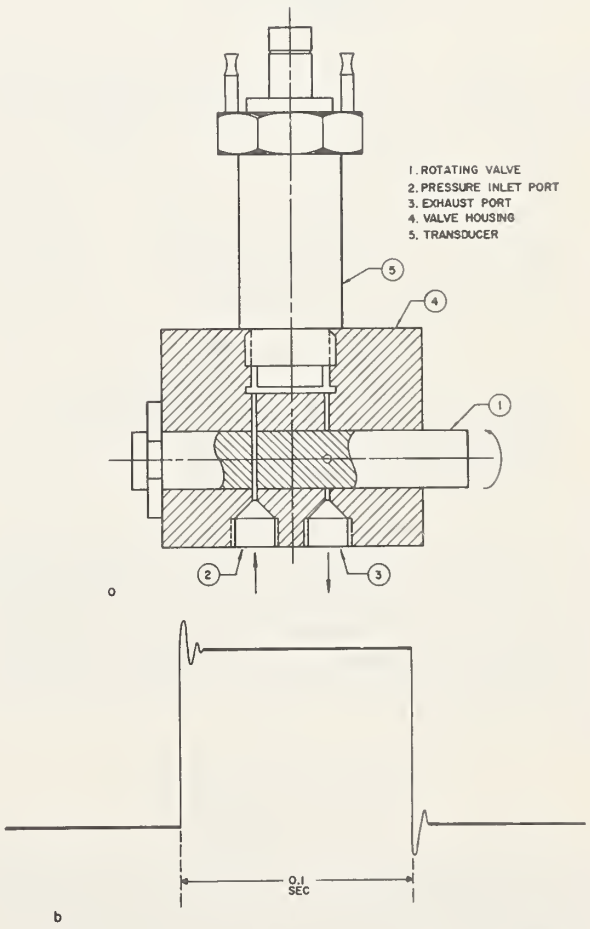

FIGURE 7.2. *Rotating valve pulse-function generator.*

(Reproduced from [1] with permission from Franzis-Verlag)

(a) Constructional features of pressure calibrator
(b) Representation of oscillograph trace for single-step calibration

[2] Figures in brackets indicate the literature reference on p. 95.

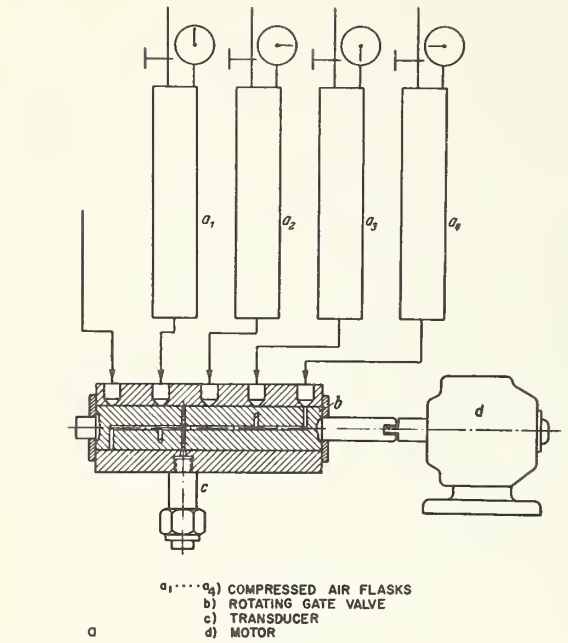

FIGURE 7.3. *Rotating-valve staircase-function generator.*

(Reproduced from [2] with permission from R. Oldenbourg Verlag)

(a) Schematic of pressure calibrator
(b) Calibration of curves derived from apparatus shown in (a) at two different motor speeds

10 to 15 psi per step as compared to 200 psi).

A major disadvantage of the rotating-valve generator is the presence of the relatively long tube between the transducer under test and the rotating-valve mechanism. In effect, it introduces a half-wave resonator into the calibration system which limits the effectiveness of the generator at high frequencies.

4. Sirens [3, 4, 5, 6, 7]

4.1. Description

The siren-tuned-cavity oscillator is a useful device for generating periodic (but not necessarily sinusoidal) pressure waves for the calibration of microphones and other low- and medium-pressure transducers. The essential elements of the generator are a cylindrical chamber with an axial orifice in one end and a revolving disk or flanged wheel with a number of equally spaced holes

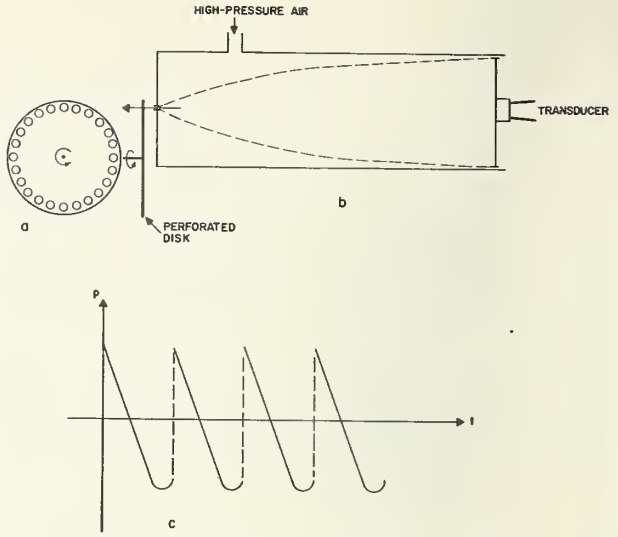

FIGURE 7.4. *Siren-tuned-cavity generator.*

(a) Rotating disk
(b) Tuned cavity
(c) Typical waveform

arranged around its periphery. The wheel is positioned such that the holes in its periphery are close to the axial hole in the cylinder and, as the wheel rotates, the flow of air from the cylinder is interrupted. A schematic representation of this arrangement is shown in figure 7.4 with a sketch of the waveform produced by such a generator.

As the name "siren-tuned-cavity oscillator" implies, two adjustments are necessary in order to operate the generator effectively. For each rotational speed of the siren (which, with the number of holes, determines the frequency of the pressure waves), the length of the cylinder must be adjusted so that it will act as a half-wave resonator; thus, the speed of the wheel determines the basic pulse length (frequency) and the tuning adjustment reinforces the pressure wave and determines its amplitude at the transducer location (fig. 7.4).

For purposes of calibration, the value of pressure at the cavity-transducer interface is measured with a previously calibrated transducer, or it is computed using methods described by Oberst [8] When measured pressures are used as a standard, the calibrated gage must be an instrument with a uniform frequency response up to frequencies several times higher than the test frequency.

Oberst [8] shows that the maximum pressure magnitude at the transducer, figure 7.4, is given by

$$|P_0| = P_e/\beta l.$$

Here P_e is static pressure (as measured with a Bourdon gage) at the end of the tube where the opening is located (called excess pressure by Oberst), and l is the tube length. The term $\beta(=8\mu\pi^2 f^2/\rho_{av}a^3)$ is the attenuation constant per unit tube length for a plane wave of frequency f in

a medium of mean equilibrium density ρ_{av}. In the expression for β, a is the velocity of sound. The actual damping for waves in air is small for moderate frequencies ($\beta=0.24\times10^{-8}$ for $f=1000/2\pi$ in air), but increases rapidly with increasing frequency.

4.2. Evaluation of Test Data

The saw-tooth shape of the pressure wave at the pressure transducer can be approximated by the series

$$P=\frac{P_0}{\pi}\sum_{k=1}^{n}\frac{1}{k}\sin k\omega t,$$

where P_0 is the peak value of pressure. Thus, although the basic pulse length is established by speed of rotation of the siren wheel, each of the pulses consists of many harmonic components whose respective amplitudes are an inverse function of frequency.

The saw-tooth shape is due to the nature of the reinforcement making any pulse steeper-fronted as the wave propagates. Even quasi-sinusoidal pulses are distorted and originally steep-fronted pulses (such as can be generated by a siren) become close approximations of the saw-tooth shape.

It has been shown that a saw-tooth wave will develop within the tunnel cavity when the pressure pulse generated at the orifice is greater than 10 percent of the pressure of the air flowing in the cavity. Peak pressures of about 30 psi (equivalent to over 190 db re 0.0002 microbar) are possible. Basic repetition rates from 50 to 1000 pulses per second can be achieved without difficulty.

5. Piston-in-Cylinder Steady-State Generators

5.1. General

A generator which can produce a steady-state (rather than repetitive-pulse) forcing function (sinusoidal at low amplitudes, distorted sinusoids at high amplitudes) has many advantages, as has been mentioned in this chapter and earlier. In particular, nonlinear effects occur when an attempt is made to generate pressure waves characterized by both high frequency and high amplitude. Thus, low-frequency, low-amplitude pressure waves can be sinusoidal, whereas high-frequency, high-amplitude waves are not sinusoidal and, in many cases, may exhibit shock characteristics.

The obvious way to produce a sinusoidal pressure variation is by means of a piston-in-cylinder device. Pressure changes produced in this manner can be reinforced by resonance effects at frequencies related to the geometry of the cylinder and the physical properties of the fluid. There is an extensive literature on the distortion of pressure waves due to nonlinearities in these properties under dynamic conditions [9, 10].

In particular, Schmidt [9] and Betchov [11] have studied the formation and behavior of oscillating shock waves which are generated by the coalescence of compression waves.

5.2. Theory

A theory for the forced motion of gases in tubes is developed by Betchov [11]. It is assumed that the calibration device is a long tube, closed at one end with a piston at the other (fig. 7.5). The motion of the piston is sinusoidal with circular frequency $\omega(=2\pi f)$. The gas in the tube is assumed to behave as an ideal gas ($P=\rho RT$). In this one-dimensional theory, for small motions (i.e., u, the pressure wave velocity is small), a linear solution is a close approximation of the actual motion. As in all idealizations of dynamical systems which do not account for friction in its various forms, infinite amplitudes are predicted at the resonant frequencies for which the length of the tube is a multiple of the half-wavelength $\left(=\frac{a}{l}, a \text{ is the velocity of sound in air.}\right)$

In an actual piston-in-cylinder device, the motions of the gas are not necessarily small (and the linear solution is not valid). In turn, the

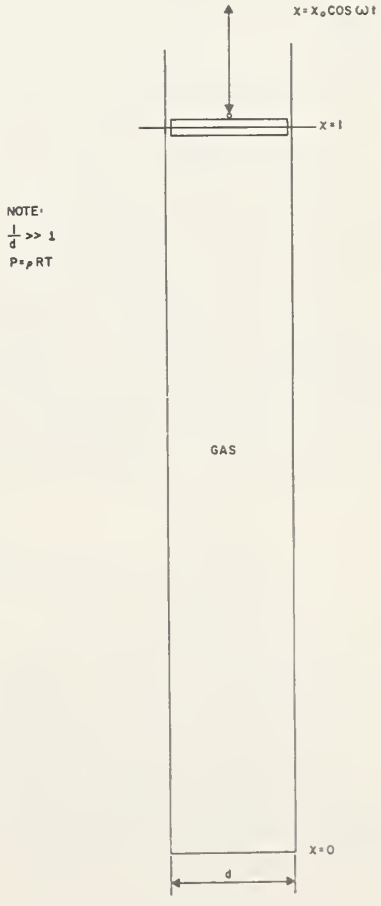

FIGURE 7.5. *Piston-in-cylinder model.*

shape of the pressure wave is determined by the piston motion, the gas-dynamics and acoustic factors associated with the phenomena, frictional effects at the lateral boundaries and inherent in the gas and, when the motion of the gas is forced into the nonlinear domain, shock fronts.

The shock fronts, whether strong or weak, tend to distort the shape of the pressure wave and form oscillating shock waves in the tube length. Energy is dissipated in the formation and continued motion of the shock waves. It is sufficient to raise the gas temperature slightly, but not so much that the resonant frequencies are affected appreciably. Losses (watts dissipated per unit piston area) may, in fact, exceed the average power delivered.

From the observations of Schmidt and others it is clear that, at resonance, oscillating shock waves are always present in the gas column of a piston-in-cylinder device. Even at nonresonant frequencies, the motion of the gas is sufficiently complex that it can safely be assumed the amplitude and phase of the gas will not agree with that of the piston motion. The nonlinear and cumulative effects of friction can be seen in the transformation of an initially shockless and almost-sinusoidal motion into one characterized by shock waves and a distorted pressure-wave shape.

Some pressure-wave generators use a liquid as the active medium instead of gas. The principle differences between liquid- and gas-piston-in-cylinder devices are associated with the incompressibility of liquids. The dynamics of long, liquid-filled tubes have been studied by several investigators [12, 13, 14, 15]. Their studies have included resonance effects, coupled vibration, cavitation, and the softening effect of entrapped air.

A basic factor in each of these studies is the bulk modulus (or its inverse, compressibility) of liquids. It is defined as the ratio $-\frac{\Delta P}{\Delta V/V}$ where ΔP is the increment of pressure applied to the volume of liquid V to cause a decrease in volume $-\Delta V$. Bulk modulus has the dimensions of pressure and depends upon both pressure and temperature

The stiffness of a liquid-filled, piston-in-cylinder device can be computed from the equation

$$-K=\frac{A}{l}K_m,$$

where A and l are the cross section and length, respectively, and K_m the bulk modulus. Typical values of K_m for several liquids are

Liquid	K_m
	psi
Water (68 °F)	3.5×10^5
Methyl alcohol (68 °F)	1.76×10^5
Carbon tetrachloride	1.63×10^5
Kerosene	1.91×10^5

5.3. Equipment

The basic elements of a piston-in-cylinder calibrator consist of a piston in a liquid-filled cylinder to which the transducer is connected. The cylinder can be pressurized and the piston is connected to a sinusoidal-motion driving mechanism. In a recent report, Cobb [16] describes such a device for which the driving force is furnished by one or two electromagnetic exciters, each capable of delivering up to 2500 lb-force at frequencies up to 2000 c/s. A plastic diaphragm seal is fastened to the end of cylinder with the piston acting against the side of the diaphragm away from the liquid. This arrangement permits separate application of the static and dynamic components of pressure.

Cobb suggests two systems: one in which the cylinder is mounted rigidly to a stiff structural frame and the piston to the exciter, and a second in which both the piston and cylinder are secured to the armatures of separate exciters arranged to operate out of phase. The second arrangement performed in a more satisfactory manner.

5.4. Evaluation of Test Data

Cobb [16] reports the two-exciter calibrator system is capable of supplying ± 150 psi with a static pressure of 500 psi in the cylinder and at frequencies between 10 and 1000 c/s. Above 500 c/s there is a tendency to distortion at the larger pressure-variation amplitudes. A major difficulty in operating the device is the softening effect of entrapped gas on cavity stiffness. This tends to lower the frequency at which the first resonance occurs and is the principal reason for limiting the effective range of the calibrator to 500 c/s.

6. Electrical and Mechanical Exciters [17, 18, 19]

6.1. General

The source of force (or motion) in many pressure-transducer calibration systems is an electrical, mechanical or electromechanical vibration exciter capable of delivering sinusoidal excitation to the transducer over a wide range of frequencies. Among the most useful of such generators are the following types: piezoelectric, mechanical direct-drive and force-reaction, hydraulic, pneumatic, and electrodynamic. They cover the frequency spectrum from almost-zero c/s to 10,000 c/s and can deliver force amplitudes as high as several thousands pounds. No one machine can span these ranges, but from this group, machines can be selected which cover large portions of them.

If a range of calibration frequencies from 5 to 10,000 c/s is desired, the electrodynamic-type machine most nearly satisfies the requirements of the ideal calibrator. For high-frequency, high-

force applications, the piezoelectric type is most useful, despite its limitation of being capable of producing only very small displacements. The latter disadvantage makes it difficult to use as a low frequency source. In addition, the motion of the exciter must be measured by interferometer techniques or external displacement-measuring sensors such as the capacitance pickup. Mechanical direct-drive and force-reaction types are used only for low-frequency (less than 100 c/s) applications. Hydraulic and pneumatic exciters are used least of all as sources of vibration, but (as we have mentioned earlier in this chapter) they are used directly in pressure-transducer calibration. When used as vibration exciters their limitations (sensitivity to distortion, low-force output at high frequencies) outweigh their advantages (force transmitted can be calibrated under static conditions, the generated force can be interrupted abruptly). Conversely, their direct use (that is, when the transducer is an integral part of the fluid chamber) is well established and is reported earlier in this chapter.

A vibration generator which is to be used in calibration work should provide:

1. Distortion-free sinusoidal forces (or motions).
2. Stepless variation of frequency and output within specified limits, easily adjustable during operation.
3. Horizontal as well as vertical motion, if required.
4. Features permitting the use of absolute calibration methods when calibrating the calibrator.
5. True rectilinear motion normal to the main axis of the exciter without the presence of other motions.

6.2. Piezoelectric Exciters

The piezoelectric vibration machine uses a stack of piezoelectric elements as a source of mechanical vibration. The piezoelectric elements are cut from crystals having piezoelectric properties or are made from ferroelectric ceramics. When the elements are subjected to mechanical pressure, electrical charges proportional to the pressure are generated. If the element is compressed between two electrically connected metal plates applied to opposite faces of the element, and a metal band is placed around the middle of the element between the band and the end plates, an electromotive force of considerable magnitude will be developed between the band and the end plates, upon small changes of pressure between the end plates. The piezoelectric effect is reversible. A variable voltage applied between the plate and the band will cause the element to expand and contract mechanically in synchronism with the varying applied voltage [20, 21].

Three types of materials are used in transducers and exciters which make use of this effect. These are Rochelle salt, ammonium dihydrogen phosphate (ADP), and barium titanate ($BaTiO_3$). In either case, a strain across the element results when a voltage is applied. The direction of the strain depends upon the orientation of the crystallographic axes of the original crystal relative to the crystal element, or in the direction of polarization of the ceramic element, and on the location of the electrodes. The strain in the piezoelectric stacks of elements (as shown in fig. 7.6) alternately causes an increase and decrease in the thickness of the elements, thereby imparting motion to the liquid-loaded plate of the calibrating chamber.

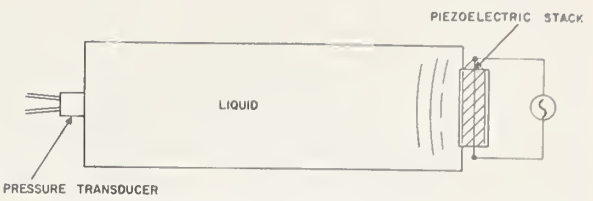

FIGURE 7.6. *Piezoelectric exciter for a pressure-transducer calibration system*

These exciters are usable in the range from 1,000 to 20,000 c/s, the span of the range depending upon the configuration and size of the particular unit; the peak-to-peak displacements are 0.001 in. or less. As a consequence of the latter, mounting the piezoelectric stack is important. A massive backup base holds fixed the end of the stack away from the liquid. In order to terminate the end of the stack in an essentially infinite mechanical impedance, the base material is preferably highly damped and the base itself made as massive as possible.

When a voltage is applied to the electrodes of the piezoelectric stack, the magnitude of the deformation produced is dependent upon the frequency of the applied voltage and the frequency response of the electromechanical system. If the mass of the load carried by the piezoelectric element in combination with the stiffness of the element gives a resonant frequency well above the highest operating frequency, the system is spring controlled, providing a displacement proportional to the voltage and independent of frequency. For a liquid loading, which is essentially mass-like and produces a resonant frequency in or near the operating frequencies, a typical resonance effect is observed.

The principal features of the piezoelectric exciter are:

1. The design can be made compact and rigid, providing good high-frequency (with high-amplitude) operation.
2. Normally, only small-displacement (and, as a result, relatively high-frequency) operation is possible.
3. The electrical load presented to the power source is highly reactive and is of high impedance. Unless it is possible to use many piezoelectric elements (connected electrically in parallel but mechanically in series) several kilovolts may be required in order to produce the requisite output.

6.3. Electrodynamic Vibration Machine

Electrodynamic exciters are used in pressure transducer calibration in one of two ways: as sources of sinusoidal motion for diaphragms, or in piston-in-cylinder calibrators such as that reported by Cobb [16]. In the former case, a pressure transducer is placed in the end of a liquid-filled chamber at the opposite end of which is the driven diaphragm. The latter example is discussed in section 5 of this chapter.

The electrodynamic exciter derives its name from the method of force generation: the force causing the motion of the table (to which the load is attached) is produced electrodynamically by the interaction between an alternating current flow in the driver coil and the intense magnetic field which cuts the coil (fig. 7.7).

A wide range of frequencies is possible, with a properly selected electric power source, from 0 to 20,000 c/s. Small, special-purpose machines have been made with the first axial resonance mode above 26,000 c/s, giving a resonance-free, flat response to 10,000 c/s [17]. Frequency and amplitude are easily controlled by adjusting the power-supply frequency and voltage. In the case of an electronic power supply, the vibration machine load is not reflected back to the oscillator signal source, giving zero frequency regulation at any load.

Rated force (continuous sinusoidal peak value) varies according to manufacturer and unit design, but the smallest self-contained units deliver approximately 1 lb, the largest, about 25,000 lb. For most transducer calibration applications, machines rated between 200 and 2500 lb are used.

Pure sinusoidal table motion can be generated at all frequencies and amplitudes. Inherently, the table acceleration is the result of a generated force proportional to the driving current. If the electric power supply generates pure sinusoidal voltages and currents, the waveform of the table motion will be sinusoidal and background noise will not be present. Operation with table waveform distortion of less than 10 percent through a displacement range of 10,000 to 1 is common.

Random vibration, as well as sinusoidal vibration, or a combination of both, can be generated by supplying an appropriate input voltage.

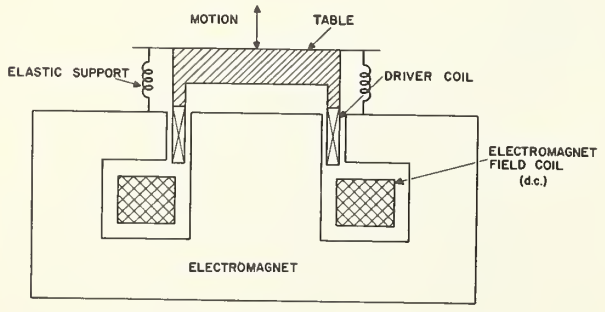

FIGURE 7.7. *Electrodynamic vibration machine.*

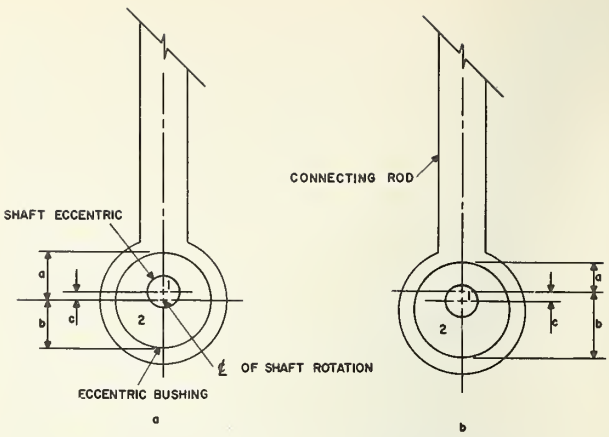

FIGURE 7.8. *Displacement adjustment method.*

(a) $a=b$. Displacement $=b-a=0$
(b) $a\neq b$. Displacement $=2c$ (PEAK-TO-PEAK)

6.4. Low-Frequency Pneumatic Sinusoid Generator

For low-frequency, low-amplitude calibration, a pneumatic generator has been developed [22]. The generator consists of an electric motor operating through a variable-speed reducer to drive a cam which positions the input crank of displacement-balance, pneumatic-pressure transmitter. In figure 7.8 is a method of providing stepless adjustability of crank offset between zero and full displacement. The boundary surfaces between shaft eccentric 1 and eccentric bushing 2 and between 2 and the connecting rod are circular cylinders. For a fixed-displacement setting, the eccentric 1 and the eccentric bushing 2 remain fixed relative to each other but rotate about the rotation center of the driving shaft. The displacement adjustment is made by rotating eccentric bushing 2 relative to shaft eccentric 1 [17].

Nominally, the pressure transmitter has an output range of from 5 to 25 psi, but different ranges can be obtained by adjusting the operating stroke at the input crank.

6.5. Electromagnetic Methods for Calibrating Some Pressure Transducers

Transducers which use diaphragms of magnetic materials can be calibrated by a direct-excitation technique. E. J. Diehl and H. Visser of the internal combustion laboratory of the Technische Hogeschool in Delft are reported to have used an iron core (solenoid) placed coaxially in close proximity to the diaphragm (fig. 7.9). The oscillating motion of the diaphragm is sensed by a capacitance pickup.

The damping present in the diaphragm assembly can be sensed and measured by recording the decay of the diaphragm vibration on a level recorder. From these decay-rate measurements, the logarithmic decrement can be computed directly.

Very low-pressure, acoustical transducers can

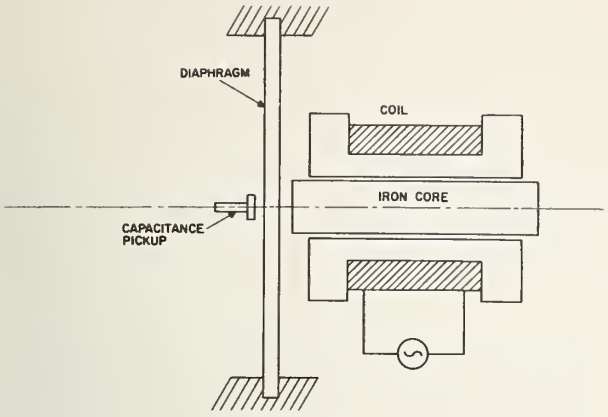

FIGURE 7.9. *Electromagnetic excitation of a transducer diaphragm.*

be calibrated by fastening them directly to the table of an electrodynamic vibration machine [23]. By exposing the pressure-sensitive diaphragm to the atmosphere, the oscillatory motion of the transducer produces a corresponding pressure variation on the sensitive element. The absolute movement of the diaphragm can be sensed and measured optically (at low frequencies) or by a capacitance pickup. The frequency range over which this method has been used is reported to be 3000 c/s under normal conditions and, with special equipment, 8000 c/s [23]. Pressure levels are low (usually no more than 50 to 60 db or, say, 0.1 dyne/cm^2).

7. References

[1] P. Hermann and G. Stiefelmayer, Contribution to the electrical measurement of pressure changes (in German), Elektronik, No. 4, 94–98 (1956).

[2] E. Eisele, Calibration of gages, II dynamic calibration (in German), Arch. Tech. Messen, J137–7 (May 1951).

[3] C. H. Allen and B. G. Watters, Siren design procedure, J. ASA **31,** 842 (1959).

[4] C. H. Allen and B. G. Watters, Siren for producing controlled wave forms with amplitude modulation, J. ASA **31,** 463 (1959).

[5] C. H. Allen and B. G. Watters, Siren for producing controlled wave forms with high intensities, J. ASA **31,** 177 (1959).

[6] R. Clark Jones, A fifty-horsepower siren, J. ASA **18,** 371 (1946).

[7] C. H. Allen and I. Rudnick, A powerful high-frequency siren, J. ASA **19,** 857 (1947).

[8] H. Oberst, A method for producing extremely strong standing sound waves in air (in German), Akust. Z. **5,** 27–38 (1940). English translation by L. L. Beranek, J. ASA **12,** 308–309 (1940).

[9] E. Schmidt, Large amplitude oscillation of gas columns in piping (in German), Z. VDI **79,** No. 22, 671–673 (June 1935).

[10] C. Mayer-Schuchard, Oscillation of air columns with large amplitude (in German), VDI Forsch. **376** [B], 1, 13–22 (Jan.–Feb. 1936).

[11] R. Betchov, Non-linear oscillation of a gas column, Phys. Fluids **1,** 205 (1958).

[12] R. W. Boyle and D. Froman, Vibrations of liquids in cylindrical tubes, Nature **126,** No. 3181, 602 (Oct. 18, 1930).

[13] R. D. Fay, Waves in a liquid-filled cylinder, J. ASA **24,** 459 (1952).

[14] G. S. Field, Longitudinal and radial vibrations in liquids contained in cylindrical tubes, Can. J. Research **5,** 131 (1931).

[15] Y. C. Lee and C. C. Miesse, On the forced vibration of a tank of liquid, Shock & Vib. Bull. No. 22, USNRL, 125 (July 1955).

[16] A. W. Cobb, Design of a dynamic calibrator for pressure transducers, MS Thesis, UCLA Engrg. Dept., UCLA Engrg. Lib. (1956).

[17] C. O. Harris and C. E. Crede, Shock and Vibration Handbook, Vol. I, Ch. 16; Vol. II, Ch. 25, McGraw-Hill Book Co., Inc. (New York, N.Y., 1961).

[18] L. Beranek, Acoustic Measurements, John Wiley & Sons (New York, N.Y., 1949).

[19] E. Rule and T. A. Perls, Hand-held calibrator for pressure-measuring systems, J. ASA **32,** 535 (1960).

[20] W. P. Mason, Piezo Electric Crystals and Their Applications to Ultrasonics, Appendix D, Van Nostrand Co. (Patterson, N.J., 1950).

[21] W. G. Cady, Piezoelectricity, McGraw-Hill Book Co., Inc. (New York, N.Y., 1946).

[22] D. P. Eckman and J. C. Moise, A pneumatic sine-wave generator for process control study, Proc. ISA **7,** 13 (1952).

[23] W. Erler, Measurement methods for the calibration of structure-borne vibration and sound-measuring instruments (in German), Hochfrequency Technik und Elektroakustik **68,** 18 (May 1959).

8. The Electronic Compensator

E. L. Michaels [1] and G. F. Paskusz [2]

1. General

The electronic compensator is an electronic device designed to provide a transfer function which is the inverse of the transfer function of a given transducer. When an electronic compensator, whose transfer function is exactly the inverse of a given transducer transfer function, is incorporated into that transducer system, the result is that the input or driving function waveform and the output waveform are exactly alike.

It was pointed out in chapter 2, section 1.4, that knowledge of a transducer's transfer function and of the system response is sufficient for the determination of the system driving function. Thus, if a pressure transducer's output and transfer characteristics are known, its input can be obtained. That the operations necessary for this determination may often be laborious must be obvious from the preceding chapters. Moreover, the results are valid only for output ranges severely limited by the transducer frequency response.

It is therefore generally desirable to extend the usable frequency range of a transducer system and to reduce the labor involved in the determination of the driving function. The electronic compensator discussed in this chapter is designed to perform both of these functions.

2. The Principle of the Compensator

A general scheme for the representation of transducer systems was developed in chapter 2, and is in part repeated in figure 8.1.

In this scheme the effect of the transducer on the system is represented by a "transfer function." Basically, this transfer function is a description of the input-output relationship, and so it may be an equation, a set of equations, or one or more characteristic curves. Equation (1.1), characteristic of the transducers described in this report, is reproduced here:

$$m\ddot{x}+c\dot{x}+kx=f(t), \tag{1.1}$$

where

$f(t)$=driving function, a function of time
x=response of system, a function of time
m, c, k=physical constants previously defined.

The transfer function is an operator implicit in the equation. The equation may be written in operator form as

$$\left[m\frac{d^2}{dt^2}+c\frac{d}{dt}+k\right]x=f(t), \tag{8.1}$$

where the expression in the brackets is considered as operating on x. If this operator is designated by $1/T$, the equation may be rewritten as

$$[T^{-1}]x=f(t). \tag{8.2}$$

The response of the system may be obtained by the inverse operation. The inverse operation, $[T]$, is defined by eq (8.3) as

$$[T][T^{-1}]x=x=[T]f(t), \tag{8.3}$$

where $[T]$ is the operation which, when applied to $[T^{-1}]x$, will yield x.

The operator $[T]$ in the time domain thus represents all the main operations involved in solving the differential equation.

Equation (8.3) relates the known output of the system, x, to the driving force $f(t)$ which is to be determined. The solution to this equation may be obtained by the same scheme as that employed for the solution of the transducer eq (8.2), i.e., by the use of the inverse operation. Thus

$$[T^{-1}][T]f(t)=f(t)=[T^{-1}]x. \tag{8.4}$$

The electronic compensator, by performing the operation implied in eq (8.4), thus generates a system output (an output voltage) which is analogous to $f(t)$, the driving function.

The transducer system, including the compensator, may thus be described by the diagram of figure 8.2.

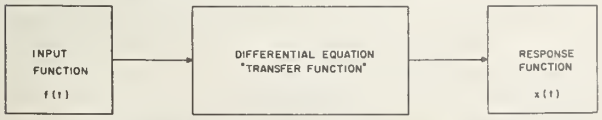

FIGURE 8.1. *A general transducer system.*

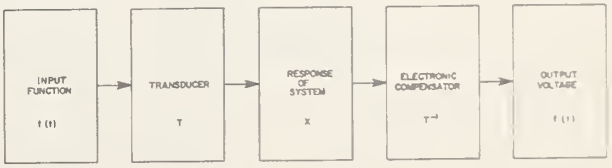

FIGURE 8.2. *The transducer system with compensation.*

[1] Chairman of Electrical Engineering, The University of Houston.
[2] Associate Professor of Electrical Engineering, The University of Houston.

3. Compensator Circuit

The electronic compensator is an electronic circuit whose transfer function is the inverse of the transfer function of the transducer. The compensator is resigned to perform the operation $[T^{-1}]$, i.e., to solve the differential eq (1.1). It is convenient for the discussion of compensator operation to modify this equation by using some of the conventional substitutions discussed in chapter 2. Thus, in terms of the undamped natural frequency, ω_n, and the damping ratio, ζ, eq (1.1) may be written in the form

$$\frac{1}{\omega_n^2}\ddot{x}+\frac{2\zeta}{\omega_n}\dot{x}+x=\frac{f(t)}{k}=g(t), \tag{8.5}$$

where $g(t)$ differs from $f(t)$ only by the constant scale factor k. This is an ordinary, second-order, linear differential equation with constant coefficients. Equations of that type are of the form

$$A\ddot{x}+B\dot{x}+Cx=g(t), \tag{8.6}$$

where both x and $g(t)$ are functions of time and A, B, and C are constants. Solution of this equation by electronic analog computer is simple and may be accomplished by use of an analog computer scheme similar to the one shown in figure 8.3, where d/dt represents a differentiator; A, $-B$, and C represent constant multipliers and Σ represents a summation amplifier.

Here the transducer output, x, is differentiated twice to yield $\dot{x}$ and $\ddot{x}$, respectively. Then x is multiplied by C, $\dot{x}$ by B, $\ddot{x}$ by A, and the three terms $A\ddot{x}$, $B\dot{x}$, and Cx are summed, thus resulting in the computer output $g(t)$.

A slightly more detailed diagram of the electronic compensator is shown in figure 8.4 [1].[3] Two amplifiers are used per stage to provide negative signals corresponding to the variables x, $\dot{x}$, and $\ddot{x}$, for summation, and for final inversion after summing. Amplifiers labeled CF are cathode followers; those numbered 1, 2, 4, and 6 are phase inverters or sign changers; and those numbered 3 and 5 are differentiators. Amplifier 6 is also an adder or summing amplifier as well as a phase inverter. Constant multiplication is achieved by means of potentiometers. A is adjusted by means of the ganged potentiometer while B is adjusted by the single potentiometer shown. C is unity in this case and thus needs no adjustment.

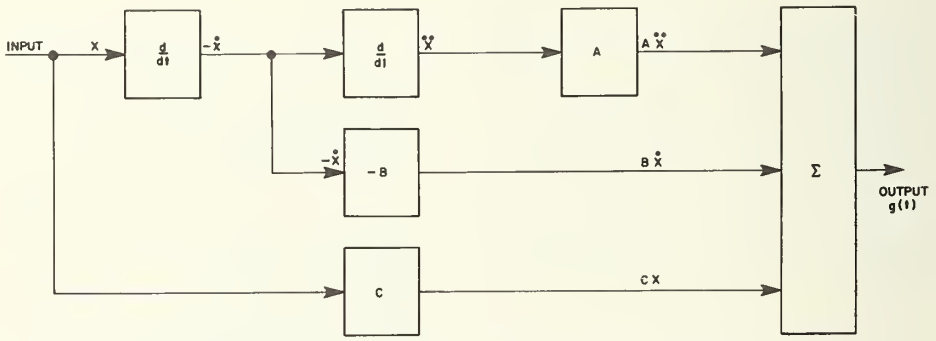

FIGURE 8.3. *Analog computer schematic for solution of eq (8.6).*

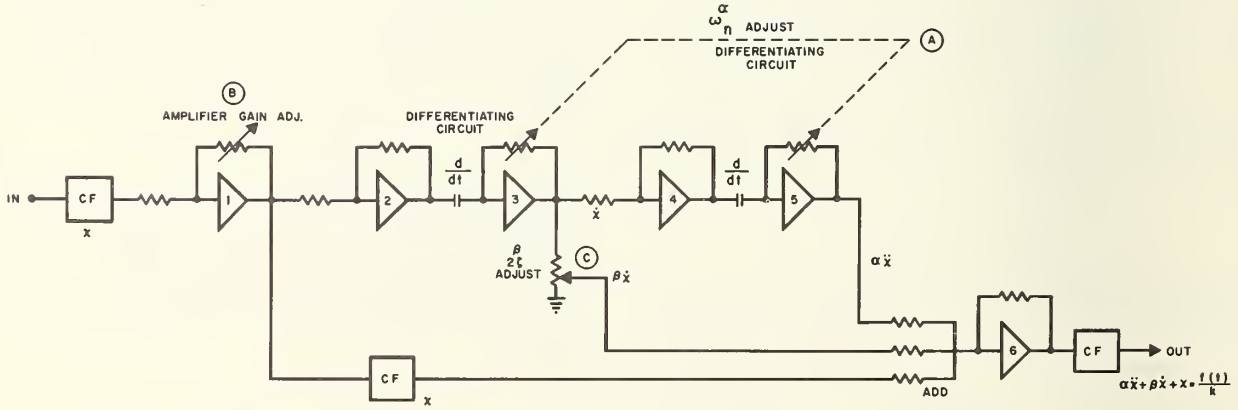

FIGURE 8.4. *Analog computer schematic diagram of electronic compensator.*

[3] Figures in brackets indicate the literature references on p. 104.

4. Calibration and Operation of the Compensator

The calibration and operation of the electronic compensator involve (1) determination of the constants in eq (8.6) by static or dynamic calibration methods, and (2) setting the compensator constants.

4.1. Calibration

Static calibration methods may yield results with an error no greater than 0.01 percent for quartz crystals. Piezoceramic transducers, which are more sensitive than quartz crystals, have a much lower internal resistance. The time constant of the piezoceramic transducer is thus reduced and the calibration accuracy at any given reading speed is much reduced below that of the quartz crystal. It then becomes mandatory to use ceramic calibration by periodic, step, or impulse function excitation.

A comparison of eqs (8.5) and (8.6) shows that the constants ω_n, ζ, and k specify completely the constants needed for the compensator eq (8.6). The natural frequency without damping (ω_n) may be derived from the damped frequency (ω_d) if the damping ratio ζ is known. The damping ratio, in turn, may be obtained from the logarithmic decrement in the following way.

It was shown in chapter 2 that the response of a slightly damped system to step function excitation is of the form

$$x=Ae^{-\alpha t}\sin \omega t, \tag{8.7}$$

which is a damped sinusoid of the form shown in figure 8.5.

At successive peaks, e.g., x_2 and x_3, $\sin \omega t \approx 1$ and therefore

$$x_2 \approx Ae^{-\alpha t_2}$$

$$x_3 \approx Ae^{-\alpha t_3} \tag{8.8}$$

and the ratio between two successive peaks is

$$\frac{x_2}{x_3} \approx e^{-\alpha \tau} \tag{8.9}$$

where $\alpha\tau$ is called the logarithmic decrement. The time of one period, τ, is related to the frequency by

$$f=\frac{1}{\tau}. \tag{8.10}$$

Also, $2\pi f=\omega$, and $c/2m=\alpha$ (see chapter 2), so that, from eq (2.11),

$$\zeta=\frac{\alpha\tau}{2\pi}. \tag{8.11}$$

Thus, the damping ratio may be determined from a dynamic calibration. From the damping ratio and the equation

$$\omega=\omega_n\sqrt{(1-\zeta^2)} \tag{8.12}$$

the damped natural frequency ω can be found [3, 4].

The remaining system constant, k, may be determined statically.

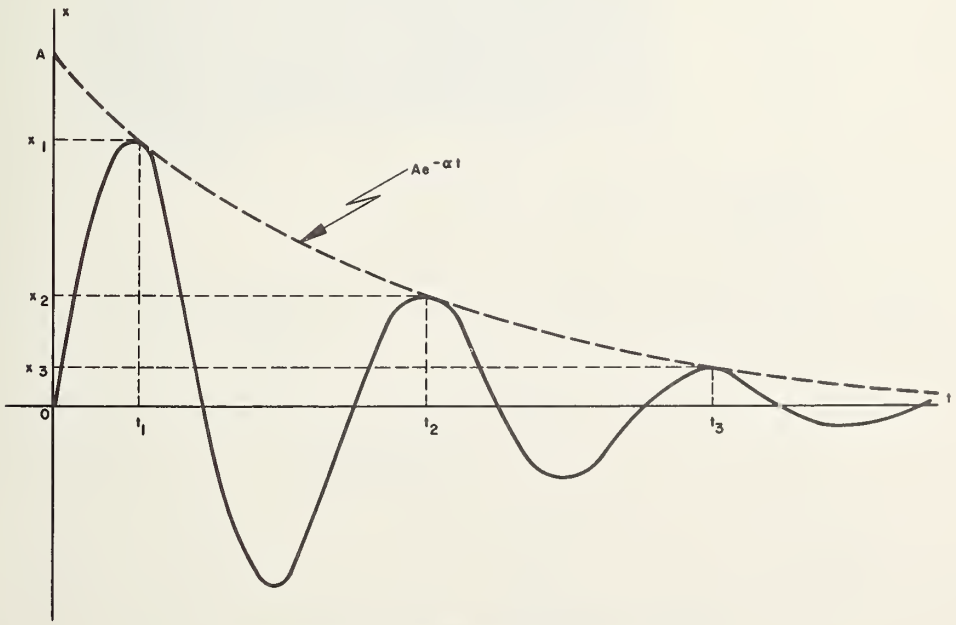

FIGURE 8.5. *Exponentially decaying oscillations.*

4.2. Setting the Compensator Constants

To set the constant A into the compensator, a sine-wave generator of frequency ω_n (the undamped natural frequency of the transducer) is connected to the input terminals, the B potentiometer is set to zero, and the A potentiometer is adjusted until a small output is obtained.

Under these conditions the signal is

$$x=V_1 \sin \omega_n t. \tag{8.13}$$

Substitution of this function into eq (8.5) results in the output

$$g(t)=\frac{f(t)}{k}=\frac{1}{\omega_n^2}\,(-\omega_n^2 V_1 \sin \omega_n t) + \frac{2\zeta}{\omega_n}\,(\omega_n V_1 \cos \omega_n t)+V_1 \sin \omega_n t. \tag{8.14}$$

This simplifies to

$$g(t)=2\zeta V_1 \cos \omega_n t. \tag{8.15}$$

If the B potentiometer is now set to zero, $(B=2\zeta/\omega_n)$, the output must be zero.

This sets the potentiometer A. The B potentiometer can now easily be set by adjustment until the output amplitude is $2\zeta V_1$.

5. Frequency Response

Ideally, amplitude and phase response of transducer and compensator are the inverse of each other, resulting in a flat overall system characteristic. The characteristics of such an ideal system are shown in figure 8.6.

In any real system the frequency characteristics and sensitivity of the amplifiers, and the noise generated in the amplifiers and in the transducer, will naturally adjust the capability of the overall system. This is particularly important at the high frequency end, where the transducer response falls off and the compensator response increases as shown in figure 8.6a, thus tending to exaggerate high-frequency noise.

Real transducer characteristics were discussed in chapter 1. The similarity between real and ideal compensator characteristics may be judged from figure 8.7, which shows the characteristics of an early model compensator [1]. The characteristics were obtained by setting the compensator's α control for the natural frequency of the trans-

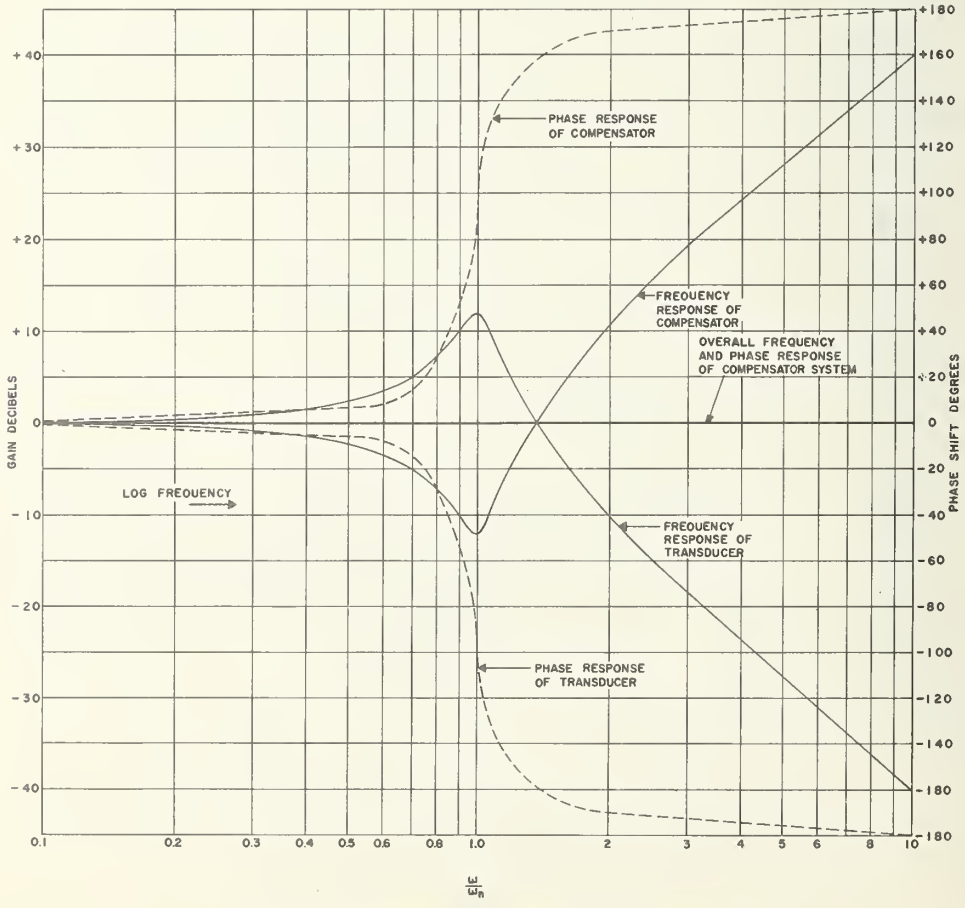

FIGURE 8.6. *Frequency response of ideal system.*

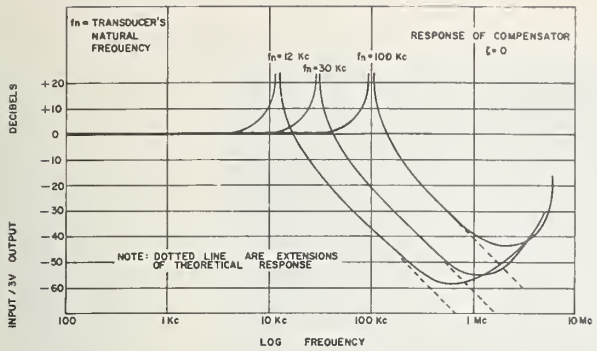

FIGURE 8.7. *Attenuation characteristic of early model compensator.*

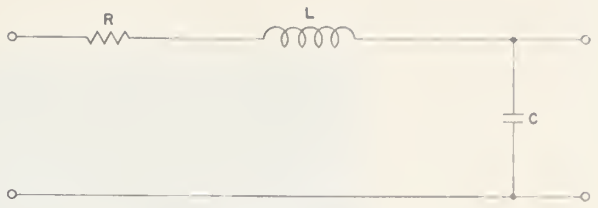

FIGURE 8.8. *Electrical analog transducer.*

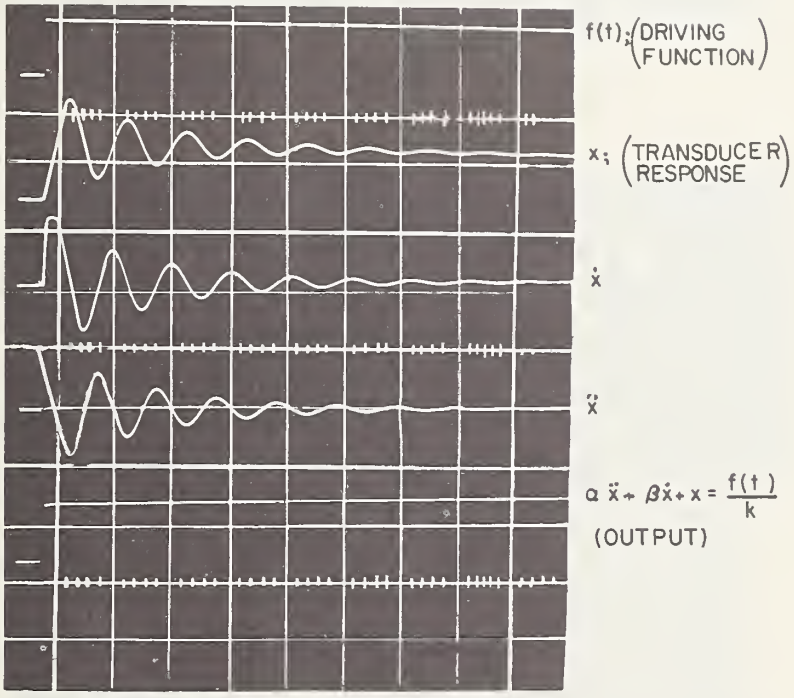

FIGURE 8.9. *Functional representation of simulated transducer and compensator system.*

ducer used, and adjusting the input to obtain constant output. The plotted attenuation is then the inverse of the compensator gain.

Compensator characteristic determination can be made somewhat more independent of transducer characteristics by replacing the physical transducer by an analogous electrical circuit such as that shown in figure 8.8. (We say "somewhat" because lumped electrical elements are known not to be entirely independent of frequency either).

Signals present at various parts of this pseudo-system excited by an electronic pulse of less than 0.1 microsecond rise time are shown in figure 8.9.

Figure 8.10 shows a three-μsec pulse, the pseudo-transducer output, and the reconstructed driving function (compensator output) [1].

Expansion of the first part of figure 8.10 in figure 8.11 makes apparent the $\frac{1}{2}$=μsec rise and decay times, and the 0.3-μsec delay of the compensator output.

An improved version of the compensator is capable of 20-μsec rise times.

The effect of the compensator on recordable system output is graphically demonstrated by figures 8.12 and 8.13. Figure 8.12 shows the response of a capacitance-type transducer to a complex waveform produced by a shock tube.

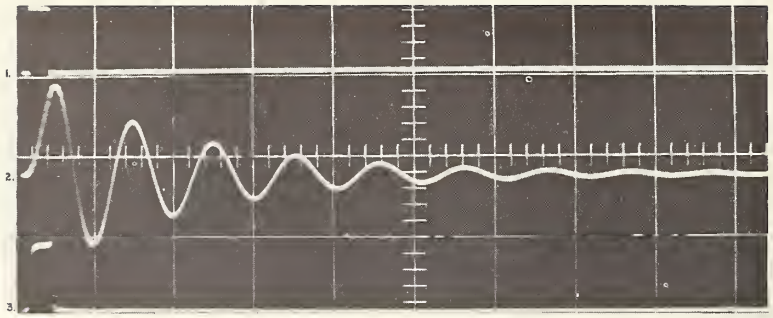

FIGURE 8.10. *Comparison of driving function, pseudo-transducer output, and compensator output.*

1. $f(t)$ (driving function)
2. x (transducer response)
3. $\alpha\ddot{x}+\beta\dot{x}+x=\frac{f(t)}{k}$ (output)

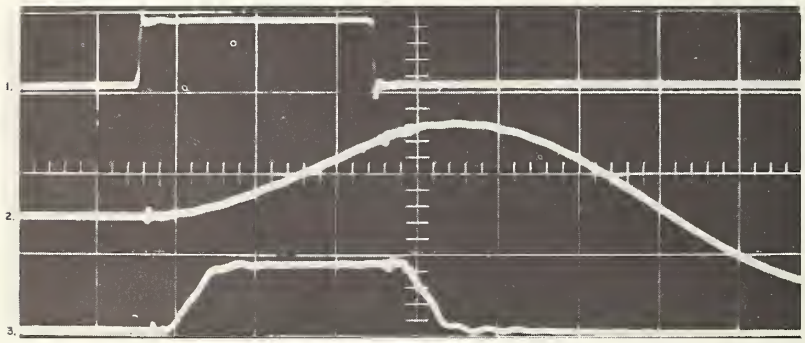

FIGURE 8.11. *Expansion of first part of figure 8.10.*

1. $f(t)$ (driving function)
2. x (transducer response)
3. $\alpha\ddot{x}+\beta\dot{x}+x=\frac{f(t)}{k}$ (output)

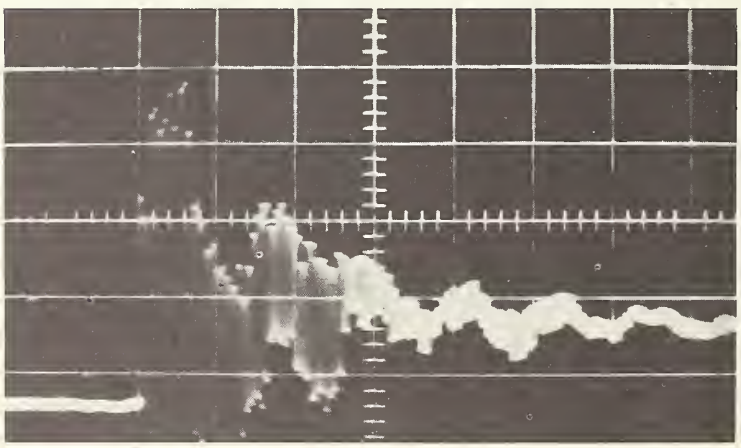

FIGURE 8.12. *Transducer response without compensator.*

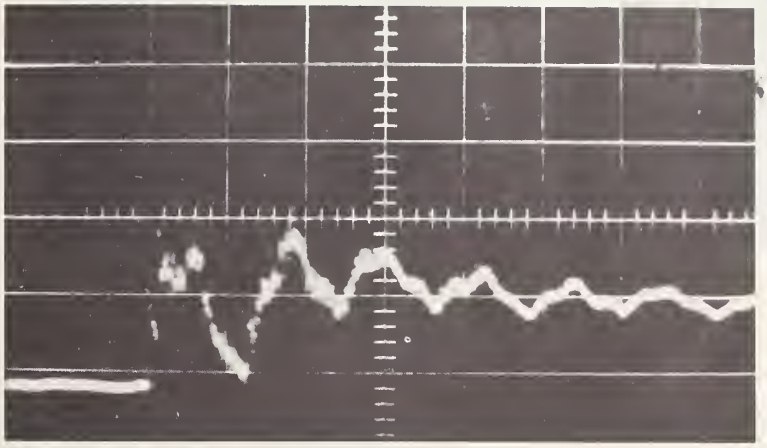

FIGURE 8.13. *Transducer response with compensator.*

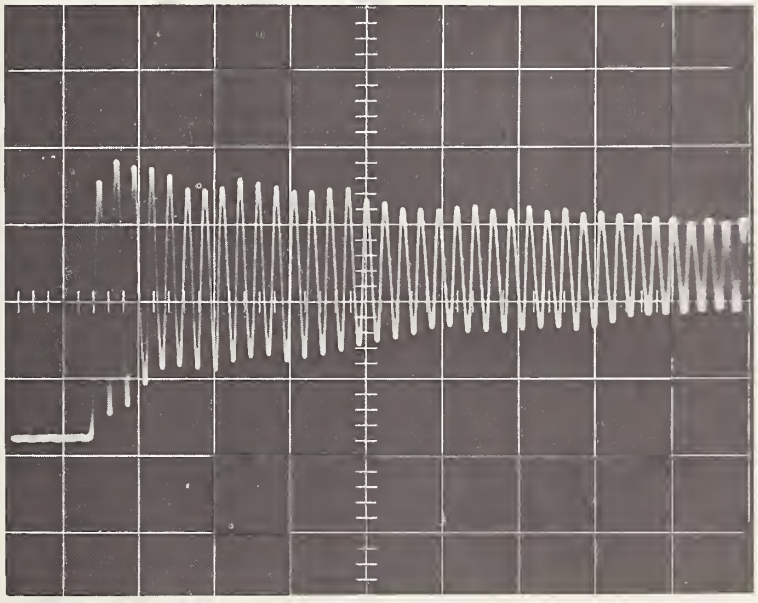

FIGURE 8.14. *Response of transducer to shock wave.*

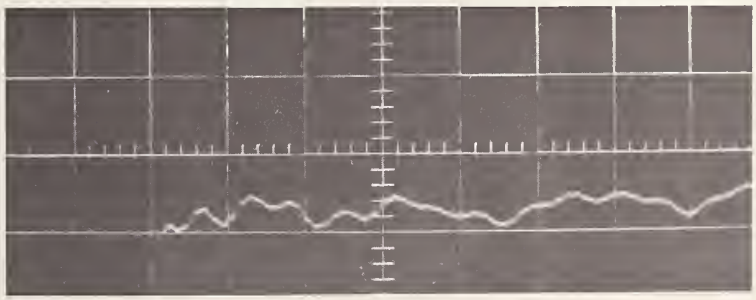

FIGURE 8.15. *Response of figure 8.14 using compensator.*

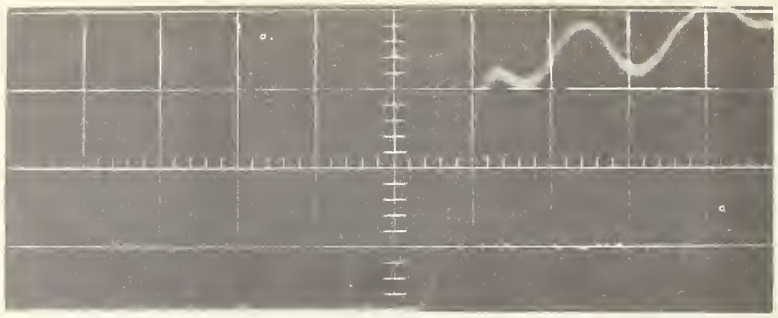

FIGURE 8.16. *Response of figure 8.15 with expanded sweep.*

Figure 8.13 shows the same response with compensator.

A similar improvement for a shock-excited transducer is shown in figures 8.14, 8.15 and 8.16.

6. Limitations

The limitations of the compensator are of two kinds: first, the compensator is essentially limited in the high-frequency region, where the compensator performance deviates appreciably from the desired characteristic. (See fig. 8.7.) A second, and possibly more severe, limitation lies in the basic principle of the compensator operation: namely, the compensator will faithfully reproduce the system input, *provided that the transducer is adequately described by an ordinary linear differential equation of the second order and with constant coefficients.*

And so nonlinearities or other deviations from these ideal transducer characteristics will result in erroneous system output even at frequencies which would yield readable results which could be accurately related to system input functions without use of the compensator.

Without the electronic compensator, any vibration frequencies that may be present in the transducer system will appear generally in distorted form in the output, the amount of distortion depending on the nature of the amplitude and phase characteristic of the transducer at those frequencies. With the compensator in the system, however, any vibration frequencies that may be present will appear unaltered in amplitude and phase in the output, provided that the vibration frequencies occur in the frequency range over which compensation is effective. If the vibration frequencies occur outside the range over which compensation is effective, they will be altered in amplitude and phase depending on the nature of the overall transfer function of the system at those frequencies.

7. References

[1] F. F. Liu, and T. W. Berwin, Extending transducer transient response by electronic compensation for high speed physical measurements, Rev. Sci. Instr. 29, 1, 14–22 (Jan. 1958).

[2] J. P. Den Hartog, Mechanical Vibration, McGraw-Hill Book Co., Inc., 3d ed. (New York, N.Y., p. 37).

[3] Gordon J. Murphy, Control Engineering, p. 89, D. Van Nostrand Co., Inc. (Princeton, N.J., 1959).

[4] C. S. Draper, Walter McKay, and Sidney Lees, Instrument Engineering, p. 249, vol. 11, McGraw-Hill Book Co., Inc., (New York, N.Y., 1953).

U.S. GOVERNMENT PRINTING OFFICE: 1963 O—694-211

THE NATIONAL BUREAU OF STANDARDS

The scope of activities of the National Bureau of Standards at its major laboratories in Washington, D.C., and Boulder, Colorado, is suggested in the following listing of the divisions and sections engaged in technical work. In general, each section carries out specialized research, development, and engineering in the field indicated by its title. A brief description of the activities, and of the resultant publications, appears on the inside of the front cover.

WASHINGTON, D.C.

Electricity. Resistance and Reactance. Electrochemistry. Electrical Instruments. Magnetic Measurements. Dielectrics. High Voltage. Absolute Electrical Measurements.
Metrology. Photometry and Colorimetry. Refractometry. Photographic Research. Length. Engineering Metrology. Mass and Volume.
Heat. Temperature Physics. Heat Measurements. Cryogenic Physics. Equation of State. Statistical Physics.
Radiation Physics. X-ray. Radioactivity. Radiation Theory. High Energy Radiation. Radiological Equipment. Nucleonic Instrumentation. Neutron Physics.
Analytical and Inorganic Chemistry. Pure Substances. Spectrochemistry. Solution Chemistry. Standard Reference Materials. Applied Analytical Research. Crystal Chemistry.
Mechanics. Sound. Pressure and Vacuum. Fluid Mechanics. Engineering Mechanics. Rheology. Combustion Controls.
Polymers. Macromolecules: Synthesis and Structure. Polymer Chemistry. Polymer Physics. Polymer Characterization. Polymer Evaluation and Testing. Applied Polymer Standards and Research. Dental Research.
Metallurgy. Engineering Metallurgy. Metal Reactions. Metal Physics. Electrolysis and Metal Deposition.
Inorganic Solids. Engineering Ceramics. Glass. Solid State Chemistry. Crystal Growth. Physical Properties. Crystallography.
Building Research. Structural Engineering. Fire Research. Mechanical Systems. Organic Building Materials. Codes and Safety Standards. Heat Transfer. Inorganic Building Materials. Metallic Building Materials.
Applied Mathematics. Numerical Analysis. Computation. Statistical Engineering. Mathematical Physics. Operations Research.
Data Processing Systems. Components and Techniques. Computer Technology. Measurements Automation. Engineering Applications. Systems Analysis.
Atomic Physics. Spectroscopy. Infrared Spectroscopy. Far Ultraviolet Physics. Solid State Physics. Electron Physics. Atomic Physics. Plasma Spectroscopy.
Instrumentation. Engineering Electronics. Electron Devices. Electronic Instrumentation. Mechanical Instruments. Basic Instrumentation.
Physical Chemistry. Thermochemistry. Surface Chemistry. Organic Chemistry. Molecular Spectroscopy. Elementary Processes. Mass Spectrometry. Photochemistry and Radiation Chemistry.
Office of Weights and Measures.

BOULDER, COLO.

CRYOGENIC ENGINEERING LABORATORY

Cryogenic Processes. Cryogenic Properties of Solids. Cryogenic Technical Services. Properties of Cryogenic Fluids.

CENTRAL RADIO PROPAGATION LABORATORY

Ionosphere Research and Propagation. Low Frequency and Very Low Frequency Research. Ionosphere Research. Prediction. Services. Sun-Earth Relationships. Field Engineering. Radio Warning Services. Vertical Soundings Research.
Troposphere and Space Telecommunications. Data Reduction Instrumentation. Radio Noise. Tropospheric Measurements. Tropospheric Analysis. Spectrum Utilization Research. Radio-Meteorology. Lower Atmosphere Physics.
Radio Systems. Applied Electromagnetic Theory. High Frequency and Very High Frequency Research. Frequency Utilization. Modulation Research. Antenna Research. Radiodetermination.
Upper Atmosphere and Space Physics. Upper Atmosphere and Plasma Physics. High Latitude Ionosphere Physics. Ionosphere and Exosphere Scatter. Airglow and Aurora. Ionospheric Radio Astronomy.

RADIO STANDARDS LABORATORY

Radio Standards Physics. Frequency and Time Disseminations. Radio and Microwave Materials. Atomic Frequency and Time-Interval Standards. Radio Plasma. Microwave Physics.
Radio Standards Engineering. High Frequency Electrical Standards. High Frequency Calibration Services. High Frequency Impedance Standards. Microwave Calibration Services. Microwave Circuit Standards. Low Frequency Calibration Services.
Joint Institute for Laboratory Astrophysics-NBS Group (Univ. of Colo.).